Schriftenreihe des Lehrstuhls für Kontinuumsmechanik und Materialtheorie der Technischen Universität Berlin

Herausgegeben von Prof. Dr. rer. nat. Wolfgang H. Müller

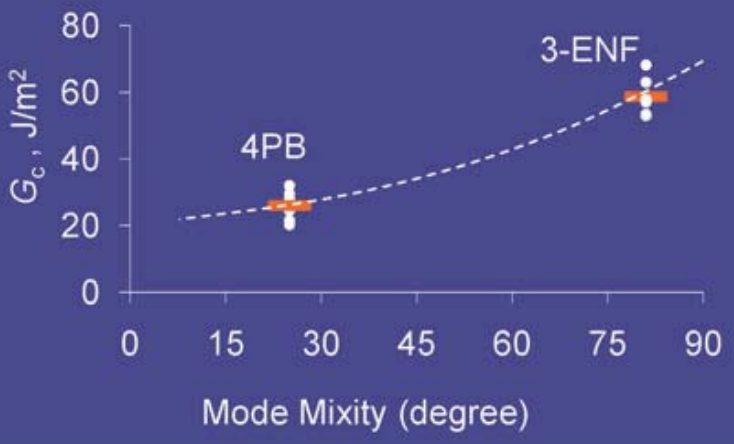

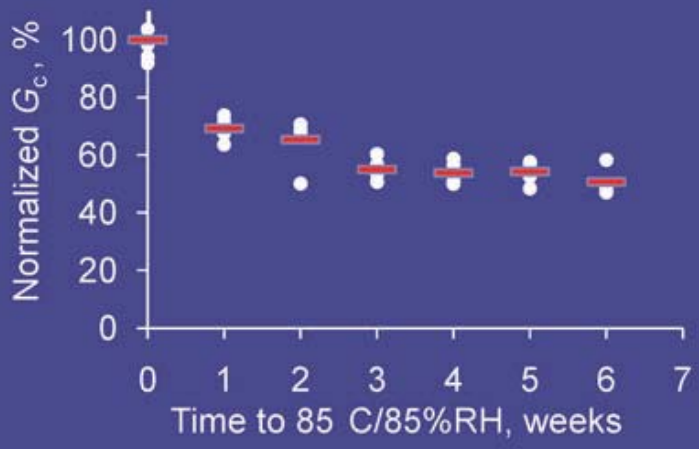

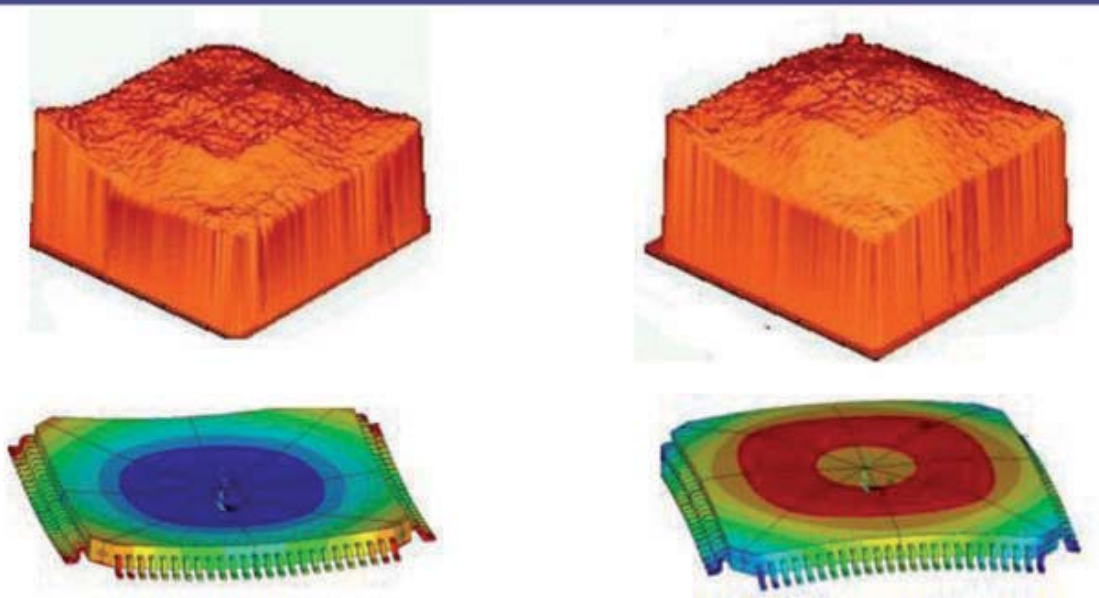

Mohammad Hossein Shirangi

Simulation-Based Investigation of Interface Delamination in Plastic IC Packages under Temperature and Moisture Loading

Cuvillier Verlag Göttingen
Internationaler wissenschaftlicher Fachverlag

Simulation-based Investigation of Interface Delamination in Plastic IC Packages under Temperature and Moisture Loading

Vorgelegt von
Mohammad Hossein Shirangi

Von der Fakultät V
Verkehrs- und Maschinensysteme
der Technischen Universität Berlin
zur Erlangung des akademischen Grades
- Doktor-Ingenieur (Dr. -Ing.) -

genehmigte Dissertation

Promotionsausschuss:

Vorsitzender:	Prof. Dr. -Ing. habil. Utz von Wagner
Gutachter:	Prof. Dr. rer. nat. habil. Wolfgang H. Müller
Gutachter:	Prof. Dr. rer. nat. habil. Bernd Michel

Tag der wissenschaftlichen Aussprache: 16.07.2010

Berlin 2010

D 83

Bibliografische Information der Deutschen Nationalbibliothek
Die Deutsche Nationalbibliothek verzeichnet diese Publikation in der Deutschen Nationalbibliografie; detaillierte bibliografische Daten sind im Internet über http://dnb.d-nb.de abrufbar.
1. Aufl. - Göttingen : Cuvillier, 2010
Zugl.: (TU) Berlin, Univ., Diss., 2010

978-3-86955-433-4

Nonnenstieg 8, 37075 Göttingen
Telefon: 0551-54724-0
Telefax: 0551-54724-21
www.cuvillier.de

1. Auflage, 2010
Gedruckt auf säurefreiem Papier

978-3-86955-433-4

Acknowledgement

I would like to take an opportunity to thank all people who helped and supported me during my PhD studies from 2006 to 2009 in Reutlingen and Berlin. I must admit that it was my greatest chance that I was able to do my work at two renowned and prestigious organizations in Germany. Being employed by the Robert Bosch GmbH in Reutlingen and being allowed to spend half of the research at Fraunhofer Institute IZM in Berlin, it gave me the greatest opportunities in my career to improve my personal and technical capabilities. I learned the discipline, teamwork, and self-confidence by being an employee of the Bosch Group. At the same time I enjoyed being a member of Micro Materials Center Berlin (MMCB) at Fraunhofer IZM, and learned how the most famous researchers in electronic packaging industry develop novel techniques.

First of all, I would like to thank my supervisor, Prof. Dr. Bernd Michel, head of Micro Materials Center of Fraunhofer IZM, for giving me the opportunity to do the major part of my research in his department. I sincerely thank him for providing motivating, encouraging, and enthusiastic environment during my pursuit of doctoral research. It was his steady support and inspiring guidance that brought this dissertation to its fruition. It was a great pleasure for me to conduct my work under his mentoring.

I would like to express my sincere thanks to my doctoral advisor, Prof. Dr. Wolfgang H. Müller, from Technical University of Berlin, who is a tremendous mentor. I thank him especially for revising this thesis and adding value to its content. I am grateful to have had the opportunity to work under his guidance and direction. I will always reflect on the numerous discussions we had in his office.

I must confess that if there is anything I miss more, it is the work in the group AE/EIM4 especially during the collaboration time with my previous advisor Dr. Metin Koyuncu. Apart from several technical issues I learned from Metin, working with him was simply enjoyable. I remember those beautiful days that we were arranging the plan of dissertation. During those discussions, I learned more from him than he will probably ever fully realize.

I would like to express my sincere thanks to my group leader Dipl.-Phys. Andreas Fischer. During the three-year work in his group, I received all kinds of supports from him. I really enjoyed

working in his group and I am thankful for all the time he spent for me especially at the end of my work in Reutlingen for my employment. I would like also to thank Dr. Cornelia Otto for courageously undertaking the responsibility of advising a PhD student who is half through his work. Additionally I would like to thank all the colleagues of the AE/EIM4 group who helped me several times with giving me valuable advices. I will do my best not to forget my Swabian dialect that I owe EIM4. I also want to express my sincere thanks to Dr. Peter van Staa, head of the department "Development ASIC- & Power Packages" of Robert Bosch GmbH, division Automotive Electronics in Reutlingen. It was for me a pleasure to be a member of his successful team and I thank him for all the suggestions, comments, and supports.

I would like to thank Dr. Hans Walter from Fraunhofer IZM, for the great support and letting me do whatever I want in his lab. I want to acknowledge the great efforts of my dear friend Dr. Marc Dreßler, from Robert Bosch GmbH in Waiblingen. A great part of my work couldn't have been done without his voluntarily supports. I really thank Marc for his patience.

I would like to thank also a very good friend of mine, Prof. Xuejun Fan from Lamar University, USA. It was my best luck to collaborate with him, who is the absolute expert in the area "moisture in electronic packaging". I got several positive feedbacks from Prof. Fan that motivated me during my research. The precious advices that he gave me on several topics together with his nice personality remain always in my mind. I am very glad that part of my doctorate thesis was published in his new book on moisture in electronic assemblies.

I also would like to thank all the colleagues and friends of Micro Materials Center for those nice days we had with each other. Especially I would like to thank Dr. Jürgen Auersperg, Prof. Bernhard Wunderle and Dr. Olaf Wittler for giving me advices, whenever I needed.

When I write this acknowledgment, the list of those I want to acknowledge keeps increasing. For all those who helped me, although their name may not be listed explicitly, my heart goes to you in gratitude.

Finally, on the personal side, my parents deserve special thanks, for providing continuous support, admirable endurance and endless faith. I would like to thank them for their unconditional love.

M. Hossein Shirangi

Berlin, 2010

Zusammenfassung

Grenzschicht-Delamination zwischen verschiedenen Materialien ist eine der größten Herausforderungen für die strukturmechanische Zuverlässigkeit von Mehrschichtsystemen. Viele Produkte, wie beispielsweise mikroelektronische Baugruppen, enthalten polymer-basierte Materialien. Da Polymere Feuchtigkeit aufnehmen, stellen die mit Feuchtigkeit verbundenen Phänomene erhebliche Probleme für die Zuverlässigkeit dieser Produkte dar und können als eine Hauptursache für viele vorzeitige Ausfälle betrachtet werden.

In der Halbleiterindustrie haben sich als Verkapselungsmaterialien Epoxid-Moldmassen, sogenannte Epoxy Molding Compounds (EMCs) etabliert. Die Grenzfläche zwischen EMC und Kupfer-basierten Leadframes in Plastic verkapselten IC-Packages ist als schwächste Grenzfläche identifiziert. Die meisten Risse in Plastic Encapsulated Microcircuits (PEMs) beginnen und vergrößern sich an dieser Grenzfläche. Diese Dissertation bietet eine umfassende Untersuchung der Mechanismen, die für die Grenzschicht-Delamination verantwortlich sind.

Die experimentellen und numerischen Untersuchungen dieser Forschung lassen sich in vier Kategorien unterteilen:

- Die prozessinduzierten Spannungen werden untersucht, darunter Spannungen infolge Schrumpfung der Epoxid-Moldmasse und Spannungen aus dem Unterschied zwischen den thermischen Ausdehnungskoeffizienten der Grenzschicht-Materialien. Eine numerische Lösungsmethode wird vorgeschlagen und durch den Vergleich der Verwölbung eines einfachen Bi-Material Streifens mit den Ergebnissen aus der Finite Elemente (FE) Analyse verifiziert.
- Es werden Experimente zur Untersuchung der Feuchtediffusion (Absorption, Desorption und Re-Sorption) mit EMC Proben durchgeführt. Mehrere Probengeometrien und Alterungsbedingungen werden verwendet, um das ungewöhnliche Verhalten dieser Materialien in Bezug auf Feuchtigkeit zu verstehen. Zwei der wichtigsten Erkenntnisse sind die Ermittlung der zweistufigen (*dual stage*) Feuchtigkeitsaufnahme während der Absorption und Restfeuchte nach dem Desorptions-Test. Zudem wird die Feuchtediffusion in den EMCs

durch FE-Analyse nachgestellt. Da die Standard FE-Tools nur das Problem der konventionellen FICK'schen Diffusion direkt lösen können, werden neuartige Simulationsverfahren vorgeschlagen und überprüft, um die Nicht-FICK'sche zweistufige Feuchtigkeitsdiffusion zu berücksichtigen.

- Die hygroskopische Quellung der Polymere aufgrund der Feuchtigkeitsaufnahme verändert den Ausdehnungsunterschied zwischen den Materialien und kann so die Zuverlässigkeit von PEMs verringern. Der Koeffizient der hygroskopischen Schwellung kann experimentell durch Vorwölbungsmessung der Bimaterial-Streifen ermittelt und in den FE-Code umgesetzt werden.
- Zur Bestimmung der Haftfestigkeit in Bezug auf Grenzflächenbruchzähigkeit sind bruchmechanische Experimente durchgeführt worden. Dabei waren die Einflüsse von Temperatur, Alterung in trockenen und feuchten Bedingungen und Mode-Winkel zu untersuchen. Die Lagerung eines Cu/EMC Bi-Material Streifens in Feuchtigkeit führt zu einer Verschlechterung der Adhäsion zwischen EMC und Leadframe. Diese Adhäsionsverschlechterung kann auf den Bindungsabbau zwischen Polymermolekülen und Leadframe zurückgeführt werden und ist das Ergebnis der Diffusion von Wasser in die Grenzfläche. Bei Proben, die sich kurzfristig in einer feuchten Umgebung befanden, ist der Abbau teilweise durch die Anwendung einer geeigneten Hitzebehandlung reversibel. Dagegen verursacht eine langfristige Lagerung in feuchten Zustand eine ständige Abnahme der Haftfestigkeit, die auf die Wirkung von Wasserstoffbrücken zwischen Wassermolekülen und Polymerketten an der Grenzfläche zurückgeführt wurde.

Die Untersuchung der Delamination in einem Plastic IC Package durch FE-Analyse zeigt, dass die vorgeschlagene Methode erfolgsreich eingesetzt werden kann, um die kritische Risslänge in einem Package zu bewerten. Darüber hinaus kann die Methode verwendet werden, um die Delamination durch optimiertes Design zu vermeiden. Das im Rahmen der Dissertation entwickelte Modell kann als Werkzeug eingesetzt werden, um geeignete Materialkombinationen auszuwählen. Es ermöglicht eine schnelle Bauteilbewertung durch Methoden der experimentellen und numerischen Bruchmechanik.

Summary

Interface delamination between dissimilar materials is one of the major threats to the structural integrity and reliability of multi-layered structures. In many of these structures, such as microelectronic assemblies, one or more of the materials are made of polymers. In this case, moisture poses a significant threat to the reliability of these products and can be regarded as one of the principal causes of many premature failures.

Epoxy Molding Compounds (EMCs) are widely used as encapsulating materials in semiconductor packaging industry. The interface between EMC and the copper-based leadframe in plastic IC packages has been found to be one of the weakest joints. Most of cracks in plastic encapsulated microcircuits (PEMs) initiate and propagate in this interface. The crack propagation facilitates, when the EMC materials absorb moisture from the environment. This research provides a comprehensive understanding of the primary mechanisms responsible for the interfacial delamination due to the presence of moisture.

The experimental and numerical investigations of this research can be divided into four categories:

- The process-induced stresses due to cure shrinkage of the epoxy molding compound and thermal mismatch between the materials in plastic IC packages were investigated. A numerical solution was proposed and the method was benchmarked by comparing the warpage of a simple bimaterial beam with the results from Finite Element (FE) analysis.
- Moisture diffusion (absorption, desorption and re-sorption) experiments were carried out on bulk EMC samples. Several sample geometry and aging conditions were used to understand the anomalous behavior of these materials in terms of moisture uptake. The results of these tests explain the complicated mechanism of moisture diffusion in epoxy molding compounds. Two highlights of these experiments are identifying the dual-stage moisture absorption during exposure to humid environments and residual moisture content upon baking the plastic parts. Additionally, the moisture diffusion in the plastic package was modeled by FE analysis. Since the standard FE tools can only solve the problem of conventional Fickian diffusion, novel si-

mulation techniques were suggested and verified to account for the non-Fickian dual stage moisture diffusion during moisture absorption and residual moisture content upon baking of these products at elevated temperature.

- The hygroscopic swelling of the polymers upon moisture absorption is also a major threat to the reliability of PEMs. The value of the coefficient of hygroscopic swelling was determined experimentally by warpage analysis of bimaterial beams and implemented in the FE code.
- Fracture tests were carried out to measure the interfacial adhesion in terms of interfacial fracture toughness. Effects of temperature, aging in dry and humid conditions and mode angle were investigated. It was observed that the exposure of a Cu/EMC bimaterial beam to moisture prior to fracture tests results in a degradation of the adhesion. This degradation is the result of the diffusion of water in the interface. For samples that were shortly exposed to humid environment the degradation was partially reversible by applying an appropriate heat treatment at mild annealing conditions. However, long-term aging in humid condition caused a permanent adhesion loss, which was attributed to the effect of hydrogen bonding between water molecules and polymer chains at the interface.

The investigation of the delamination risk in a plastic IC package by FE analysis showed that the proposed method can be well used to evaluate the critical crack length in a package. Additionally, the method may be used in order to reduce the delamination risks by design optimization. Moreover the predictive model provides a useful tool for selecting proper material combinations. This enables rapid virtual qualification technique by experimental and numerical fracture mechanics approach.

Table of Content

List of Figures

List of Tables

List of Symbols

Latin symbols

a	Crack length	J	Rice contour integral
A	Crack surface	K	Stress intensity factor
B	Thickness of body or specimen	K_{I}	Stress intensity factor for mode I
C	Moisture concentration	K_{1}	Inhomogeneous stress intensity factors for interface cracks
C_{∞}	Saturation moisture concentration	M	Moment of applied load
$C_{1\infty}$	First saturation moisture concentration up to quasi-saturation	$M(t)$	Mass of moisture at time t
$C_{2\infty}$	Second saturation moisture concentration for dual-stage diffusion	M_{residual}	Residual mass of moisture upon desorption
C_{residual}	Residual moisture concentration	P	Applied force
D	Diffusion coefficient (Fickian model)	P_{c}	Critical force
D_{1}	Diffusion coefficient of the 1st diffusion phase	r	Distance of a point to the origin
D_{2}	Diffusion coefficient of the 2nd diffusion phase	t_{EMC}	Thickness of the EMC layer
E	Young's modulus	t_{Cu}	Thickness of the copper leadframe layer
E	Total energy of cracked body	T	Temperature
E_{i}	Young's modulus of the layer i of interface	T_{i}	Traction
ΔE	Activation energy	u	Nodal displacement
G	Strain energy release rate	w	Warpage, also nodal displacement
G_{I}	Strain energy release rate of mode I	W_{s}	Surface energy
G_{c}	Critical strain energy release rate	X	Nodal force at crack front in x direction
G_{Ic}	Critical strain energy release rate of mode I	Y	Nodal force at crack front in y direction
I	Second moment of area for beam	Z	Nodal force at crack front in z direction

Greek symbols

α	Dundurs parameter and coefficient of thermal expansion
β	Dundurs parameter and coefficient of hygroscopic swelling
δ	Crack opening
ε	Strain and interface mismatch parameter
μ_i	Shear modulus
ν	Poisson ratio
σ	Stress
ϑ	Constant depending on the plane strain or plane stress
ψ	Mode angle (mixity)
Γ	Contour surrounding the crack tip
Π	Potential energy
Ψ	Mode angle (mixity) for characteristic length

Abbreviations

3-ENF	Three-point End Notch Flexure
4-ENF	Four-point End Notch Flexure
4PB	Four-Point Bending
APDL	ANSYS Parametric Design Language
CHS	Coefficient of Hygroscopic Swelling
CT	Compact Tension
CTE	Coefficient of Thermal Expansion
DMA	Dynamic Mechanical Analysis
EMC	Epoxy Molding Compound
FE	Finite Element
FEA	Finite Element Analysis
HAST	Highly Accelerated Stress Test
JEDEC	Joint Electron Device Engineering Council
LEFM	Linear Elastic Fracture Mechanics
PEM	Plastic Encapsulated Microcircuit
RH	Relative Humidity
SAM	Scanning Acoustic Microscopy
SEM	Scanning Electron Microscopy
SERR	Strain Energy Release Rate
SHRT	Solder Heat Resistance Test
SMT	System Mount Technology
TGA	Thermo- Gravimetric Analysis
TMA	Thermo- Mechanical Analysis
VCE	Virtual Crack Extension
VCCT	Virtual Crack Closure Technique

Chapter 1 Introduction

Few markets have experienced such rapid growth that the semiconductor market experienced during its relatively short history. The development and growth of production of semiconductors in its history of half of a century has been a real impressive one (KPMG group, Survey of Industry Executives, 2005). This growth was very intense; one only needs to look at the decade between 1985 and 1995, during which the total sales of semiconductors tripled to exceed $150 billion of sales. Since the integrated circuits became available commercially in 1961, the number of transistors doubles every 18~24 months in a single chip, the so-called "Moore's law. Over the past 40 years, Moore's law was remarkably true and remains to be true as markets continue to demand maximum performance and minimum cost.

Electronic packaging refers to the science and technology of providing a suitable environment for an electronic device to perform reliably over a given period of time. The functions of an electronic package are to protect, power, and cool the microelectronic chips or components and provide electrical and mechanical connection between the microelectronic part and the outside world (Tummala, 2001). Although the exact date attributed to the advent of electronic packaging is difficult to establish due to the diversity in opinion as to what exactly constitutes an electronic package, the beginning of modern electronic packaging can probably be dated around 1950, shortly after the invention of the transistor in 1949 by Brattain, Bardeen, and Shockley at Bell Labs (Brown, 1999). Early transistors were housed in plastic packages, which made them highly susceptible to environmental degradation. With a push for increased reliability from the military, these transistors were quickly replaced by the development of the metal Transistor Outline (TO) package, which hermetically sealed the transistor within an inert atmosphere using a metal lid. By the 1960s, the need to reduce manufacturing costs in conjunction with satisfying the large number of input/output (I/O) requirements for the Integrated Circuit (IC) led to the development of the ceramic flatpack, metal flatpack, and Dual-In-line Package (DIP) packages. In response to the need for a higher density Printed Wiring Board (PWB), the 1970s and 1980s observed the development of the Quad-Flat Package (QFP) and Surface Mount Technology (SMT). Driven by the need to make electronic products smaller, more powerful, and available at a lower cost, the Ball Grid Array (BGA) package and Chip Scale Package (CSP) were developed in the 1990s.

These packages offered several advantages to the QFP package, including higher I/O density by utilizing the full area for I/O connections and shorter electrical paths yielding better electrical performance (Tummala *et al*., 1997). Both of these packages emerged from flip chip technology, which utilizes the area underneath the chip for I/O connections rather than just the perimeter of the chip.

Automotive semiconductor products are found in multiple systems - from the powertrain and safety applications to cockpit electronics. The market for semiconductors in automotive applications is growing at a compound annual growth rate of 8.5 percent, and should reach $22.7 billion by 2014. The fastest-growing segments include optoelectronics, sensors, logic, and processors. Analog and microcontrollers are the largest segments, with market shares of 29 percent and 24 percent, respectively (Automotive Semiconductors Report, 2009). The automotive electronics market is being driven by several factors. A few would include increasing global competition, longer vehicle life (more upgrade possibilities), consumer and regulatory demands for more safety systems, the need for greater fuel efficiency, and growing demand for new in-vehicle entertainment devices. These trends all point toward increasing automotive electronics density and complexity, which lead to higher levels of components integration and more silicon content. So, as the number of components increases, space requirements are shrinking.

The miniaturization, new processes, and new materials, among many other means, are essential to these demands. Meanwhile, all those changes result in profound challenges to the reliability in all aspects. For example, thin film cracking, interfacial delamination of organic and metallic interfaces, solder joints detachment at first and second level interconnects, electromigration in conductor lines, vias, bumps, and package traces, potential moisture ingress on die edge seal and low-k dielectrics, stress-induced voiding in copper lines due to thermal mismatch and electromigration, integrity of package assembly, etc. (Zhang, 2007).

As the market demands continue to force product performance to reach its technological limits, the tradeoff between performance and lifetime must be tailored to the needs of different market segments. The advanced semiconductor devices, for example modern plastic IC packages, require increased effort from reliability assessments if the industry is to keep Moore's Law on course. To fulfill the reliability challenges, these products require that accurate reliability models and tools for lifetime estimation be available during the product design and development stage. More efficient reliability-assessment approaches must be employed to identify the potential failures and evaluate their kinetics and impact based on the specific application conditions. Since the structural integrity of these devices is still a persistent challenge, improved understandings of failure mechanisms of these devices, together with virtual qualification methods are required in order to reduce their qualification costs and the time-to-market.

Chapter 2 Reliability in Electronic Packaging

2.1 Introduction to Packaging Processes

The manufacturing phase of an integrated circuit can be divided into two steps. The first, wafer fabrication, is a sophisticated and intricate process of manufacturing the silicon chip. The second, assembly, is a highly precise and automated process of packaging the die. Those two phases are commonly known as “Front-End” and “Back-End”, respectively (quoted from STMicroelectronics).

Plastic Encapsulated Microcircuits (PEMs) are manufactured through a series of sequential processes, widely using metals and polymers in various forms such as in leadframes, encapsulants, adhesives, underfills, molding compounds and coatings (Seraphim *et al.*, 1989; Tummala, 2001). Fig. 2.1 shows typical processes undertaken to fabricate these plastic IC packages.

In the first step, large wafers containing up to several semiconductor chips are fabricated in a wafer fab. These finished wafers coming out of the wafer fab are electrically tested by contacting the exposed bond pads with a probe card. The purpose of this pretest is to early sort out circuits that will not likely result in functional products (van Roosmalen, 2006). The next step after the manufacturing of wafers is the packaging. Typically the wafers must be first prepared to gain the chip with required dimensions. In the following, the main steps from chip preparation to final steps of chip packaging will be reviewed (Tummala, 2001, van Driel 2007, van Roosmalen, 2006):

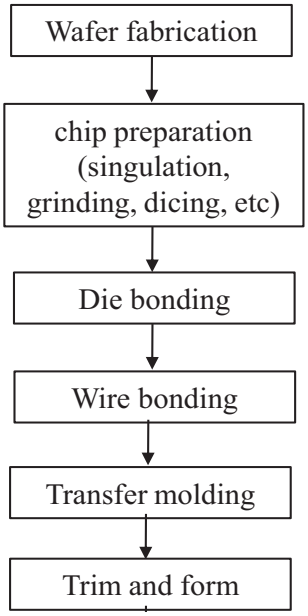

Figure 2.1 Manufacturing process of electronic IC packages.

1. *Chip preparation*: A typical thickness for many compact packages today is ~0.5 mm, almost the same as a standard wafer thickness, implying that most of the wafer backside will need to be removed to fit the eventual outline, this process is called *grinding*. Next, the ICs are cut out of the wafer and can be used for further 'single' processing. This is done at room temperature using a circular sawing or a laser cutting process (*sawing*).
2. *Die bonding*: The packaging process itself involves die attach and encapsulation, each cluster being a conglomerate of shapes and processes in itself. In the die bonding process, the single IC is attached on a carrier material, usually a metal called leadframe, by using some kind of polymeric die attach materials or in some cases by solder materials. Typical process temperature is 150-175°C for die attach and up to 300°C for solder die attach.
3. *Wire bonding:* To connect the die to its environment, the basic choice is between wire bonding and flip-chip technology. In a wire bonding process, the die is fixed into position with a metal-filled epoxy film or paste adhesive or, to allow operation at high die power dissipation, through soldering. A continuous wire, usually gold, is connected to the first bond pad by ultrasound-enhanced thermal compression, then stretched out and welded to the corresponding pin on the external connection structure. That structure will typically be a strip holding multiple patterns, meant to be encapsulated in the molding process, the so-called leadframe. After the weld is made, the wire is cut with a flame of electric arc and brought to the next bond pad, restarting the sequence. In power applications, the thin gold wires may be replaced by thick copper wiring or by aluminum straps. Wire bonding is still the major form of first level interconnection in the world today. At present, over 95% of the manufactured packages (in volume) are wire bonded and the majority of wire bonding is done with thermosonic gold ball bonding. A typical process temperature is 200-220°C.

4. *Chip coating*: For protection of the IC top surface a chip coat material can be used. The chip coat is a highly viscous liquid or paste that encapsulates the IC – mostly epoxies or silicones, with some inorganic filler. A typical process temperature is 150°C.
5. *Transfer molding process*: Transfer molding is the process most commonly used for die encapsulation. Epoxy resin liquefied by high temperature and pressure is forced through a mold chase over the die and leadframe and into the cavity on the frame where the die was placed earlier. The hardened epoxy eventually forms the body of the final package. In this process, the semiconductor IC, wires, and carrier are encapsulated by an epoxy-based material called Epoxy Molding Compound (EMC). The process temperature is about 175°C, followed by a 3 to 6 hours curing step at 175°C. The EMC materials as well as the transfer molding process will be introduced in Chapter 3 in more detail.
6. *Mark*, *Trim and Form*: Finally, the packages are marked and by a trim and form process redundant materials are removed.

Fig 2.2 shows some plastic packages, some of which will be used for reliability investigation in this work. In addition, the cross-section of a TQFP-epad package is illustrated in Fig. 2.3. In this epad package type, the leadframe is exposed to bottom surface of the package for increasing thermal capabilities.

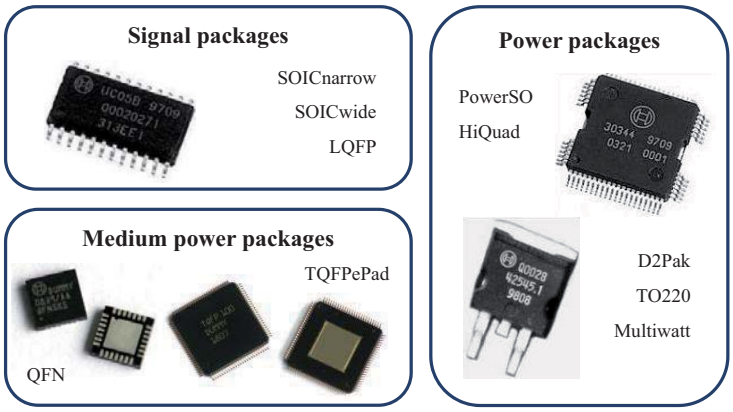

Figure 2.2 Some plastic packages used in automotive industry (courtesy of Robert Bosch GmbH).

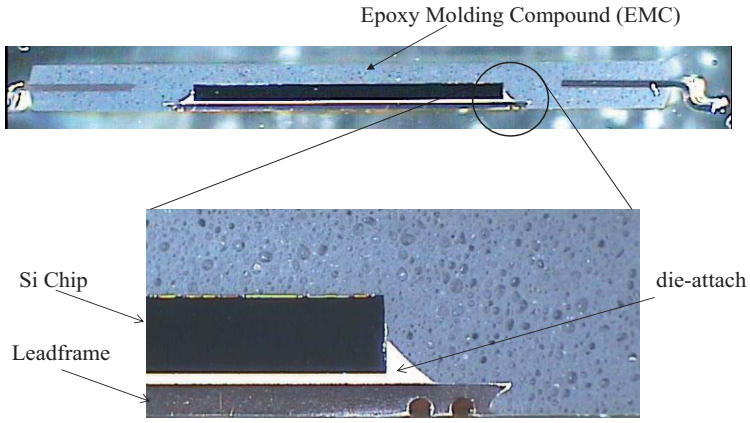

Figure 2.3 Cross-section of a TQFP-epad package.

After the IC packages are fabricated and qualified, they will be store and transported until they are used for their finial surface mount technology via a soldering process to mount these devices on the Printed Circuit Board (PCB). Reflow soldering is the most common method of attaching IC packages and other surface mount components to a circuit board. The goal of the reflow process is to melt the solder alloy particles within the solder paste without overheating and damaging the electrical components. Heating may be accomplished by passing the assembly through a reflow oven or under an infrared lamp or by soldering individual joints with a hot air pencil.

Today, environmental considerations force the so-called lead-free solder materials and the removal of lead materials from microelectronic systems. The materials used so far for the soldering are conventional PbSn eutectic soldering materials that induce automatic alignment of misplaced or non-flat die by surface tension. This phenomenon, together with the quite limited temperature budget imposed by advanced Si wafer technologies, limits the range of reliable alternatives. The alloy SnAgCu is a frequently used lead-free solder replacement for the solder reflow process (van Roosmalen, 2006). These lead-free solder materials need higher temperatures up to 260°C due to their higher melting point. These elevated reflow temperatures are more damaging for the reliability of the IC devices and cause several reliability problems.

2.2 Reliability Tests of Electronic Packages

In the early 1950s, the reliability problems drew attention due to the needs to understand the failure mechanism of unreliable components in US Air Force equipment and quickly, many problems were investigated on a wide front, such as measuring, predicting, and testing of the parts, equipments, even the system reliabilities (Zhang, 2007). However, the microelectronics industry had started booming in the late 1950s. The rapid progress of new designs, new materials, manner of fabrications, operation conditions, application criteria, etc. negated the existing data and models. The establishment of new reliability data on the new devices required expensive testing and was time-consuming. Even further, the improvement of analysis of new data could not catch up the development of new devices. Hence, reliability physics, or “physics of failure”, was created in the early 1960s. Researchers tried to establish the quantitative reliability requirements for devices, and related the fundamental physical and chemical behavior of materials to reliability parameters.

As the emphasis for decreasing costs and time to market in the semiconductor industry becomes even stronger, efficient and effective reliability qualification of products becomes more critical. Reliability qualification is often the last step before manufacturing release of a product and can thus directly impact the time to market. To uncover specific construction, material, and/or process related marginalities, semiconductor devices are qualified using specially designed tests in order to ensure that they have sufficient life so that failures do not occur during the normal usage period. These tests are called reliability tests and their specific purpose is to determine the

failure distributions, evaluate new designs, components, processes and materials, discover problems with safety, collecting reliability data, and to perform reliability control (van Driel, 2007). Reliability tests are classified under various names according to the test format, purpose, method of applying stress, and other factors. In reliability tests, environmental conditions (temperature, moisture) are extrapolated such as to accelerate the circumstances under which the product could fail. Historically, a number of standard tests have been defined by worldwide consortia such the Joint Electron Device Engineering Council (JEDEC), the institute for Interconnection and Packaging electronic Circuits (IPC) and the International Electro-technical Commission (IEC). Table 2.1 describes some of these testing methods (Siliconfareast, 2009, van Driel, 2007).

Table 2.1 Common reliability testing methods of semiconductor packages.

Reliability Test	Reference Specs	Conditions
Solder Heat Resistance Test (SHRT)	JEDEC JESD22-A113	- 24 hours Bake at 125C - Temperature/Humidity Soak based on MSL - 3X IR Reflow at the prescribed peak temperature (about 235C for non-Pb-free parts; 260C for Pb-free)
Temperature Cycle Testing (TCT)	JEDEC JESD22-A104	- Mil Std 883 Method 1010: - Must be conducted for a minimum of 10 cycles
Thermal Shock (TS)	JEDEC JESD22	- Must be conducted for a minimum of 15 cycles
Autoclave or Pressure Cooker Test (PCT)	JEDEC JESD22-A102	- Preconditioned - Soak at 121C/100% RH for 168 hours - Pressure = 2 atm - Unbiased
Highly Accelerated Stress Test (HAST)	JEDEC JESD22-A110	- Preconditioned - Soak at 130C/85% RH for 96 to 100 hours - Biased
Temp Humidity Bias (THB) Test	JEDEC JESD22-A101	- Preconditioned - Soak at 85C/85% RH for 1000 hours - Biased

In the following, some of these reliability tests together with the failure mechanisms expected from the test will be discussed.

Solder Heat Resistance Test (SHRT): As its name implies, SHRT is a reliability test for assessing the ability of a device to withstand the thermal stresses of the soldering process. It is also sometimes referred to as 'preconditioning' if it precedes another reliability test. Preconditioning is usually done for surface-mount devices prior to PCT, THB, and HAST, all of which accelerate corrosion if the package cracks after preconditioning. Preconditioning may also be done prior to temperature cycling or thermal shock, both of which aggravate incipient mechanical failures induced by the precondition. In effect, preconditioning simulates the board soldering process while the tests following it simulate the stresses that the device will experience after mounting.

In order to perform moisture preconditioning on plastic IC packages, different conditioning levels are available, each posing a different degree of damage on the plastic parts. Moisture Sensitivity Levels (MSL) are introduced by JEDEC standards and for each IC package the MSL level with which the package was successfully qualified should be reported. MSL levels are 1 to 6, with 1 being the most severe and 6 being the less severe one. For example, in an MSL1 assessment, the IC package should withstand experimental conditions of 85%RH (Relative Humidity) at 85°C for a period of 168 hours. However, in an MSL6 assessment, the IC package should withstand experimental conditions of 60%RH/30°C for a period of 6 hours.

Temperature Cycle Testing (TCT): TCT determines the ability of parts to resist extremely low and extremely high temperatures, as well as their ability to withstand cyclic exposures to these temperature extremes. A mechanical failure resulting from cyclical thermo-mechanical loading is known as a fatigue failure. During this test, IC packages are subjected to a typical temperature change from, *e.g.,* -50°C to 150°C for a number of cycles. Typical numbers of cycles are 200 to 1000 or more, and depend on the application. For instance, the demand for IC packages aimed for an automotive application is higher than those aimed for customer application.

Thermal Shock (TS): TS is performed to determine the resistance of the part to sudden changes in temperature. The parts undergo a specified number of cycles, which start at ambient temperature. The parts are then exposed to an extremely low (or high) temperature and, within a short period of time, exposed to an extremely high (or low) temperature, before going back to ambient temperature.

Autoclave Test, or **Pressure Cooker Test (PCT):** This test is a reliability test performed to assess the ability of a product to withstand severe temperature and humidity conditions. It is used primarily to accelerate corrosion in the metal parts of the product, including the metallization areas on the surface of the die. It also subjects the samples to the high vapor pressure generated inside the autoclave chamber. Autoclave testing consists of soaking the samples for 168 hours at 121°C, 100% RH, and 2 atm. Intermediate read points at 48H and 96H may also be employed.

Temperature, Humidity, Bias (THB): THB is a reliability test designed to accelerate metal corrosion, particularly that of the metallizations on the die surface of the device. Aside from temperature and humidity which are enough to promote corrosion of metals in the presence of contaminants, bias is applied to the device to provide the potential differences needed to trigger the corrosion process, as well as to drive mobile contaminants to areas of concentration on the die. THB testing employs the following stress conditions: 1000 hours at 85°C, 85% RH, with bias applied to the device. The main drawback of THB is its long duration, necessitating weeks before useable data are obtained.

Highly Accelerated Temperature/Humidity Stress Test (HAST): This test was developed as a shorter alternative to THB Testing. If THB testing takes 1000 hours to complete, HAST results are available within 96-100 hours. Like THB testing, HAST accelerates corrosion, particularly that of the die metal lines and thin film resistors. HAST requires preconditioning and is conducted with electrical bias at 130°C and 85% RH for 96-100 hours.

As a consequence of the reliability tests, which mimic the storage and operation of the plastic IC devices, failures may occur in the IC packages. One of these failures is interface delamination between two adjacent materials, which is one of the major problems in microelectronic devices. Moisture ingress, either through the bulk epoxy or along the interface can accelerate delamination in plastic IC packages. A common method to identify the interface delamination in microelectronic devices is using C-mode Scanning Acoustic Microscopy (C-SAM). The method will be described in next chapter. Fig. 2.4a shows a C-SAM picture of a Hiquad (MO-188) package after reflow soldering. The red regions in this picture indicate the delaminated areas between leadframe and the EMC of the package. Fig. 2.4b shows a Scanning Electron Microscopy (SEM) picture of the cross-section of the same package in the region of interface between the leadframe and epoxy molding compound. In contrast to C-SAM analysis, this method is destructive and requires preparation of the sample at the cross-section. However, the fracture path can be observed more clearly.

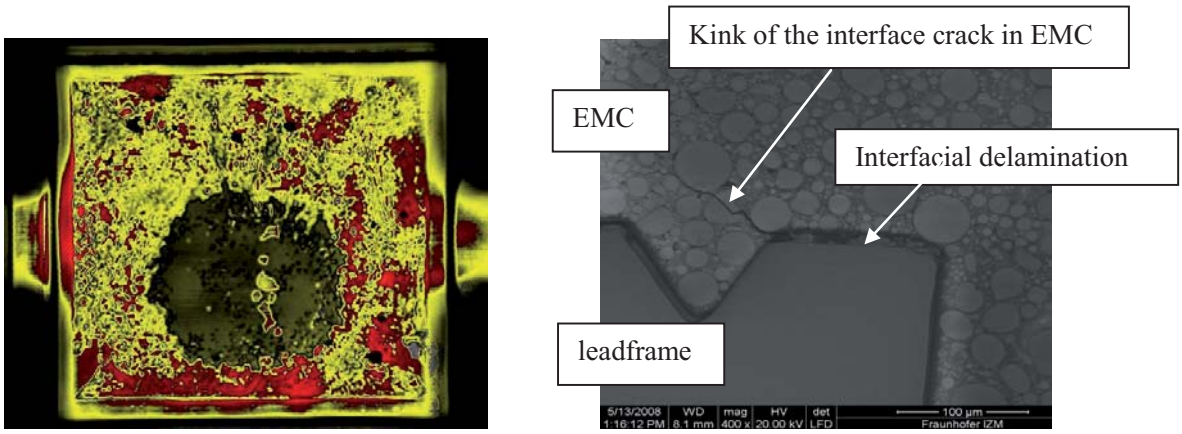

(a) (b)

Figure 2.4 Identification of interface delamination in an IC package: (a) C-SAM picture: red regions indicate delamination, (b) SEM picture of the cross-section of the package.

2.3 Effects of Moisture on the Reliability of Electronic IC Packages

As observed in Table 2.1, many reliability tests of electronic packages contain moisture precondition. This is due to the fact that electronic packages are normally prone to humid environments during their storage and service. In order to mimic these humid conditions, the reliability tests attempt to simulate the process of long-term exposure to humid conditions. Moisture diffusion in Plastic Encapsulated Microcircuits (PEMs) is one of major problems in electronic packaging industry. Moisture diffusion can happen either through the bulk Epoxy Molding Compound (EMC) which is used as the encapsulant for protecting the silicon chip, or through the interface between the EMC and leads. Fan *et al.* (Fan *et al.*, 2009) studies various effects of moisture and summarized a large number of works done in moisture-related reliability issues in electronic

packages. They reported three major types of failure modes arising when the electronic devices are exposed to humid condition. The first type of failure is often referred to 'popcorn failure' at soldering reflow during rapid heating. The second type of moisture-induced failure mechanism concerns the package reliability during a life-long service period under various field environmental conditions due to swelling-induced and adhesion degradation damage. The third type is due to electrochemical migration (corrosion) in the presence of both electrical bias and moisture. Dentritic growth and conductive anodic filament (CAF) growth are typical corrosion phenomena observed in high-density substrates.

The mechanical behavior of polymeric systems is affected significantly by the absorption of moisture. Absorbed moisture may lead to plasticization of the material and, thereby, affect the material's mechanical performance (Ferguson, 2006, Fan *et al.,* 2008a, b, c and 2009, Dermitzaki *et al.,* 2008a, b). By acting as an external plasticizer to the polymer adhesive, the water spreads the polymer molecules apart and reduces the polymer-polymer chain secondary bonding. This provides more room for the polymer molecules to untangle and move around, which results in a softer, more easily deformable mass (Rosen, 1993). Plasticization, on the molecular level, leads to increased intermolecular space or free volume, and may involve the weakening or braking of selective interpolymer bonds. Plasticization implies intimate mixing, such that plasticizer is dissolved in a polymer or a polymer is dissolved in a plasticizer (Franks, 1988). Moreover, the absorbed water can act as a crazing agent by continuously decreasing the mechanical strength of epoxies with exposure time in water (Lu *et al*., 2001). This is supported by scanning electron micrographs of epoxies, which have shown cavities and fractured fibrils that could only be explained by a moisture induced crazing mechanism. Consequently, the moisture induced swelling creates dimensional changes and internal stresses that can ultimately craze and/or crack the material. As a result, lightly cross-linked networks will be more susceptible to crazing than highly cross-linked networks (Morgan *et al*., 1980).

Fig. 2.5 summarizes a number of effects associated with moisture diffusion in polymeric materials of electronic packages. Obviously, the prerequisite to investigate any moisture effect is to ascertain the diffusion (absorption and desorption) mechanism of moisture. Among the various effects listed in Fig. 2.5, three mechanisms are extremely important for the reliability of plastic IC packages from the structural mechanics point of view. First, the adhesion between the epoxy molding compound and other package materials (this work focus on the copper-based leadframe) is of particular importance. This is because of the fact that under poor adhesion, the structural integrity of the package may be threatened, which may lead to disruption in sending electrical signals to the board. Second, the hygroscopic swelling is of particular concern. When epoxy molding compounds of plastic IC packages absorb moisture, they expand in dimensions which change the stress state in these parts. The third mechanism associated with moisture absorption is the effect of vapor pressure (Wong *et al*., 1998 and 2000, Fan *et al*., 2005, Van Gils *et al.*, 2007, Xie *et al*., 2009). This mechanism has normally significant influence at elevated temperatures of the solder reflow process. The main reason for the vapor pressure effect is the evaporation of condensed water molecules in molding compounds. This is especially important at lead-free sol-

dering temperatures because of the exponential increase of vapor pressure at these temperatures. Vapor pressure can be categorized in to two types. One type is the micromechanics-based vapor pressure that causes the volume of the molding compound to increase, and hence, causes an additional mismatch between volumetric changes inside the package. The second type is the effect of gathered vapor molecules in those delaminated areas. This acts as an additional driving force for the crack propagation and finally popcorn cracking of the package.

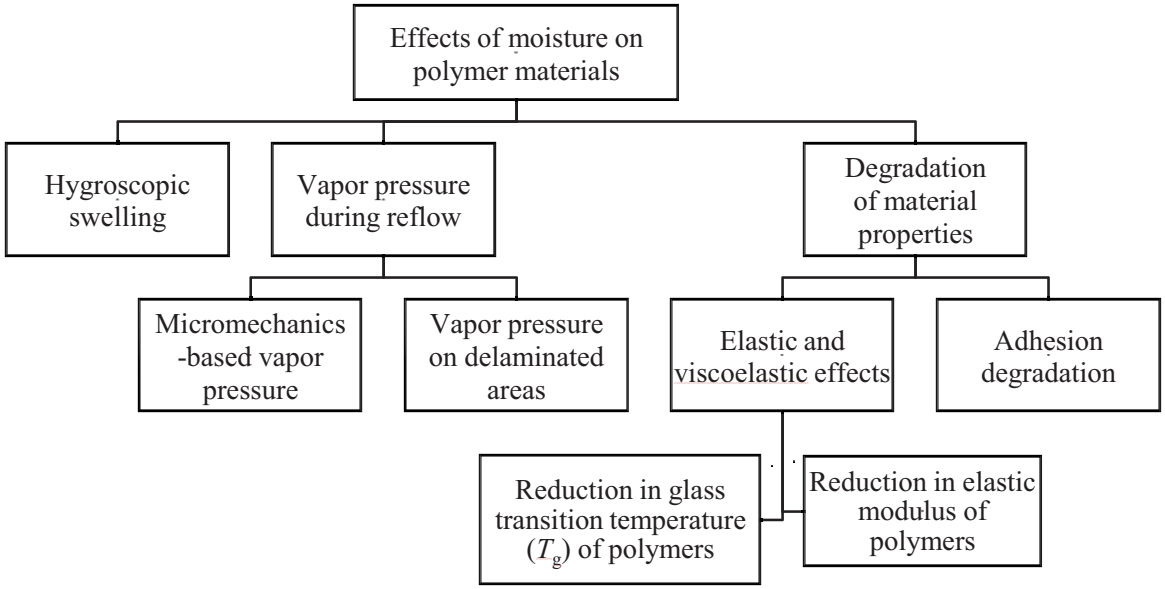

Figure 2.5 Different aspects of moisture-related reliability issues in plastic IC packages.

Other mechanism associated with moisture absorption in polymeric materials may be of different degree of importance for different materials. For example, there is an associated reduction in the polymer glass transition temperature, which reduces the maximum allowable operating temperature of material. Moreover, it has been observed that for a large number of polymers without filler contents the elastic modulus decreases with increasing moisture content (Ferguson, 2006, Dermitzaki, 2008). The reduction of Young's modulus in an epoxy molding compound is of course much less than that in pure epoxy resins. This is because of the fact that a large volume percent of molding compounds (up to 89% in volume) is filled with silica fillers, which are impermeable to moisture.

A common failure arising from moisture precondition is the popcorn cracking in plastic IC packages. Popcorn cracking is a sudden crack propagation in the EMC encapsulant of an IC package, which results from the release of high internal vapor pressure at elevated reflow temperatures during soldering. This is the primary failure mechanism accelerated by SHRT. Popcorn cracking has been the subject of a large number of studies in the past, due to its extreme importance. However, with improving quality of EMC materials many problems associated with popcorn cracking have been solved. Unlike popcorn cracking, the problem of interface delamination is still the subject of many current studies. This is due to new trends in electronic devices regarding

their continuous miniaturization. New products are challenged by more components in smaller geometries, which increase the number of interfaces in these devices.

2.4 Outline of the Dissertation

As the title of this work implies, this study attempts to provide a conceptual understanding of the interface delamination in plastic IC packages driven by moisture and thermal loading. When talking about interface delamination, two fundamental characteristics should be considered. First, the driving force debonding adjacent materials should be known. This driving force may be the consequence of any mechanical, thermo-mechanical or hygro-mechanical loadings. The second factor is the adhesion between the two materials. In order to ascertain the mechanism of interface delamination, both of these characteristics should be well understood.

Fig 2.6 illustrates the methodology that will be used in this work to deal with the moisture-induced interface delamination in electronic packages. The blocks on the right hand of this diagram represent the required steps to determine the driving force of crack in a package, while the blocks on the left side represent the required steps to determine the adhesion characteristics.

Obviously, material characterization lies at the heart of every thermo-mechanical analysis. Moreover, since the Finite Element Method (FEM) simulation tools require complete material data, the prerequisite of a successful analysis is obtaining all required material parameters. It is clear that several instruments are required to obtain these material data. Additionally, in order to fully understand the failure modes in electronic packages a detailed investigation shall be performed which also needs special instruments. A large number of experimental characterizations and several analyses of physics of failure were carried out during this work. Chapter 3 provides a brief overview of some of the instruments and materials used in this study.

In order to determine the fracture driving force in an IC package thermo-mechanical Finite Element Analysis (FEA) is performed. The prerequisite to do such an analysis is implementing the residual stresses from the manufacturing process of these devices in the models. Chapter 4 provides some information about the residual stresses arising from the fabrication process of plastic encapsulated microcircuits.

In order to understand the effect of moisture on the delamination, both driving forces and adhesion characteristics shall be investigated. This is especially important to analyze, because a lot of failure modes observed in electronic packages arise from the diffusion of moisture during storage and service-life of these devices. Several key issues are investigated in Chapters 5, such as moisture absorption, desorption and re-sorption in epoxy molding compound. In addition in Chapter 6 the hygroscopic swelling effect of the moisture is discussed in detail.

The second factor associated with the prediction of interface delamination is the determination of the adhesion characteristics. Since one of the weakest joints in plastic IC packages is the interface between the epoxy molding compounds and the copper-based leadframes, in this work atten-

tion is paid to this interface. However, the method presented in this work is similarly applicable for other polymer/metal interfaces in multi-layer structures, such as composite materials.

In order to deal with the delamination problems, a fracture mechanics approach is used in this study. When using this method, two parameters must be compared against each other in order to determine whether an existing crack will propagate. The first parameter is the Strain Energy Release Rate (SERR or shortly G) which is the driving force for crack propagation. Chapter 7 presents the associated fundamental fracture mechanics approach and some numerical methods to determine this parameter.

The second parameter is the critical value of G, known as interfacial fracture toughness (G_c), which represents adhesion strength. Chapter 8 presents some experimental testing methods performed in this work in order to determine the interfacial fracture toughness between epoxy molding compound and the copper-based leadframe.

In Chapter 9 the intrinsic effect of moisture and temperature on the interfacial fracture toughness between epoxy molding compound and the leadframe is investigated. Finally, the last block in Fig. 2.6 shows how a comparison between the driving force G and material parameter G_c can be used as a crack propagation criterion. Chapter 10 gives some examples that show the application of the developed method for the reliability analysis of plastic IC packages.

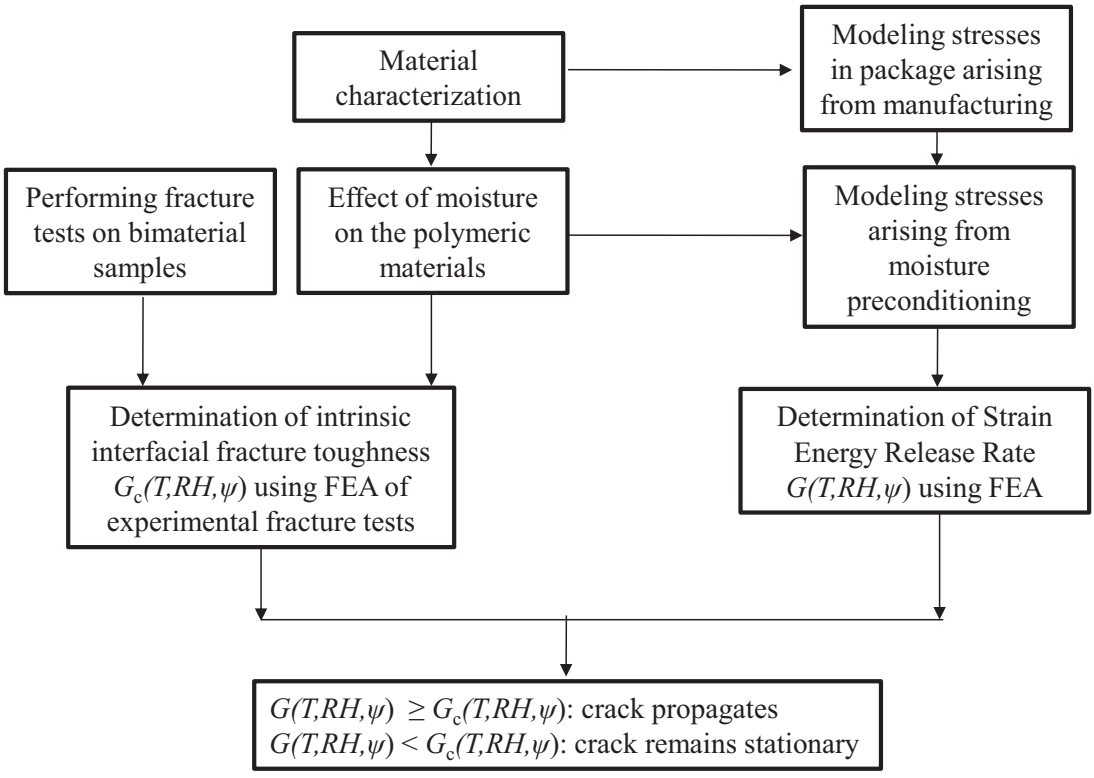

Figure 2.6 Methodology to predict the interface delamination by a combined fracture mechanics and thermo-mechanical analysis.

Chapter 3 Materials and Instrumentations

3.1 Introduction

This chapter presents a brief introduction to the materials as well as the experimental techniques used throughout this study. The interface between an epoxy molding compound and a copper-based leadframe is the main subject of this study. In order to provide a conceptual understanding of the delamination of this joint, it is necessary to ascertain the behavior of each material under in-service conditions. Moreover, in order to use simulation methods for reducing the time-to-market of electronic assemblies via virtual qualification, the materials used in these devices must be fully characterized. In addition, the simulation results should be validated by experimental verifications in order to be used for the design and qualification of these devices. This chapter attempts to present a brief introduction to the instrumentations, testing equipments and the particular testing methods performed in this research. This will aid future research to extend the results and conclusions obtained from this study to advance the understanding of moisture and its role in affecting interfacial adhesion.

Section 3.2 provides brief information about both epoxy molding compounds and copper based leadframes. In Section 3.3 the transfer molding process will be introduced. This is the most common method to encapsulate the silicone chip in plastic encapsulated microcircuits. Finally, in Section 3.4 the equipments used to characterize the materials will be briefly introduced.

3.2 Materials

3.2.1 Epoxy Molding Compound

Epoxy molding compounds (EMCs) are used for protecting the semiconductor chips from the external environment, specifically from external physical forces, such as impact and pressure, and external chemical forces, such as moisture, heat, and ultraviolet rays, maintaining the electric insulating property, and providing the semiconductor package with a form allowing easier mount-

ing on a printed circuit board (Komori and Sakamoto, 2009). Various raw material ingredients are added to an epoxy molding compound in order to meet the requirements on reliability, physical properties and moldability. Examples of some typical ingredients are epoxy resins, phenolic resins, fused silica as filler, coupling agents, curing promoter, and a release agent, all of which are important raw materials that influence the adhesion strength and moldability of the resulting product. These raw materials are mixed and kneaded under heat into a homogeneous mixture in a kneader or a roll mixer. Generally, the materials are kneaded while cooled into a sheet shape, which is then pulverized. The powdery material is pelletized into pellets, which are used in the transfer molding step. Fig 3.1 shows various pellets with different dimensions.

Figure 3.1 Examples of epoxy molding compounds in powder and pellet forms (Komori and Sakamoto, 2009).

Novolac epoxy resins have been commonly used for increasing the cross-linking density of epoxy network after curing. Cross-links are covalent or ionic bonds that link one polymer chain to another. When polymer chains are linked together by cross-links, they lose some of their ability to move as individual polymer chains. Fillers are being used increasingly at higher amounts for reducing water absorption by semiconductor packages and reducing the dimensional changes. Phenol novolac resins have been commonly employed as hardeners for EMCs because of their excellent performance in terms of heat resistance, moisture resistance, electrical properties, curing property, and storage stability. Silica fillers are commonly used in EMCs for reducing the Coefficient of Thermal Expansion (CTE) and reducing the moisture absorption of the EMCs. The curing promoter is a catalyst promoting the reaction between the epoxy resin and the hardener (Komori and Sakamoto, 2009). The silane-coupling agents have long been utilized for strengthening the interface between an inorganic filler and an organic resin matrix are also used in EMCs (Hozoji *et al*., 1990). The product of the EMC for semiconductor should satisfy the flammability rating. For this purpose, a flame retardant is usually added into EMC formulations.

In this work, three commercial epoxy molding compounds from different vendors are investigated. These three materials are marked as **MC-1**, **MC-2** and **MC-3** throughout this study, with **MC-1** being the focus of this study. Most of the material parameters were characterized using the in-house instruments, even though some of these data are provided by the manufacturer. Except for the samples in form a of plate disk, other samples were fabricated using the in-house transfer molding machine. The EMC pellets were provided by the vendors and kept in the refri-

gerator at freezing temperatures (below -10°C) to avoid undesired chemical change or contaminations. Table 3.1 lists some items that are reported by the EMC vendors in the material datasheets.

Table 3.1 Material composition of three EMCs investigated in this study (from material datasheets).

Item	Unit	Epoxy Molding Compound		
		MC-1	**MC-2**	**MC-3**
Epoxy resin	-	Multi Aromatic + Biphenyl	N/A	Multi Aromatic + Biphenyl
Hardener	-	Low Water Absorption	N/A	Low Water Absorption
Z Silicone	-	No	N/A	Yes
Flame retardant system	-	No FR	NO FR	No FR
Filler content	(weight/volume %)	88 / 80	88 / 80	88 / 80
Filler shape	-	All spherical (average 50µm diameter)	All spherical (average 50µm diameter)	All spherical (average 50µm diameter)
Spiral flow	Inch	45	47	45
Gelation time (175°C)	Sec	30	38	30
Flexural Modulus	kgf/mm^2	2450	2800	2350
Flexural strength	kgf/mm^2	15	19.5	15

3.2.2 Leadframe

A leadframe is a thin layer of metal that connects the wiring from tiny electrical terminals on the semiconductor surface to the large-scale circuitry on electrical devices and circuit boards. The leadframe used in this study is a copper-based alloy with the chemical composition listed in Table 3.2. The leadframe plates were provided by the manufacturer in the desired dimensions and their surface was spotted by Nickel-Palladium-Gold (NiPdAu).

Table 3.2 The composition of the copper-based leadframe used in this study (in percent).

Cu	Fe	P	Pb	Zn
balance	2.1-2.6	0.015-0.15	0.03(max)	0.05-0.2

3.3 Transfer Molding Process

Transfer molding is normally the preferred method used for encapsulating or packaging a semiconductor chip with an epoxy molding compound. Transfer molding has been around for decades. It is generally a fast, consistent manufacturing technique that results in high-quality parts. This relatively simple process can be simply automated, which makes it a suitable choice for a lean manufacturing line (Komori and Sakamoto, 2009, Hitachi-chemical, 2009).

In this work, a special bimaterial leadframe/EMC sample is used in order to determine cure shrinkage, hygroscopic swelling and adhesion between the copper leadframe and the epoxy molding compound. The transfer molding process used for the bimaterial samples is similar to that for the plastic encapsulated microcircuits as shown in Fig. 3.2. Fig. 3.2a shows the special mold form designed for the fabrication of these samples. The transfer molding process includes the following steps:

1. Set the leadframe (substrate) connected to the semiconductor chip (here only the leadframe plate) into the cavities of a heated mold (Fig. 3.2b).
2. Set the molding compound tablet into the pot of the molding machine.
3. Close the mold die tightly and, melt the molding compound under mold temperature conditions of 170-180°C, and pour it into the mold under pressure (Fig. 3.2c).
4. After applying pressure for 45-90 seconds, when the molding compound has been fully cured, open the mold and release the molded parts. This completes the encapsulation process.

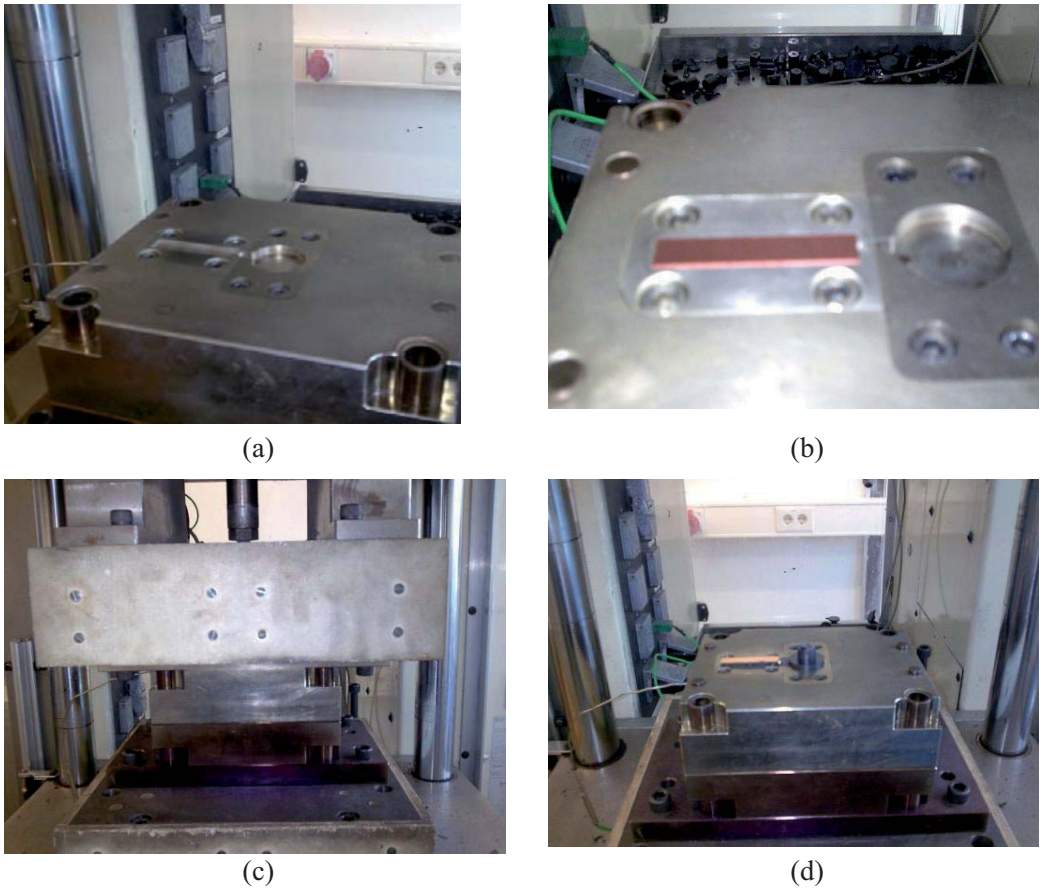

Figure 3.2 Transfer molding for fabricating Cu/EMC samples. (a) Mold form (b) Leadframe placed in the mold form. (c) Injection of EMC. (d) Release of the molded sample from the mold form.

In order to fabricate the bimaterial samples, leadframe plates were machined into $50\times10\times0.4$ mm^3 strips and were molded. After the transfer molding, the samples were placed in an environmental chamber for the post-mold curing at 175°C for six hours to complete the polymerization process of the epoxy molding compound.

3.4 Testing Equipments

3.4.1 Load Frame

One of the main objectives of the experimental part of this work is developing a measurement technique for characterization of the interfacial adhesion between the epoxy molding compounds and copper leadframes. To accomplish this objective, fracture tests are needed to be performed, for which a precise testing machine is required. A computer controlled Instron 5848 Micro Tester load frame shown in Figure 3.3 was used for the interfacial fracture toughness testing. Flexural bend testing was performed using both three-point and four-point bending fixture to determine the adhesion. The computer inputs for all interfacial fracture testing were as follows: 1 N preload, 2 mm/min preloading rate, and different testing rates from 0.1 to 10 mm/min. Load displacement curves were generated for each individual fracture test specimen to determine the critical load at fracture.

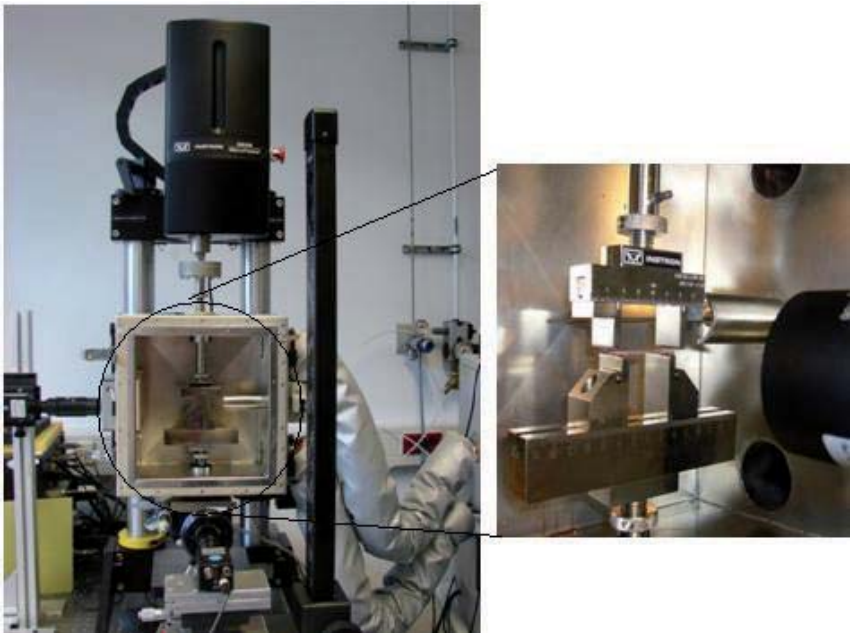

Figure 3.3 The load frame used for the measurement of interfacial fracture toughness (left) and the four-point bend fixtures (right).

The testing system was equipped with a temperature chamber to perform the material characterization at various temperatures ranging from -40°C to 300°C. Moreover, the system was equipped

with two computer-controlled cameras that allowed for taking high resolution images during the testing. Up to 60 images per second were taken for some fracture tests that made the monitoring of the crack propagation via image correlation possible.

3.4.2 Shadow Moiré Interferometry

Measuring the exact deflection of the microelectronic devices is one of the challenges in electronic packaging industry. The deflection of plastic IC packages due to the manufacturing process and residual stresses is within some microns and consequently special equipment is needed to measure their warpage (deflection in out-of-plane direction). One of the most common measuring techniques is based on the principle of shadow Moiré interferometry. The TherMoiré PS200 which was used in this work is a metrology solution that utilizes the shadow Moiré measurement technique combined with automated phase-stepping to characterize out-of-plane displacement for samples up to 150 mm ×200 mm. With time temperature profiling capability, the instrument captures a complete history of a sample's behavior during a user-defined thermal excursion.

Shadow Moiré uses geometric interfaces between a reference grating and its shadow on a sample to measure relative vertical displacement at each pixel position in the resulting interference pattern image (Pan *et al.,* 2007). It requires a grating (alternating clear and opaque lines of equal thickness and constant pitch imprinted on a high temperature glass), white line source at approximately 45 degrees to the grating, and a camera perpendicular to the grating. Fig 3.4 shows a schematic picture of the warpage measurements by this technique.

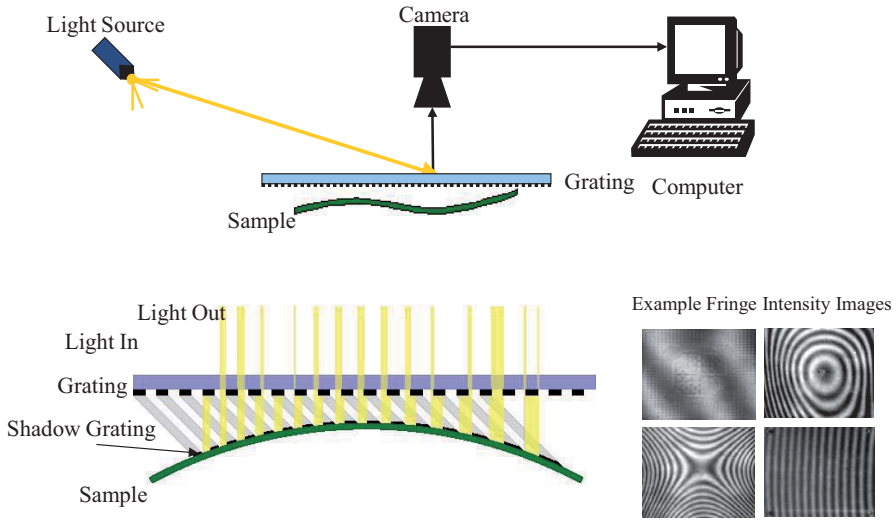

Figure 3.4 Schematic picture of the warpage measurement by TherMoiré equipment.

In order to measure the warpage values at various temperatures, the measurement system was equipped with an infrared chamber which was controlled with a computer. Fig 3.5 shows the measurement equipment used throughout this study for measuring the warpage of bimaterial beams. The system provides measurement results with a vertical resolution of ± 10 µm and a lateral resolution of 640×480 pixels.

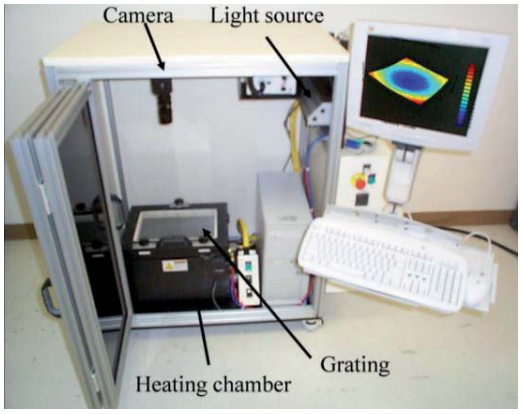

Figure 3.5 TherMoiré equipment used for the warpage analysis of bimaterial samples.

3.4.3 MicroProf with Chromatic Sensor

In order to obtain a topographical picture of packages the FRT MicroProf® with the chromatic sensor (CWL) was used. This is important, because the plastic packages investigated in this study are small in dimension and the effect of moisture on their shape could be well studied with this instrument. The chromatic sensor illuminates the sample by white light source, measures the wave-length dependent (chromatic) distribution of the reflected light, and determines the absolute height information. This analysis can be performed only at room temperature and can provide a topographical picture of the surface of the sample.

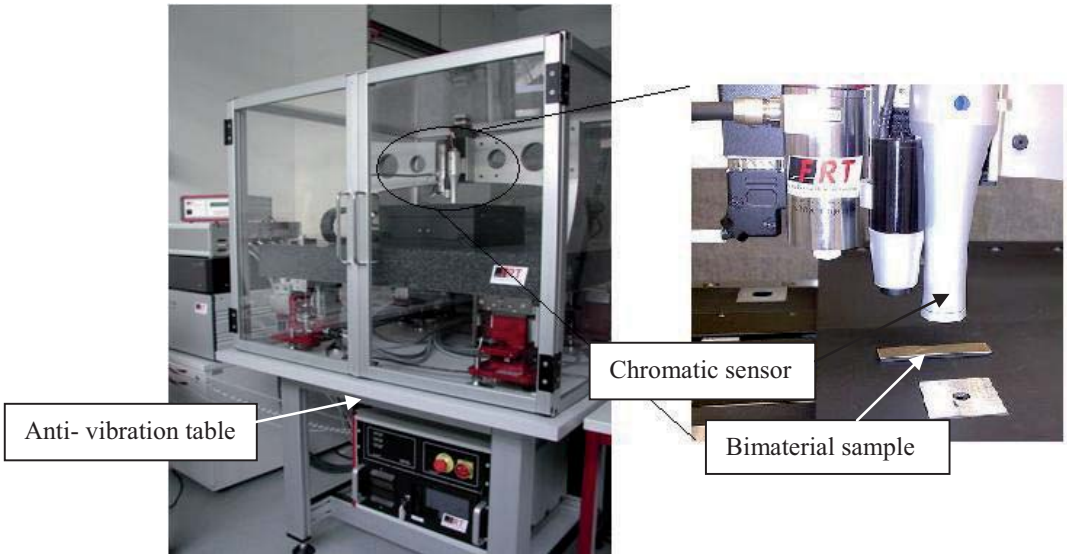

Figure 3.6 MicroProf chromatic sensor used to produce a topographical picture of the surface of the samples.

3.4.4 Dynamic Mechanical Analysis (DMA)

Dynamic Mechanical Analysis (DMA) provides information about a material's time and/or temperature dependent modules and energy-dissipative mechanisms. The DMA equipment used in this study for characterizing the viscoelastic response of epoxy molding compounds was the GABO QUALIMETER model with a maximum 100 N load capacity as shown in Fig.3.7. The use of DMA in polymer characterization has proven to be extremely useful in identifying the major molecular relaxation (Wittler, 2003, Walter *et al.*, 2009a, b). In the DMA instrument, the specimen is exposed to a forced vibration and the response of the material is followed. The extent of damping to which the cyclic strain lags behind the applied stress wave is measured. The use of oscillating force enables the differentiation of the material response to elastic and plastic components. The elastic modulus is the part of the applied stress that is in phase with the oscillation and for this reason is called the storage modulus, whereas the loss modulus represents the part of the applied stress that is out of phase with the oscillation and is completely dissipated (mostly in the form of heat). In this study, the frequency was set between 1 to 20 Hz and the experiments were conducted over a temperatures range of -40°C to 250°C. This results in the presentation of the responding force as a function of temperature, which is then converted to a stress/temperature diagram. The test configuration was put in tension and a full temperature-frequency measurement took normally between 8 to 12 hours.

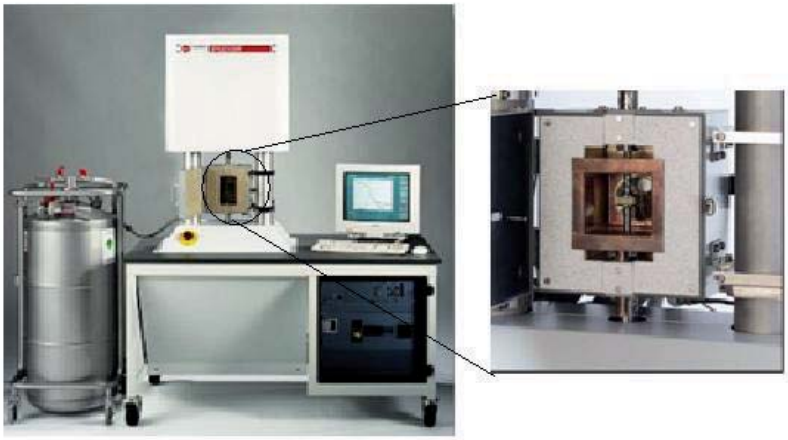

Figure 3.7 The DMA equipment to characterize the time-temperature elastic modulus of EMC materials.

The system is also equipped with an Atomic Force Microscope (AFM) which was used to determine the surface roughness of the leadframe plates. The set-up of the warpage analysis is illustrated in Fig. 3.6. The system allows a scan range of 200×200 mm and provides a vertical resolution of ± 0.1 μm.

3.4.5 Thermo-Mechanical Analysis (TMA)

Thermo-Mechanical Analysis (TMA) is a technique of measuring the dimensional changes in a specimen as a function of time under constant or variable temperatures. In its purest form, the changes of material's dimensions under minimal load are recorded and used as an indicator of the changes in the material's free volume. This data allows for the calculation of the Coefficient of Thermal Expansion (CTE) as well as the detection of the glass transition temperature (T_g) in the polymeric materials. The vertical design of the TMA systems makes it possible to work with very low loads applying only negligible force to the sample. The TMA equipment used in this study was a TMA-202 model provided by Netzsch Company as shown in Fig. 3.8.

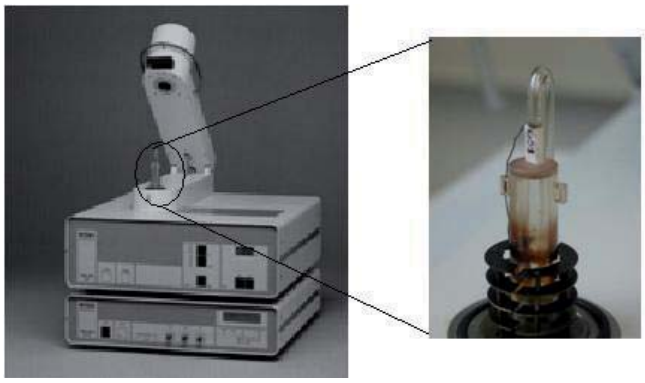

Figure 3.8 The TMA equipment used for the CTE measurements. This apparatus was also used for measuring the hygroscopic strains.

In order to measure the CTE values of the epoxy molding compounds, a small specimen of around 2 mm length was cut from an EMC plate and placed in the chamber of the TMA apparatus. A temperature ramp of 5 K/min was used to measure the thermal strains from room temperature to 250°C. The slope of the strain-temperature curve represents the coefficient of the thermal expansion of such materials. As shown in Fig. 3.9, the CTE curve is composed of two regions. The kink point in this curve represents the glass transition temperature of the material. This temperature is associated with the transition of the polymeric materials from a glassy to a rubbery state. As shown in Fig. 3.9 a unique point to be assumed as this value cannot be identified. Different operational definitions of the glass transition temperature are in use, and several of them are endorsed as accepted scientific standards. Nevertheless, all definitions are arbitrary, and all yield different numeric results. At best, values of T_g for a given substance agree within a few Kelvin. It is also possible to define the T_g value from the DMA analysis, where the elastic modulus of the EMC drops suddenly as the temperature is raised. However, the T_g value may be slightly different. In order to refrain from any inconsistency, the TMA measurements were used to determine the T_g values and the method shown in Fig. 3.9 was used to determine the glass transition temperature T_g. In this method, the linear parts of the strain curves are extended and the point these curve meet is regarded as the glass transition temperature.

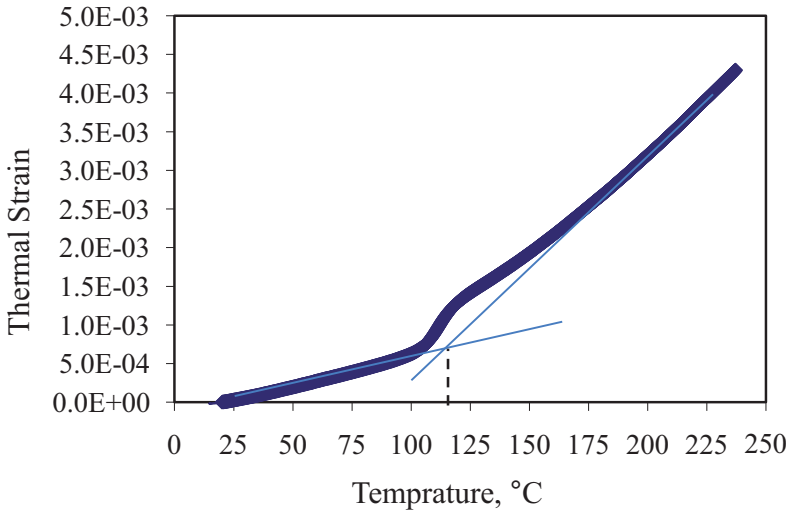

Figure 3.9 A typical TMA measurement curve of EMC materials.

3.4.6 Scanning Electron Microscopy (SEM)

Scanning Electron Microscopy (SEM) provides morphological, topographical and elemental information about solid surfaces. In this work, the SEM measurement technique was used to investigate the surface of the leadframe to investigate the fracture locus. Moreover, the equipment was used to provide high resolution pictures during some fracture tests, which were performed on a micro-load stage inside the chamber of the SEM. The SEM equipment used in this study was a Zeiss 1540XB Crossbeam model.

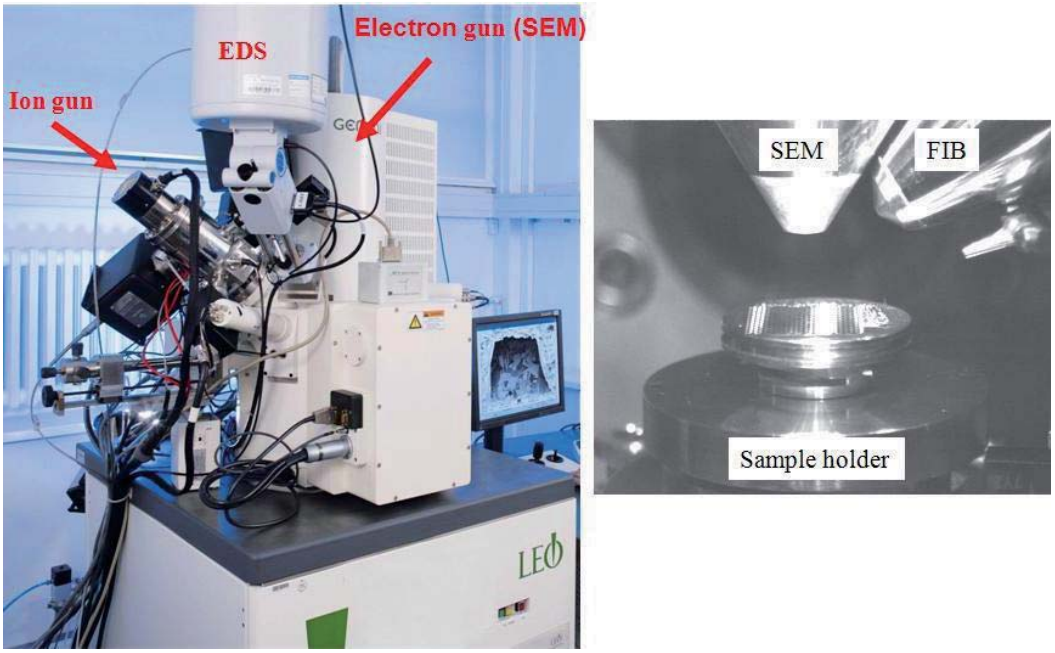

Figure 3.10 The SEM equipment used to find the fracture locus of the Cu/EMC interfaces.

Fig. 3.10 shows the SEM equipment used in this study to provide high resolution images of fracture tests. Additionally, a Force Ion Beam (FIB) was used to investigate the oxidization of the leadframe upon exposure to elevated temperatures.

3.4.7 Scanning Acoustic Microscopy (SAM)

Plastic encapsulated microcircuits are constructed of many adhesive materials. In order to manufacture reliable parts the interfaces, such as die / die-attach, EMC / die, and EMC / leadframe, must be strong enough to ensure the structural integrity of the package. However, it has been found that under certain stress conditions the interfaces could lose adhesion (or delaminate). This delamination can be detected with an analytical tool called C-mode Scanning Acoustic Microscopy (C-SAM). This analysis is a type of Acoustic Micro Imaging (AMI) that uses reflection-mode (pulse-echo) technology in which a single, focused acoustic lens mechanically raster-scans a tiny dot of ultrasound over the sample. As ultrasound is introduced (pulsed) into the sample, a reflection (echo) is generated at each subsequent interface and returned to the sending transducer for processing (Sandor and Evans, 2000). Proper lens selection and proprietary high-speed digital signal processing allow information to be gathered from multiple levels within a sample. Fig. 3.11 presents a schematic picture of the delamination analysis by C-SAM method. The equipment used in this study was a D9000™ C-SAM© model manufactured by Sonoscan company.

Figure 3.11 C-SAM equipment (left), schematic representation of the C-mode scanning acoustic microscope (right).

Chapter 4 Process-Induced Stresses in Plastic IC Devices

4.1 Introduction

Plastic Encapsulated Microcircuits (PEMs) use normally Epoxy Molding Compounds (EMCs) for the environmental and mechanical protection of IC devices. The encapsulation is performed via a transfer molding process in which the uncured EMC pellets are heated and injected into the mold form under a hydraulic pressure. The cross-linking, and hence the formation of the polymer networks during the transfer molding leads normally to a decrease in the volume of the EMC during its solidification process. This phenomenon is normally called "*cure shrinkage*" and the strains that arise from this effect are called cure strains. Furthermore, when these devices are cooled down to room temperature, the mismatch between the Coefficients of Thermal Expansion (CTEs) of different materials causes an additional deformation.

Fig 4.1 shows various dimensional changes that occur during the manufacturing and storage of PEMs. Each of these changes (shrinkage or swelling) may change the overall stress balance in the whole system. These stresses can cause adhesive failure by leading to the formation of cracks which tend to initiate at bimaterial interface corners or edges. In the following each of these mechanisms leading to the residual stresses will be shortly presented:

- In the first step, the pellets of epoxy molding compound melt at 175°C and are injected in the cavity of the mold form for the encapsulation of the silicon die. At this moment, no significant mechanical stresses are available in the system, because the EMC material is still in liquid form and does not jet adhere to the substrate.
- Next the EMC adheres to other parts such as the copper leadframe and the silicon die. During this process the solidification of the EMC begins.
- Due to some chemical reactions, the epoxy molding compounds loose volume and shrink during their solidification and polymerization. This decrease in volume is known as the cure shrinkage of the EMC and causes a deflection of the system. Additionally, a post-mold cure

process is usually performed after the fabrication of these devices. This is due to the observation that during the molding process some of the polymer chains remain uncured and the material needs more time to reach a final fully cured state. It is also believed that during this post-mold process the EMC materials shrink further.

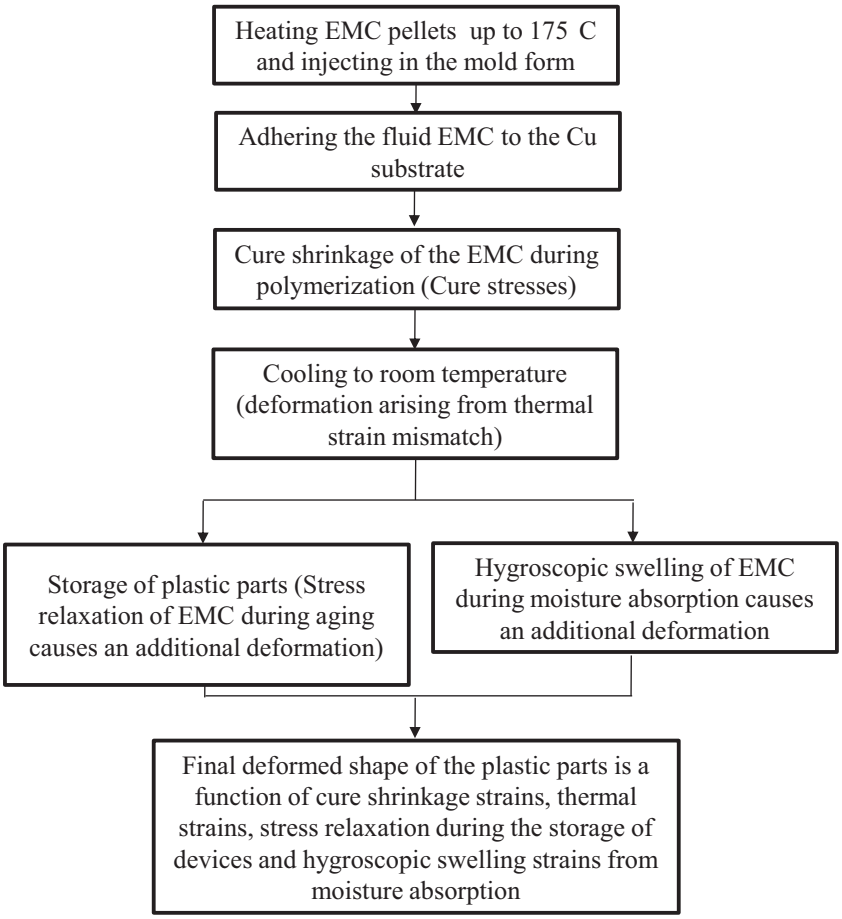

Figure 4.1 Different mechanisms influencing the final deformed state of plastic IC packages.

- After their fabrication the plastic packages are cooled down to room temperature. During this cooling process, each material changes its dimension proportionally to its CTE. However, since different materials in the plastic package have different CTE values, they change their dimension differently. This leads to *thermal strains* due to the *CTE-mismatch* between materials and causes further deflection in the package.
- When the plastic IC packages are stored before the surface mount technology, there are two effects that may also change the overall stress balance of these devices. One mechanism is the stress relaxation of the polymeric materials. This is due to the fact that the packages are under residual stresses. These stresses change with time, because the polymers are viscoelastic materials. As a consequence both stresses and warpage of the package also change with storage time. Another mechanism that normally occurs during the storage of plastic IC

devices is the diffusion of moisture which is the subject of the next two chapters. From the structural mechanics point of view, the moisture absorption causes hygro-thermal strains which also change the stress balance in plastic IC devices.

4.2 Cure Shrinkage of Epoxy Molding Compounds

In this section, the cure shrinkage of the epoxy molding compounds during the polymerization will be investigated. It should be noted that a detailed analysis of the effect of cure shrinkage requires kinetic modeling of the evolution of material changes, which is beyond the scope of this study. In this chapter the effect of cure shrinkage will only be studied by an empirical approach in order to consider its effects on the fracture results presented in Chapters 8 and 9.

The polymerization or cure process of the EMCs is associated with the cross-linking of the epoxy resin during the transfer molding process, at which the rheology and kinetics of the molding compound changes drastically. Yang *et al.* (2004) proposed a cure-dependent viscoelastic constitutive model to describe the evolution of material properties during the curing process, and measured the chemical shrinkage strain with an online density measurement process based on Archimedes principle. They implemented their model in FEA and predicted the warpage of a plastic package. Their result confirms the significant effect of cure shrinkage on the warpage of the plastic packages.

Schreier-Alt *et al.* (2008) applied a stress measurement chip, using an embedded fiber optic Bragg grating (FBG) sensor, and determined the stress condition on the surface of the silicone chips during the encapsulation process. They observed at the gelling point the polymer transforming from a fluid to viscoplastic solid. By cross-linking the molecules enclosed the glass fiber and coupled mechanically to the polymer. They also observed the transfer of shrinkage strains of the polymer onto the fiber sensor to which it was contacted. Moreover, Wang *et al.* (2008) developed an integrated measurement technique based on a fiber Bragg grating for calculating simultaneously the effective chemical shrinkage and the modulus of the polymeric materials as a function of time during polymerization.

Hwang and Chang (2006) measured the isothermal and isobaric volume shrinkage by a single-plunger type dilatometer for an epoxy molding compound. They proposed a mathematical model for Pressure-Volume-Temperature-Cure (P-V-T-C) behavior leading to a relation between the volume shrinkage, pressure, temperature and conversion (degree of cure). Vreugt *et al.* (2008) reported that the curing process associated with the cross-linking of the epoxy resin and the hardener results in a reduction in the volume. This amount of shrinkage was reported for highly filled molding compounds in the order of 0.6-0.8 volumetric percent. Chew and Tan (2003) investigated the effect of Post-Mold Cure (PMC) on the viscoelastic properties of the low stress epoxy molding compounds. They observed that the glass transition temperature typically increases with increasing PMC time as cross-linking density increases and suggested that the pro-

gressive attachment of the silicone particles to the cross-link network of the encapsulant is active during the PMC that decreases the modulus with increasing PMC time.

In order to find out how the residual stresses influence the overall behavior of the bi-material samples in terms of the beam warpage, the process-induced stresses will be investigated in next sections. Additionally, the Finite Element Analysis (FEA) results will be verified by comparing the warpage results from simulation with those found in experiments.

4.3 Sample Fabrication and Material Characterization

In order to investigate the effect of chemical cure shrinkage due to the cross-linking of the epoxy resin in the epoxy molding compound a bi-material beam of Cu/EMC was designed and manufactured. The fabrication process of these samples via transfer molding was describes in Chapter 3. Fig. 4.2 shows the dimensions of the bi-material beam.

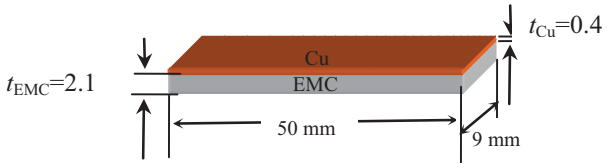

Figure 4.2 Bi-material Cu/EMC beam for the characterization of the residual stresses.

The sample geometry used in this study results in a warpage at room temperature as shown in Fig. 4.3, for which the term “positive warpage” is used.

In order to conduct structural analysis, cure shrinkage and moisture-induced strains need to be incorporated into the stress-strain constitutive relation of the materials as:

$$\{\sigma\} = [\mathrm{K}]\{\varepsilon^{\mathrm{el}}\} = [\mathrm{K}]\{\varepsilon^{\mathrm{total}} - \varepsilon^{\mathrm{cure}} - \varepsilon^{\mathrm{th}} - \varepsilon^{\mathrm{h}}\}, \tag{4.1}$$

where $\{\sigma\} = \{\sigma_x, \sigma_y, \sigma_z, \tau_{xy}, \tau_{yz}, \tau_{xz}\}^{\mathrm{T}}$ is the stress vector, $[\mathrm{K}]$ is the stiffness matrix of the materials, and $\{\varepsilon^{\mathrm{el}}\} = \{\varepsilon_x^{\mathrm{el}}, \varepsilon_y^{\mathrm{el}}, \varepsilon_z^{\mathrm{el}}, \gamma_{xy}^{\mathrm{el}}, \gamma_{yz}^{\mathrm{el}}, \gamma_{xz}^{\mathrm{el}}\}^{\mathrm{T}}$ is the elastic strain vector. In addition, $\{\varepsilon^{\mathrm{cure}}\}$ is the strains arising from the cure shrinkage of the EMC and $\{\varepsilon^{\mathrm{th}}\}$ is the thermal strain vector which can be found from:

$$\{\varepsilon^{\mathrm{th}}\} = \begin{cases} \Delta T \left[\alpha_{\mathrm{Cu}} \quad \alpha_{\mathrm{Cu}} \quad \alpha_{\mathrm{Cu}} \quad 0 \quad 0 \quad 0\right]^{\mathrm{T}} & \text{for Cu} \\ \Delta T \left[\alpha_{\mathrm{EMC}} \quad \alpha_{\mathrm{EMC}} \quad \alpha_{\mathrm{EMC}} \quad 0 \quad 0 \quad 0\right]^{\mathrm{T}} & \text{for EMC,} \end{cases} \tag{4.2}$$

where α_{Cu} and α_{EMC} are the CTE values of Cu and EMC, respectively. Moreover, $\Delta T = T - T_{\mathrm{ref}}$, where T_{ref} is the so-called stress-free and T is the final temperature. $\{\varepsilon^{\mathrm{h}}\}$ is the hygroscopic strain vector which can be found from:

$$\{\varepsilon^{\mathrm{h}}\} = C\left[\beta \quad \beta \quad \beta \quad 0 \quad 0 \quad 0\right]^{\mathrm{T}}, \tag{4.3}$$

where C is the local moisture concentration and β is the coefficient of hygroscopic swelling of the EMC. Obviously, for the dry samples the term $\{\varepsilon^{\mathrm{h}}\}$ in Eq. (4.1) vanishes.

Note that, simple reasoning implies that the CTE-mismatch between the copper and the EMC should induce a negative warpage at room temperature, because the CTE value of the copper (17 ppm/K) is higher than the average equivalent CTE of the EMC when it is cooled from the mold temperature (175°C) to room temperature (25°C). Since the exact value of the $\{\varepsilon^{\mathrm{th}}\}$ can be found analytically and the total strain $\{\varepsilon^{\mathrm{total}}\}$ can be found experimentally by warpage measurement, the cure strain may be estimated from $\{\varepsilon^{\mathrm{cure}}\} = \{\varepsilon^{\mathrm{total}} - \varepsilon^{\mathrm{th}} - \varepsilon^{\mathrm{h}}\}$.

However, an important factor is the time-dependent behavior of the EMC materials, which makes it difficult to extract the value of cure shrinkage. Consequently, a detailed FE analysis which includes viscoelastic properties of the EMC materials will be used to model the residual stresses in these materials.

Several sample geometries were produced to investigate the effect of the cure shrinkage analytically. For example, samples with an EMC thickness below 0.6 mm showed a zero or negative warpage at room temperature. These samples were not suitable for the cure shrinkage measurement, because the measurement of very small warpage with the available equipments was not possible. That is why the optimum sample geometry was found to be the one in Fig. 4.2.

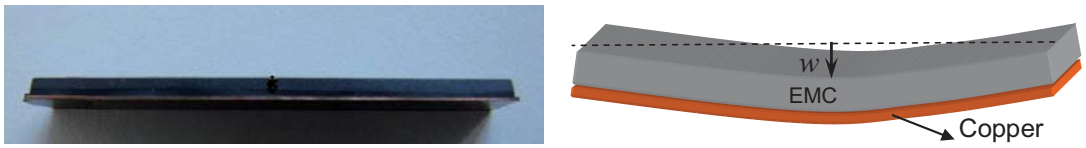

Figure 4.3 Warpage (w) of the bi-material beam at room temperature.

Three commercial molding compounds from different vendors are selected for this study. The warpage is defined as the out-of-plane displacement at the middle of the sample as shown in Fig. 4.3. The bi-material beam which used **MC-1** as the molding compound had the largest warpage at room temperature among all three samples. The warpage of samples with **MC-2** and **MC-3** at room temperature were almost the same, although their glass transition temperatures and CTEs were different. This implies that the chemical cure shrinkage of the two materials must be different. Table 4.1 lists the CTE values measured by Thermo-Mechanical Analysis (TMA). CTE1 and CTE2 denote the coefficients of thermal expansion below and above the glass transition temperature T_{g}, respectively.

Table 4.1 Coefficient of Thermal Expansion (CTE) of three EMC materials.

	T_g [°C]	CTE1 [10^{-6}/K]	CTE2 [10^{-6}/K]
MC-1	109	8.9	29.6
MC-2	104	6.9	25.1
MC-3	109	7.5	28.9
Cu	-	17	

Dynamic Mechanical Analysis (DMA) was used to evaluate the viscoelastic properties of the EMCs. The method utilizes the tension test by applying a sinusoidal force which results in a sinusoidal deformation of the sample. By performing the test under a continuous frequency range, a time lag between the applied stress and the resultant strain causes the ratio of stress and strain to be a complex number. The real part is called the storage modulus and the imaginary part is called the loss modulus. Fig. 4.4 shows the multi-frequency response of the storage modulus as well as the ratio of loss modulus to storage modulus in the temperature range of -40°C to 250°C for the material **MC-1**. The same method was used for the other EMC samples **MC-2** and **MC-3**.

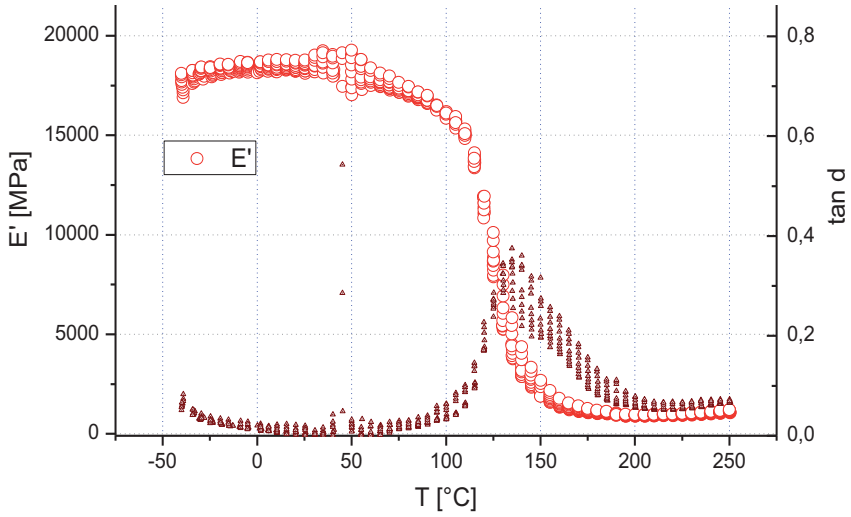

Figure 4.4 Viscoelastic characterization of the material **MC-1**.

Based on the time-temperature superposition a master curve was gained and fitted by Prony coefficients for the FEM software ANSYS. More details about the viscoelastic materials and numerical implementation can be found in (Walter *et al.* 2009a,b), and (Wittler, 2004).

4.4 Experimental Warpage Measurements

In order to find out how the warpage values of the beams change with increasing temperatures, the principle of shadow Moiré interferometry was applied. TherMoiré is a metrology solution that utilizes the shadow moiré measurement technique combined with automated phase-stepping

to characterize the out-of-plane displacement. The measurement system was equipped with an infrared chamber controlled by a computer. The temperature rise of the system was programmed as shown in Fig. 4.5. The temperature of the oven was increased stepwise every 20 K. The temperature was held constant at each step for 10 minutes and then increased linearly to reach the next step. The warpage measurements around 100°C, which is near the glass transition temperature of all three EMCs, was performed using a 10 K temperature rise between each two steps in order to increase the accuracy of measurement in this temperature region. The warpage value was documented at the beginning and at the end of each step in order to investigate the effect of the 10 minutes viscoelastic relaxation at constant temperature.

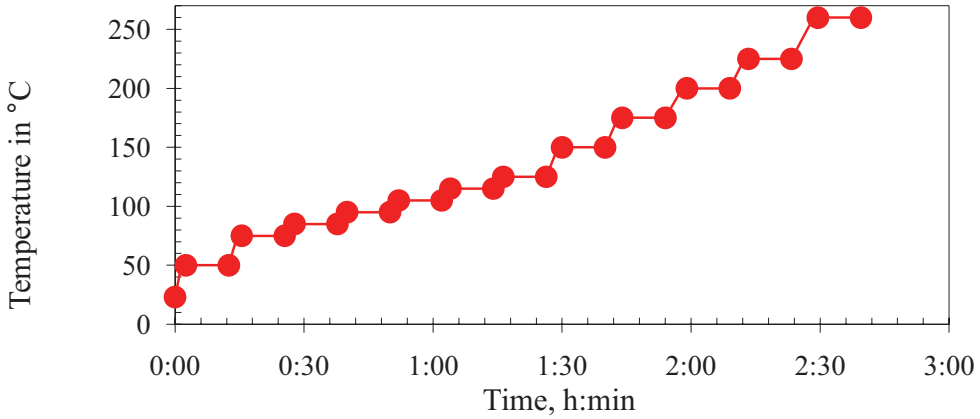

Figure 4.5 Temperature-Time profile for the measurement of the warpage of Cu/EMC beams by shadow Moiré technique.

Fig. 4.6 shows some pictures of warpage measurement by shadow Moiré technique. As it is shown in this picture, at 260°C (reflow temperature), the direction of the deflection was completely different than that at room temperature.

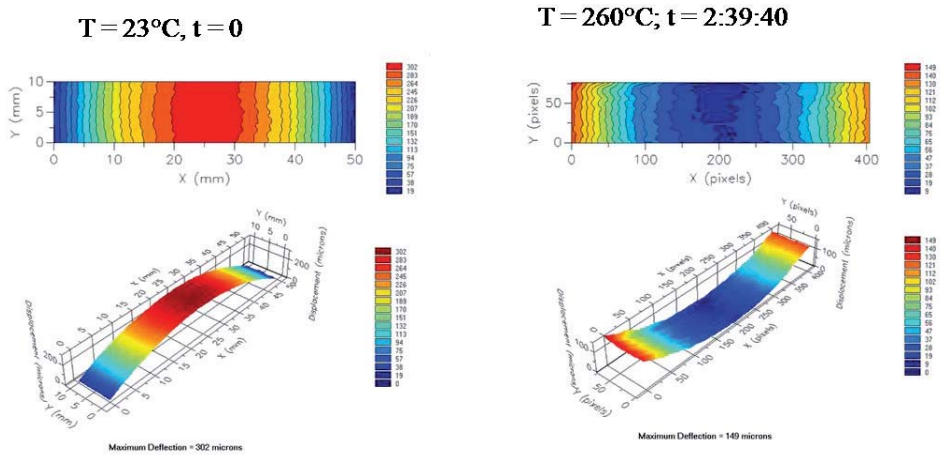

Figure 4.6 Example of warpage results at two temperatures by shadow Moiré interferometry.

Recall that the warpage measurements were taken at the upper surface of the bimaterial beam with EMC layer facing up as shown in Fig. 4.3 (right).

Fig. 4.7 shows the experimental warpage values of each sample as a function of temperature. A jump of the warpage curves at the measured temperatures can be observed, especially at temperatures above the glass transition temperature of EMCs. The first point at each vertical jump represents the warpage measured immediately after the sample reached the desired temperature, while the second point represents the warpage at the same temperature upon 10 minutes storage at a constant temperature. In the temperature range of 25°C to around 110°C the first measurement point shows a higher warpage value, whereas above 110°C the first measurement point shows a lower warpage value. This means that the viscoelasticity has two different effects at temperatures above and below the glass transition temperature of EMC. The significance of the time-dependent behavior of the EMCs can be observed in this figure. At low temperatures the viscoelasticity seems to have no significant influence within small times. However, at temperatures above the glass transition temperature, even short time relaxation induces a significant warpage change due to the drastic stress relaxation of the molding compound.

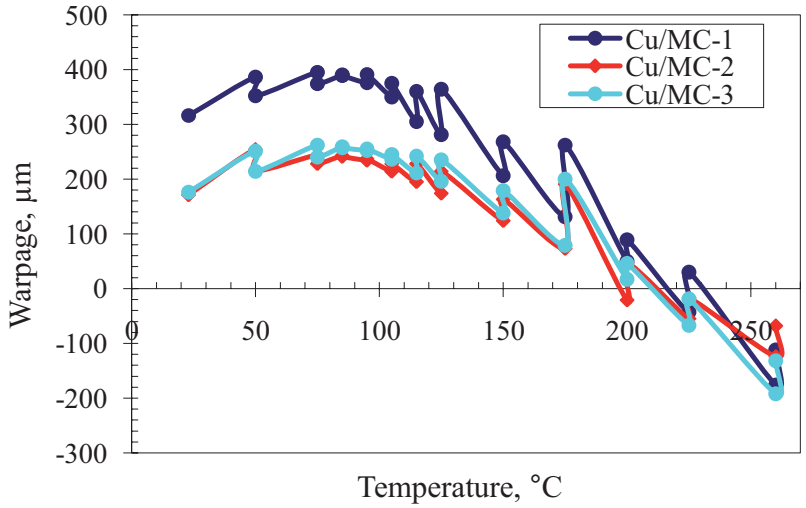

Figure 4.7 Warpage changes of three Cu/EMC bi-material beams as a function of temperature.

Another important observation is that a unique state of zero warpage does not exist, because the warpage curve crosses the abscissa more than once. Since the warpage of the samples varies largely at elevated temperatures due to time-dependency of the EMCs, it is not possible to state a stress-free temperature. However, for all of the three samples the temperature at which the warpage curve reached the abscissa for the first time, *i.e.* w=0, was found to be above 200°C. This is the direct result of the effect of chemical cure shrinkage, which makes the so-called stress-free temperature of the samples higher than the mold temperature of 175°C.

4.5 Viscoelastic FE Analysis Considering Cure Shrinkage

In this section the procedure to model the behavior of bimaterial samples is presented. An FE model is used in the next chapters to model the residual stresses in the bimaterial systems. For a bimaterial beam the FE model must primarily be able to predict the response of the materials to thermal loading, which is associated with the time and temperature dependence of the warpage. Considering the complex temperature and load-rate dependence of EMCs, it was tried to develop a simple geometry-independent FE model that predicts the warpage of the bimaterial beams correctly. For the verification of the FE model the time-temperature data in Fig. 4.5 were used as input to the FE model and the resultant warpage values were compared to the experimental results of Fig. 4.7.

In order to model the cure stresses the value of the cure shrinkage strain must be known first. However, the EMC material suppliers usually do not provide these data. Consequently, an empirical method was used to find this value. The total strains can be found from experimental warpage analysis and the thermal strains can be found by simulation the cooling process of the sample from mold temperature to room temperature. In the absence of moisture the total residual strain consists of cure strains and thermal strains as:

$$\varepsilon^{\text{residua}} = \varepsilon^{\text{cure}} + \varepsilon^{\text{th}}. \tag{4.4}$$

Fig 4.8 shows the procedure used to model the cure shrinkage of the EMC materials. The cure shrinkage strain was implemented in the FE program as a fit value as follows: First, a guess value ($\varepsilon^{\text{cure\_guess}}$) of the cure strain was assigned to the model. Then the cooling process from the molding temperature (175°C) to the room temperature (25°C) was added. Finally the heating of the sample according to Fig. 4.5 was modeled and the simulated warpage was compared against the experimental results of Fig. 4.7. If the predicted warpage curve did not fit to the experimental one, the value of the $\varepsilon^{\text{cure\_guess}}$ was changed so that the predicted warpage curve fits the experimental one.

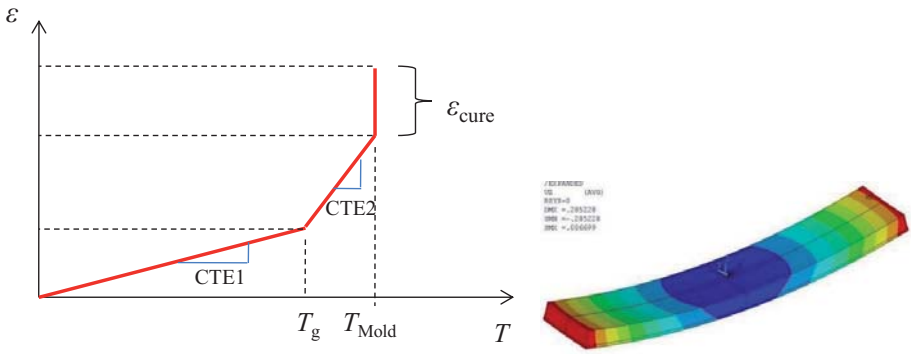

Figure 4.8 Material model for the determination of the cure strain (left) and the FE analysis of the fabrication process of the bimaterial Cu/EMC beam (right).

As stated earlier, two warpage analyses were performed at each temperature with a 10 minute time lag in between. The results of warpage from FE simulation together with the corresponding

experimental curves are shown in Figs. 4.9a-4.9c. Only one set of the warpage data at each temperature is shown in these figures to ease the comparison between the experimental and numerical warpage results. It seems that the method works very well at temperatures below 150°C, and the discrepancy between the experimental and simulation warpage results at elevated temperatures can be attributed to the poor accuracy of the temperature ramping of the testing machine. More importantly, it must be stated that the accuracy of the warpage at low temperatures, where the epoxy molding compound is still in glassy state and the elastic modulus is high, is more important. The warpage at the elevated temperature is still important to be modeled correctly; however, since the epoxy molding compound is in rubbery state with a low Young's modulus, the stresses are not as susceptible to warpage as they are at lower temperatures.

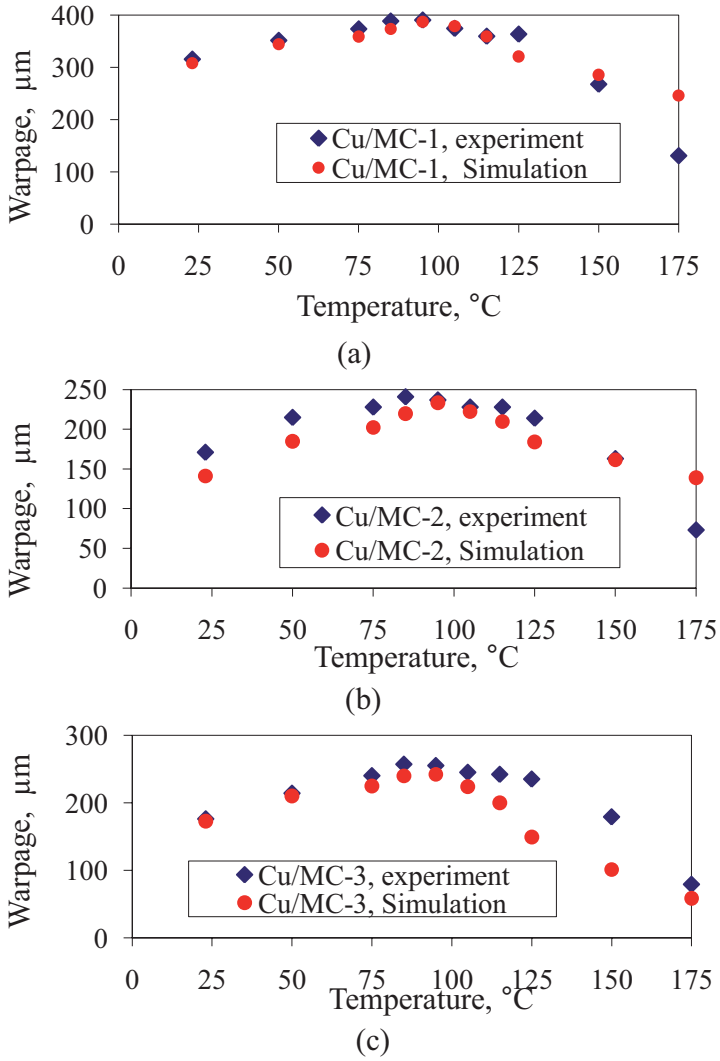

Figure 4.9 Temperature-dependent warpage found by simulation compared to that found experimentally (a) Cu/**MC-1**, (b) Cu/**MC-2**, (c) Cu/**MC-3**.

The results from the FE calculations reveal that among the three EMC materials investigated, the **MC-1** material has the highest cure shrinkage followed by **MC-2** and **MC-3**, respectively. These

results are in agreement with the data provided by the EMC vendors that estimated a value of 0.18% volume shrinkage for **MC-1** and 0.8% for **MC-3**, respectively.

It should be reiterated that the purpose of this chapter was only to propose the simplest method to consider the residual stresses in the bimaterial system. The presented method works very well for FE models that deal with isotropic conditions. However, the evolution of the cure strains during polymerization may cause a non-uniform degree of cure in the system. In this work we assume that the system has reached a fully cure state. A comprehensive study of the cure shrinkage in epoxy materials was done by Dermitzaki *et al*. (2008), who investigated six pure epoxy resins where the structure was systematically changed in terms of stoichiometry and molecular weight, leading to structures with various crosslink densities. Density experiments with the aid of a dilatometer showed that all of them underwent a chemical shrinkage of about 8.84%.

4.6 Conclusions

Internal residual stresses can significantly affect the stress condition and hence the durability of bimaterial interfaces. These stresses can cause adhesive failure by leading to the formation of cracks which tend to initiate at bimaterial interface corners or edges. Residual stress in structure with dissimilar materials, such as adhesives joints and coatings, can originate from processing or solidification of the adhesive. If there is a difference in the Coefficient of Thermal Expansion (CTE) between the adhesive and substrate, heating or cooling will lead to such stresses. Moreover, when the polymeric adhesives absorb moisture, the hygroscopic swelling due to moisture absorption also leads to some residual stresses.

Internal residual stresses in adhesive joints can either be contractive or expansive in nature. A combination of the volume shrinkage of the adhesive with a CTE-mismatch between the adhesive and substrate determines if the adhesive joint is under tension or compression.

In this chapter, the effect of the shrinkage of the epoxy molding compounds during the solidification was investigated. The proposed method consists of both experimental and numerical analyses. In the experimental parts the following steps were undertaken:

- First, a proper bimaterial sample of a Cu/EMC interface was designed and fabricated.
- The required material parameters were characterized experimentally. The main material parameters of the EMC material are the glass transition temperature (T_g), CTE values below and above the T_g (CTE1 and CTE2, respectively), Poisson's ratio, and finally, viscoelastic material data. The copper leadframe was modeled as an elastic material, for which CTE value and E modulus were also characterized.
- The warpage (out-of-plane deflection) of the bimaterial beam was measured at various temperatures. Since the EMC material showed a time and temperature dependence, the warpage also changed as function of time and temperature.

- FE analyses of the fabrication process of the bimaterial beam were performed. The amount of cure shrinkage strain was used as a fit parameter, while other material parameters were known and implemented in the FE model. The cure strain was fitted to the FE analysis, so that the FE warpage of the beam agreed with the experimental values over a large range of temperatures.

The fact that the viscoelastic FE analysis could accurately predict the warpage at selected time and temperatures was a strong reason that the residual stresses were also calculated correctly. This is an important issue, especially when fracture mechanics is used for the prediction of interfacial delamination in bimaterial interfaces.

Chapter 5 Mechanism of Moisture Diffusion in Epoxy Molding Compounds

5.1 Introduction

In order to design and manufacture robust electronic packages, it is important to understand the response of materials and interfaces to the conditions to which they will be subjected. Moisture diffusion in Epoxy Molding Compounds (EMCs) is one of the major reliability concerns in Plastic Encapsulated Microcircuits (PEMs), because many failure modes observed in these devices are believed to arise from the diffusion of moisture during manufacturing, storage or operation.

The use of epoxy-based encapsulating materials for protecting semiconductors against environmental attacks is believed to be a turning point in electronic packaging industry. PEMs have many advantages, such as lower cost, lighter weight and better performance, over hermetic packages. They are generally applied in all industrial areas including automotive industry, consumer electronics, military, and space applications. Despite all of their advantages, one important disadvantage of PEMs is that the EMC absorbs moisture when exposed to a humid environment. EMCs are composite materials made up of an epoxy matrix that encompasses silica fillers, stress relief agents, flame-retardants, and other additives (Pecht *et al*., 1995). The commonly used resin in epoxy molding compounds for electronic packaging is Epoxy Cresol Novolac (ECN) and the common hardener and filler are Phenolic Novolac (PN) and Fused Silica (FS), respectively (Ardebili *et al.*, 2002).

Moisture behavior of EMC is mainly dominated by the diffusion of water through epoxy resin. However, it is also possible that the amount of filler and its shape can influence the moisture diffusivity. Diffusion of moisture in epoxy resins is affected by several factors; however, surface topology and resin polarity are the primary aspects that affect the equilibrium moisture uptake. Soles and Yee (2000) found that water traverses the epoxy through a network of nanopores that is inherent to the epoxy structure. They determined the average size of nanopore diameter to vary from 5 to 6.1 Å and account for 3-7 % of the total value of the epoxy material. Since the approximate diameter of a kinetic water molecule is just 3.0 Å, moisture can easily traverse into the

epoxy via the nanopores. They found that the volume fraction of nanopores does not affect the diffusion coefficient of water in any of the resin studied and argued that polar groups coincident with the nanopores are the rate-limiting factor in the diffusion process, which could explain why the diffusion coefficient is essentially independent of the nanopore content.

There are many speculations regarding the state of water molecules in polymers. Adamson (1980) proposed that moisture can transfer in epoxy resins either in the form of liquid or vapor. Tencer (1994) suggested it is also possible that vapor water molecules undergo a phase transformation and condense to the liquid phase. The condensed moisture was reported to be either in the form of discrete droplets on the surface or in the form of uniform layers. These water layers are often quantified in terms of monolayers of water necessary to initiate and support corrosion of the metallization in PEMs.

Moisture diffusion in a polymer can be analyzed using the so-called thermal-moisture analogy. The method has been developed by a number of researchers (Galloway *et al.,* 1997, Wong *et al.,* 1998) to overcome the discontinuity problem of moisture concentration across the bi-material interfaces using normalized variables. More recently, a Direct Concentration Approach (DCA) has been proposed by Xie *et al.* (2009) to study the moisture diffusion with varying temperature and humidity conditions such as in soldering reflow.

Prediction of the problems associated with moisture in PEMs requires a full understanding of the mechanism of moisture diffusion in these materials. In this chapter a detailed analysis of the role of moisture in EMC performance is presented. Moisture diffusion in epoxy molding compounds will be first investigated quantitatively by gravimetric analysis (weight gain measurements) of plastic packages as well as standard bulk EMC samples. Then the characteristics of moisture absorption will be studied by performing moisture desorption and re-sorption tests at various baking conditions. The results of this chapter will be used for the interpretation of adhesion tests.

5.2 Moisture Diffusion in Plastic Encapsulated Microcircuits

The objective of this section is to study the diffusion of moisture in plastic encapsulated devices. Four types of plastic packages were selected to investigate how their moisture content changes with time at 85°C/85% RH (Relative Humidity). Table 5.1 lists the type and initial dry weight of these packages. All of these packages were stored more than one year in unprotected conditions after their fabrication. Since these packages absorb moisture from air during storage, they should be first baked to reach the dry state. The bake-out condition is believed to depend on the geometry and storage time of the packages. However, a typical and standard baking condition in electronic packaging is 24 hours baking at 125°C. This baking condition may not necessarily lead to a fully dry state as will be discussed in the next sections. Despite this fact, the bake-out condition for all packages was assumed to be as standard (24 h at 125°C) in order to facilitate a consistent comparison between the moisture contents of these devices.

Table 5.1 Four types of plastic IC packages for the investigation of moisture diffusion.

Sample name	Package type	Package dry weight (mg)	EMC used in Package	Package dimensions (mm^3)
P1	MO-188	2209.01	**MC-1**	14×14×2.75
P2	SOIC-24	672.13	**MC-2**	15.4×7.5×2.45
P3	SOIC-16	451.18	**MC-2**	10.3×7.5×2.45
P4	PLCC-44	2540.47	**MC-3**	16.5×16.5×3.8

Package P1 is an MO-188 type which uses solder for the die bonding, while other packages use an epoxy die-attach for bonding the die on leadframe. The packages P1 and P2 use molding compounds **MC-1** and **MC-2**, respectively. Packages P2 and P3 are both SOIC packages that use the same type of molding compound (**MC-2**). The only difference between P2 and P3 is that P2 is larger and has more pins compared to P3. Package P4 is a PLCC package and is the largest among the four packages. In order to measure the dry weight of the plastic parts, all plastic packages were first baked at 125°C for 24 hours, then their weight was measured using an electronic balance (0.01 mg) and finally they were placed in a moisture chamber (85°C/85% RH). The plastic parts were removed periodically from the moisture chamber, their weight was measured after reaching room temperature, and they were placed in the chamber for further sorption. Assuming an initial dry sample at the start of the sorption tests, the weight gain of the packages during the sorption experiment corresponds to the weight of moisture available in the package. Fig. 5.1a shows the mass of moisture *vs.* square root of exposed time. The illustration of mass uptake versus square root of time instead of time is due to the fact that the initial sorption curves show a linear relation with square root of time. This makes an estimation of the diffusion coefficient and a comparison of diffusion behavior easier, as will be seen in Section 5.3. In package P1, the epoxy molding compound is the only organic material that absorbs moisture. The other packages use epoxy die-attach for bonding the silicon die to the leadframe. However, the thickness of the die-attach is very low (20-50 μm) and has therefore no significant influence on the overall mass gain of the plastic package. Hence, it is reasonable to assume for all four packages, that only the EMC is responsible for the moisture absorption of the package and other components are whether impermeable to moisture or have no significant contribution to the package mass gain.

The mass uptake of the plastic parts at time t can be determined from

$$\text{Mass uptake (\%)} = \frac{M(t) - M_{\text{Dry}}}{M_{\text{Dry}}} \times 100 , \tag{5.1}$$

where $M(t)$ is the weight of the sample at time t and M_{Dry} is the dry weight before moisture preconditioning. In order to ensure that the result of bulk material diffusion can be compared reasonably to that of the package, the weight of the molding compound of each plastic package was estimated using the data provided by the manufacturer and used in Eq. (5.1), meaning that the dry weight in Eq. (5.1) represents the weight of the molding compound of the package only and not the whole weight of the package. Using Eq. (5.1), the mass uptake of the packages was

calculated and the results as a function of the square root of exposure time are shown in Fig. 5.1b. These graphs are more suitable for a meaningful comparison between the moisture uptakes of different packages, because they provide comparable information about the moisture uptake of molding compounds.

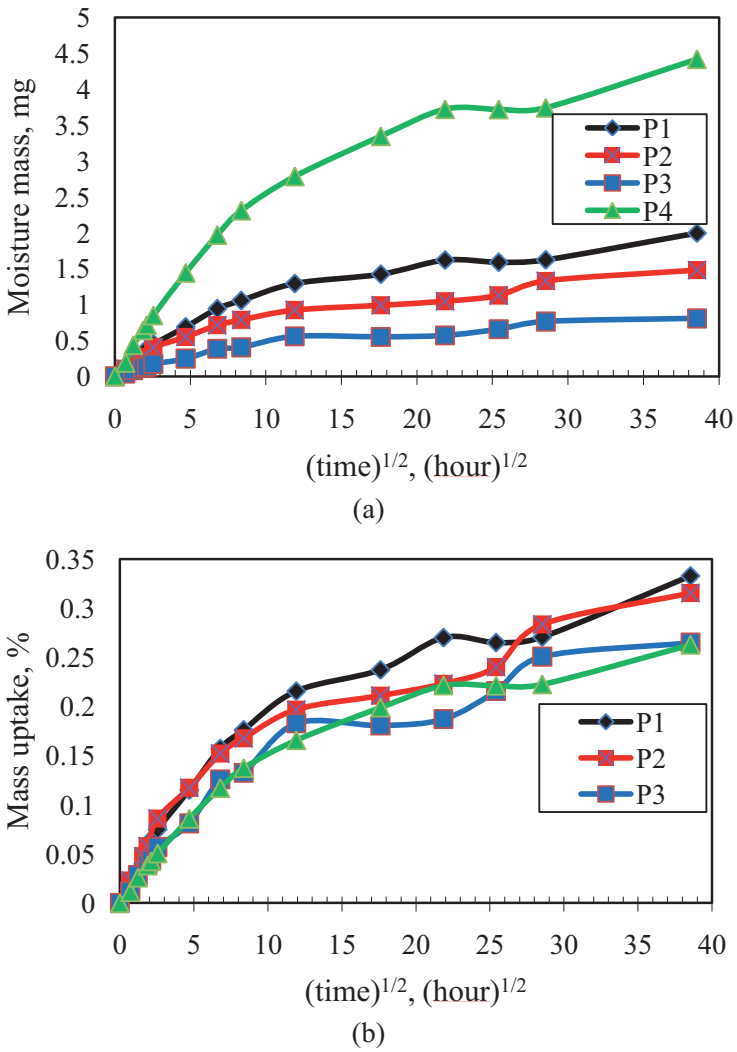

Figure 5.1 Moisture absorption of four plastic IC packages at 85°C/85%RH: a) mass of moisture (mg) in package with square root of time, b) mass uptake (%) with square root of time.

The sorption results shown in Fig 5.1 reveal that the behavior of plastic packages in terms of moisture absorption manifests similar trends. However, the amount of moisture and its diffusion rate depend on the shape and size of the packages and the EMC material used for their encapsulation (*cf.*, Table 5.1). It should be noted that from the moisture curves of these plastic IC packages it is not possible to find the moisture diffusion coefficient exactly, because in order to estimate the diffusion coefficient two prerequisites must be fulfilled. First, the specimen geometry should be so that the moisture diffusion can be assumed almost one-dimensional. This assumption does not hold true for the plastic IC packages due to the diffusion path along all sides of the package.

Second, in order to estimate the diffusion coefficient and the saturation value of the moisture concentration the diffusion path should be only through the bulk material. However, as will be seen in the next sections, the moisture diffusion through the interfaces of the package contributes also to the overall moisture absorption of the plastic IC packages.

From these discussions it can be postulated that a thin bulk specimen is needed in order to find the moisture-related material properties of the polymers exactly. However, there are some important results by comparing the package diffusion with standard bulk EMCs, which will be discussed in the next subsections.

5.2.1 Moisture Diffusion in a Package *vs.* Bulk EMC

Using the same transfer molding process, bulk samples of EMCs (**MC-1** and **MC-2**) were provided by the manufacturers in the form of molded disks of 100 mm diameter and 2 mm thickness. Their moisture uptake was also measured using the method described above. Fig. 5.2 shows the moisture uptake curve of a plastic package compared to the moisture uptake curve of the bulk epoxy molding compound used in that package.

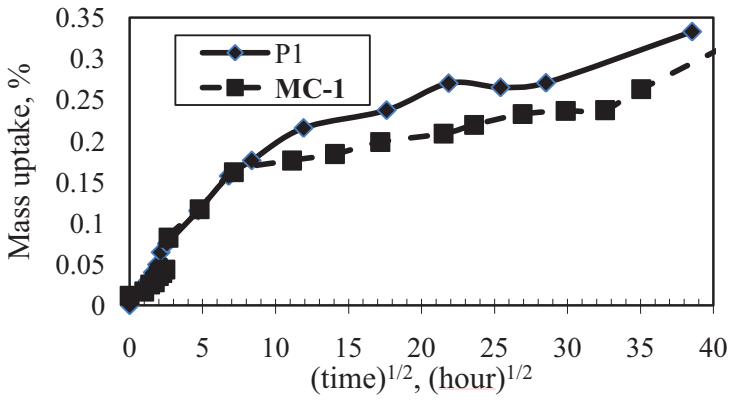

(a)

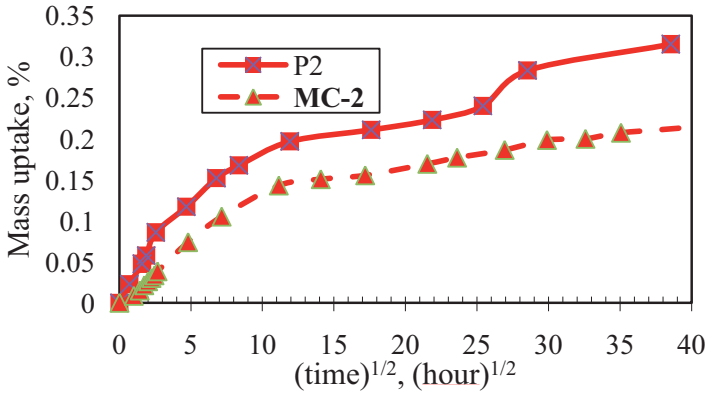

(b)

Figure 5.2 Moisture absorption of a plastic IC package compared to its bulk EMC: (a) P1 *vs*. MC-1, (b) P2 *vs*. MC-2.

The results of Fig. 5.2 suggest that the plastic packages and their respective bulk EMCs manifest similar behavior in terms of moisture absorption. For both IC package and bulk EMC, a linear part of moisture absorption curve at the early stages of sorption is followed by a slight plateau and finally a second linear phase. However, there are some differences between a plastic package and its bulk EMC in terms of the diffusion rates, which suggest that for plastic packages additional mechanisms may exist which are explained in the following sections.

5.2.2 Interfacial Moisture Diffusion

From Figs. 5.2a and 5.2b, it can be postulated that the diffusion of moisture in both packages is faster than that of the corresponding bulk molding compounds. This can be attributed to the three-dimensional nature of diffusion in the package and also to a higher diffusion rate through the leads / EMC interfaces, while for the thin plates, the diffusion is almost one-dimensional.

A review of the diffusion rates available in the literature reveals that, in general, the diffusion rate along the interface of adhesive/substrate is faster than that of the bulk adhesive and it becomes more critical to the lifetime of the adhesive joints as the strength of the interface decreases. Vine *et al*. (2001) studied the moisture uptake of an epoxy bonded to aluminum substrates with various surface treatments. They observed faster diffusion in three-layer sandwich specimens than predicted based on mass-uptake experiments performed on bulk diffusion specimens. They attributed this behavior to the presence of micro-cavities in the adhesive layer.

Davis *et al*. (2000) utilized the technique of electrochemical impedance spectroscopy and investigated epoxies bonded to aluminum with various surface preparations that resulted in either a weak or strong interface and observed that the rate of crack growth was slower for strong interfaces. However, for weak interfaces crack growth was detected almost immediately as moisture appeared at the interface and resulted in a fast rate of crack growth. Zanni *et al.* (1993) compared the calculated diffusion rates between non-bonded adhesive specimens and bonded adhesive joints. They observed that the interfacial diffusion coefficient was greater than of bulk adhesives and hypothesized the phenomenon of “capillary diffusion”, where the higher surface energy of the dry adhesive effectively pulls moisture along the interface. They used Fickian diffusion to measure water diffusion into bonded joints and related enhanced rates of moisture ingress to water diffusion occurring rapidly in the interface region.

These examples all suggest that the diffusion of water into the adhesive joints is not a simple process and may involve several pathways for the moisture ingress, dependent on the system chemistry and the interfacial morphology.

5.2.3 Moisture Accommodation at Interfaces

An important observation in Fig. 5.2 is the higher amount of maximum moisture content in a package compared to its corresponding bulk molding compound. This difference can be attributed to the accommodation of water molecules at the interfaces between molding compound and the leadframe. This hypothesis is supported by the study of Chan *et al.* (2007) who performed

Fourier Transform Infrared Spectroscopy (FTIR-MIR) technique measurements that showed the maximum moisture concentration at an interface is higher than that at the saturation state of a bulk molding compound.

There are many other evidences in the literature on the accumulation of water at the interfaces. Buchwalter (1996) suggested that for weak interfaces, where secondary bonds forces dominate the adhesion, failure occurs almost immediately as water contacts the interface. O'Brien (2003) suggested that it is possible for the water to be present in the bulk and interface of the adhesive, yet the integrity of the adhesive bond can be preserved if the interface is strong. This is the case where covalent bonds are present. For strong interfaces, the role of interfacial diffusion becomes less important and the rate-limiting step for failure becomes the chemical reaction at the interface.

Wu *et al*. (1995) used neutron scattering by D_2O to show high concentration of water at polyimide interfaces. They showed that the concentration of water at interfaces without adhesion promoters was significantly higher than with. Nguyen *et al.* (1995) used infrared spectroscopy to measure the accumulation of water at an epoxy / SiO_2 interface and correlated it to weakened adhesion. They detected significant diffusion at the interface for poorly adhered adhesive systems where adhesion forces are governed by secondary interactions. Bowden and Throssell (1951) found that on aluminum, iron, and SiO_2 surfaces, the layer can be up to 20 molecular layers thick at ambient temperatures and humidity. Takahashi (1990) used AC impedance spectroscopy to show that at a relative humidity of 80% the interfacial capacitance increased abruptly, suggesting the formation of water clusters in the bulk and at the interfacial regions.

Another possible reason for a slightly higher amount of moisture content in plastic packages compared to that of bulk molding compounds may be the presence of residual stresses in packages which cause some nano-scale damages along the interfaces. Buchwalter (1996) studied the effect of applied stresses on the moisture-induced damage at interfaces of a plastic package and used a wedge test to load the adhesive bonds externally and concluded that mechanical stresses can work in concert with moisture to cause interfacial damage other than that caused by moisture alone.

Since there are many uncertainties if a package is used for the understanding of moisture diffusion in EMCs, the rest of this work will focus on moisture absorption of bulk molding compounds. **MC-1**, which is a commercial molding compound, will be used further for a systematic investigation of moisture absorption and desorption in EMCs. Moreover, other samples required for the characterization of hygroscopic swelling and interfacial adhesion are produced from the material **MC-1**.

5.3 Fickian Model of Moisture Diffusion

Diffusion of water in polymers has been widely investigated and for most cases the rate of diffusion has been assumed to be constant (Fickian diffusion). Fick's second law can be applied to describe the moisture diffusion process in many polymeric materials as (Shen, 1976)

$$\frac{\partial C}{\partial t} = \nabla \cdot (D \nabla C), \tag{5.2}$$

where D [mm^2/s] is the diffusion coefficient, C [g/mm^3] is the moisture concentration, t [s] is the time and x [mm] refers to Cartesian coordinates. For isotropic materials with a constant diffusion coefficient, Fick's second law can be simplified to

$$\frac{\partial C}{\partial t} = D\left(\frac{\partial^2 C}{\partial x^2} + \frac{\partial^2 C}{\partial y^2} + \frac{\partial^2 C}{\partial z^2}\right). \tag{5.3}$$

If the one-dimensional case of an infinite plate of thickness l with appropriate boundary conditions is considered, the analytical solution, giving the temporal and spatial moisture concentration, C, at time t and distance x from the mid-plane is given by (Shen, 1976):

$$\frac{C_t - C_0}{C_\infty - C_0} = 1 - \frac{4}{\pi}\sum_{n=0}^{\infty}\frac{(-1)^n}{2n+1}\exp\left(\frac{-D(2n+1)^2\pi^2}{4l^2}t\right)\times\cos\left(\frac{(2n+1)\pi}{2l}x\right). \tag{5.4}$$

C_∞ is the maximum equilibrium moisture concentration and C_0 is the initial moisture content, D is the Fickian diffusion coefficient. Since it is not possible to measure the moisture concentration at a point experimentally, the above expression is integrated over the thickness of the bulk film and the fractional mass uptake of the specimen as a function of time becomes:

$$\frac{M_t}{M_\infty} = 1 - \frac{8}{\pi^2}\sum_{n=0}^{\infty}\frac{1}{(2n+1)^2}\exp\left(\frac{-D(2n+1)^2\pi^2}{4l^2}t\right), \tag{5.5}$$

where M_t is the mass of moisture after absorption time t and M_∞ is the mass of saturated sample. If the moisture absorption curve reaches a saturation level, then the saturation value of moisture concentration can be found from $C_\infty = M_{\text{moistue}}/V$, where M_{moistue} is the mass of moisture in the sample and V is the volume of the specimen. Eq. (5.5) implies that the moisture mass of a polymeric sample exposed to a humid environment obeys an asymptotic behavior, for which a saturation state exists. In other words, if two samples with different thicknesses are exposed to a humid environment, the final moisture uptake defined by Eq. (5.5) is the same for both samples; however, the time to reach this maximum value depends on the thickness of the sample as shown in Fig. 5.3.

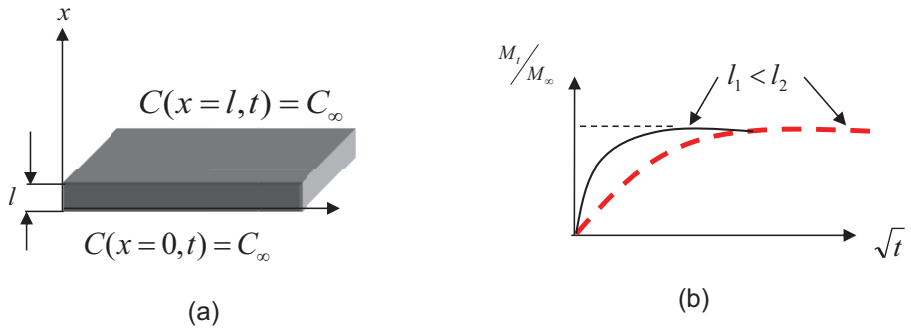

Figure 5.3 One-dimensional Fickian diffusion in a plate.

5.4 Non-Fickian Dual-Stage Moisture Diffusion

As observed in Figs. 5.2a and 5.2b, a state of saturation in moisture absorption cannot be realized even after long-periods of moisture sorption. At the beginning of this study, it was suspected that this phenomenon may be due to the larger thickness of the bulk samples (2 mm). However, further investigations showed similar dual-stage moisture absorption curve for all sample geometries which will now be explained.

In order to investigate the role of geometry in the moisture performance of bulk EMCs, two different sample geometries of the material **MC-1** were produced. The sample with thickness 1 mm has a diameter of 50 mm and the sample with thickness 2 mm has a diameter of 100 mm, meaning that for both samples the one-dimensional moisture diffusion can be assumed. Fig. 5.4 shows the percentage of moisture content as a function of $\sqrt{t}/l$, where t is the time of exposure to moisture and l is the thickness of the bulk EMC.

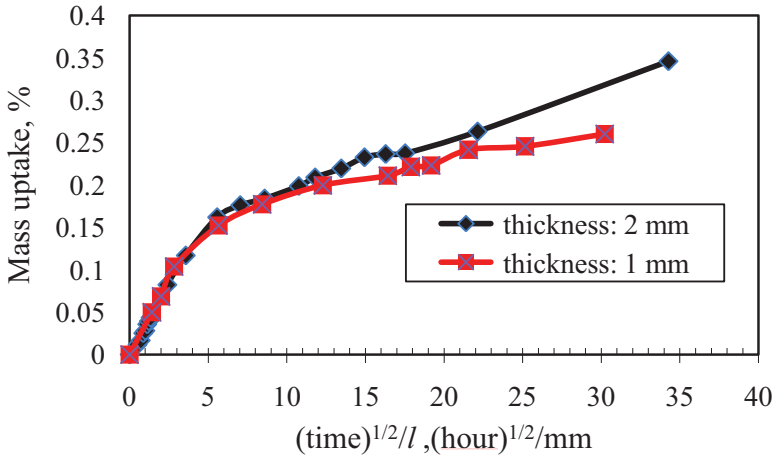

Figure 5.4 Effect of sample thickness on the non-Fickian behavior.

It can be observed that the rate of mass uptake per thickness was the same for both sample geometries at the beginning of the exposure to moisture, which is a typical behavior of Fickian mois-

ture diffusion in polymers. However, after the $\sqrt{t}/l$ ratio of around 13, the curves started to deviate from each other. This ratio corresponds to one week of sorption for the sample with 1 mm thickness and approximately 3-4 weeks for the sample with 2 mm thickness, respectively. This sorption time will be denoted as *quasi-saturation* in this work and will be used as a virtual border between the two phases of the moisture absorption.

It is important to note that in Eq. (5.3) the diffusivity D in Fickian diffusion is assumed to be independent of moisture concentration C. This assumption may not hold true for many polymers and, consequently, Equations (5.3)-(5.5) cannot be used directly for the case of non-Fickian diffusion. A prominent feature of non-Fickian diffusion is that there is no characteristic equilibrium mass uptake. There are various types of non-Fickian moisture absorption reported in literature. Chen and Zhao (2005) reported that the moisture absorption in some molding compounds can be characterized by linearly decreasing diffusivity as a function of average moisture content. However, Celik *et al.* (2007) found that for highly non-Fickian diffusion of some organic substrates a power-law relation between the diffusivity and moisture content exists.

Non-Fickian behavior may be the consequence of a relaxation process in polymer molecules and/or the result of an irreversible reaction between polymer and moisture, such as formation of hydrogen bonds. Weitsman (2006) proposed various types of non-Fickian moisture absorption and used a combined damage/diffusion model to interpret the non-Fickian moisture uptake of fiber-reinforced polymeric composites. Loh *et al.* (2005) suggested that non-Fickian diffusion is generally considered to occur when the relaxation of the polymer influences the uptake behavior. Such responses are conventionally divided into two groups. One is known as Class II (Class I being Fickian diffusion) and generally occurs when the relaxation rate controls the uptake. The other group is termed as *anomalous* uptake and generally occurs when diffusion and relaxation have comparable rates. Two-stage or dual-uptake diffusion has been observed in many polymeric materials and is one of the most common types of anomalous moisture uptakes.

It must be noted that the aging at 85°C/85% RH (MSL1) is one of the most severe moisture sensitivity level (MSL) reliability tests condition. Fig. 5.5 shows the moisture absorption curves of the material **MC-1** in two aging conditions. The rate of diffusion and the maximum mass uptake at MSL1 are higher than that at MSL3 condition (30°C/60% RH). The dual-phase moisture absorption can be observed at the MSL1 condition more significantly. However, there seems to be a slight permanent increase in the mass uptake curve at 30°C/60% RH, which suggests that the second phase of moisture absorption may exist even at low temperatures.

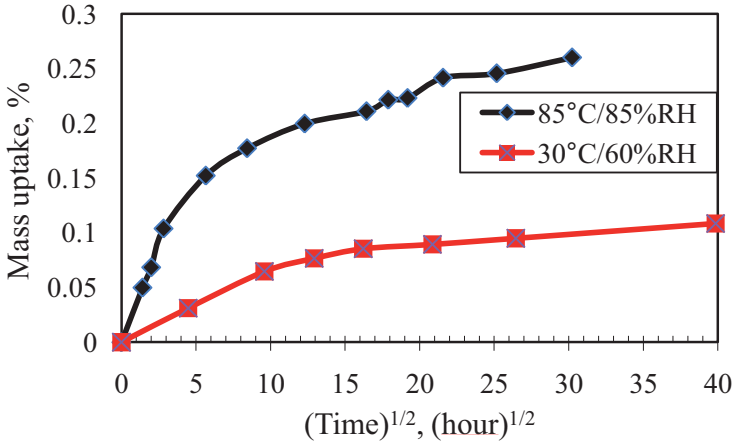

Figure 5.5 Effect of sorption conditions on the non-Fickian behavior.

Another mechanism leading to a non-Fickian behavior of moisture absorption may be swelling of the polymer matrix, which increases the number of active sites available for sorption. Also a chemical degradation of epoxy resins and/or epoxy/filler interface may cause non-Fickian diffusion. In the latter case, Lekatou *et al.* (1997) observed that the water diffusion initially follows the Fickian model, but then the deviations from the ideal behavior are explained by the flow of water molecules along the filler-matrix interface followed by diffusion into the bulk resin and transport of water by microcracks.

Most likely the dual-phase moisture absorption in epoxy molding compounds can be explained with the two mechanisms of absorbing water by polymers. During the early stages of sorption the absorbed molecules reside in the free volumes in the polymer. However, their transfer to a bound state with a different energy level requires overcoming some energy barriers and occurs relatively slowly. Possibly the two bound and unbound mechanisms act simultaneously. However, due to the faster diffusion in free volumes at the beginning of the sorption, the effect of the bonding mechanism can be observed later more clearly, when the first mechanism slows down by reaching its saturation state. In this case, most of the bonded water causes non-Fickian diffusion behavior that typically causes a gradual increase of moisture uptake with time. These statements are supported by the results of desorption tests after various sorption times, which will be discussed in Section 5.5. It will be shown that the non-Fickian behavior during the absorption process is responsible for a non-reversible sorption process. This supports the hypothesis that there is an energy level for the transition from free volume diffusion to molecular bondings.

By using Eq. (5.5), the diffusion coefficient of bulk materials can be found from the slope of the initial linear part of the moisture uptake curve together with the sample weight at saturation state. The initial stage of moisture absorption ($M_t / M_\infty < 0.5$) can be simplified as:

$$\frac{\mathrm{d}}{\mathrm{d}t}\left(\frac{M_t}{M_\infty}\right)=\frac{8D}{l^2}\frac{1}{2}\sum_{n=0}^{\infty}\exp\left(-\frac{(2n+1)^2\pi^2 Dt}{l^2}\right)2$$

$$\approx\frac{8D}{l^2}\frac{1}{2}\int_0^{\infty}\exp\left(-\frac{x^2\pi^2 Dt}{l^2}\right)\mathrm{d}x=\frac{4D}{l^2}\frac{1}{\pi\sqrt{Dt}}\frac{\sqrt{\pi}}{2}=\frac{2}{l}\sqrt{\frac{D}{\pi t}}\,.$$

So the relative moisture content can be simplified as:

$$\frac{M_t}{M_\infty}=4\sqrt{\frac{Dt}{\pi l^2}}\quad . \tag{5.6}$$

However, the problem of moisture diffusion in epoxy molding compounds is that from Figs. 5.4 and 5.5, no specific saturation point can be observed. Hence, an estimate of the diffusion coefficient by using M_∞ in Fick's law is not possible.

In order to investigate the amount of errors caused by applying the Fickian model for the EMC materials various sorption times were considered as saturation levels and the diffusion coefficient found from each level was calculated from the Fickian model. By considering a quasi-saturation level after 168 hours, a first value of diffusion coefficient can be estimated. Using a longer soaking time as saturated level will result in obtaining a smaller Fickian diffusion coefficient. This is repeated for various sorption times until a relation between D and M_∞ can be obtained. After having the corresponding values of D and M_∞, a transient Finite Element (FE) analysis is performed for each pair of data and the average moisture content at the end of diffusion process is calculated. Fig. 5.6 shows the relation between the apparent diffusion coefficients with the average moisture content in the sample. It indicates clearly that the diffusion coefficients of both materials decrease with increasing moisture content.

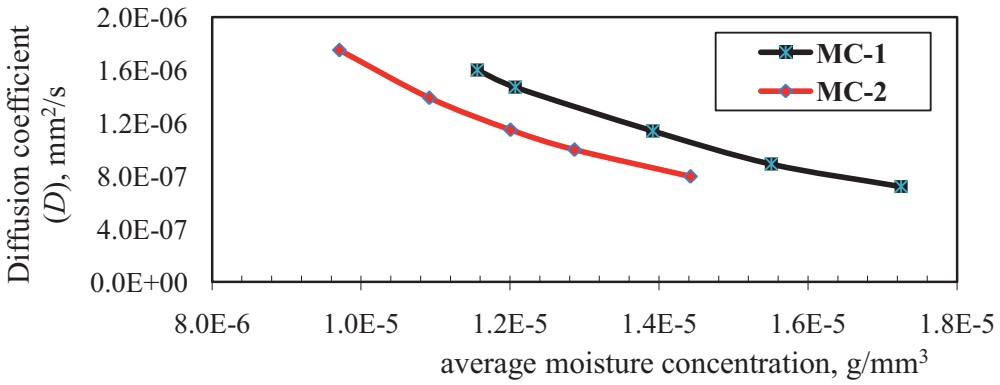

Figure 5.6 Diffusion coefficient of two bulk EMC materials as a function of average moisture content at 85°C/85%RH condition.

In order to compare the Fickian and non-Fickian models of the moisture diffusion in the bulk EMC disk, three-dimensional transient finite element analyses was performed using the thermal-moisture analogy by the simulation tool ANSYS. The dashed lines in Fig. 5.7 show the simula-

tion results of the weight gain process when using the Fickian model and assuming a final saturated level at the end of absorption process (1000 hours sorption at 85°C/85%RH). For this Fickian simulation, D was extracted from the last point in Fig. 5.6 and C_∞ was assumed to be the saturation moisture concentration, which can be found from $C_\infty = M_\infty / V$, V being the specimen's volume.

As shown in Fig.5.7, the Fickian model can only describe the early stages of moisture diffusion correctly. However, the main problem of Fickian model is that it predicts a saturation level and uniform moisture concentration at longer sorption times. This is obviously not true, because as observed earlier, the moisture content increases further and consequently no uniform moisture concentration will be achieved in practice.

In order to model the non-Fickian dual-stage diffusion properties, the following method proposed by the author (Shirangi, 2008) is used: The method is based on the assumption that the dual-stage moisture absorption consists of two diffusion mechanisms. The first mechanism starts directly after exposing the EMC samples to moisture, while the second mechanism starts after a certain time (quasi-saturation). Each of these mechanisms can be modeled using the Fickian diffusion model and the sum of the moisture content of each mechanism will give the total diffusion results. In other words, a first Fickian diffusion with the diffusion coefficient D_1 and saturated content level of $C_{1\infty}$ is followed by a second Fickian (with diffusion coefficient D_2 and saturation content level $C_{2\infty} = C_\infty - C_{1\infty}$) after a specific time (quasi-saturation found from experiment). Three independent variables (D_1, D_2 and $C_{1\infty}$) can be found by using a least mean-square approach to produce the best fit to the experimental curve. The Fickian (D and C_∞) and non-Fickian (D_1, D_2 and $C_{1\infty}$) diffusion parameters are listed in Table 5.2.

Table 5.5.2 Fickian and non-Fickian absorption parameters.

	Fickian diffusion model		Non-Fickian dual-stage diffusion model		
	D mm^2/s	C_∞ g/mm^3	D_1 mm^2/s	D_2 mm^2/s	$C_{1\infty}$ g/mm^3
MC-1	0.7e-6	5.4e-6	1.9e-6	1.5e-6	3.7e-6
MC-2	0.8e-6	4.5e-6	2.3e-6	1.2e-6	3.1e-6

The moisture mass gain results from the non-Fickian dual-stage model proposed in this section are also shown in Fig. 5.7. The results suggest that the non-Fickian model that is composed of two parallel Fickian diffusions can be used to obtain the mass uptake of the molding compounds quite exactly.

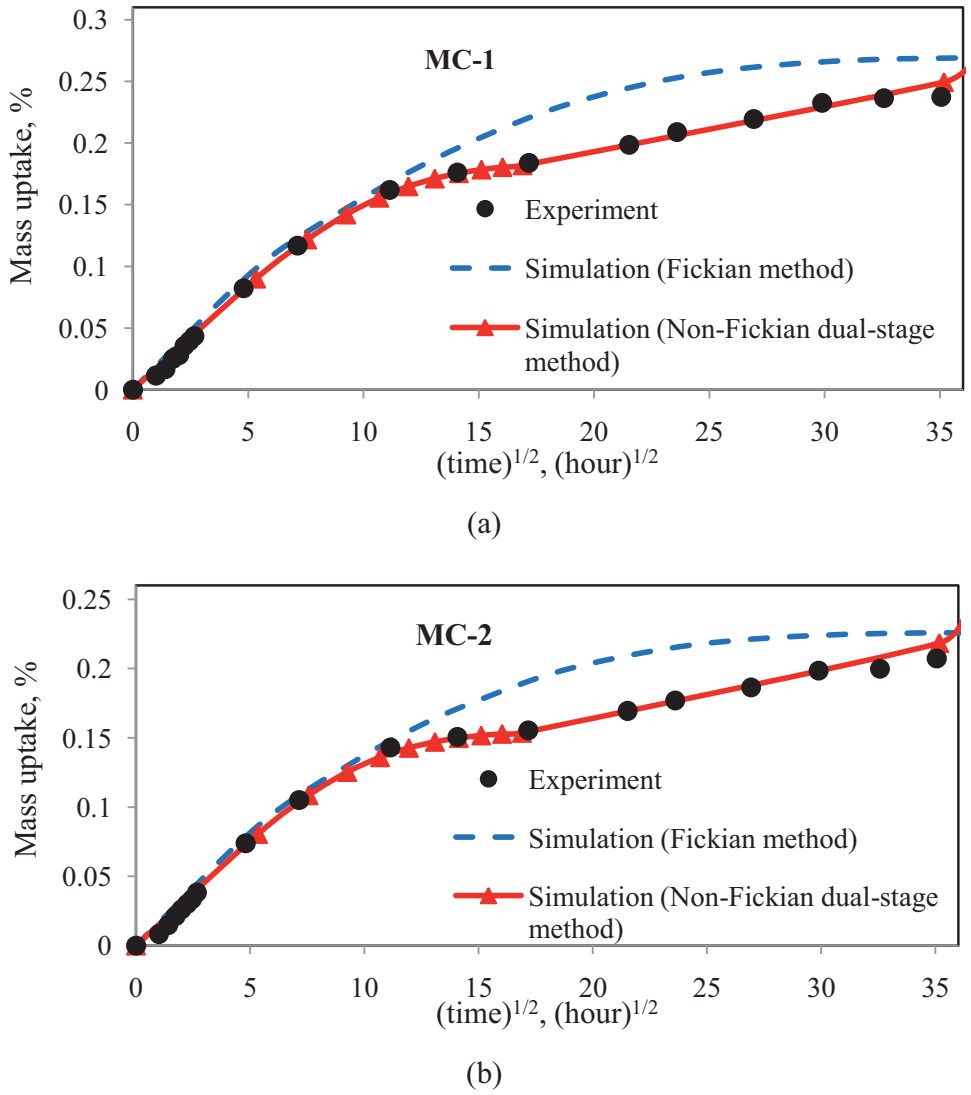

Figure 5.7 Comparison of the Fickian and non-Fickian simulation of the moisture absorption with the experimental data. (a) **MC-1**, (b) **MC-2**.

The fitting parameters D_1, D_2 and $C_{1\infty}$ are so far used to get the best fit of the experimental results. However, they could be used for investigating the dual-stage moisture diffusion and interpret different mechanisms. As stated earlier, there are at least two major active mechanisms during the moisture absorption of the EMC materials. The first mechanism involves the diffusion of moisture via free volumes of the polymer matrix or polymer/Silica interfaces. This mechanism can be described by using the Fickian model with the diffusion coefficient of D_1 and the saturation level of $C_{1\infty}$. In many polymeric materials this is the only mechanism available and, consequently, the moisture absorption curves reach a plateau. In the case of epoxy molding compounds a second mechanism of the moisture absorption is also available. This mechanism involves a hydrogen bonding between the water molecules and the polymer matrix and can be de-

scribed by the diffusion coefficient of D_2 and the saturation level of $C_{2\infty}$. This mechanism seems to start after the first mechanism reaches its saturation level and manifests a linear relation between the moisture concentration and the exposure time.

5.5 Moisture Desorption

Moisture desorption in epoxy molding compounds happens primarily during reflow processes, where the most severe reliability problems are observed. Moreover, it is important to understand the mechanism of moisture desorption, since during the assembly of PEMs, the packages undergo baking to remove moisture and thus reduce the probability of moisture induced failures such as popcorn cracking and interfacial delamination.

Experiments on the moisture desorption behavior of the plastic packages listed in Table 5.1 were performed at various temperatures. The packages investigated in this study were stored in an unprotected environment before the sorption tests and thus initially contained moisture due to long-period storage in air. The plastic parts were first baked at 125°C for 24 hours to remove the initial moisture content. The weight after baking was considered as the dry weight. However, results found from desorption curves of the packages and also from desorption of bulk EMCs revealed that the condition of 125°C baking for 24 hours may not fully remove all of the moisture content. After baking, the packages (3 packages for each test category) were placed in a moisture chamber at 85°C/85% RH for a sorption time of 168 hours. Afterwards, the desorption experiments were performed in four infrared chambers at four baking temperatures, namely 75°C, 110°C, 160°C, and 220°C. Since the glass transition temperature of the EMCs used in the packages range from 95°C to 130°C, the aim was thus to run the desorption experiments at two temperatures below and two temperatures above the glass transition temperature. The desorption period (baking time) was chosen to be 96 hours for baking at 75°C, 70 hours for baking at 110°C, 48 hours for baking at 160°C and 4 hours at 220°C, respectively. The weight measurements of the plastic parts were performed periodically by removing the parts from the oven and measuring their weight at room temperatures similar to the procedure explained in Section 5.2. Figs. 5.8a-5.8d show the temperature dependent desorption results of the packages P1-P4, respectively.

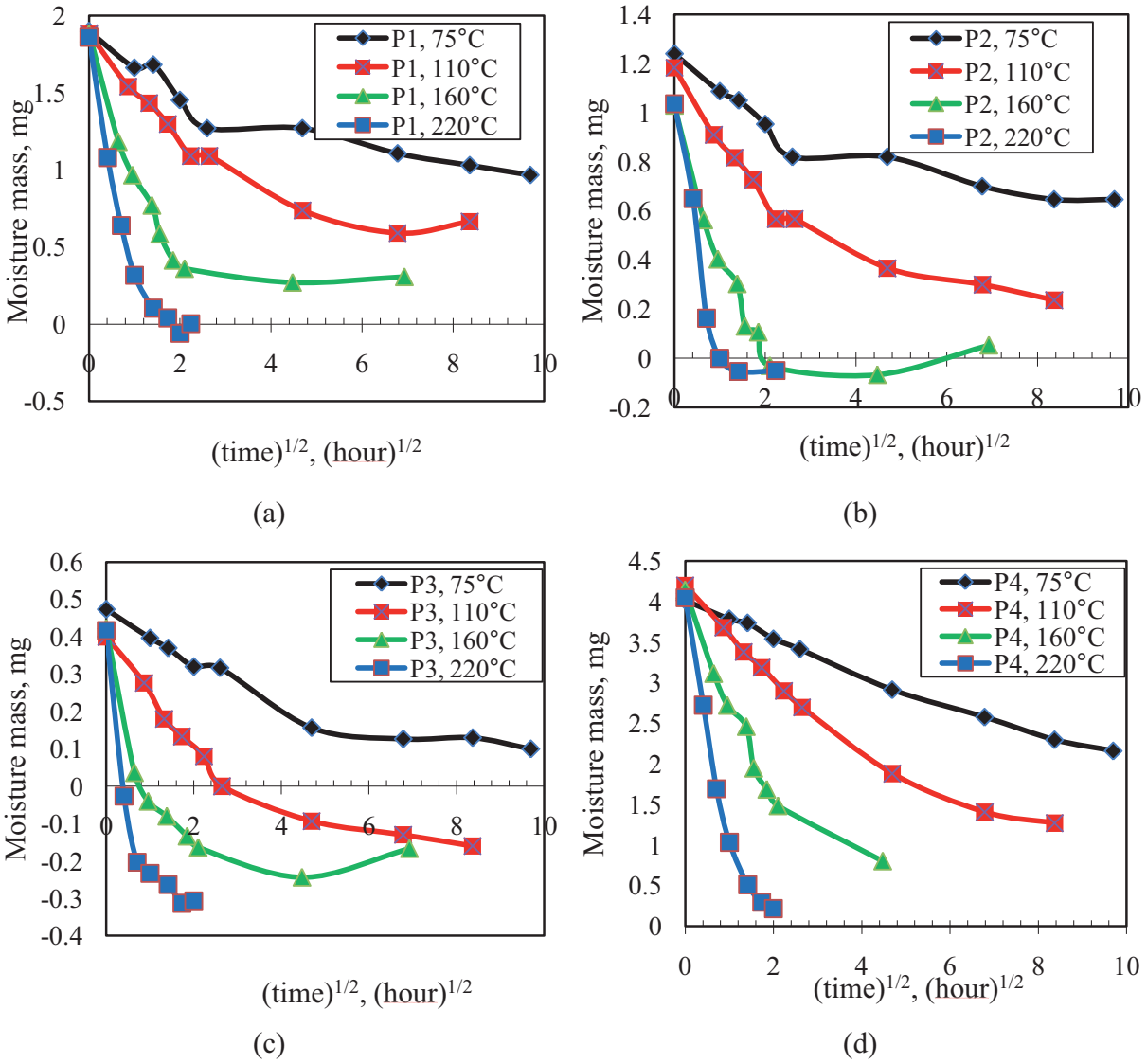

Figure 5.8 Moisture desorption of four types of plastic IC packages at various temperatures: (a) MO-188, (b) SOIC-24, (c) SOIC-16, and (d) PLCC-44.

The results of Fig. 5.8 indicate that for all packages studied, the baking condition at 75°C cannot lead to a complete removal of moisture content. Even baking at 110°C seems to be inappropriate for the removal of moisture from the packages. Interestingly, for the package P3, which is the smallest amongst the packages, the final weight of the sample at the end of bake-out was lower than the apparent initial dry weight, which explains why the moisture mass in Fig. 5.8c was a negative value at longer baking times. This can arise from two possible reasons. The first reason may be the out-gassing of the polymer during the baking condition. This assumption proved not to hold true due to the results found from Thermal Gravimetric Analyzer (TGA) measurements of dry bulk EMC samples that showed insignificant out-gassing even at 220°C. The second reason is that, principally, the assumption of gaining a dry package upon 24 hours baking at 125°C

might have been wrong. In other words, plastic packages that have been stored in humid environments for a long time may still contain some moisture after this standard baking condition. It seems that this baking condition did not lead to a complete removal of the moisture content and the apparent dry samples contained moisture in reality. It appears to be difficult to understand the mechanism of moisture desorption from the results of baking of plastic IC packages, because other phenomena like interfacial diffusion and moisture accumulation may lead to a misinterpretation of the desorption results. That is why standard bulk samples were used later to understand the intrinsic mechanism of moisture desorption.

5.5.1.1 Moisture Desorption of bulk EMC Disks

Epoxy molding compounds, similar to other polymeric materials, lose their moisture content when they are exposed to dry environments at high temperatures. However, for plastic packages, it was observed that not all of the moisture may escape even upon exposure to high temperature. In this section a systematic approach is presented in order to find out at which state of the moisture absorption the formation of the *residual moisture content* may take place. Samples of bulk EMC (both geometries with 1 and 2 mm thickness of the material **MC-1** presented earlier in Section 5.2) were placed in humid conditions (85°C/85% RH). Some samples were removed after 2 weeks sorption while the others were removed after 4 weeks. After the removal from the moisture chamber, the weights of samples were measured and then they were placed in a dry infrared oven for subsequent baking. Their weight during the baking process was also measured by removing them from the dry chamber, letting them cool down to room temperature and measuring the weight by an electronic scale. Figs. 5.9a and 5.9b illustrate the weight loss of samples at 110°C and 160°C baking temperatures, respectively. Higher initial moisture content in these figures indicates that the sample was aged for a longer time in humid condition prior to baking and hence the moisture absorption had reached a higher level (the second absorption phase). This longer aging in a moist environment has a direct influence on the subsequent baking curves. It should be noted that the baking tests were generally performed for longer periods than those indicated in these figures and some fluctuations in desorption curves were observed at longer sorption times.

From these desorption curves the following results can be postulated:

- A complete removal of moisture was not achieved for any of the samples within the time period investigated. Samples with higher initial moisture content show a higher final residual content, suggesting that a longer time of exposure to moisture leads to a higher amount of "non-reversible" moisture content at a certain temperature. Baking at elevated temperatures (*e.g.*, 160°C) leads to more moisture release and a lower amount of residual moisture content. This may mean that for the debonding of hydrogen bounds between water molecules and polymer chains a certain amount of energy is needed, which is not available at lower temperature (*e.g.*, 110°C).

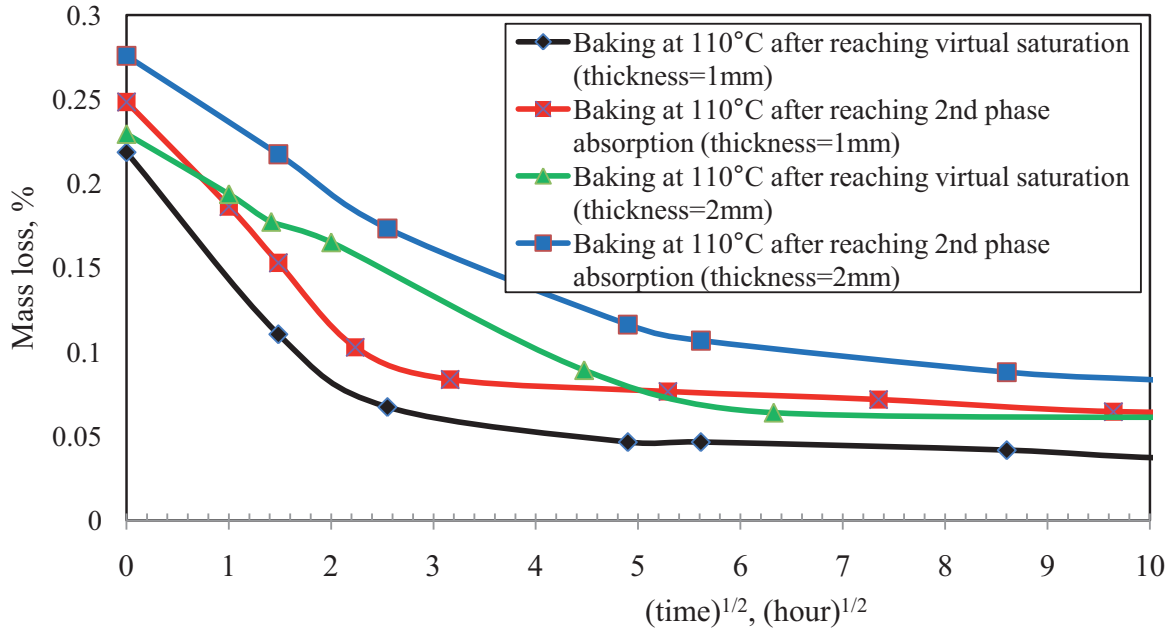

(a)

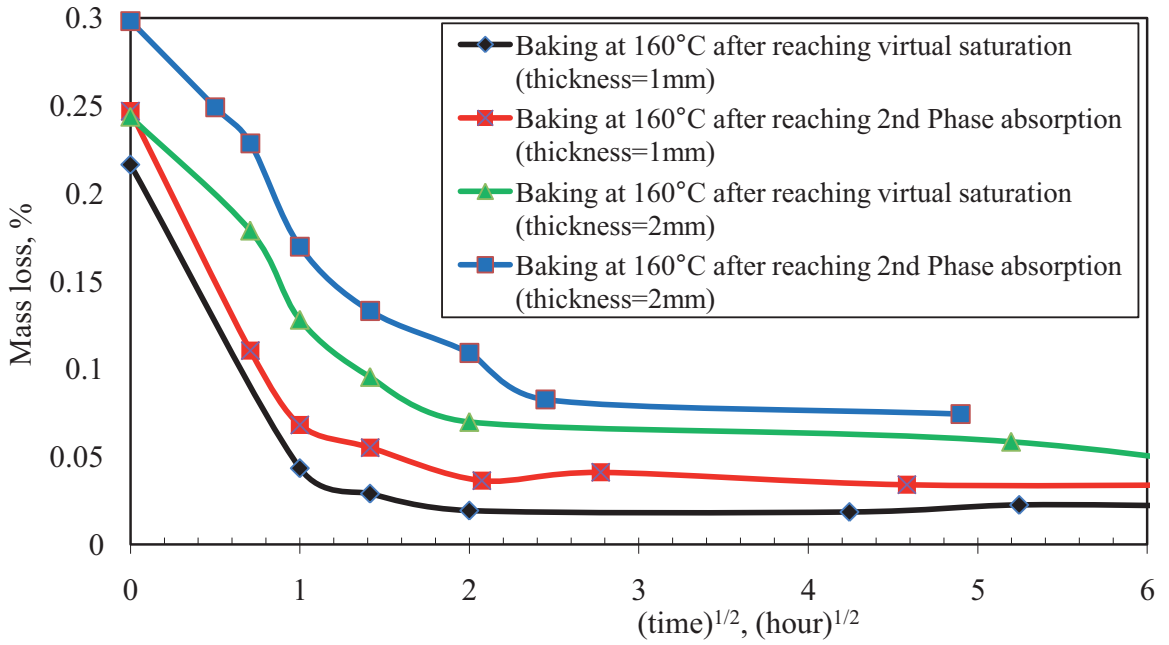

(b)

Figure 5.9 Desorption of the EMC material as function of exposure time to dry environment. (a) Desorption at 110°C. (b) Desorption at 160°C.

- The thicker samples (2 mm thickness) show to retain a higher amount of residual moisture content when compared to the thinner samples (1 mm thickness). This observation seems to be reasonable, since the thicker samples normally need more time to reach a certain amount of mois-

ture content during the moisture absorption. A longer exposure to moisture prior to desorption tests, results in higher amounts of non-reversible hydrogen bounds and consequently a higher value of residual moisture contents upon the subsequent baking process. This suggests that hydrogen bonding is active from the early stages of exposure to moisture; however, its influence is more dominant when the Fickian mechanism decelerates upon reaching a quasi-saturation. It should be reiterated that the quasi-saturation is defined in this study as a virtual border between the first and the second phases of the moisture absorption curve. The term virtual is here used, because if the absorption tests are not long enough and are

- It should be reiterated that the "quasi-saturation" level defined in this study is assumed to be the border between the first and the second phases of the moisture absorption curves. The term "virtual" is here used, because in reality there is no saturation level at the end of the first absorption phase as described earlier in the last sections. The term "virtually dry" state is similarly used for the isothermal baking tests. Since in those samples with long-term sorption history the moisture content cannot be released fully upon the isothermal desorption tests, the remaining amount of moisture is considered as the "residual moisture" content, and the sample is termed as "virtually dry." This is due to the observation that the weight of the samples upon the isothermal desorption tests exceeds their initial dry weight before any moisture preconditioning.
- An interesting observation is the parallel initial linear parts of the desorption curves of the samples with similar thickness values, but with different initial moisture content. For a certain geometry at a constant temperature, the desorption curves of samples with different histories are in parallel. A longer exposure to moisture results in a higher amount of nonreversible absorption mechanism, however, the desorption rate at a constant temperature does not depend on the sorption history and depends only on the baking condition. This means that the nonreversible mechanism arising from the second absorption phase has only influence on the residual moisture content and not on the desorption coefficient.

In order to find the local moisture concentration during the baking of plastic IC devices, such as heating during solder reflow processes, finite element analysis shall be used. The finite element analysis of the moisture desorption using the Fickian model is similar to that of the absorption analysis since both obey the same diffusion equation. However, the boundary conditions are different. For the FE modeling of moisture desorption it is necessary to define in the FE model an initial moisture content for all nodes and zero moisture contents for the surfaces that are exposed to dry condition. However, there are essentially two problems when the Fickian model is used for the analysis of moisture desorption in epoxy molding compounds. First, the initial moisture content is not necessarily uniform, because as stated earlier the moisture absorption did not reach a saturation level and consequently the assumption of uniform moisture content at time zero of the analysis is wrong. Second, the boundary condition for Fickian diffusion implies that the moisture content at the boundaries is zero and the final state of the polymer is dry. This is obviously wrong, because as shown in Figs. 5.9 a,b, the final state of the samples is not dry. In

other words, the Fickian model does not consider the ability of the materials to keep a certain amount of water after a long-term baking. It is worth noting that upon one week baking at 110°C, a residual moisture content of around 40% of the saturated level was observed in the thick samples. The dashed lines in Figs 5.10a,b,c represent the moisture mass data of the desorption process when the Fickian model is applied and show poor agreement with the experimental data, especially at longer bakng times. A simple non-Fickian moisture desorption model is suggested in this work, which can solve this problem with conventional FE simulation tools.

The proposed non-Fickian desorption model is based on the assumption that the non-Fickian desorption behavior of epoxy molding compounds consists of two mechanisms. One mechanism is conventional Fickian desorption that occurs in most polymers and leads to a fully dry system if adequate time is given. The other mechanism is a competing mechanism that does not allow for a fully removal of moisture content and is responsible for the presence of the residual moisture content. In other words, in order to model the overall behavior of the moisture desorption, two parallel diffusion simulations are performed. The first one is a desorption process with the diffusion coefficient D_1 with boundary conditions similar to a Fickian desorption (initial nodal moisture concentration of all nodes being $C = C_\infty$ and applying $C = 0$ on the external surfaces of the model). The second one is a parallel absorption process of an originally dry sample with the diffusion coefficient D_2 and the boundary conditions being $C = C_{\text{residual}}$ on the external surfaces of the model. The nodal moisture concentration at each specific time of the first analysis should be added to that at the corresponding time of the second analysis. The results are a non-Fickian moisture desorption with the controlled desorption coefficient and, more importantly, with the residual moisture concentration C_{residual}.

The residual moisture content can be simply found from experimental data by calculating the residual moisture concentration from $C_{\text{residual}} = M_{\text{residual}} / V$, where M_{residual} is the residual moisture mass in the sample at the end of desorption process and V is the volume of the sample.

The parameters D_1 and D_2 can be found by fitting the results to the experimental curve, similar to the approach described in the previous section. Table 5.3 summarizes the fitted parameters of the non-Fickian model and compares them with the values of Fickian desorption.

Table 5.3 Fickian and non-Fickian desorption parameters.

	Fickian desorption model	**Non-Fickian desorption model**		
T (°C)	D mm^2/s	D_1 mm^2/s	D_2 mm^2/s	C_{residual} g/mm^3
110	0.7e-6	3.5e-6	5.5e-6	2.2e-6
160	2.5e-5	8.5e-5	8.5e-5	1.5e-6
220	15.5e-5	20e-5	19e-5	0.6e-6

The non-Fickian desorption model is compared with both experimental data and Fickian model in Fig. 5.10. As observed, the proposed model can describe the behavior of the epoxy molding compounds quite well.

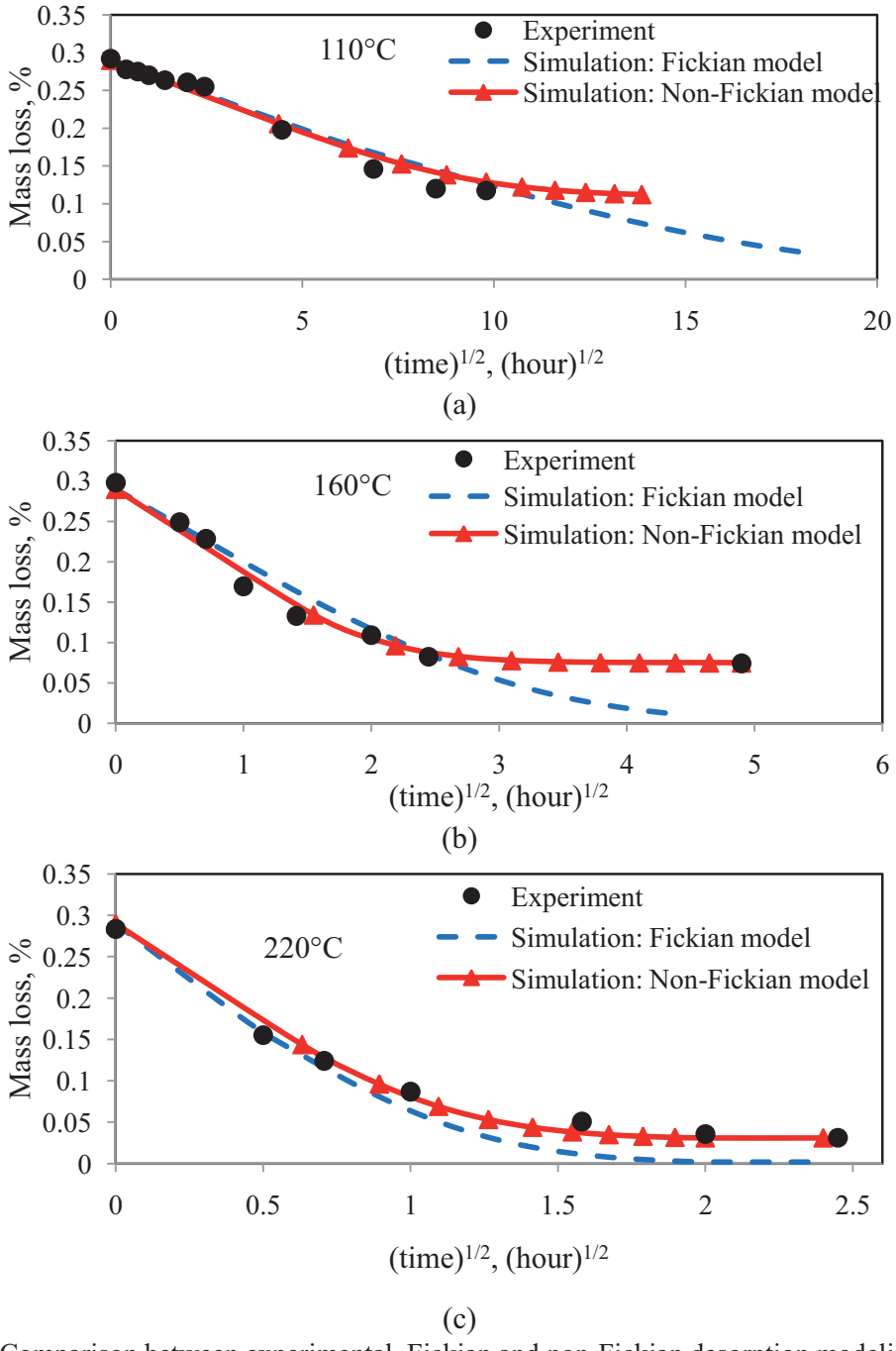

Figure 5.10 Comparison between experimental, Fickian and non-Fickian desorption modeling of the EMC material (a): 110°C, (b):160°C, (c): 220°C.

It must be mentioned that the desorption experiments were performed in an infrared oven, with possibly some humidity in the air. Some of the residual moisture content in the materials could

be the result of a competing parallel absorption due to the moisture available in the air. Another source of error arises from a short time needed for the weighing of the specimens after they are removed from the oven. Since the electronic balance scale is sensitive to the heat, a time of approximately 5 minutes is needed, so that the hot samples reach room temperature. Within this time some moisture uptake from the atmosphere is possible.

In contrast to the results presented in this section there are some other studies that suggest a complete removal of moisture content upon baking. He and Fan (2007) performed in-situ measurements of moisture absorption/desorption on thin film Bismaleimide-triazine resin/glass fiber laminates and observed repeatable moisture absorption. It is possible that in these cases only the first phase of moisture absorption was activated within the time period of the recycled test.

Assuming Fickian desorption, the desorption coefficient can be estimated from the initial linear part of the experimental data by using Eq. (5.6). The temperature-dependent desorption coefficient of the EMC material **MC-1** is shown in Fig. 5.11. It can be observed that the desorption coefficient fulfills the following equation:

$$D = D_0 \exp(-\frac{\Delta E}{kT}). \tag{5.7}$$

The diffusion coefficient D depends on an initial diffusion constant, D_0, temperature, T, and activation energy, ΔE, where k is Boltzmann's constant. For the sample **MC-1**, the activation energy can be estimated as 0.55 eV.

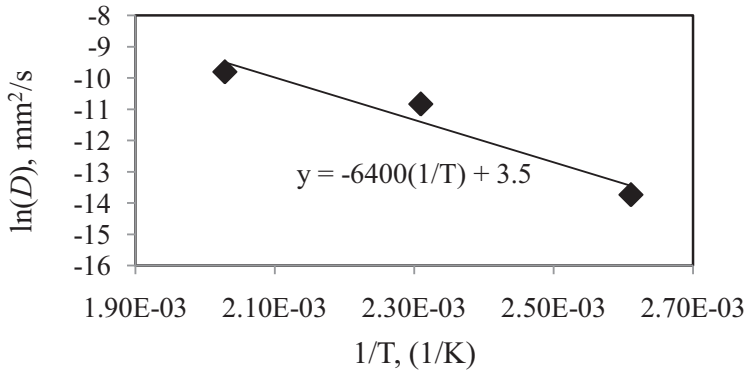

Figure 5.11 Desorption coefficient of the EMC material MC-1 against adverse temperature and calculation of the activation energy.

5.6 Second Run of Absorption (Re-sorption)

The complex mechanism of moisture absorption suggests that a second run of moisture absorption after an absorption/desorption cycle would be even more complicated. In order to achieve logically comparable re-sorption curves, the first run of absorption was stopped after 1 and 2 weeks sorption for thin and thick samples, respectively. This sorption time corresponds to the

time needed to reach the first plateau in sorption curves and will be denoted as "quasi-saturation." After the first sorption, the EMC samples were removed from the humidity chamber and placed in two infrared dry ovens at temperatures of 110°C and 160°C to release their moisture at a constant temperature. After reaching a "virtual dry state" (the final desorbed state in Figs. 5.9a and 5.9b), the samples were placed in the same humidity chamber again for a second run of moisture absorption at 85°C/85% RH. Since the samples had undergone an absorption/desorption cycle, they had an initial moisture content (residual moisture content at the end of desorption) as described in the previous section. This initial content was relatively low, because the absorption was stopped as soon as the samples reached quasi-saturation and before they reach the second diffusion phase, which is responsible for large residual moisture contents. Figs. 5.12a and 5.12b show the comparison between the first run of moisture absorption and the second run after baking at 110°C and 160°C for the thin and thick samples, respectively.

From these curves the following results can be postulated:

- After the desorption at 110°C, the second absorption curve before quasi-saturation was found to be almost identical to the first run for both 1 mm and 2 mm samples. This means the moisture absorption due to the first phase of moisture diffusion is mostly repeatable. The moisture desorption at 110°C happens below the glass transition temperature, at which the relaxation of polymer chains and the change of free volumes are not significant;
- However, the desorption at 160°C affected the second run of moisture absorption significantly. The rate of moisture absorption at the second run was found to be higher than that at the first run. The increase in the rate of moisture uptake can be attributed to the expansion of free volumes in the polymeric materials due to the storage of the material, which was baked at 160°C, well above the glass transition temperature. For the thin samples (Fig. 5.12a) the difference between the first and second runs of moisture absorption is much less than the thicker samples (Fig. 5.12b), because of less exposed time to elevated temperature. Consequently, the formation of new free volumes is less, as this is dependent on the time exposure to high temperatures.

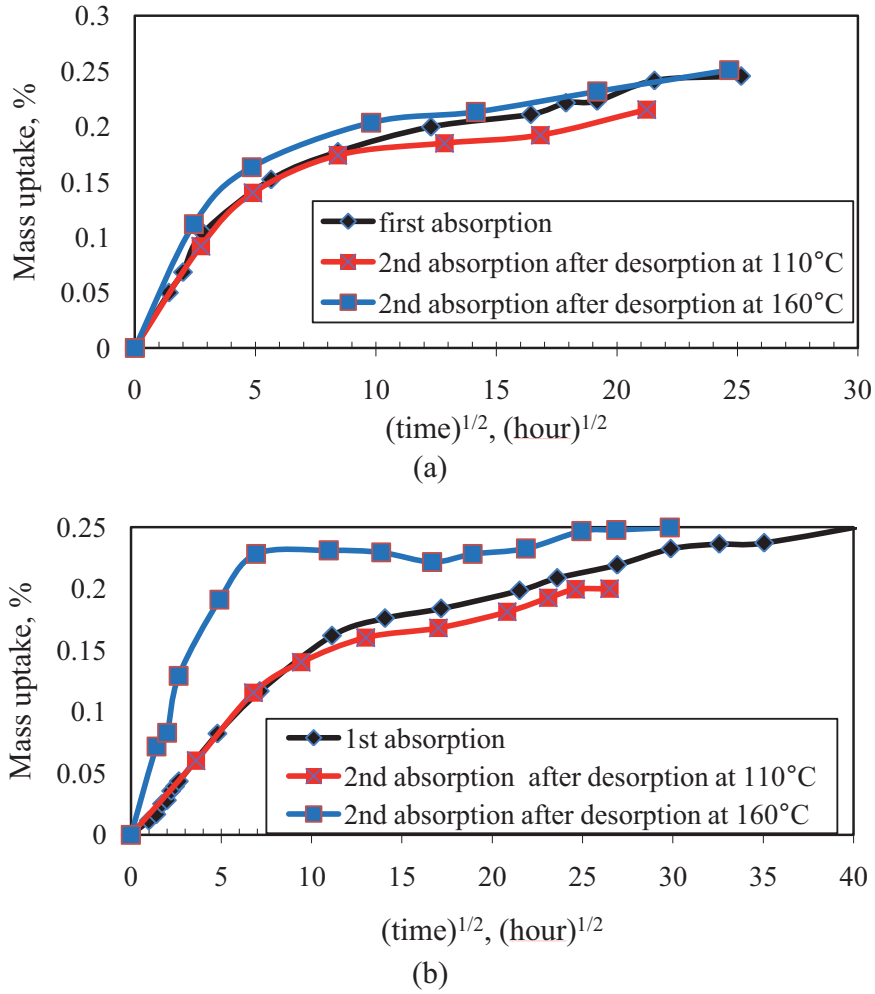

Figure 5.12 Re-sorption experiment of bulk samples after two baking temperatures of 110°C and 160°C (a) thin samples: thickness 1 mm (b) thick samples: thickness 2 mm.

5.7 Conclusions

In this chapter a systematic investigation of absorption and desorption of moisture in epoxy molding compounds was conducted. Absorption of moisture can be explained by an empirical dual-stage non-Fickian behavior. This means that the conventional simulation tools cannot model the diffusion process in epoxy molding compounds correctly and additional consideration is needed for an exact modeling of diffusion behavior. In order to model the moisture diffusion in a plastic IC package correctly, the first step is extracting the non-Fickian material data from the experimental results of standard bulk EMC samples. Fig. 5.13 shows the recommended methodology to model the dual-stage moisture diffusion in plastic IC packages. The left part of this figure is required to find the non-Fickian diffusion parameters. A simple method to verify these parameters is running the proposed non-Fickian FE analysis by using these parameters and comparing the simulation results with the experimental sorption curves. The next step is implement-

ing these parameters and running an FE analysis for IC packages that share the same molding compound. Obviously, experimental sorption curves of the plastic packages can be used to benchmark the FE results.

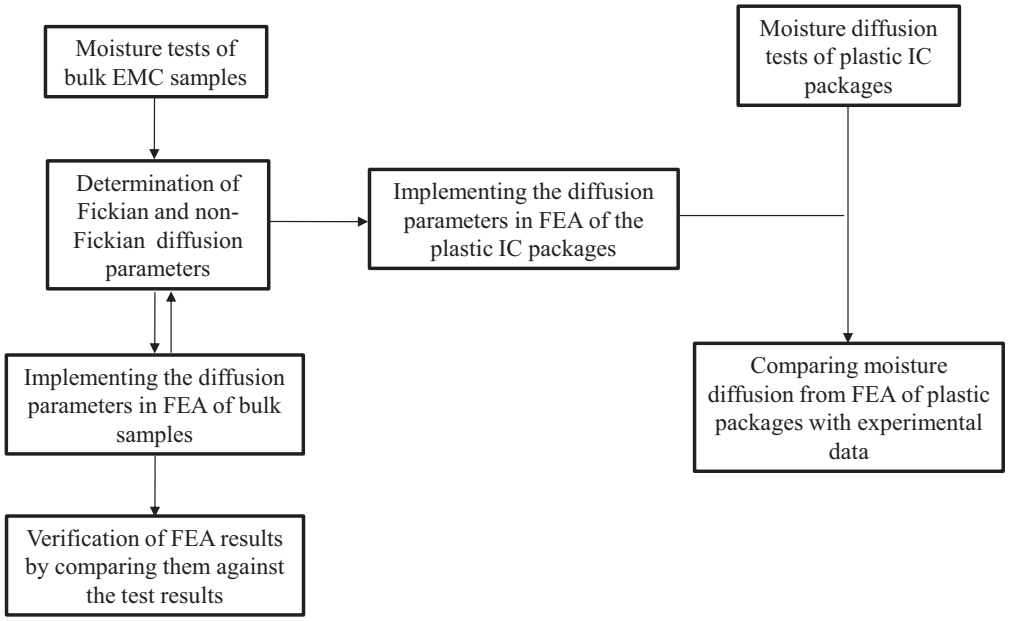

Figure 5.13 Recommended methodology to investigate the non-Fickian diffusion parameters.

When EMC samples are baked to remove their moisture and to reach a dry state, the sorption history prior to baking was found to play an important role in the desorption curves of these materials. The exposure of an EMC sample upon a quasi-saturation (end of the first absorption phase) to a dry environment was found to lead to an almost dry state with only slight residual moisture content at the end. However, a dry state was not achieved when the samples with higher initial moisture content (which were kept in humid environment for a longer time) were baked in dry conditions. A residual moisture content was available upon baking which was a complex function of time, sample geometry and baking temperature. The schematic picture of the influence of sample history may be depicted as shown in Fig. 5.14. Samples which reached point A (quasi-saturation during the absorption process) show lower residual moisture content upon baking when compared to the samples reached point B (a representative point from the second absorption phase). However, the rate of desorption for both cases was the same, indicating that at least two mechanism are active during the diffusion of moisture. One is a reversible mechanism that dominates the diffusion rate. The other is a non-reversible mechanism that is a function of time, temperature and sample geometry.

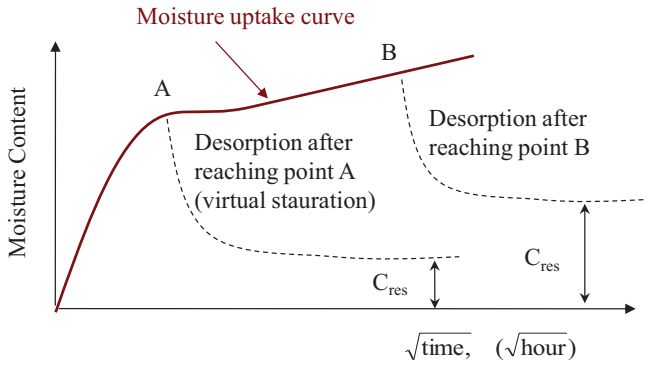

Figure 5.14 Schematic model for the residual moisture content upon desorption of moisture.

The second run of moisture absorption showed also some differences from the first run. The sample sorption history was found to be the dominating factor. The rate of moisture absorption at the second run was found to be higher than that at the first run. The increase in the rate of moisture uptake can be attributed to the formation of new voids in the polymeric materials, which facilitates the transformation of water molecules in the sample. Higher temperatures lead to the formation of more new free volumes. A schematic picture of the effect of sample history on the rate of the second run of moisture absorption may be depicted like the one in Fig. 5.15.

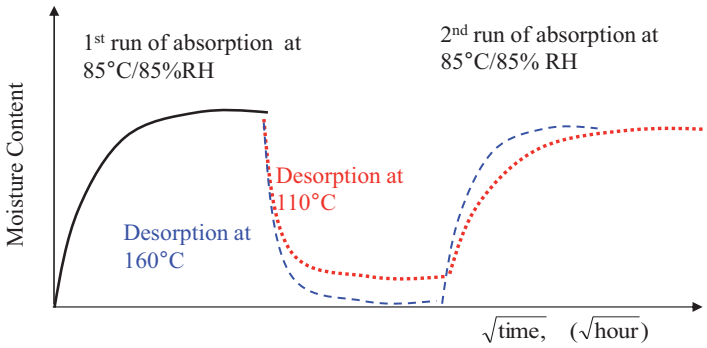

Figure 5.15 Schematic model of the second run of the moisture absorption after an absorption/desorption cycle

Chapter 6 Mechanism of Hygroscopic Swelling in Epoxy Molding Compounds

6.1 Introduction

There are essentially three sources that lead to deflection of polymer/metal systems and formation of residual stresses. The first two mechanisms (cure and thermal strains) were explained in Chapter 4. The main objective of this chapter is to provide conceptual understandings of the mechanism of moisture-induced volumetric expansion of molding compounds. This phenomenon is known as hygroscopic swelling and is responsible for an additional mismatch between epoxy molding compound and other package materials.

The hygroscopic strain is similar to the thermal strains. However, one should take two essential differences between these two into consideration. The first difference arises from the relatively lower value of the moisture diffusion coefficient in polymers when compared to thermal diffusion coefficient. This leads usually to a non-uniform moisture concentration state in the EMC of the package, while, in case of very thin IC packages, the temperature distribution in the packages reaches a uniform state much faster. This means that the thermal stresses of very thin devices arise mainly from the CTE-mismatch of the materials and to a less extent from the temperature gradients inside the package. However, hygroscopic stresses usually arise not only from a mismatch in coefficient of hygroscopic swelling of the materials, but also from gradients in moisture distribution inside a polymeric material. This non-uniform moisture concentration causes that different locations of the EMC swell differently, because the swelling is proportional to the amount of the local moisture concentration. In other words, those EMC molecules that are first affected by moisture will swell and cause hygroscopic strains while other dry molecules will not. The second difference between thermal and hygroscopic strains is that essentially the nonorganic materials, such as leadframes, are impermeable to moisture. This means that while the epoxy molding compound in a package increases its volume due to moisture absorption, the copper leadframe is not affected by moisture and preserves its dimensions. This makes the deflection due to moisture absorption to be more pronounced.

Water molecules in polymeric materials have been identified to have two distinct states. "Free" or "unbound" state of water is attributed to water molecules that are present in voids and nano-pores of the material (Fan *et al.*, 2005, 2008a,b, O'Brien, 2003, Dermitzaki *et al.*, 2008) and can easily move through the free volumes of polymer. Another state is formed by water molecules that disrupt interchain polymer ties, which are called "bonded" water molecules. The "bound" water molecules may react with the polymer chains via hydrogen bonding. It is believed that only the bonded water molecules contribute to the hygroscopic swelling of the polymers and the water molecules in free polymer volumes do not change the volume of the polymer. This identification is further supported by measurement of the ratio of hygroscopic volume expansion to the volume of absorbed water which is less than unity (Ardebili *et al.*, 2003), indicating that some of the absorbed water does not contribute to swelling. The hygroscopic mismatch strain at the interfaces between molding compounds and metallic components in a package could be as important as the thermal mismatch strains (Stellrecht *et al.*, 2004, Ardebili *et al.*, 2003, Shi *et al.*, 2008).

In order to recognize the impact of the hygroscopic swelling on the overall shape of plastic packages, the surface topography of a package was investigated. The measurements were performed via an FRT MicroProf with a chromatic sensor (CWL). Fig. 6.1 shows the out-of-plane shape of a TQFP-epad package which uses the molding compound **MC-1** introduced in previous sections. The surface topography of a dry package at room temperature is shown in Fig. 6.1a. The sample was then placed in a humidity chamber at 85°C/85%RH for 168 hours (MSL1). After sorption the sample was removed from the humidity chamber and exposed to ambient temperature. Upon cooling to room temperature, the warpage was again measured as shown in Fig. 6.1b. By comparing the warpage of a dry and a moisture preconditioned package, it becomes clear that the hygroscopic swelling of EMCs alters the overall stress balance in plastic packages. The warpage direction of the package changed from a "smiling" shape to "crying" after moisture preconditioning. When the packages absorb moisture, the hygroscopic swelling of the EMC affects the warpage direction of the package by introducing the moisture-induced expansion to the epoxy molding compound.

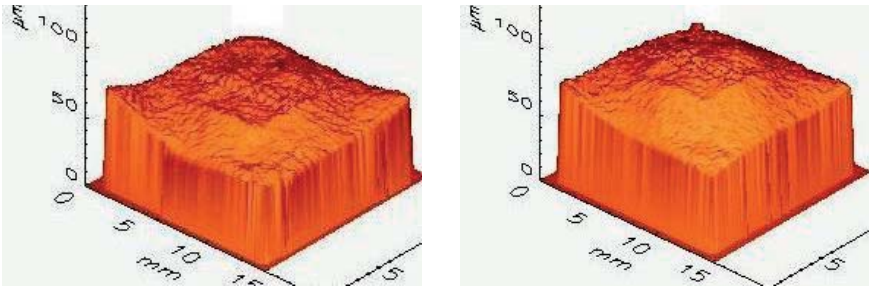

a) b)

Figure 6.1 Topography of the upper surface of a TQFP-epad package: (a) Dry package at room temperature. (b) The same package at room temperature after 168 hours aging at 85°C/85%RH.

The amount of hygroscopic strain found from dimensional change is normally assumed to be linearly proportional to the moisture concentration as (Wong *et al*., 2000)

$$\varepsilon^{h} = \beta C \tag{6.1}$$

where ε_h is the hygroscopic strain, β [mm^3/g] is the Coefficient of Hygroscopic Swelling (CHS) and C [g/mm^3] is the moisture concentration.

There has been a long debate and some discrepancy between the different studies over a suitable method in order to find the coefficient of hygroscopic swelling (Ardebili *et al.*, 2003, Stellrecht *et al.*, 2004, Zhou *et al*., 2005 and 2006, Shi *et al.*, 2008). The aim of all these works is finding the hygroscopic swelling strain and relating it to the local moisture concentration. The next sections of this study provide useful information about the direct effect of hygroscopic swelling by measuring the deflection of the specially designed bimaterial beams and comparing the results with those found from a well-established characterization method, namely the TMA/TGA approach.

6.2 Characterization of CHS by Warpage Measurement of Bimaterial Beams

Since the direct impact of the hygroscopic swelling is affecting the warpage of the plastic packages, a simple way of understanding this effect is investigating the warpage change of a bimaterial system. To do this, bimaterial beams of Cu/EMC with two different EMC thicknesses were designed and manufactured as shown in Figs. 6.2a and 6.2d. These samples will be also used in Chapter 9 for the characterization of interfacial fracture toughness between EMC and the copper leadframe. The sample fabrication was described in Chapter 4, where these samples were used to determine the cure shrinkage of the EMC materials during the polymerization.

Figs. 6.2b and 6.2e show the warpage of thin and thick beams in dry state, respectively. This warpage arises from the cure shrinkage of EMC during the sample fabrication and the CTE-mismatch between the EMC and copper leadframe during cooling to room temperature as discussed in Chapter 4. After fabrication of the samples and measurement of their warpage at room temperature, they were placed in a humidity chamber at 85°C/85% RH and were removed periodically from the moisture chamber, their warpage was measured each time at room temperature and then they were placed in the humidity chamber for further sorption. During the moisture absorption, the warpage of the thin samples (with an EMC thickness of 0.6 mm) changed from concave to convex shape (see Figs. 6.2b and 6.2c). The convex shape increased and reached a constant value of approximately 185 micrometers after 1 week of sorption. Further exposure to moisture did not affect the warpage significantly. The thicker samples (with an EMC thickness of 1.0 mm) had an initial warpage of 186 micrometers at room temperature in the fully dry state. During sorption, their warpage decreased to around 31 micrometers and remained almost constant after 2 weeks of sorption as shown in Figs. 6.2e and 62.f. The warpage values of both samples as a function of exposure time to moisture are shown in Fig. 6.3.

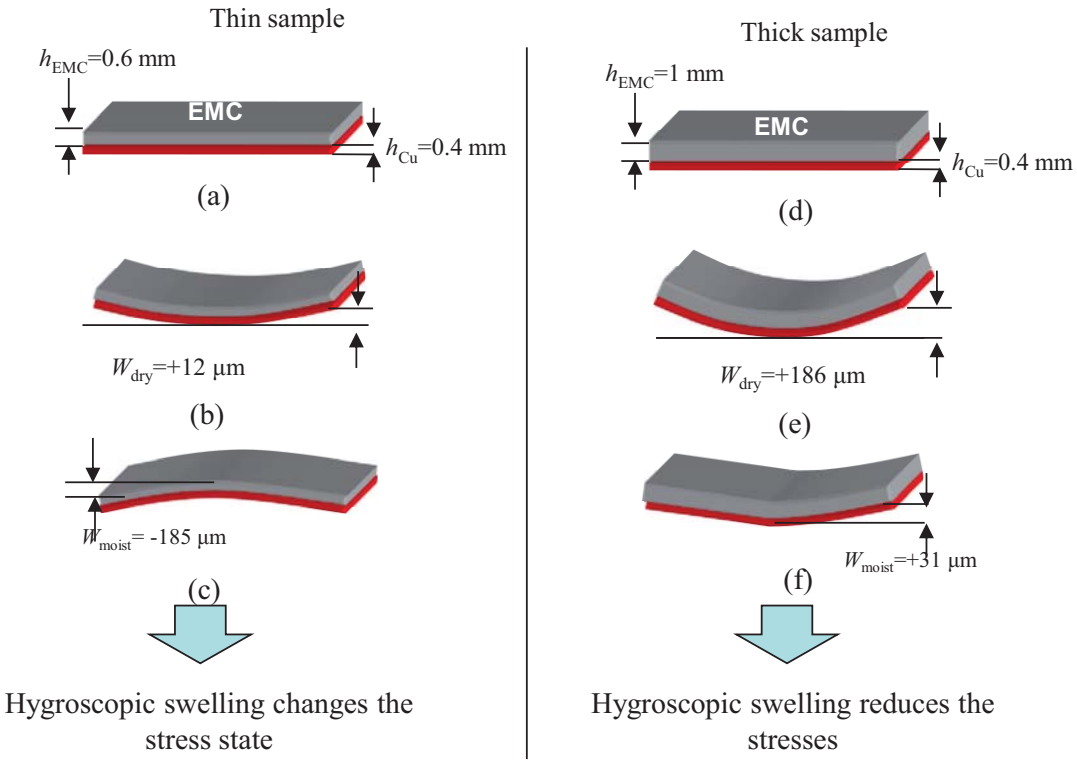

Figure 6.2 Effect of hygroscopic swelling on the warpage of the bimaterial beam.

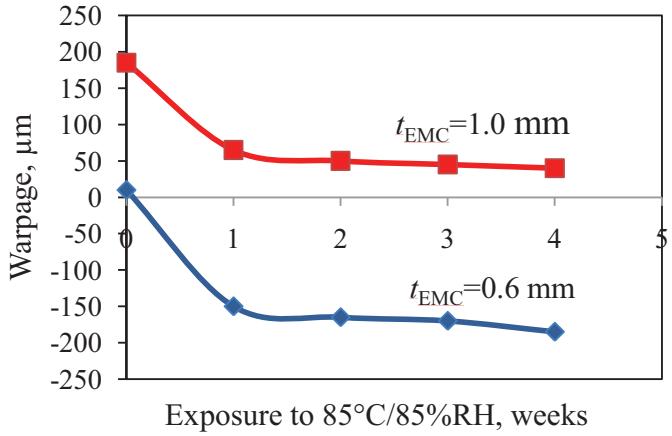

Figure 6.3 Warpage change of two geometries of bimaterial Cu/EMC beams during the moisture absorption.

The reduction of the warpage for the thicker bi-material beams and the change in the warpage from "smiling" to "crying" shape for the thin beams are due to the hygroscopic swelling across the exposed surface of the epoxy molding compound. However, since the epoxy molding compounds are viscoelastic, stress relaxation causes also a change in the warpage during the moisture aging at 85°C/85%RH (Shirangi *et al.*, 2009a,b and 2010). This was confirmed by a separate test

regarding the aging of bimaterial samples in a dry condition at 85°C in order to isolate the effect of the thermal aging and to assess the pure effect of the hygroscopic swelling at 85°C/85%RH. Nevertheless, in order to calculate the pure hygroscopic swelling strain, one needs the exact amount of the cure and thermal strains.

The total amount of residual strains in the absence of moisture of a bimaterial beam was presented in Chapter 4. When moisture is present, then the hygroscopic swelling also contributes to the total residual strains in the system as stated in the following equation:

$$\varepsilon^{\text{residual}} = \varepsilon^{\text{cure}} + \varepsilon^{\text{th}} + \varepsilon^{'\text{h}}, \tag{6.2}$$

where $\varepsilon^{\text{residual}}$ is the total residual strain at temperature T, $\varepsilon^{\text{cure}}$ is the cure strain due to the shrinkage of the EMC material during the solidification, ε^{th} is the thermal residual strain due to different CTE values of the EMC and Cu, and ε^{h} is the hygroscopic strain due to the expansion of the EMC material during moisture absorption.

In Chapter 4 it was shown that a simple modification in the CTE values together with an application of a viscoelastic model can accurately predict the warpage of these bi-material samples. In this section, the same model will be applied to determine the hygroscopic strain of the epoxy molding compound. The glass transition temperature (T_g) of the EMC material **MC-1** was measured and found to be 109°C and the CTE1 and CTE2 (CTE values below and above the T_g) were measured at 8.9 and 29.6 ppm/K, respectively, as reported in Chapters 3 and 4. The cure shrinkage during the molding process of the samples was found also by warpage analysis as shown in Chapter 4. The sample history was modeled with the FE program ANSYS as follows. First, the cure shrinkage at the molding temperature was accounted for by applying the cure strain to the molding compound. Afterwards the thermal strains arising from the cooling process from mold temperature (175°C) to room temperature (25°C) were taken into account. Finally, the moisture diffusion during the aging in humidity chamber and the resulting stress relaxation during the aging at 85°C/85%RH were modeled. The hygroscopic strain was obtained from the finite element calculation by a trial and error technique. In this technique, the CHS values were varied so that the final amount of warpage from FE analysis is the same as the experimentally measured warpage after sorption process of the bimaterial beam. From these methods the hygroscopic strain mismatch in the bimaterial system was found to be almost 0.061 %. The moisture content of the EMC was measured in Chapter 5 and was reported to be between 4.45×10^{-6} to 6.7×10^{-6} g/mm^3, depending on the sorption history. From the sorption tests of the bimaterial samples, it was found that long-term sorption does not have a remarkable influence on the warpage values. Consequently, the moisture concentration of 4.45E-6 g/mm^3 together with the hygroscopic strain value of 0.061 % gives the best estimate of CHS. By using Eq. (6.1), the coefficient of hygroscopic swelling can be estimated as an average value of 134 mm^3/g.

In addition, some samples were removed from moisture chamber after the saturation and were placed in a dry infrared oven at 110°C. The warpage values of the samples were measured after 10 days of baking. This was done to investigate as to whether hygroscopic swelling is reversible.

As expected, not all of the moisture-induced warpage due to moisture absorption was recovered. This suggests that the measurement of the hygroscopic swelling by any method that deals with the dimensional change during the desorption process of the samples may be wrong and should be avoided, at least for the polymeric materials that show such nonreversible hygroscopic swelling. In the next section another method based on the dimensional measurement of EMCs during the baking will be investigated and the results will be compared to that from the above method.

6.3 Characterization of CHS by TMA/TGA

Hygroscopic swelling of EMCs has been usually investigated by performing two parallel analyses (Wong *et al*., 2000): In the first analysis the weight loss of a saturated sample during desorption at a constant temperature is measured. This can be done via a TGA (Thermal Gravimetric Analysis) or running a finite element simulation of the desorption process of the sample as proposed by Shirangi *et al.* (2008a). In the second analysis the dimensional changes of a sample, with the same size as for TGA, during the baking at an elevated temperature is measured. A TMA (Thermal Mechanical Analysis) (Wong *et al.*, 2000) or shadow Moiré interferometry (Stellrecht *et al*., 2004) is normally used for the in-situ measurement of the hygroscopic strains. In all of these methods the dimensional changes of the sample during the isothermal desorption is measured and it is assumed that the behavior of the polymeric materials in terms of swelling and shrinkage during the absorption and desorption is the same, respectively. However, the main problem of this assumption is that, similar to the residual moisture content upon desorption of the molding compounds reported previously, a residual hygroscopic strain may also exist. In other words, not all of the swelling during the moisture uptake may be recovered after desorption.

In order to determine the CHS of the material **MC-1**, moisture preconditioned samples of 8 mm length were placed in the TMA for the strain measurement at different temperatures. The average elastic strain along the measuring line was reported by Zhou *et al.* to be close to zero (Zhou *et al.*, 2005). The presence of elastic strain due to hygroscopic stress contributes relatively small analysis error in the determination of the coefficient of hygroscopic swelling (Zhou *et al.*, 2006), compared to the error caused by non-uniform hygroscopic swelling. To eliminate the role of thermal expansion during desorption with TMA, a dry sample was used as reference so that only hygroscopic strains were documented.

For the TGA measurement with the available equipments, samples must have a maximum length of 2 mm to fit to the equipment, which makes it difficult to couple the moisture concentration results from TGA with strains from TMA because of different sample geometries. As an alternative to TGA, a finite element analysis of the desorption process was performed and used for the mass loss calculation using the desorption data from Table 5.3. Fig. 6.4 shows the experimental results of TMA and the corresponding TGA simulations at three temperatures.

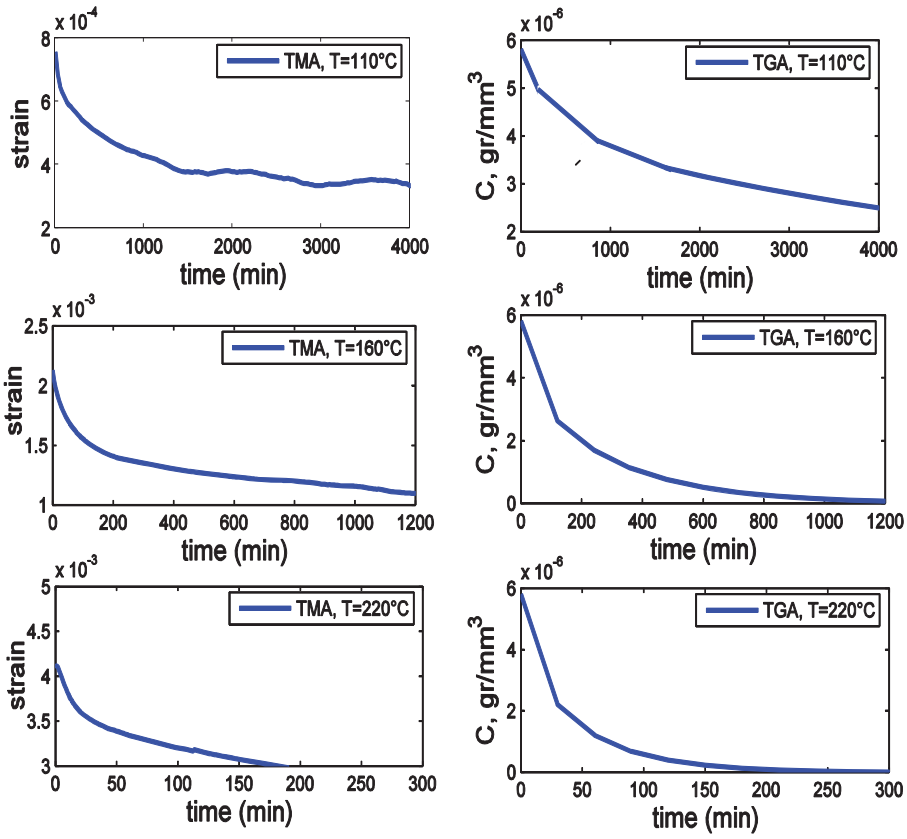

Figure 6.4 Results of TMA analysis at three temperatures (left) together with results of TGA from simulation at corresponding temperature (right).

From each pair of isotherm TMA/TGA curves of Fig. 6.4 a CHS value can be obtained by fitting a linear line and calculating its slope as depicted in Fig. 6.5. The curves do not cross the origin due to the inaccuracy of the TMA at longer stages of desorption. The results show a smooth increase of CHS at higher temperatures due to vapor pressure-induced expansion of EMC at elevated temperatures.

It must be mentioned that the results from Fig. 6.5 show that the CHS increases with increasing baking temperature. This is the problem of estimating the CHS when using TMA/TGA approach, because during the strain measurements by TMA, especially at elevated temperatures, the expansion of EMC due to high vapor pressure is also documented. Consequently, the results at lower temperatures seem to be closer to the real hygroscopic expansion during the sorption at 85°C/85%RH.

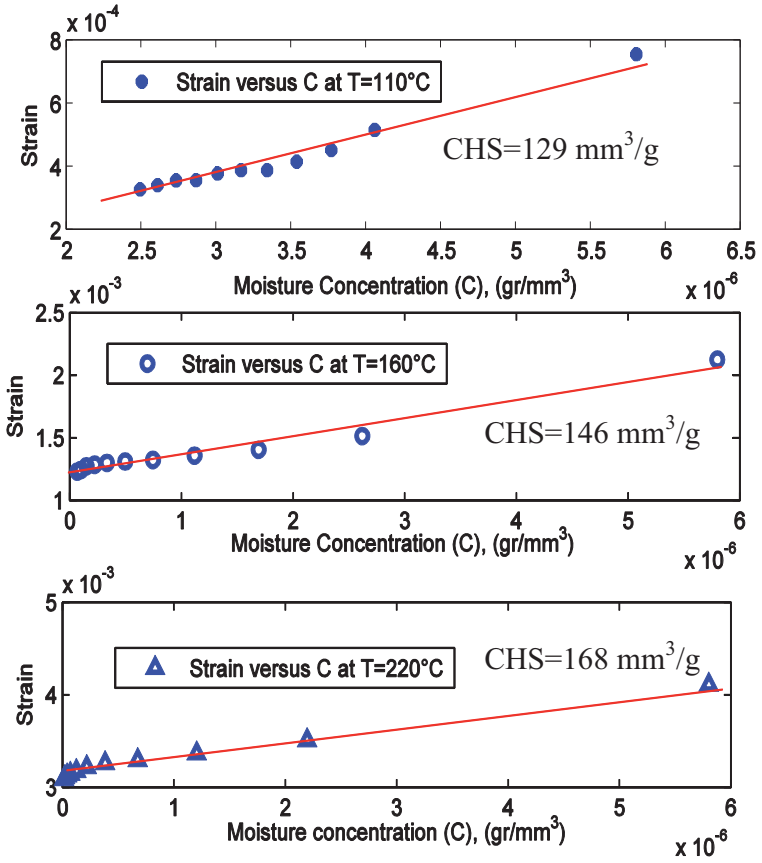

Figure 6.5 Calculation of CHS by combining the results of TMA and TGA from Fig.6.4.

The CHS results found from the TMA/TGA method are of the same order of magnitude as the CHS value determined using the warpage analysis as compared in Table 6.1. However, to the authors' experience, the warpage analysis should be preferred to estimate the CHS value. This is because of the fact that the hygroscopic swelling develops during the moisture preconditioning and not during the desorption. Its direct effect is changing the package warpage. Consequently, the method can be benchmarked by applying the CHS value in the FE analysis of a bimaterial beam and comparing the simulated warpage to the experimental one. This enables the verification of the whole stress analysis, which includes cure, thermal and hygroscopic strains.

Table 6.1 CHS results from different approaches.

Method	**CHS [mm^3/g]**
TMA/TGA at 110°C	129
TMA/TGA at 160°C	146
TMA/TGA at 220°C	168
Warpage analysis of a bi-material beam	134

6.4 Conclusions

The coefficient of hygroscopic swelling is normally found by relating the dimensional change of a saturated sample to its mass loss during isothermal desorption. However, this method may cause significant errors because essentially it was observed that not all of the absorbed moisture may be released upon baking of a specimen. Moreover, swelling of the EMC upon moisture intake was not recovered completely after its moisture desorption. Consequently, the hygroscopic strains may not be directly correlated to moisture mass and other methods based on the absorption process should be used for estimation of the coefficient of hygroscopic swelling. Warpage measurements of a bi-material beam could be a possibly a better approach. However, a detailed finite element analysis is required, because significant stress relaxation may occur when the sample is aged for long times. A detailed analysis of the warpage via FEA which considers the effect of cure shrinkage, stress relaxation due to viscoelasticity, and moisture-induced swelling was performed. This method allows for the calculation of the CHS during the moisture absorption of the EMC materials.

It is recommended that the CHS values should be determined from the warpage analysis of bimaterial beams. However, this method may be very expensive and time consuming. Usually fabrication of bimaterial beams is an expensive and time-consuming procedure and requires several modifications in the molding process. Moreover, the measurement of warpage for the implementation in FE analysis might be difficult and a large number of material characterizations are needed for a correct FE modeling. An alternative way to determine the CHS is using the TMA/TGA method and by replacing the TGA with an FE analysis of desorption process. This may solve many problems such non-uniform moisture content in the sample.

Chapter 7 Theory of Fracture Mechanics and Numerical Implementations

7.1 Introduction

One of the major objectives of this work is providing a conceptual understanding of fracture at the interface of a polymer (here epoxy molding compound) and a metal (here copper-based leadframe). Interfacial debonding (delamination) may be studied by using fracture mechanics, where delamination is modeled as a crack propagating along the interface between two dissimilar materials. This chapter presents a summary of fracture mechanics theory of isotropic materials as well as fracture mechanics characteristics of interfacial cracks.

In general, crack growth in ductile materials is likely to experience fatigue and stable crack growth before the occurrence of fast fracture and complete failure (unstable crack growth). Fatigue is a process of cumulative damage that is caused by repeated fluctuating loads. Fatigue crack propagation can be characterized by crack growth-rate models that predict the number of loading cycles required to propagate a fatigue crack to a critical size. Stress Intensity Factors (SIFs) under fatigue loading are below the critical value for quasi-static or unstable crack propagation. Under such circumstance, Linear Elastic Fracture Mechanics (LEFM) suffices to characterize the crack growth-rate model.

Both stable and unstable crack growth may occur in electronic packages. Subcritical stable crack growth may be driven by residual stresses, thermo-mechanical cycling, and mechanical or vibration loadings. Thermal expansion mismatch and polymer curing strains generate residual stresses in packages during fabrication and in use. The high temperatures employed for the solder reflow process and service thermal and moisture cycles during operation may produce significant thermo- and hygro-mechanical cycling. During thermal cycle loadings, a micro-scale defect in any of the materials or at the interface between any two materials can cause initiation and propagation of cracks. Consequently, fatigue crack growth occurs during the service life of these devices and determines their lifetime. Prominent examples of stable crack growth in electronic devices are the fatigue crack in solder joints (Wunderle, 2003) and encapsulant materials (Leblanc, 2004).

Another problem of cracking in electronic packages is associated with unstable crack growth (Wittler, 2004, Keller, 2005) either within a material or at the interface between two materials. The most significant examples of such crack propagations are popcorn cracking (Dudek, 2002) during the solder reflow process and interface delamination (Fan *et al.*, 1999, 2008, Auersperg, 2005, Dreßler *et al.*, 2006, Shirangi *et al.*, 2008b, 2009a,b,c, Schlottig, 2009 and 2010).

When the effect of moisture on crack initiation and propagation is investigated by fracture mechanics, the theories of fracture get more complex. This is because of the fact that the diffusion rate of moisture affects the rate and velocity of crack growth. Consequently, problems of moisture-driven subcritical crack growth must be treated with particular attention. Moisture, which lowers the debond driving energy required for extension of the debond, may be present in the materials themselves, in operating environments, or accumulated during processing steps which involve exposure to aqueous environments. The kinetics of interfacial debonding growth varies with a stress-dependent chemical reaction and mass transport of the environmental species (*e.g.*, moisture) to the debond tip (Kook and Dauskardt, 2002).

Since the interfacial delamination of electronic devices during the solder reflow process is essentially an unstable crack growth problem, in this work only the unstable crack growth will be investigated. The interface of interest is the joint between an epoxy molding compound and a copper-based leadframe.

In Section 7.2 the basic theories of fracture mechanics in isotropic materials will be presented. In Section 7.3 the problem of an interface crack between two dissimilar materials will be explained. In Section 7.4 a review of numerical methods and their implementation techniques in FE programs will be presented. Since the aim of this chapter is providing numerical methods for the use in next chapters, the numerical methods introduced in Section 7.5 will be validated for some basic fracture examples, for which an analytical solution exists. The verification of these numerical methods will allow us to use them in more complex fracture problems that we will face during the rest of this study in next chapters.

7.2 Brief Introduction to Fracture Mechanics in Isotropic Materials

When a system goes from a non-equilibrium to an equilibrium state, the potential energy of the whole system will decrease according to the first law of thermodynamics. In 1920 Griffith applied this theorem and suggested that a crack may form (or an existing crack may grow) only if such a process causes the total energy to decrease or remain constant. The critical condition for fracture can be defined as the point where the crack growth occurs under equilibrium condition, which means that there is no net change in the total energy.

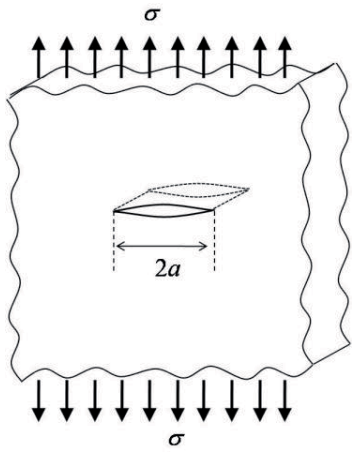

Figure 7.1 Crack in an infinite plate under uniform tension.

The Griffith consideration can be illustrated with a crack of length $2a$ in an infinite plate as shown in Fig. 7.1. In this case the plate width and length are much larger than $2a$ and plane stress condition can be assumed. If the crack is going to increase in size, a sufficient amount of potential energy must be available in the plate in order to overcome the surface energy of the material. If the above mentioned consideration is applied, the following energy balance can be formed for an incremental increase in crack area, $\mathrm{d}A$:

$$\frac{\mathrm{d}E}{\mathrm{d}A}=\frac{\mathrm{d}\Pi}{\mathrm{d}A}+\frac{\mathrm{d}W_{\mathrm{s}}}{\mathrm{d}A}=0\Leftrightarrow-\frac{\mathrm{d}\Pi}{\mathrm{d}A}=\frac{\mathrm{d}W_{\mathrm{s}}}{\mathrm{d}A}, \tag{7.1}$$

where E is the total energy, Π is the potential energy supplied by internal strain energy and external forces and W_{s} is the energy required to create new surfaces (surface energy). This energy balance is also called the *Griffith energy balance*.

Irwin (1957) defined the *Griffith energy* G , also called the Energy Release Rate (ERR), or Strain Energy Release Rate (SERR) as a measure of the energy available for an increment of crack extension as follows:

$$G=-\frac{\mathrm{d}\Pi}{\mathrm{d}A}. \tag{7.2}$$

Furthermore, by use of the Griffith energy balance, the critical Griffith energy balance, or the *critical energy release rate*, can be defined as:

$$G_{\mathrm{c}}=\frac{\mathrm{d}W_{\mathrm{s}}}{\mathrm{d}A}. \tag{7.3}$$

G_{c} is also called the *fracture toughness* of the material. Using these definitions, the Griffith fracture criterion can be stated in terms of the parameters above. In other words, the Griffith energy balance implies that the necessary condition to grow the crack is that the amount of the strain energy release rate exceeds the fracture toughness.

Irwin was also among the first to deliver the singular stress field close to a sharp crack field in plane stress or strain for a homogeneous, isotropic elastic solid. Hutchinson and Suo (1992) proposed that this stress field (as shown in Fig 7.2) can be defined in the following polar form:

$$\sigma_{ij} = \frac{K_{\mathrm{I}}}{\sqrt{2\pi r}}\sigma_{ij}^{\mathrm{I}}(\theta) + \frac{K_{\mathrm{II}}}{\sqrt{2\pi r}}\sigma_{ij}^{\mathrm{II}}(\theta) + T(r,\theta)\,\delta_{i1}\delta_{1j}, \tag{7.4}$$

where δ_{ij} is the Kronecker delta, T the non-singular stresses parallel to the crack surface. The two functions $\sigma_{ij}^{\mathrm{I}}(\theta)$ and $\sigma_{ij}^{\mathrm{II}}(\theta)$ define the shape of the stress filed. Note that the $1/\sqrt{r}$ represents the singularity of the stress fields at the crack tip. K_{I} and K_{II} are called the *stress intensity factors*.

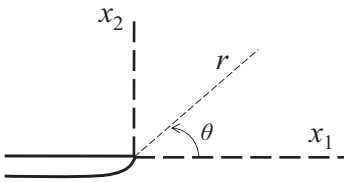

Figure 7.2 Near tip crack field definitions in homogeneous materials.

In Fig. 7.3 the basic fracture modes of crack tip deformation are illustrated. Mode I is opening or tensile mode where the crack surfaces move directly apart. Mode II is sliding or in-plane shear mode where the crack surfaces slide over one another in a direction perpendicular to the leading edge of the crack. Mode III is out-of-plane shear mode or tearing mode where the crack surfaces move relative to one another and parallel to the leading edge of the crack.

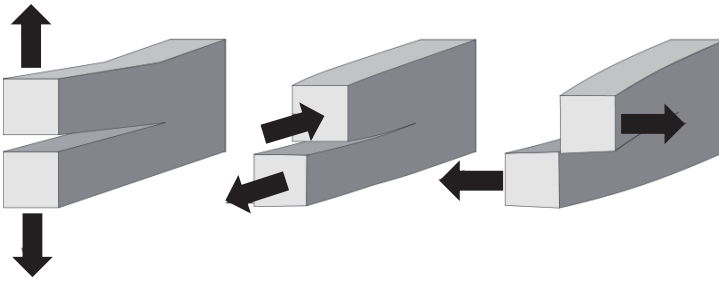

Figure 7.3 Basic fracture modes.

When a two-dimensional (2D) problem is assumed, only the two first modes are available. For this case, a pure mode I field will be symmetric with respect to the crack line. K_{I} and K_{II} are then defined as stress amplitudes according to

$$\sigma_{22} = \frac{K_{\mathrm{I}}}{\sqrt{2\pi r}} \qquad \sigma_{12} = \frac{K_{\mathrm{II}}}{\sqrt{2\pi r}} \qquad \text{for} \qquad \theta = 0\,, \tag{7.5}$$

The mode mixity for a certain stress filed can be then defined as:

$$\Psi = \arctan\left(\frac{K_{II}}{K_I}\right). \tag{7.6}$$

Irwin also defined a relationship between the stress intensity factors and the Griffith energy for straight ahead quasi-static crack propagation:

$$G = \frac{K_I^2 + K_{II}^2}{\overline{E}}, \tag{7.7}$$

where $\overline{E}$ is given as Young's modulus for plane stress problems. For plane strain problems the relationship $\overline{E} = E/(1-\nu^2)$ is applicable, where ν is the Poisson's ratio.

In three-dimensional (3D) problems the total energy release rate in mixed mode fracture can be obtained by summing up the energy release rates for each mode:

$$G = G_I + G_{II} + G_{III} = \begin{cases} \dfrac{K_I^2}{E} + \dfrac{K_{II}^2}{E} + (1+\nu)\dfrac{K_{III}^2}{E} & (\text{plane stress}) \\ (1-\nu^2)\dfrac{K_I^2}{E} + (1-\nu^2)\dfrac{K_{II}^2}{E} + (1+\nu)\dfrac{K_{III}^2}{E} & (\text{plane strain}). \end{cases} \tag{7.8}$$

It is important to note that the derivation of both the stress intensity factor and the strain energy release rate is independent of the actual fracture process, hence critical conditions of the materials. In other words, these relations only represent the driving force for crack growth and bear no relation to materials' resistance against fracture. The resistance of materials against fracture needs experimental material characterizations which are the subject of the next two chapters. In summary, the above theory is known as Linear Elastic Fracture Mechanics (LEFM) in homogeneous materials. This theory is applicable to brittle materials where the failures process zone and the crack tip plasticity is very limited and is much smaller compared to the *K*-dominated zone.

7.3 Theory of Interface Fracture

This section reviews some key concepts and the definitions relating to the problem of a crack along an interface between two dissimilar materials. A bimaterial interface is the conjoining surface between two materials that are typically fused or bonded together. It is often observed that a crack in the homogeneous materials advances in mode I fracture. Even though the mixed mode crack situation can happen in homogeneous materials, the crack will immediately try to kink in to a path where pure mode I exists. It must be noted that a pure mode I or mode II does not exist for the crack at interfaces and the crack propagation at interface is mostly under mixed mode condition.

7.3.1 Nature of Interface Cracks

The governing analytical solution for a plane interface crack between two elastic isotropic materials was obtained by Williams (1959) who performed an asymptotic analysis of the elastic field at the tip of an open crack and found that the stress field possesses an oscillatory character of the type $r^{-1/2+i\varepsilon}$, where r is the radial distance from the crack tip, $\xi = -1/2 + i\varepsilon$ is the complex eigenvalue , $i = \sqrt{-1}$ and ε is the bimaterial constant defined as

$$\varepsilon = \frac{1}{2\pi} \ln\left[\frac{1-\beta}{1+\beta}\right], \tag{7.9}$$

where

$$\alpha = \left[\frac{\overline{E}_1 - \overline{E}_2}{\overline{E}_1 + \overline{E}_2}\right] \text{ and } \beta = \frac{\mu_1(\vartheta_2 - 1) - \mu_2(\vartheta_1 - 1)}{\mu_1(\vartheta_2 + 1) + \mu_2(\vartheta_1 + 1)}. \tag{7.10}$$

α and β are the so-called Dundurs parameters (Dundurs, 1967 and 1969) and $j = 1,2$ represents material 1 and 2, respectively (Fig. 7.4).

Furthermore, $\vartheta_j = (3 - 4\nu_j)$ and $\overline{E}_j = E_j/(1-\nu_j^2)$ for plane strain, and $\vartheta_j = (3-\nu_j)/(1+\nu_j)$ and $\overline{E}_j = E_j$ for plane stress where E_j is the elastic modulus, ν_j is Poisson's ratio, and $\mu_j = E_j / 2(1+\nu_j)$ is the shear modulus for material j .

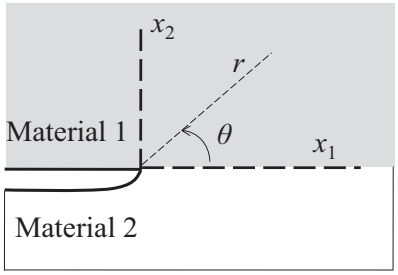

Figure 7.4 Geometry of bimaterial interface crack.

The oscillatory singularity is given by:

$$r^{i\varepsilon} = \cos(\varepsilon \ln r) + i\sin(\varepsilon \ln r). \tag{7.11}$$

The geometry of interface crack is illustrated in Fig. 7.4. The problem is treated as planar, in plane strain, and linear elastic fracture mechanics (LEFM) is assumed to hold true.

7.3.2 Complex Stress Intensity Factor

Using the convention for an interface crack defined in Fig. 7.4, the complex stress intensity factor, K, is given by (Rice and Sih, 1965)

$$K = K_1 + iK_2 = |K| e^{i\Psi^*}, \tag{7.12}$$

where K is the complex stress intensity factor, which has the unit of $\mathrm{N\,m^{-2}}\sqrt{\mathrm{m}}\,\mathrm{m}^{-\mathrm{i}\varepsilon}$ and Ψ^* is the mode mixity (phase angle). It should be noted that in the above equation, the stress intensity factors K_1 and K_2 do not refer to the individual stress amplitudes for the respective mode I and mode II any more. This is due to the mixed-up of the traditional stress intensity definition in bi-material fracture mechanics. This mix-up is also the reason for the different choice of mode designation with Arabic numerals, in order to distinguish between homogeneous and inhomogeneous stress intensity factors.

Just ahead of the crack tip ($\theta = 0°$) the stresses are dominated by a singular stress field of the form (Rice, 1988):

$$\sigma_{yy} + \mathrm{i}\sigma_{xy} = \frac{1}{\sqrt{2\pi}} K\, r^{\mathrm{i}\varepsilon - 1/2}, \tag{7.13}$$

where σ_{yy} is the tensile and σ_{xy} is the shear stress components.

The stress intensity factors of classical type K_{I} and K_{II}, represent the stress intensity factors of two different modes of fracture and can be defined as:

$$K_{\mathrm{I}} + \mathrm{i}K_{\mathrm{II}} = K l^{\mathrm{i}\varepsilon} = |K| e^{\mathrm{i}\psi}, \tag{7.14}$$

where l is an arbitrary chosen reference length, ψ is the mode mixity of $K l^{\mathrm{i}\varepsilon}$ and K_{I} and K_{II} are based on the reference length $r = l$. By using the concept of a reference length, an alternative definition of Stress Intensity Factors (SIFs) was suggested by Rice (1988) and Hutchinson and Suo (1992) as:

$$\sigma_{yy} + \mathrm{i}\sigma_{xy} = \frac{K_{\mathrm{I}} + \mathrm{i}K_{\mathrm{II}}}{\sqrt{2\pi r}} \left(\frac{r}{l}\right)^{\mathrm{i}\varepsilon}. \tag{7.15}$$

It should be noted that the stress intensity factors defined by Eq. (7.15) have the units of the isotropic stress intensity factors, *i.e.* $\mathrm{N\,m^{-2}}\sqrt{\mathrm{m}}$. However, as stated by Rice (1988) and Hutchinson and Suo (1992), the stress intensity factors K_{I} and K_{II} for a crack at bimaterial interface with $\beta \neq 0$ are not directly analogous to mode I and mode II stress intensity factors for homogeneous materials, because a characteristic reference length must always be specified.

The (stress-based) mode mixity then for an interface crack is expressed as:

$$\psi = \tan^{-1}\left(\frac{\mathrm{Im}[Kr^{\mathrm{i}\varepsilon}]}{\mathrm{Re}[Kr^{\mathrm{i}\varepsilon}]}\right)_{r=l} = \tan^{-1}\left(\frac{\sigma_{xy}}{\sigma_{yy}}\right)_{r=l}. \tag{7.16}$$

The mode mixity ψ defined above is a local mode mixity of $Kl^{\mathrm{i}\varepsilon}$ and the stresses and SIFs are local quantities evaluated at a point defined by reference length ahead of the crack tip. ψ can be related to Ψ^* according to (Hutchinson and Suo, 1992):

$$\psi = \Psi^* + \varepsilon \ln(l). \tag{7.17}$$

The characteristic length l has the effect that the phase of mode mixity is shifted when the length is chosen arbitrary. Generally, this length has no physical meaning but is normally chosen, so that the minimum encountered in the distribution of the critical energy release rate is located at $\psi = 0$.

The relation between two mode mixities ψ_1 and ψ_2 obtained from two arbitrary reference lengths of l_1 and l_2, respectively, can be derived as (Agrawal and Karlsson, 2007):

$$\psi_2 = \psi_1 + \varepsilon \ln\left(\frac{l_2}{l_1}\right). \tag{7.18}$$

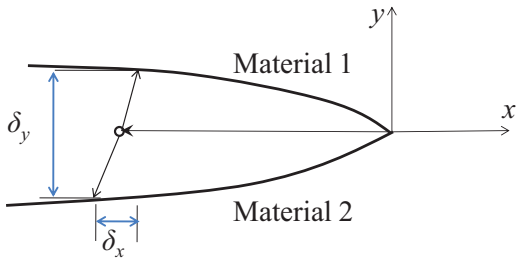

Figure 7.5 Displacement jump close to the crack tip.

The displacement jumps (Fig. 7.5) close to the crack field can be expressed in terms of stress intensity factors as (Hutchinson and Suo 1992):

$$\delta_y + \mathrm{i}\delta_x = 8\frac{K_\mathrm{I} + \mathrm{i}K_\mathrm{II}}{(1+2\varepsilon)E^* \cosh(\pi\varepsilon)\sqrt{2\pi}}\sqrt{r}\left(\frac{r}{l}\right)^{\mathrm{i}\varepsilon}, \tag{7.19}$$

where $\frac{1}{E^*} = \frac{1}{2}\left(\frac{1}{\bar{E}_1} + \frac{1}{\bar{E}_2}\right)$.

Here δ_x and δ_y are the displacement jumps between two points located on opposite crack faces at a distance r behind the crack tip, along x- and y- coordinates, respectively.

The total strain energy release rate for an interface crack G is not oscillatory and can be expressed as (Malyshev and Salganik, 1965):

$$G = \frac{1-\beta^2}{E^*}|K|^2, \tag{7.20}$$

where $|K|^2 = (K_1^2 + K_2^2) = (K_\mathrm{I}^2 + K_\mathrm{II}^2)$.

Similar to that for the homogeneous materials, the strain energy release rate for an interface crack has the dimension of J/m^2 or Nm^{-1}.

7.4 Methods of Computational Fracture Mechanics

In order to calculate the strain energy release rate (SERR) G and the mode mixity for cracks at bimaterial interfaces, finite element analysis can be applied. There are several methods to extract the SERR from FE tools. However, most of these methods have not been yet implemented in commercial general purpose finite element codes such as ANSYS. Consequently, in order to find the SERR, these methods must be implemented and then be benchmarked by comparing their results against analytical solutions from the literature. Among various methods available in literature to determine SERR from finite element results, four of them, which have been the focus of recent studies, are selected in this work. In this section, these methods will be introduced and the SERR values estimated from these methods will be compared. The four methods which will be discussed in this study are:

- The crack closure method using two analysis steps
- The Virtual Crack Closure Technique (VCCT)
- The Virtual Crack Extension (VCE) method
- The J integral

7.4.1 The Crack Closure Method Using Two Analysis Steps

This method is based on Irwin's crack closure integral (Irwin, 1957). According to Irwin, the work required to extend a crack by an infinitesimal distance is equal to the work required to close the crack to its original length. Thus, for homogeneous, isotropic, linear elastic materials, the components of strain energy release rate for mode I and mode II can be expressed as (Irwin, 1957):

$$G_{\mathrm{I}} = \lim_{\Delta a \to 0} \frac{1}{2\Delta a} \int_0^{\Delta a} \sigma_{yy}(\Delta a - r)\delta_y(r)\,\mathrm{d}r, \tag{7.21}$$

$$G_{\mathrm{II}} = \lim_{\Delta a \to 0} \frac{1}{2\Delta a} \int_0^{\Delta a} \sigma_{xy}(\Delta a - r)\delta_x(r)\,\mathrm{d}r, \tag{7.22}$$

where Δa is a small crack extension; σ_{yy} and σ_{xy} are the normal and shear tractions, at a distance r ahead of the crack tip and δ_x and δ_y are the displacement jumps at a distance r behind the crack tip, along the x (sliding mode) and y (opening mode) directions, respectively.

The crack closure method assumes that the energy ΔE released when a crack is extended from the length a (Fig. 7.6 left) to $a + \Delta a$ (Fig. 7.6 right) is identical to the energy required to close the crack between locations l and i in these figures.

For a crack modeled with two-dimensional four node elements as shown in Fig. 7.6, the work ΔE required to close the crack along one element side can be calculated as (Krueger, 2002):

$$\Delta E = \frac{1}{2}[X_{1l}\,\Delta u_{2l} + Z_{1l}\,\Delta w_{2l}], \tag{7.23}$$

where X_{1l} and Z_{1l} are the shear and opening forces at nodal point l and Δu_{2l} and Δw_{2l} are the difference in shear and opening nodal displacements at node l. This method requires two separate FE analyses with the same mesh size along the crack font. The forces may be obtained from the first FE analysis. The displacements should be obtained from a second FE analysis while the crack has been extended to its new length $a+\Delta a$ as shown in Fig 7.6.

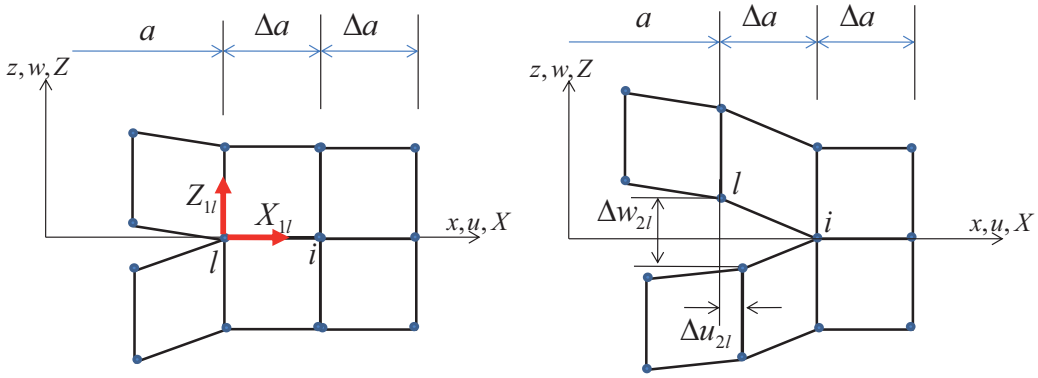

Figure 7.6 The two-step crack closure method.

7.4.2 The Virtual Crack Closure Technique (VCCT)

The Virtual Crack Closure Technique (VCCT), originally proposed in 1977 by Rybicki and Kanninen is also based on the Irwin's integral. Additionally, it is assumed that the crack extension of Δa from $a+\Delta a$ to $a+2\Delta a$ does not significantly alter the state at the crack tip (Fig. 7.7). Therefore, the displacements behind the crack tip at node i are approximately equal to the displacements behind the original crack tip at node l. This method can be used with conventional (non-singular), linear finite element solutions to get accurate strain energy release rate values. The energy ΔE released when the crack is extended by Δa from $a+\Delta a$ to $a+2\Delta a$ is identical to the energy required to close the crack. For a crack modeled with two-dimensional, four-node elements, as shown in Fig. 7.7, the work required to close the crack along one element side can be calculated as (Krueger, 2002):

$$\Delta E = \frac{1}{2}[X_i\,\Delta u_l + Z_i\,\Delta w_l]. \tag{7.24}$$

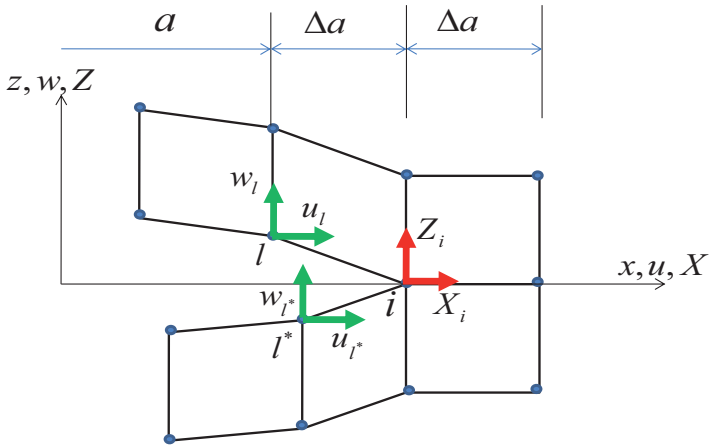

Figure 7.7 the virtual crack closure technique (VCCT).

For three-dimensional solid elements, the three components of strain energy release rate can be calculated from the following formula (Krueger, 2002):

$$G_{\mathrm{I}} = -\frac{1}{2\Delta A} Z_{Li}(w_{Ll} - w_{Ll^*}),$$

$$G_{\mathrm{II}} = -\frac{1}{2\Delta A} X_{Li}(u_{Ll} - u_{Ll^*}),$$

$$G_{\mathrm{III}} = -\frac{1}{2\Delta A} Y_{Li}(v_{Ll} - v_{Ll^*}), \tag{7.25}$$

with $\Delta A = b\,\Delta a$ as shown in Fig.7.8. Here ΔA is the area virtually closed, Δa is the length of elements at the crack front, and b is the width of the elements. X_{Li}, Y_{Li} and Z_{Li} denote the forces at the crack front in column L, row i.

The total energy release rate G is calculated from the individual mode components as:

$$G = G_{\mathrm{I}} + G_{\mathrm{II}} + G_{\mathrm{III}}. \tag{7.26}$$

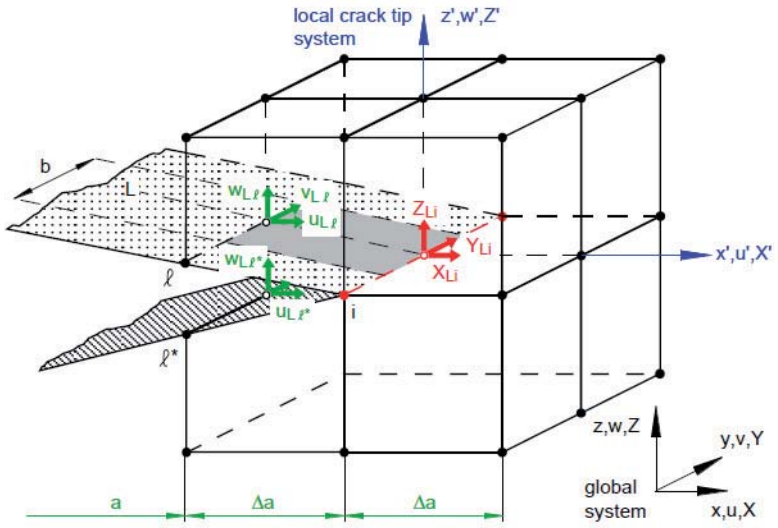

Figure 7.8 Three-dimensional VCCT (Krueger, 2002).

The equations for determining the strain energy release rate from the two-dimension eight-node elements are similar to the equations above. The summation of the product of corresponding nodal forces and displacements results in the calculation of the strain energy release rate. Fig. 7.9 shows the corresponding nodes ahead and behind the crack tip for such elements.

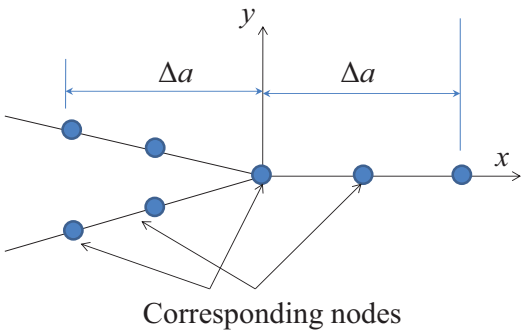

Figure 7.9 Corresponding nodes ahead and behind crack tip to calculate the SERR from 2D eight-node elements.

In contrast to the previous two-steps crack closure method, the VCCT required only one set of FE analysis. Another advantage of VCCT is its relatively low CPU time. Furthermore, convergence analyses were applied in this study and it was revealed that moderately dense mesh near crack tip is sufficient for getting acceptable SERR results. However, it must be noted that the VCCT results in non-converging mode mixity for the problem of crack at interfaces. Consequently, the mode mixity gained from the VCCT for bimaterial problems must be modified. This problem will be explained in Section 7.6.

7.4.3 The Virtual Crack Extension (VCE) Method

The virtual crack extension (VCE) method is based on the general definition of strain energy release rate. In this method the whole structure subjected to crack propagation will be analyzed twice. The first analysis with a crack length of a and the second analysis with the crack length of $a+\Delta a$. Unlike the previous methods, VCE does not deal with the local forces and displacements rather it requires the potential energy of the whole system. If the potential energy values Π (strain energy) for both cases are stored, the energy release rate can be calculated from the following equation:

$$G = -\frac{\Delta \Pi}{\Delta A} = -\frac{\Pi_{a+\Delta a} - \Pi_a}{b\,\Delta a}, \tag{7.27}$$

where b is the thickness of the fracture model.

This method was also implemented in the FE program ANSYS. The method requires two separate analyses which can be regarded as a disadvantage because of being time consuming. Another disadvantage of this method is that VCE, in contrast to VCCT, does not provide any information about the mode mixity and delivers only the total amount of strain energy release rate.

7.4.4 The J-integral

The J-integral was first proposed by Rice (1968) because of the difficulties involved in computing the stresses close to the crack in nonlinear elastic or elastic-plastic materials. It can be shown that (Anderson, 2005) if a monotonic loading is assumed (without any plastic unloading) the J-integral can be used to compute the energy release rate of plastic materials for small scale deformations. In its simplest form, the J-integral can be defined as a path independent line integral that measures the strength of the singular stresses and strains near a crack tip. Eq. (7.28) is an expression for J-integral in its 2D form as shown in Fig. 7.10. It assumes that the crack lies in a local crack front in a Cartesian *x*-*y* plane, with the *x*-axis parallel to the crack and the interface.

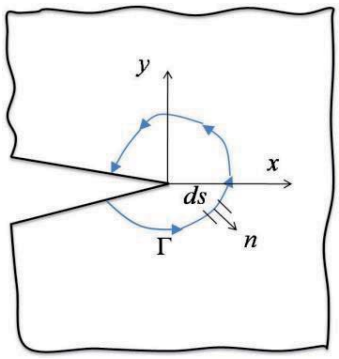

Figure 7.10 Definition of the path of 2D J-integral.

$$J = \int_{\Gamma} \left(W \, \mathrm{d}y - T_i \frac{\partial u_i}{\partial x} \mathrm{d}s \right), \tag{7.28}$$

where Γ is a path surrounding the crack tip going from the lower to the upper crack flank. W is the strain energy density defined as:

$$W = \int_0^{\varepsilon_{ij}} \sigma_{ij} \, \mathrm{d}\varepsilon_{ij}, \tag{7.29}$$

and T_i are the tractions defined as $T_i = \sigma_{ij} n_j$, where n_j is the normal to the path.

Rice (1968) showed that the J-integral is a path independent line integral and it represents the strain energy release rate of nonlinear elastic materials.

In order to implement the 2D J-integral in the FE code ANSYS, a numerical routine produced by ANSYS was used. This routine uses an option available in ANSYS that enables definition of a path. Moreover, the normal vectors and the strain energy density can also be determined. Consequently, the first part of the J-integral can be calculated by integrating with respect to the path length s. In the second part of the integral, the derivative of the displacements with respect to the *x*-direction is involved. To obtain this derivative, a new path shifted by a small distance from the first one was created and the displacements were calculated along the new path. Using the definition of derivative, a numerical estimation enables the derivative of the displacements with respect to the *x*-direction. It must be noted that this method is only required for the previous versions of ANSYS when this study was carried out. In the recent versions of ANSYS (from version 11 on) the J-integral is implemented in the program.

7.5 Verification of Implemented Fracture Methods

In this section the methods mentioned in the previous section will be implemented in the FE code ANSYS and the results of strain energy release rate will be compared against each other. Three fracture testing methods are selected, which include a Compact Tension (CT) testing method, a Four-Point Bending (4PB) delamination test and finally a Three-Point End Notch Flexure (3-ENF) delamination test. These fracture testing methods are selected due to their simplicity and because there exists an analytical solution for the energy release rate, which enables the benchmarking of the above methods by comparing the numerical result against the analytical solutions of SERR. Moreover, in this work, the two latter delamination testing methods were applied to determine the adhesion between EMC and Cu. These methods will be discussed in the next chapter in details. However, in this section the applicability of the numerical methods presented in the previous section will be discussed.

7.5.1 Compact Tension (CT) Specimen

The CT specimen is widely used for the determination of the fracture toughness of isotropic materials in mode I fracture. Many researchers have worked on the different aspects of this testing method such as limit of validity for viscoelastic materials (Wittler, 2002), subcritical crack growth (Leblanc, 2004) by optical crack tracing, and micro-deformations by digital image correlation technique (Keller, 2005).

Since in this work only the interfacial fracture toughness will be investigated, experimental fracture using a CT specimen will not be performed. However, due to its simplicity in geometry and availability of analytical solutions for the energy release rate, the CT specimen will be used for benchmarking the numerical methods presented in Section 7.4. Fig. 7.11 illustrates the geometry of this test specimen which was modeled in the FE program ANSYS. Since in most commercial programs, including ANSYS, the numerical methods for calculating the energy release rate are not implemented, for all of the methods mentioned above, a separate subroutine was written for both two- and three-dimensional FE analysis (except for the J-integral for which only a 2D subroutine was available). A large number of FE simulations were carried out to investigate the effects of element size, element type and convergence analysis for all the above mentioned numerical methods. For example, the convergence analysis revealed that for the VCCT method, an element size of $\Delta a = a/100$ (a being the crack length) with 12 elements in circumferential directions around the crack tip (Fig. 7.11 right) will produce acceptable results (Hanoi, 2009).

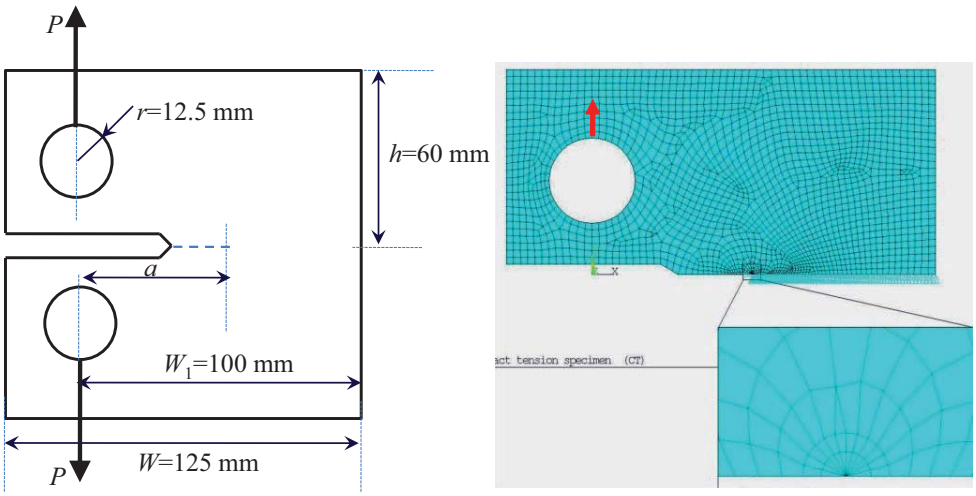

Figure 7.11 Geometry of the CT specimen (left) and the mesh generation (right).

The material used for the benchmarking of numerical methods was assumed to have an elastic modulus of E=25 GPa and a Poisson's ratio of ν=0.24 (similar to an epoxy molding compound). The applied load was P=400 N.

Fig. 7.12 compares the values of normalized energy release rates found by different numerical methods using 3D analyses. The SERR results are all normalized against the SERR from the analytical solution of the CT specimen (Anderson, 2005). Excellent agreement between the nu-

merical results and analytical solution can be observed. The largest discrepancy between the analytical and numerical solution is 0.93%, when the VCE method is used. When VCCT is compared to the analytical solution, the difference is only 0.37%. This means that the method can determine the SERR quite exactly, even though the calculation is performed in only one FE analysis.

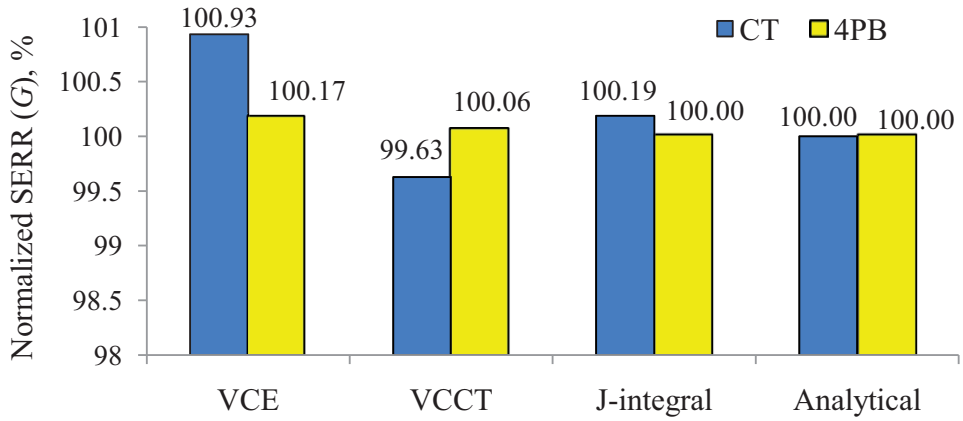

Figure 7.12 Comparison between the SERR results found by different numerical methods.

The SERR value for a CT specimen depends on geometry, crack length, materials and the applied load. The CPU time for FE analysis using 3D meshing is much higher than that of a 2D analysis. However, as will be shown in the next chapter, a 2D analysis may be acceptable only if the fracture problem is a mechanical and not a thermo-mechanical problem. For the case of thermo-mechanical loads, a 2D analysis can be erroneous, especially if the problem of bimaterial fracture is considered. The problem of crack propagation in the CT specimen was benchmarked for the 3D specimen as illustrated in Fig. 7.13. The crack propagation was modeled by decoupling the nodes across the crack path. By using the ANSYS Parametric Design Language (APDL) a parametric script was written in order to calculate the SERR values after each step of crack propagation and finally find the G value as a function of crack length. As observed in the plots of Fig. 7.13, the stress field is symmetric with respect to the crack path. This is a typical phenomenon for cracks in CT specimen for isotropic materials. Moreover, the stress intensity varies with increasing crack length.

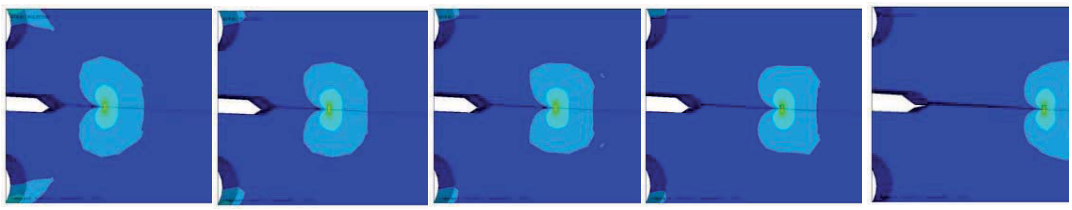

Figure 7.13 Simulation of the crack propagation in a CT specimen.

Similar to these analyses the crack propagation at the interface and the effect of crack length on the stress intensity factor for an IC package will be discussed in Chapter 10.

7.5.2 Four-Point Bending (4PB) Delamination Problem

The next example which will be used as a benchmark for the numerical methods implemented in ANSYS is a crack at the interface of a bimaterial beam in a Four-Point Bending (4PB) delamination problem. The reason for selecting this problem is that, in this work, the 4PB delamination testing method will be applied to investigate the fracture toughness of Cu / EMC interface. The test method, sample manufacturing, and the fracture results will be explained in details in next chapter. This section only attempts to verify the numerical methods to determine the SERR. The geometry of the 4PB model is illustrated in Fig. 7.14. Without loss of generality, we assume that the substrate of the bimaterial beam is copper leadframe (Cu) and the upper layer is an Epoxy Molding Compound (EMC). By applying beam theory and assuming LEFM to hold true, the strain energy release rate for an interface crack in a 4PB test can be calculated as (Charalambides, 1989):

$$G = \frac{M^2(1-\nu_{\mathrm{Cu}}^2)}{2E_{\mathrm{Cu}}}\left(\frac{1}{I_{\mathrm{Cu}}} - \frac{\lambda}{I_{\mathrm{c}}}\right), \tag{7.30}$$

where $\lambda = \frac{E_{\mathrm{Cu}}(1-\nu_{\mathrm{EMC}}^2)}{E_{\mathrm{EMC}}(1-\nu_{\mathrm{Cu}}^2)}$ and $M = PL/2b$.

I_{c} and I_{Cu} denote quantities which are proportional to the moments of inertia of the composite beam and of the Cu, respectively, and they can be calculated from:

$$I_{\mathrm{c}} = \frac{t_{\mathrm{EMC}}^3}{12} + \frac{\lambda t_{\mathrm{Cu}}^3}{12} + \frac{\lambda t_{\mathrm{EMC}} t_{\mathrm{Cu}} (t_{\mathrm{EMC}} + t_{\mathrm{Cu}})^2}{4(t_{\mathrm{EMC}} + \lambda t_{\mathrm{Cu}})}, \text{ and } I_{\mathrm{Cu}} = \frac{t_{\mathrm{Cu}}^3}{12}.$$

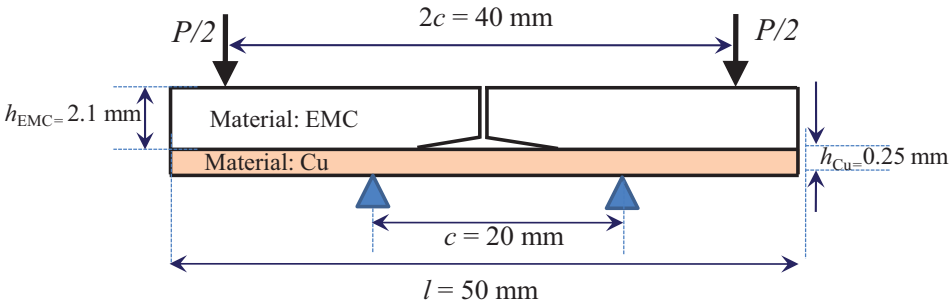

Figure 7.14 The geometry of the 4PB delamination test.

Fig 7.15 shows an FE model of the 4PB problem together with the mesh refinement at the crack tip. The mechanical parameters of the EMC were assigned similar to those shown in Section 7.5.1. Moreover, Young's modulus and Poisson's ratio of the copper leadframe were assumed as 125 GPa and 0.33, respectively. The results of SERR gained by different numerical methods are also depicted in Fig. 7.12. A very good agreement between FEA results and the analytical solution can be observed, which suggests that all the methods work for the problem of bimaterial cracks. However, among all methods, VCCT has two advantages that make it the preferred one.

First of all, for the calculation of SERR only one FE-analysis is required which reduces the required time for calculation of SERR. The second reason is the fact that VCCT delivers all of the three components of SERR in separated modes. This advantage is even more important for the case of interface fracture, because, as mentioned previously the nature of cracks at bimaterial interfaces is always a mixed mode problem. Consequently, the separation of fracture modes needs more attention when the interfacial delamination is being considered.

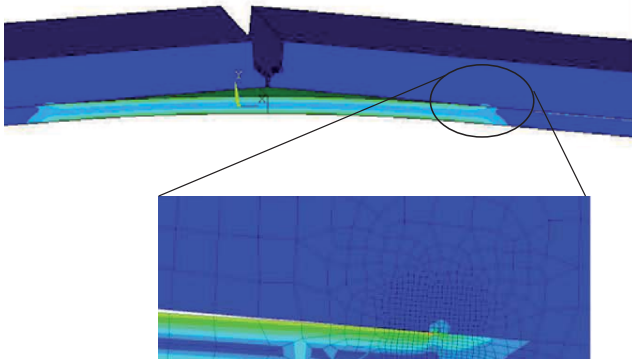

Figure 7.15 Mesh generation near the crack tip a 4PB delamination test.

7.5.3 Three-Point End-Notch Flexure (3-ENF) Delamination Problem

Another delamination test specimen which will be used in this study is the Three-Point End-Notched Flexure (3-ENF) as shown in Fig. 7.16. The fracture setup of 3-ENF tests together with other details will be discussed in the next section. The FE-analysis of this test is slightly more complex than that of a 4PB test. This complexity is primary due to two facts. First, the deformations in this test are generally larger than for a 4PB. Consequently geometric nonlinearity must be considered in the FE solver. The second problem is associated with the element penetration when the crack at the interface is modeled. In contrast to the 4PB test which is mainly dominated by mode I fracture, the 3-ENF test results in a mode II dominant fracture. A direct consequent of mode II delamination is the presence of large shear stresses across the interface crack. In this work the friction between the cracked surfaces will be neglected, because it was observed that neglecting the friction could cause only small errors in the calculation of SERR. This is due to the fact that the 3-ENF test specimen used for the characterization of interface strength delivers a fracture mode of approximately 75-85°. The small portion of mode I, 5-15°, results in that the cracked surfaces do not have large shear contacts with each other. Consequently, the cracked surfaced could be modeled with frictionless contact elements in ANSYS to prevent element penetrations. Moreover, for a few elements near the crack tip no contact elements were used in order to avoid the calculation of nodal forces and displacement around the crack tip from being affected by the constitutive laws of contact elements. Due to these nonlinearities, the CPU time of 3-ENF model was considerably higher than that of a 4PB model. Moreover, for modeling the 4PB, it is possible to benefit from the symmetry condition by modeling only one half of the problem and

applying symmetry boundary conditions which decreases the CPU time significantly. This was not possible for the 3-ENF problem where the whole model has to be analyzed.

According to beam theory and by assuming Linear Elastic Fracture Mechanics (LEFM), the energy release rate of 3-ENF test can be found by the following formula (Asao, 1992):

$$G = \frac{3}{2}\frac{P^2 a^2}{b^2}\left[\frac{1}{t_{EMC}^3 E_{EMC} + t_{Cu}^3 E_{Cu}} - \frac{(t_{EMC}E_{EMC} + t_{Cu}E_{Cu})}{k}\right] \tag{7.31}$$

where $k = 4t_{EMC}t_{Cu}E_{EMC}E_{Cu}(t_{EMC} + t_{Cu})^2 + (t_{EMC}^2 E_{EMC} - t_{Cu}^2 E_{Cu})^2$.

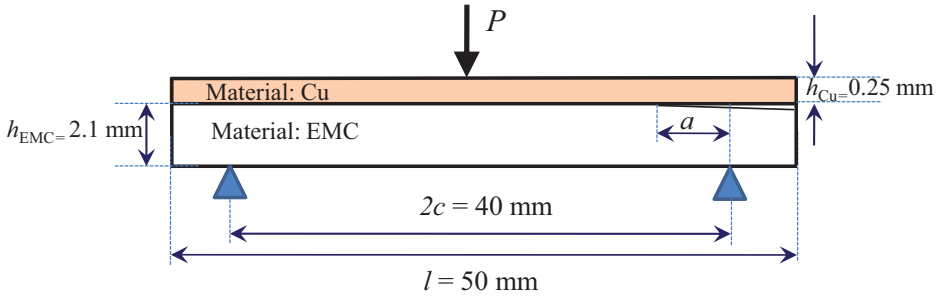

Figure 7.16 Geometry of the 3-ENF test specimen.

Among the four numerical methods suggested in the previous sections, only VCCT was applied for the 3-ENF model. This is because of the fact that the contact elements may alter the local stresses at the free edges, which may alter the total strain energy of the whole system. This may cause some numerical errors when energy-based methods such as VCE or the J-integral are used. Consequently, only VCCT was used for the 3-ENF model which showed excellent agreement with the analytical solution. For example, the VCCT method predicts for P=31N and a=10.9mm an SERR value of 40.04 J/m^2, while the analytical solution gives an SERR of 39.97 J/m^2. The successful applications of VCCT in this example together with the results and arguments from the two other examples are convincing arguments that make us believe that VCCT should be the preferred method for the calculation of the SERR. However, the main problem of VCCT for bi-material fracture is the separation of fracture modes as will be discussed in the next section.

7.6 Determination of Mode Mixity of Bimaterial Cracks

In this section a well-known numerical problem of interface cracks associated with the mode separation will be discussed. We first perform a convergence analysis of a 4PB test of the problem stated in Section 7.5.2. Without loss of generality we consider the problem in a two-dimensional FE analysis. When using the VCCT method to determine the components of the strain energy release rate, the virtual extension of the crack is determined by the length of the elements around the crack tip. In order to use the VCCT method correctly, it is required that the length of all elements across the interface at the crack tip be equal. However, a prominent problem of bimaterial

interface cracks is that, when the length of these elements in the FE meshing is changed, then the values of G components, G_{I}, G_{II} and G_{III}, also change, although the total amount of G remains constant. This problem has been observed by many researchers (*e.g.,* Sun and Qian, 1995, Hae-Soo-Oh, 2004, and Agrawal and Karlsson, 2006 and 2007). As illustrated in Fig. 7.17, the mode-separated strain energy release rates of the 4PB example of interface crack do not converge as $\Delta a \to 0$. This makes the calculation of mode mixity difficult, because it seems that mode mixity depends on the mesh size- a numerical problem that should be solved.

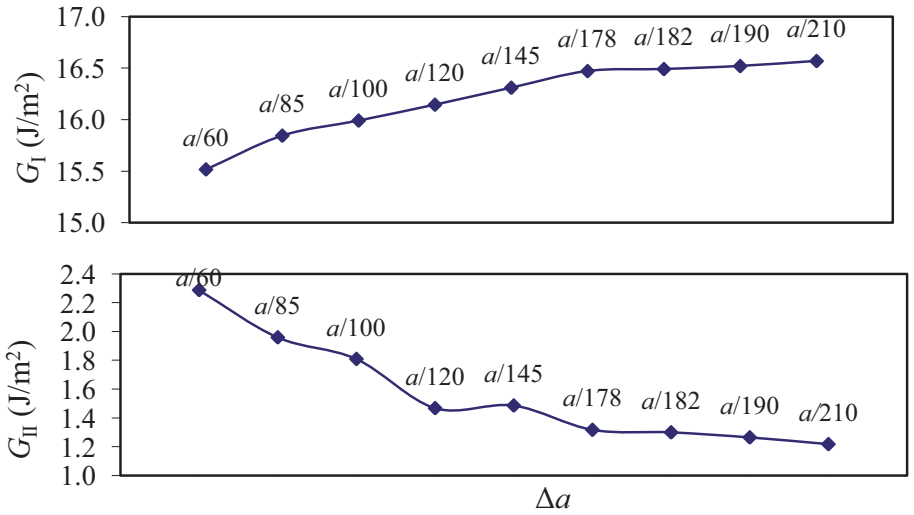

Figure 7.17 Convergence analysis: Effect of element size at crack tip (Δa) on the mode I and II values of SERR found by VCCT for a 4PB delamination test.

For a bimaterial interface crack, the solutions of the crack opening with oscillatory stress and displacement fields are given by the Eq. (7.15) and (7.19), respectively. These equations indicate that there are infinite numbers of sign changes of the normal and shear stresses as well as normal and shear displacements near the crack tip (Sun and Qian, 1997). The oscillatory zone for stress and displacement are not necessarily the same. Similarly, the oscillation zone based on the oscillatory field model and the contact zone based on the contact model are not necessarily the same (Agrawal and Karlsson, 2006). Rice (1988) proposed an elementary estimate of the contact zone as the radius of oscillation zone of displacement, which is the largest value of r for which the opening gap δ_y vanishes in the cycle of oscillation. The contact zone obtained by Rice, is very small compared to the crack size and other specimen dimensions even of large mismatch (β=0.5).

A typical way of solving the above problem is that, for bimaterial interfaces, the mode mixity is specified at a particular distance ahead of the crack tip, which is normally referred as *reference length*. Agrawal and Karlsson (2006) showed that several, apparently different, methods suggested in literature for obtaining mode mixity based on the stress intensity factors are indeed identical. However, as suggested by Beuth (1996), a Δa-independent SERR-based mode mixity can be defined by introducing a "normalizing length" parameter. It should be noted that this ref-

erence length is only a mathematical quantity with no physical meaning and is only used to enable a consistent way of reporting the mode mixity values.

It must be noted that the aforementioned problem is dependent on many factors such as geometry of the model, element types, and more importantly mismatch in the mechanical parameters (Young's modulus and Poisson's ratio) of the two dissimilar materials. Fig. 7.18 shows a convergence analysis of a 3-ENF delamination problem as introduced in Section 7.5.3. It is evident that the mode mixity for a Cu/EMC interface varies only 5 degrees when the element size is reduces to one-fifth of the initial size. This small variation in the mode mixity suggests that the variation in the mode mixity is not a major problem due to the relatively moderate β values.

An important finding of a large number of investigations of the Δa influence performed during this work can be summarized as follows: If the element size is small enough to get a convergence of the total G value, the shift of the mode mixity due to the element size is almost equal for all problems provided that the same element size is used. In other words, the results are consistent, even though a shift, whether positive or negative, in the calculated mode mixity exists.

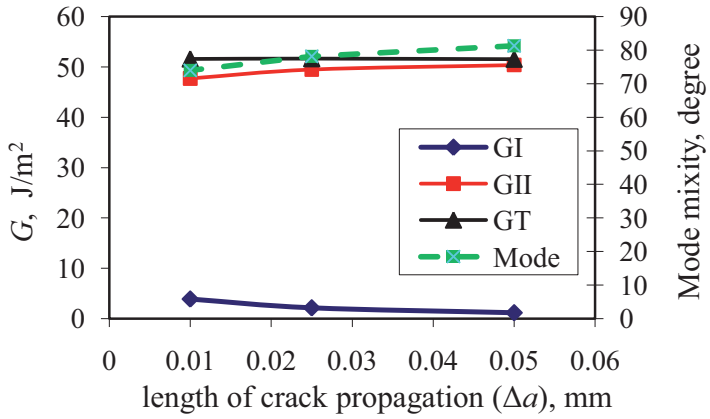

Figure 7.18 Effect of element size (Δa) on the accuracy of SERR and mode mixity values for 3-ENF delamination test.

7.7 2D *vs.* 3D FEA of Interfacial Fracture Problems

It should be noted that, generally, there is large dispute between researchers on the question as to whether the crack problem shall be treated as one of plane strain or plane stress. A major problem in numerical fracture mechanics is the relatively large degree of freedom of the FE models which causes usually long CPU times. The two-dimensional (2D) models are in many cases preferred because of less complicated modeling techniques as well as shorter computational times. Generally speaking, the problem of fracture in isotropic material, as in the CT specimen of Section 7.5.1, may be reduced to a 2D plane strain or plane stress with acceptable accuracy. Even the fracture problem of interface crack has been treated as a 2D problem in many cases. For example, Krueger and Minguet (2002) investigated the effect of a 2D assumption on the debonding

prediction of composite specimens subjected to tension and bending. They suggested that the plane stress and plane strain models provide results for skin and flange strains, as well as energy release rate, which form an upper and lower bound of the results obtained from full three-dimensional analysis. They also added that the stresses obtained from plane strain and generalized plane strain models were excessively high when compared to results from three-dimensional analysis.

Despite considerably lower computational times of 2D analyses, for the rest of this work only 3D analysis of cracks in fracture specimen will be performed. The main reasons are some uncertainties regarding the consistency of the 2D analysis when a thermo-mechanical FE simulation is applied. Since the goal of this study is the characterization of moisture driven failures, small errors in each analysis step such as moisture diffusion, viscoelasticity, and finally fracture mechanics analysis may cause some misinterpretation of the fracture results. A convincing argument on preferring a 3D fracture analysis can be deduced from Figs. 7.19 and 7.20. In these figures the thermo-mechanical stresses arising from the manufacturing process of the test specimen are implemented in the FE code. These stresses develop in the form of residual stresses as describe in Chapter4, and will be explained in Chapter 9 in more detail. The aim of these two diagrams is to present a comparison between SERR values from two and three-dimensional thermo-mechanical FE analyses. The results are normalized against the total SERR (G_T) found from a 3D thermo-mechanical analysis by using the VCCT methods. The graphs reveal that by using a 2D plane strains analysis, one would underestimate the total SERR almost 15.53% and 11.48% for 4PB and 3-ENF models, respectively. These are evidences that two-dimensional thermo-mechanical analyses for fracture problems should be avoided.

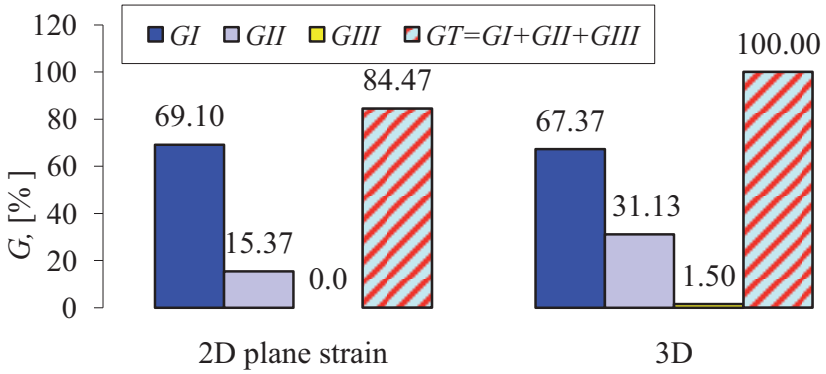

Figure 7.19 Comparison of 2D and 3D FE analyses of three components of SERR for the 4PB delamination model.

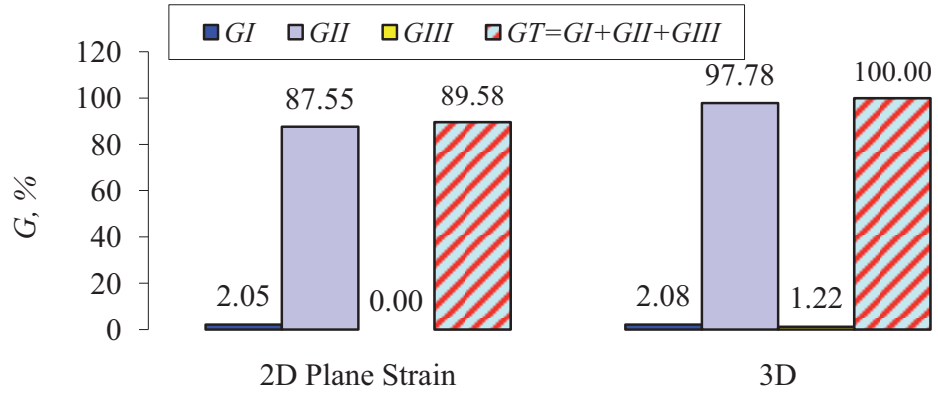

Figure 7.20 Comparison of 2D and 3D FE analyses of three components of SERR for the 3-ENF delamination model.

7.8 Conclusions

In this chapter the fundamentals of fracture in isotropic materials as well as cracks at the interface between dissimilar materials were presented. The main fracture parameter that will be used throughout this work is the strain energy release rate (G). Simply speaking, the value of G represents the amount of energy is released during the crack growth divided by the area of the new surfaces formed upon the crack propagation. There are many methods in order to determine the G values for both cracks in isotropic materials and at interfaces. For simple fracture problems, the value of G can be found by some analytical solutions, *e.g.,* from beam theory. However, in most cases, an analytical solution for the determination of G value does not exist and numerical methods should be used. The most common way of determination of G is by using the Finite Element Analysis (FEA). In this case, the problem of fracture will be first treated like a stress analysis problem. Then from the nodal values of stresses, displacement and/or strains, the value of G will be determined. Among the several methods reported and discussed in this study, the Virtual Crack Closure Technique (VCCT) is used in this work due to the following reasons:

- VCCT requires only one FE analysis and is more effective in terms of CPU and post-processing time.
- VCCT delivers the mode separated SERR values. For interface problems, mode separation is of particular concern, because the critical values of G are mode dependent.
- VCCT can be also used in three-dimensional problems and hence can deliver the mode III of SERR.
- VCCT required only the nodal stresses and displacements around the crack tip. This means that for bimaterial problems with residual stresses, the fabrication process that changes the stress state can be considered.

However, VCCT has two major drawbacks:

- The element size across the interface at the crack tip must be equal for all elements. Moreover, these elements at the crack tip must be finely meshed in order to guarantee convergence of the results. This makes the meshing of complicated models more time consuming.
- When using VCCT for fracture at interfaces, the convergence of separated modes is difficult. Consequently, a further mathematical treatment is usually required in order to solve this problem.

Despite these drawbacks, VCCT was found the superior method and will be used throughout this work for the determination of the total SERR and its components. The method was benchmarked by comparing the G values for three examples with their analytical solutions. The high accuracy of VCCT (±1% difference with analytical solution) was another reason to make this method the favorite one.

A further numerical problem arises when the fracture problem is modeled with a 2D finite element model. Although 2D models reduce the analysis time significantly, they should be avoided for the analysis of interface cracks. This is especially true, when the residual thermo-mechanical stresses are also taken into account. In this case, a 2D analysis results in G values which are neither the upper nor the lower bound of G values from 3D analysis. Depending on the materials, geometry, and fracture setup, the 2D analysis may over- or underestimate the G values, which makes the interpretation of the results very difficult. Consequently, for the rest of this work, only three dimensional analyses of the fracture models will be used, even though the numerical cost is considerably higher.

This chapter provided information on how to determine a correct value of strain energy release rate. However, a G value on its own cannot provide information if an existing crack will propagate or not. It represents only the driving force for an existing crack. In order to predict as to whether the crack will propagate, the G value must be compared against a material parameter. This material parameter is the critical value of SERR found from experimental fracture mechanics and is usually referred as *fracture toughness* denoted by G_c . A simple failure criterion for an interface crack is that, provided G exceeds G_c the existing crack will propagate, otherwise it remains fixed. To determine the interfacial fracture toughness, fracture tests must first be carried out and then the results of fracture tests should be used to determine the G_c values. Experimental fracture mechanics and the interpretation of the fracture results are very challenging and are the subjects of Chapters 8 and 9, respectively.

Chapter 8 Fracture Tests

8.1 Introduction

Interfacial adhesion between the EMC and the copper-based leadframe is one of the major concerns in the qualification of plastic packages. The characterization of adhesion between these two materials is one of the most crucial matters in electronic packaging industry. The conventional way of qualification of the EMC in the industrial sectors is using the so-called shear button tests. In this method, a conical shape of adhesive (here EMC) is molded on to the substrate (copper leadframe) and the load required to break this system is used to measure the adhesion strength. However, there are many problems associated with this method. One of the main drawbacks is that the failure locus is often not located at the interface and fracture occurs in the adhesive material close to interface. This means that the fracture load cannot be used for the measurement of adhesion. The next problem is that the adhesion results can only be measured qualitatively. In other words, these tests may help us determine which material adheres better to the substrate but the results cannot be used in FE analysis for predicting the interfacial delamination numerically. Moreover, in this chapter it will be shown that these adhesion tests may provide completely wrong answers, because there are many factors that are not considered in the analysis of adhesion by shear tests. For example material parameters such as elastic moduli of adhesive and substrate, and Poisson's ratios are not considered. Even classical experimental fracture mechanics, based on mechanical load leading to crack propagation, may not fully characterize interfacial fracture toughness, because residual stresses available in the sample are not usually considered in the analytical formulas of SERR. These stresses arise from the manufacturing process of the samples and impede or facilitate the crack progress, depending on the state of the stresses at the crack tip.

This chapter presents the experimental fracture tests performed in this work in order to characterize the interfacial fracture toughness between the EMC and leadframe. The procedure of fracture tests and their analyses will be introduced in Section 8.2. Then the delamination testing methods will be presented in Section 8.3. Since the toughness values of the interface depend on mode mixity, it is usually necessary to perform various testing methods in order to obtain the toughness

values as a function of mode angle. There are three types of testing methods that will be used: 4-Point Bending (4PB), 3-point End-Notched Flexure (3-ENF) and finally 4-point End-Notched Flexure (4-ENF). The testing methodology together with fracture results will be presented in Section 8.3.

Section 8.4 presents a methodology to determine the intrinsic interfacial fracture toughness and shows how neglecting the residual stresses may cause large errors in the determination of toughness values. The term "*apparent*" will be used, whenever the residual stresses are not considered, because in this case the calculated critical SERR values are not correct. On the contrary, the term "*intrinsic*" will be used when these stresses are considered in the analysis.

Section 8.5 presents how the combined experimental/numerical methods developed in this chapter can be applied to find the most proper EMC material for preventing the interfacial delamination in electronic packages. In Section 8.6 the effect of mode angle on the interfacial fracture toughness of Cu/EMC interface will be discussed. And finally in Section 8.7 the fracture test methods will be compared and detailed discussions will be presented.

8.2 Procedure of Fracture Tests

This section present the methodology used in this work to determine the intrinsic interfacial fracture toughness of Cu/EMC interfaces. Bimaterial Cu/EMC beams were fabricated by using the transfer molding process as presented in Chapters 3 and 4. Fig. 8.1 shows the dimensions of one of the bimaterial beams. The thickness of the copper leadframe layer (t_{Cu}) was fixed at 0.4 mm, while the thickness of EMC layer (t_{EMC}) was 1 mm for thin samples and 2.1 mm for thick samples.

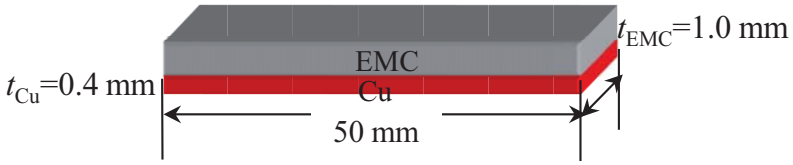

Figure 8.1 Bimaterial beam sample.

The quality of bimaterial samples plays an important role in the repeatability of the fracture test results. During this study several changes were made in the molding machine configurations, process parameters, and mold form geometry in order to fabricate suitable bimaterial samples. The quality of the adhesion at the interface was studied after each effort and if a change was necessary the process was renewed. Fig. 8.2 shows an SEM picture across the bimaterial interface between copper leadframe and the epoxy molding compound. In order to investigate the locus of fracture, samples were investigated under SEM after a few fracture tests to make sure that the locus of the crack was at the interface between the copper leadframe and the epoxy molding compound.

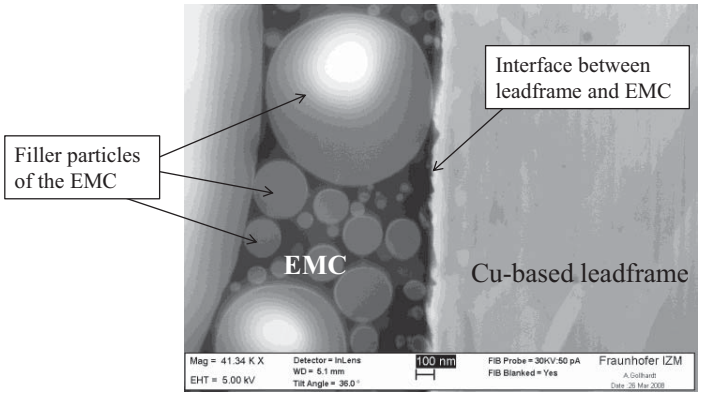

Figure 8.2 An SEM picture of the bimaterial Cu/EMC interface.

The methodology to determine the intrinsic interfacial fracture toughness used overall in this study is shown is Fig 8.3. In this diagram both experimental and numerical fracture mechanics is shown. The left part of this diagram shows the experimental part of fracture mechanics, which results in the determination of critical loads which leads to crack propagation during the fracture test. The right side of this diagram shows the numerical part of the fracture mechanics analysis. This includes primarily an FE modeling of the manufacturing process as presented in Chapter 4. Moreover, since prior to fracture tests (for 3-ENF and 4-ENF) a pre-crack is introduced at the interface of the bimaterial beam, this pre-cracking should be also modeled in the FE analysis. Finally the critical load found from experimental fracture mechanics should be applied in the model and an FE analysis should be carried out. After the FE analysis the VCCT method should be performed to determine the critical strain energy release rate (G_c).

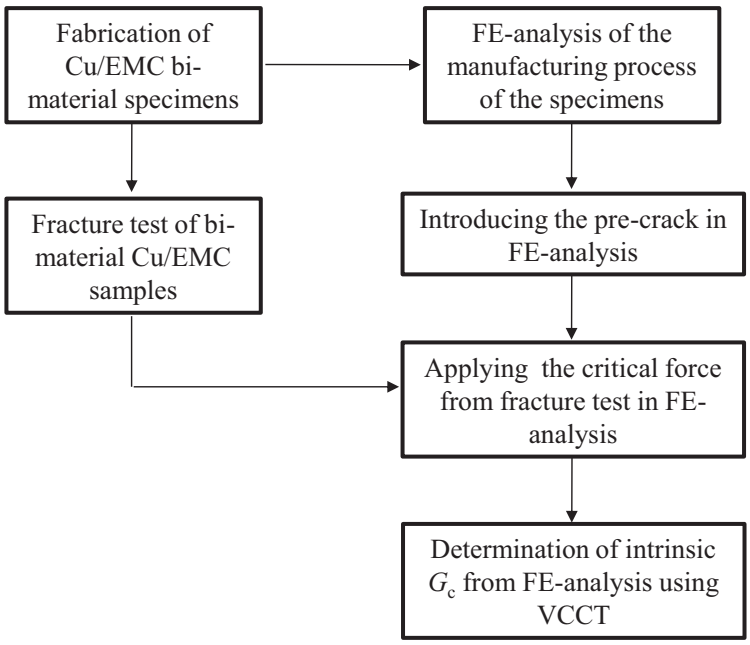

Figure 8.3 Summary of the method for the determination of intrinsic interfacial fracture toughness.

8.3 Delamination Testing Methods

8.3.1 Four-Point Bend (4PB) Delamination Test

The Four-Point Bend (4PB) delamination test was initially proposed by Charalambides *et al.* (1989) for the determination of the fracture resistance of bimaterial interfaces and is now a commonly used method to measure interfacial adhesion of thin film structures, such as semiconductor devices.

Fig. 8.4 shows a schematic picture of a 4PB setup. The bimaterial beams were placed in 4PB fixtures with adjustable inner and outer symmetrical loading pin positions. When the upper supports are moved down, bending of the samples leads to the initiation of a crack at the tip of the notch. The top layer of the EMC was carefully notched with a diamond wafering blade. The notch depth was approximately 80% of the whole thickness of the EMC.

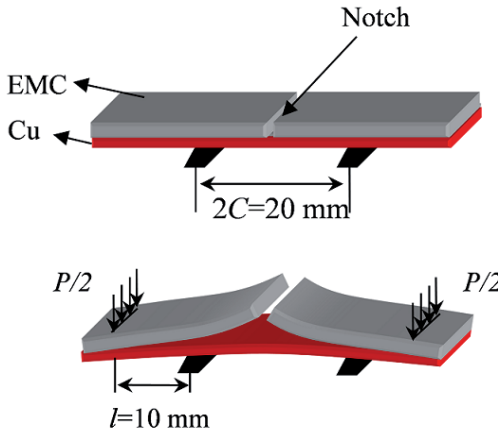

Figure 8.4 Schematic picture of a 4PB delamination test.

The nominal span between the inner and outer supports was equal to 20 mm and 40 mm, respectively. Experiments were performed using an Instron universal testing machine with a load cell of 1000 N and a temperature chamber as described in Chapter 3. A high resolution displacement gauge was used to monitor the displacements.

The strain energy release rate of 4PB delamination tests exhibits steady-state characteristics when the interfacial crack reaches a minimum length and does not exceed the distance between the inner supports ($2C$). In the absence of residual stresses, Eq. (7.30) provides the (apparent) fracture toughness, provided that the load P is substituted by the critical load P_c.

The precision of the 4PB test depends on the effects of notch depth, actuator speed, specimen geometry, and pin spacing (Shaviv *et al.,* 2005). Consequently, a large number of tests was performed in order to find out the optimum testing methodology. For the delamination tests a pressing speed of 0.1 mm/min was found suitable. This speed minimized data scattering and, more importantly, reduced the stress relaxation of the epoxy molding compounds, hence, allowed for

the assumption of linear elastic fracture mechanics. Moreover, for the tests at elevated temperatures, pressing speeds of 1-10 mm/min were used to minimize the viscoelastic effect of the EMC.

The effect of notch depth was also investigated. It was found that for a short notch depth, it was possible that the delamination did not occur symmetrically. A large notch depth was also problematic, because the vibrations during the sawing of the notch had negative influences on the interface strength by causing some micro-defects at the interface. Consequently, the notch was cut to 80% of the top EMC thickness, as also recommended by Shaviv *et al.* (2005). Moreover, the upper and lower pin distances were found to be one of the most important precision aspects of the delamination tests by 4PB method.

There are basically two factors that must be taken into considerations in order to increase the precision of the 4PB tests. First, the distance between the lower pin supports must be large enough to allow for steady-state crack propagations. Second, the distance between upper pin supports should not be too large, because in this case large displacements may be required to force the delamination propagation across the interfaces. This causes linear elastic fracture mechanics not to be applicable for such problem because of large deformations. In order to find out the optimum support distance, several FE analyses with various support distances were performed. Three aspects were of primary importance. First the copper leadframe should not be deformed plastically. Second, the strain energy release rate gained from this configuration must exceed the interfacial fracture toughness to let the crack propagate. Third, the distance between the inner supports must be large enough so that the precrack (kink from the notch to the interface) lies between these two supports. After several tests, the final distance between lower and upper supports was fixed at 20 mm and 40 mm, respectively. Despite these considerations, some local yielding may occur when the specimens are loaded. However, the critical load was found to occur in the linear elastic range of global force-displacement curve and, hence, a linear fracture mechanics model can be used to model the damage process, as was also confirmed by Zhang and Lewandowski (1997).

8.3.1.1 Single-step vs. Two-step 4PB test

In general there are two methods for measuring the critical force using the 4PB setup. The 4PB delamination test can be applied in a single-step or a two-steps way. In the former method, the whole fracture test can be performed in one step without any previous precracking requirement. Fig. 8.5 depicts the force-displacement curve of such a test.

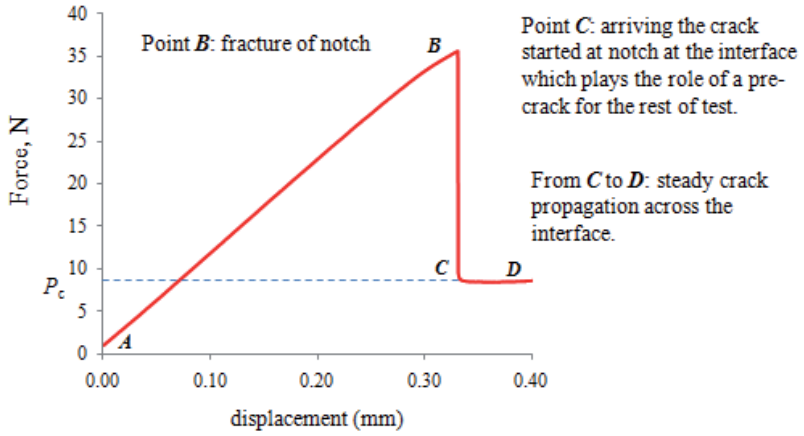

Figure 8.5 Typical load-displacement curve of a 4PB delamination test.

The slope of the linear part of the curve shown in Fig. 8.5 (point ***A*** to ***B***) corresponds to the stiffness of the whole beam. The force at point ***B*** represents the required force for fracture in the upper bulk EMC through the notch. This force is primarily a function of the shape and length of the notch and does not provide any information about the interface. When a vertical crack originated from the end of the notch formed, it moved very rapidly, reached the interface, and kinked into it (point ***C***) as the actuator ramps up the displacement. Afterwards, the crack advanced along the interface (point ***C*** to ***D***). The constant force during crack propagation (P_c) represents the critical force required to propagate the crack at the interface. Its constant value suggests that the critical energy release rate does not depend on the crack length, if a 4PB delamination test is used.

In the second method (two-steps way of 4PB), the precracking and the delamination tests were performed in two separate 4PB tests. A major prerequisite to measure the interfacial fracture toughness is introducing a sharp precrack to the interface (Huang *et al.,* 2005). First a symmetric precrack was forced to propagate from the notch along interface by means of a 4PB with the minimal inner span size of 10 mm. The sample was then loaded and, during the loading, the force-displacement curve was monitored. As soon as a decrease in the stiffness was observed, the machine was stopped. The vertical crack kinked into the interface and formed a sharp precrack at interface. After initiation of the interfacial crack, it arrested upon arriving at the inner load pins. Consequently, for all samples, a precrack length of about 10 mm was obtained. After precracking, the distance between the lower supports was increased to 20 mm and the specimens were placed into a 4PB delamination fixture again to conduct the fracture toughness measurements. Fig. 8.6 illustrates a typical curve of the 4PB delamination tests for a sample with an initial symmetric precrack. The single-step delamination test of the same sample (dotted curve) is also depicted for comparison. The slope of the linear part of the curve represents the stiffness of the whole beam, which was obviously lower for the sample with the pre-crack inside. When the sample with the precrack was loaded, the crack remained stationary up to a certain load. However, when the force reached a critical value, the crack started to advance and the reaction force reached a plateau which represented the critical force. This load was the driving force of a sta-

tionary crack to grow. It was found that the critical force found from the two-steps delamination test had the same magnitude as the critical force found from the single-step method. From the results it can be postulated that the interfacial fracture toughness found by 4PB delamination test is independent of crack length and no crack length measurement is required to determine the fracture toughness.

During all tests delamination growth was observed using a high speed camera. The images were synchronized to load and displacement data after test. The images of a few tests were later correlated using the MicroDAC software (MicroDAC, 2007) in order to find the actual crack tip position as reported by Auersperg *et al.* (2004).

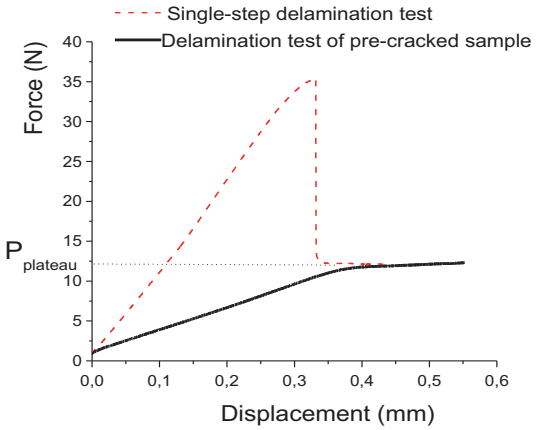

Figure 8.6 Comparison between the critical forces found from a single-step 4PB delamination test and a two-step 4PB delamination test.

In addition, some delamination tests were performed in the micro bending stage shown in Fig. 8.7. This equipment fits into the chamber of scanning electron microscopy (SEM) for in-situ delamination testing under high resolution imaging. Fig. 8.7 shows also a bimaterial sample under 4PB delamination.

A remarkable result of investigating the crack tip under SEM was that the crack tip position was not located always at the position identified by naked eye. This is of course not a major problem when the 4PB delamination testing is carried out, since a crack length measurement is not required.

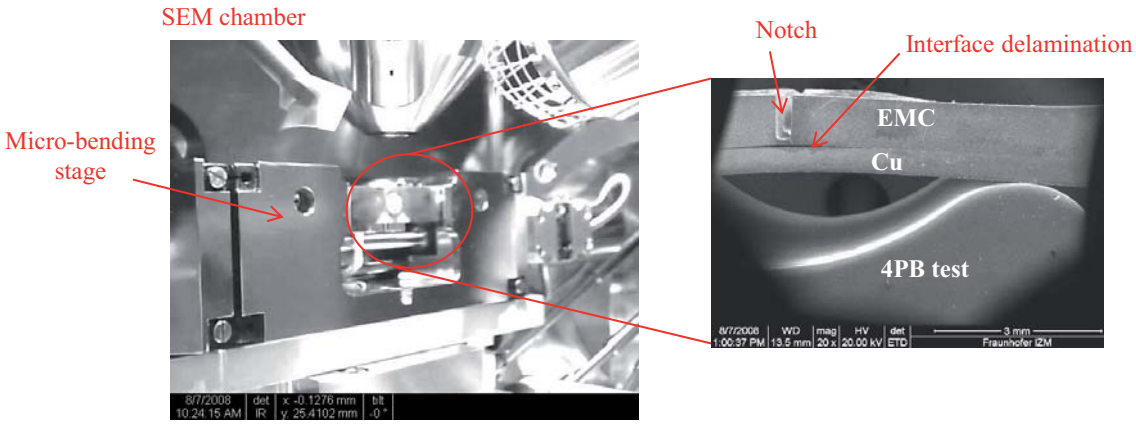

Figure 8.7 A micro bending stage in the chamber of SEM (left), SEM image during the 4PB delamination test of a bimaterial beam (right).

8.3.1.2 Symmetrical and Unsymmetrical Crack Propagation

In a conventional 4PB test, two cracks are assumed to propagate simultaneously along the beam axis direction symmetrically. The analytical solution for the strain energy release rate of such a test shown in the last chapter is also for the case of symmetrical crack growth. However, this is not always the case and in many fracture tests it is observed that only one crack starts to grow. Wang and Siegmund (2008) proposed a modified 4PB delamination test methodology that can produce crack propagation in two directions, either sequentially or simultaneously. It must be mentioned that the fracture specimens used in this work, showed in almost all cases a symmetric crack propagation for which no additional consideration is required. The good repeatability in the fracture tests is mostly due to the high stiffness of the copper substrate which makes small misalignments in the system not have big influences on the fracture results. The second reason for symmetric crack propagation was an accurately defined pre-notch, which was introduced by a precise diamond wafering blade. Fig. 8.8 shows a typical 4PB delamination test of bimaterial Cu/EMC samples (half of the beam). The symmetric crack propagation and the position of crack tip at the interface can be observed in these pictures.

Fig. 8.9a shows a bimaterial sample with a notch in the EMC layer before and after a 4PB delamination test. As shown in these pictures, after the delamination test the leadframe remains straight, indicating that it did not undergo any macroscopic plastic deformation. Fig 8.9b shows a SAM picture of the same bimaterial sample after the 4PB delamination test. The sample was immersed in water and the picture was taken from the leadframe side of the sample. The bright region indicates the delaminated areas. It can be seen that the delamination was completely symmetrical, which is an important factor for accurate fracture toughness measurements. Moreover, the crack front is not straight, which is an indication of residual stresses in the sample.

Another important observation is that the crack has arrested when it reached the position of inners supports.

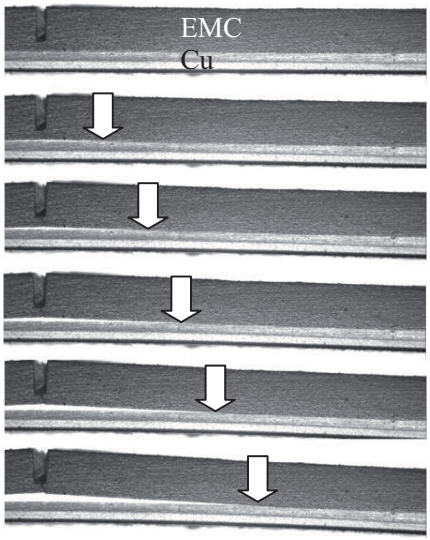

Figure 8.8 Symmetric crack propagation of bimaterial sample in a 4PB delamination test, the arrows indicate the position of the crack tip.

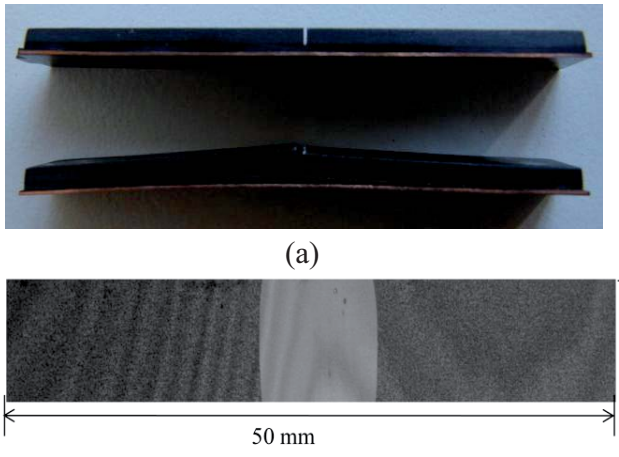

(a)

(b)

Figure 8.9 (a) A bimaterial Cu/EMC sample before and after a 4PB delamination test. (b) SAM picture of the bimaterial beam after a 4PB delamination test.

8.3.1.3 Fracture Test of Sandwich Specimens

Before producing bimaterial Cu/EMC beam structures, it was attempted to produce sandwich Cu/EMC/Cu structures in order to investigate the interfacial fracture toughness. This was primarily due to the fact that the bimaterial structures exhibit large beam deflection (warpage) due to the residual stresses. In contrast to bimaterial beams, sandwich structures do not exhibit any warpage due to asymmetric conditions. A sandwich structure is a three-layer structure consisting of a low

density and low modulus core material (here EMC) between two high modulus face sheets (Cu leadframe). This arrangement provides a structure with a high bending stiffness (Østergaard *et al.,* 2007). Suo and Hutchinson (1989) analyzed sandwich specimens with core layer thicknesses much smaller than that of the sheet layers. They found that for moderate stiffness mismatch, the difference between the mode mixity of the sandwich and the homogeneous specimen (*i.e.,* without the thin core layer) was relatively small.

A major advantage of the Cu/EMC/Cu sandwich structure is that the stiffness of the structure is higher than that of the Cu/EMC bimaterial structure. In a 4PB test of a sandwich structure, the stiffening layer suppresses the segmentation of the brittle layer and increases the stored energy in the layer and therefore the driving force for the delamination (Hofinger *et al.,* 1998). A notch must be machined through the stiffening Cu leadframe and the EMC similar to that explained in the previous section.

Fig 8.10 shows a schematic picture of the 4PB test of sandwich structures. In Fig. 8.11 the crack propagation across the interface is shown at some interval after the initiation of the fracture test. The fracture tests exhibited symmetric crack propagation almost in all of tests that were performed. The scatter of data for the successful tests was generally much smaller than that for bimaterial specimens. However, the number of unsuccessful fracture tests was relatively high. This was mainly due to problems associated with the manufacturing of sandwich samples. Due to the asymmetric shape of these samples, the specimens exhibited no warpage, which increased the residual stresses in the sample considerably. Also the molding process of these samples was much more complicated than that of bimaterial specimens. The adhesion of the upper Cu layer to the EMC was generally weaker than that of the lower Cu layer, which is associated with distribution of mold pressure during the transfer molding process.

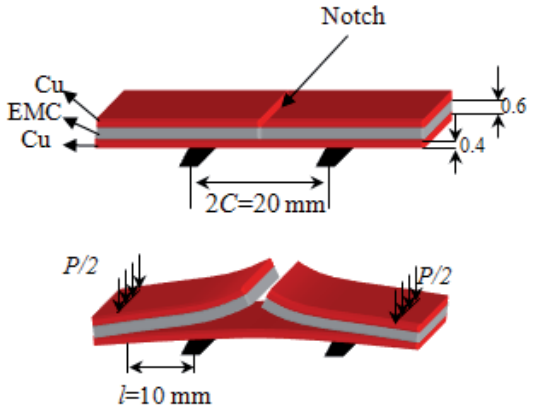

Figure 8.10 Schematic picture of the 4PB delamination test of a sandwich Cu/EMC/Cu specimen.

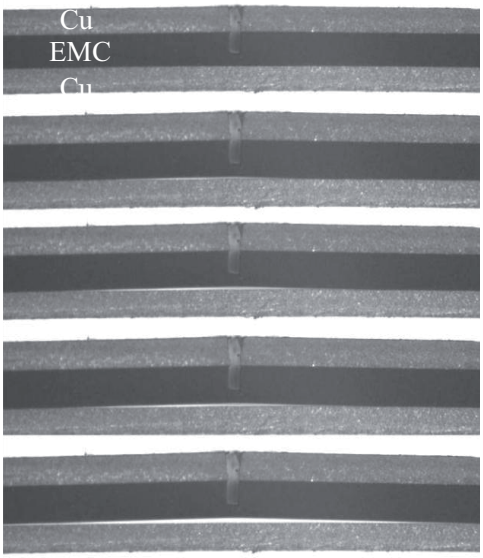

Figure 8.11 Symmetric crack propagation in a sandwich specimen during a 4PB delamination test.

Fig 8.12 shows a SAM picture of a sandwich specimen after a 4PB test. A significant problem associated with the fracture of sandwich specimens is that the crack front does not exhibit a linear shape as shown in Fig.8.12. The main reason for this unusual crack shape is the presence of residual stresses that stem from cure shrinkage of EMC and CTE mismatch between Cu and EMC during the cooling process as explained in Chapter 4. For a bimaterial beam the specimen is free to bend and these stresses induce warpage. For sandwich specimens, however, the sample is not allowed to bend due to symmetric condition and hence the interface is under multi-axial stresses. Moreover, there were other problems regarding the fabrication costs that made the sandwich specimens unfavorable. While the fabrication time for a bimaterial specimen was approximately five minutes per sample, a sandwich specimen took on average 15 minutes. The main reason was the required time to position the upper and lower leadframes in the mold frame. Especially for the positioning of the upper layer a vacuum machine was required in order to prevent it from dropping in to the mold cavity. These problems made the number of unsuccessful sample productions much larger than that for the bimaterial samples. For example almost every second sandwich samples was inappropriate for a subsequent fracture test due to manufacturing problems, such as mold flake, lack of adhesion, sliding of leadframe in the cavity, and adhering of the specimen to the mold frame. Moreover, the bimaterial specimens are more appropriate for the investigation of moisture effect on the interfacial adhesion. Since the copper leadframes are impermeable to moisture, sandwich specimens do not allow for the determination of intrinsic adhesion loss and let moisture diffuse through the interface path only, which leads to a gradient of moisture concentration across the interface. These are all convincing arguments that bimaterial samples should be preferred because they are easier to manufacture, less complex, and more appropriate for the purpose of a study regarding the effect of moisture.

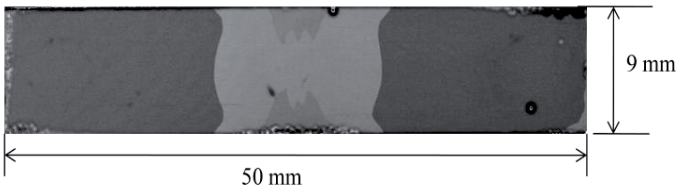

Figure 8.12 SAM picture of a sandwich Cu/EMC/Cu specimen after a 4PB delamination test.

8.3.2 Three-Point End Notched Flexure (3-ENF) Delamination Test

Since the interfacial fracture toughness is a mode-dependent parameter, two other test methods were performed to investigate the effect of mode angle on the toughness values. The End-Notched Flexure (ENF) test has been widely used to characterize the mode II fracture toughness (Schuecker and Davidson, 2000, Morais, 2004, Yoshihara, 2007, Davidson and Sun, 2005). Since there are two types of ENF tests, as will be discussed in this section, we will distinguish between these two testing methods by using the term 3-ENF for a three-point flexure and 4-ENF for a four-point flexure, respectively. A typical 3-ENF testing setup for the bimaterial interface is essentially a three-point bend (3PB) test with an initial crack of length *a* at one end of the beam as shown on Fig. 8.13. Since the upper layer undergoes a larger deflection, the sample was positioned with the copper side facing up.

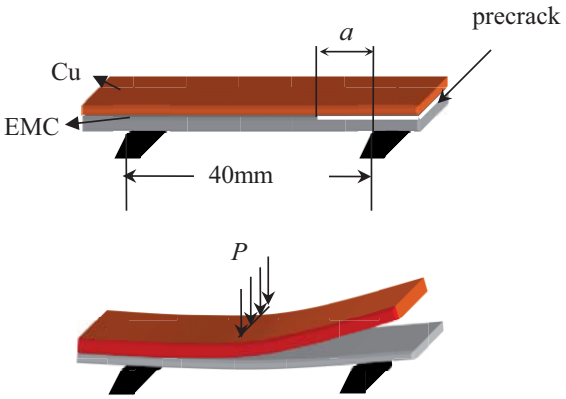

Figure 8.13 Schematic picture of a 3-ENF delamination test.

A typical load-displacement curve of a 3-ENF test is shown in Fig. 8.14. For performing each test the specimen was placed on the lower supports. Then the upper support was moved down manually and positioned just above the specimen. Next the loading was initiated and the displacement was read off upon reaching a preload of 1 N (point **A**). At the early stages of the application of the load (point **A** to **B**), a linear relation between force and displacement can be observed. The slope of the curve at this stage represents the bending stiffness of the composite Cu/EMC structure. The peak of the load profile corresponds to the critical force and the initiation of the interfacial delamination. This force will be used later as the critical load in the finite element analysis. After reaching the peak load (point **B**) the delamination propagates until it stops at a point (point **C**). After the crack propagation arrests at point **C** the load increases again linearly.

For each test condition, between four to eight specimens were used, and each peak load with its corresponding precrack length was used for a separate finite element calculation to measure the interfacial fracture toughness as will be discussed in next section.

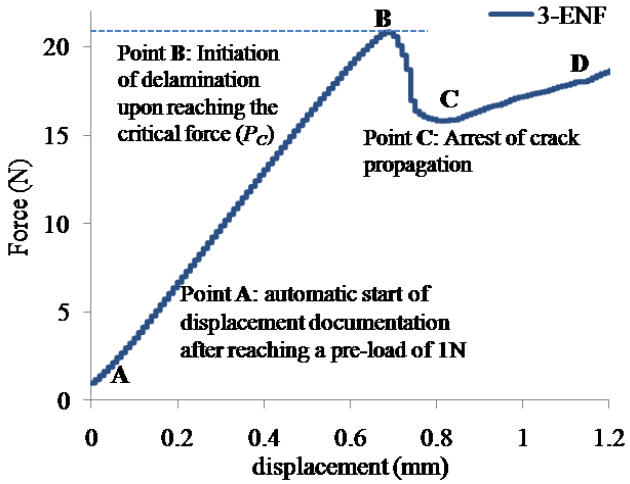

Figure 8.14 Typical load-displacement curve a 3-ENF delamination test.

In contrast to 4PB, the 3-ENF and 4-ENF delamination tests require a precrack before the fracture test can begin. Prior to fabrication of 3-ENF bimaterial samples, precracking was facilitated by coating the desired area of the leadframe with a special spray used as release agent to prevent the leadframe from adhering to the molding compound during the molding process. The adhesion at this area was weak. Hence this area was later used to generate a pre-crack by using the apparatus shown in Fig. 8.15. The sample was positioned vertically underneath the razor blade and a small load from the dropping of a weight made the desired precracking without damaging other parts of the beam. After the delamination test, there was a visible trace on the region of the copper leadframe which was pre-cracked and the precrack length was measured by using a ruler. Furthermore, the precrack length was verified for a few samples by C-mode scanning acoustic microscopy as shown in Fig. 8.16.

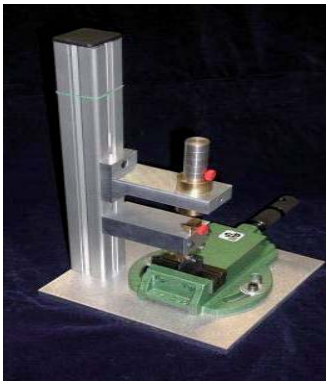

Figure 8.15 Apparatus which was used to generate a sharp precrack for a 3-ENF test.

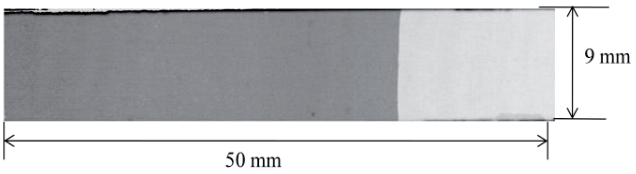

Figure 8.16 SAM picture of a bimaterial Cu/EMC specimen after a 3-ENF delamination test.

8.3.3 Four-Point End Notched Flexure (4-ENF) Delamination Test

The Four-Point Bend End Notched Flexure (4-ENF) test is also used to determine the mode II interfacial fracture toughness of laminated composites. The schematic picture of this test is shown in Fig. 8.17. The 3-ENF test has been used more extensively in the past, but the 4-ENF test is gaining more popularity in recent years due to the stable nature of crack growth. However, many observations have indicated potential errors with the 4-ENF test (Davidson and Sun, 2005). For example, 4-ENF tests produce G_{IIc} values that are typically larger than those obtained by the 3-ENF (Davidson and Sun, 2005, Yoshihara, 2007).

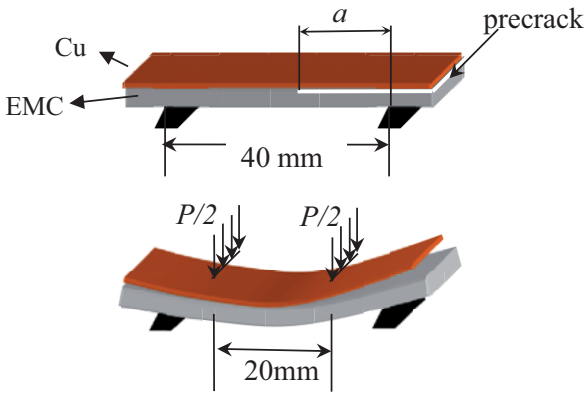

Figure 8.17 Schematic picture of a 4-ENF delamination test.

The load-displacement curve of the 4-ENF delamination test manifests the same behavior as the 3-ENF test. The peak load in the diagram is the critical load to crack propagation and is used for the characterization of fracture toughness.

8.4 Determination of the Intrinsic Interfacial Fracture Toughness

This section presents a complete overview of the problems associated with the fracture toughness of polymer/metal interfaces. As discussed in Chapter 4, polymeric materials undergo dimensional changes during their manufacturing and in-service life. In the absence of moisture, two important phenomena should be considered in order to model the behavior of a polymer/metal interface correctly. Both the cure shrinkage of the polymer during the polymerization and the mismatch between the CTE values of polymer and metal should be taken into account. This section discusses the important effect of these two factors on a correct estimation of the interfacial fracture

toughness. In order to distinguish between the fracture toughness values used conventionally and the approach suggested in this work, the following terminology will be used. If the value of interfacial fracture toughness is found directly from the mechanical load which leads to crack propagation without considering the residual stresses, then the term *apparent* interfacial fracture toughness will be used. However, if the residual stresses in the sample are also included in the FE analysis, then the term *intrinsic* interfacial fracture toughness will be used, because only in this way the "correct" value of fracture toughness can be determined.

In contrast to the effect of cure shrinkage on the apparent interfacial fracture toughness of polymer/metal samples, the effect of thermal residual stresses has been discussed widely in the literature. In one of these works, Yao and Qu (1999) measured the apparent fracture toughness of the interfaces of several epoxy based underfill adhesives and aluminum substrate experimentally. The measurements were correlated to different levels of interface thermal residual stresses resulted from the CTE mismatch of underfill and aluminum. They found that thermal residual stress plays a considerably detrimental role in the apparent interfacial toughness and added that the effect of the elastic modulus changes associated with the change of CTE may be insignificant. However, in their work, the effect of cure shrinkage was not taken into account. Roham and Hight (2006) studied the role of residual stresses in the competition between deflection and penetration energy release rate of bimaterial interfaces. Their study showed that when including residual stress in a film, the outcome depends on whether this residual stress is compressive or tensile. They suggested that compressive stresses tend to deflect the crack at the interface and the opposite is true for tensile stresses.

In order to capture the intrinsic interfacial fracture toughness of Cu/EMC interface, 3D finite element models of the fracture specimens were built with eight-node elements using the FEM tool ANSYS. The residual stresses during the manufacturing process of the samples were taken into account as follows: First the chemical cure shrinkage during the molding process was introduced in the FEA model as discussed in Chapter 4. Then the cooling process from the mold temperature (175°C) to room temperature (25°C) was taken into account. Later, the introduction of a precrack, which leads to some stress relaxations in the sample, was modeled by decoupling the selected nodes at the interface. Contact elements without friction were used for the cracked areas to avoid element penetrations (only for 3-ENFand 4-ENF). Finally, the force and the corresponding crack length found from the experimental results were applied.

Based on the results of the nodal forces and displacement obtained from the finite element analysis, the Virtual Crack Closure Technique (VCCT) was used to estimate the interfacial fracture toughness. This method was benchmarked in Chapter 7 by comparing the strain energy release rate found from VCCT with that found from analytical solution of 4PB and 3-ENF tests. It was shown that VCCT delivers SERR values which are within 1% difference compared to the analytical solution. However, the analytical solution cannot be used to determine the intrinsic toughness values, because the effects of cure and thermal residual stresses are not considered in the analytical solutions. The advantage of VCCT is that it is a post-processing method and if the FE analysis considers the residual stresses, then VCCT will deliver the intrinsic toughness values.

Since VCCT is only applicable for the case of Linear Elastic Fracture Mechanics (LEFM), it may be questionable if this approach would be suitable for the interface crack between the copper leadframe and the viscoelastic EMC. However, LEFM can be assumed to hold true, because as shown in load-displacement curves of all three fracture tests, a linear relation between the reaction forces and applied displacement up to the delamination point was always observed. Moreover, no plastic deformation was observed in the copper leadframe after the delamination tests. A more satisfactory reason to consider LEFM a true assumption for the fracture tests, is that the fracture tests were all performed with a relatively high displacement rate of 0.1 mm/min for room temperature and above 1.0 mm/min for higher temperatures. The crack propagation happened always within a couple of seconds after starting the test and took normally less than one second until the crack was arrested at the outer supports. The viscoelastic effect due to the stress relaxation within such short crack propagation time and especially at room temperature was found to be almost negligible. Consequently, the material model for EMC was assumed viscoelastic, however linear elastic fracture mechanics was assumed during the crack propagation.

Fig. 8.18 shows the influence of residual stresses on the apparent interfacial fracture toughness for a 3-ENF test (dry sample at room temperature, P=31 N, a=10.9 mm, EMC material: **MC-1**). If only the mechanical load is considered, the total value of G found by VCCT (40.04 J/m^2) agrees very well with G from the analytical formula (39.97 J/m^2), which is the verification of the FEA-based VCCT approach. If the thermal stresses (arising from the CTE-mismatch between EMC and leadframe which induces a warpage because of higher leadframe shrinkage by cooling from mold temperature to room temperature) are considered, the apparent toughness values is 30.02 J/m^2 as shown in the middle of Fig. 8.18. However, considering only thermal residual stresses may even cause more errors, because in this case the warpage of the bimaterial beam will be predicted incorrectly.

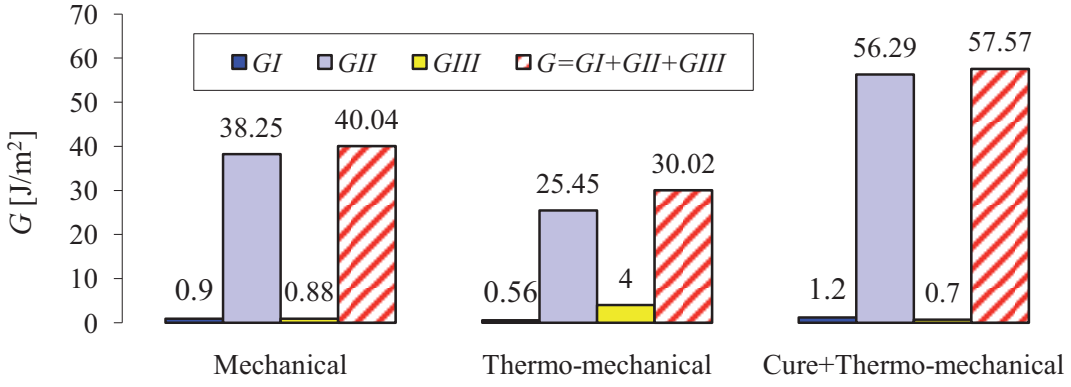

Figure 8.18 Effect of cure and thermal residual stresses on the apparent interfacial fracture toughness of a 3-ENF delamination test.

The correct way to determine the intrinsic toughness values is by considering both thermal and cure stresses as shown in the right part of Fig. 8.18 (57.57 J/m^2). These results suggest that using the analytical solutions or only consideration of the thermal stresses for the calculation of SERR

can cause errors. Compressive stresses in general impede the crack propagation while tensile stresses facilitate it. Hence, if these stresses are modeled incorrectly in the FE analysis, then the determination of energy release rate will be incorrect.

Another example for the effect of residual stresses is the fracture toughness analysis of a 4PB delamination test. The effects of both cure and thermal stresses on the apparent fracture toughness of a 4PB test are shown in Fig. 8.19. These are the toughness values found by different approaches for a 4PB delamination test that delivered a critical force of (P_c=11 N for a bimaterial sample (**MC-1** thickness =1 mm). As shown in this picture, neglecting the residual stresses would lead to underestimation of toughness values. The mechanical and thermo-mechanical analyses result in apparent toughness values of 23.51 and 22.57 J/m^2, respectively. However, the complete analysis (cure + thermo-mechanical) gives the intrinsic toughness value of 30.73 J/m^2. This difference is due to residual stresses that contribute to the stored energy in the specimen. Therefore, for the rest of this work, sample history including both cure shrinkage and thermal stresses will be considered.

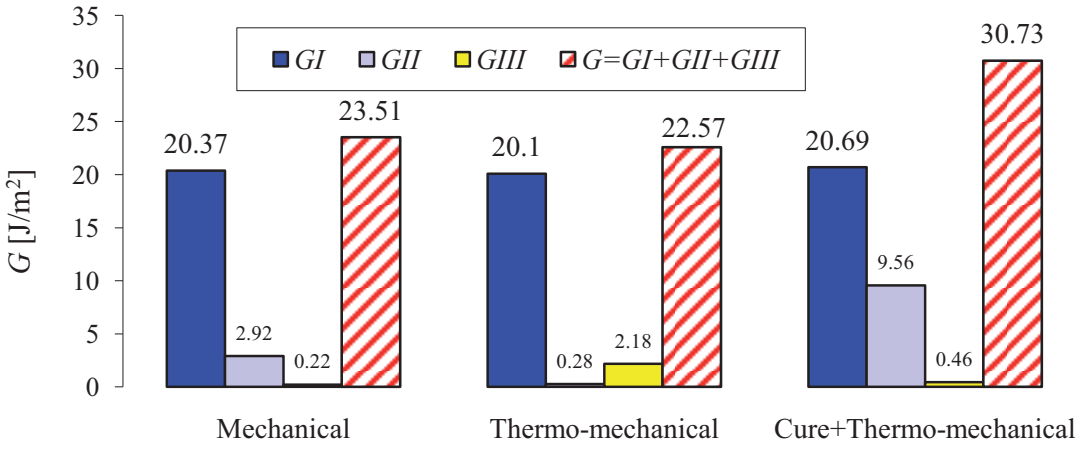

Figure 8.19 Effect of cure- and thermo-mechanical stresses on the apparent interfacial fracture toughness of a 4PB delamination test.

One advantage of VCCT in comparison to other methods for estimation of SERR is that it is possible to find the distribution of SERR across the width of specimen. A plot of the distribution of the energy release rate across the width of a 4PB specimen is shown in Fig. 8.20. As shown in this picture, the local SERR value at in the middle of the specimen is higher than at the corners. This explains the concave shape of the crack front and the reason why the crack in the middle of the specimen is longer than other parts.

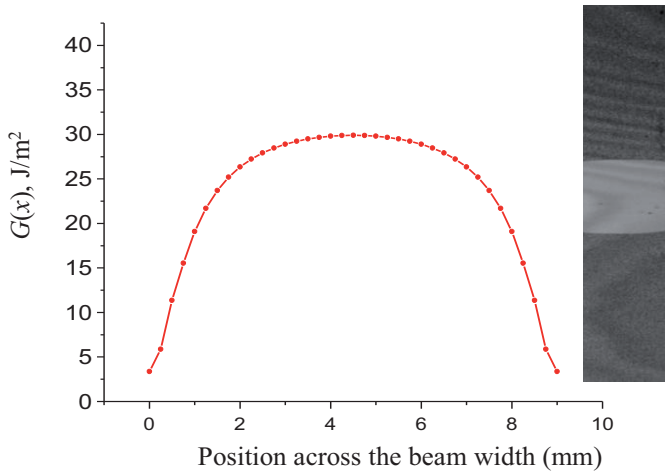

Figure 8.20 Distribution of the SERR (G) across the width of a bimaterial beam during a 4PB delamination test. This distribution agrees with the shape of the crack found.

8.5 Experimental and Numerical Fracture Mechanics to Select a Proper EMC

Interfacial adhesion between the epoxy molding compound and the copper-based leadframe is one of the major concerns in the qualification of plastic IC packages. Generally, there are two different ways of characterization of the interfacial adhesion. First, the strength of interface can be qualified based on stress analysis. In this method, the quality of interface can be measured in terms of adhesion strength by shear test, lap shear test, etc. The second method for qualification tests of interfaces is based on the fracture-mechanics approach. Although the first method is simpler to carry out, it is generally known that the interfacial fracture toughness determined from the fracture mechanics approach is more accurate and reliable than adhesion strength analysis (Park *et al.*, 2007, Loo *et al.*, 2007, van Driel *et al.*, 2005). The aim of this section is to propose an effective selection criterion for finding the most suitable epoxy molding compound in terms of the intrinsic interfacial adhesion.

Three different epoxy molding compounds introduced in Chapter 3 (**MC-1**, **MC-2**, and **MC-3**) were nominated to find the best one for adhering to a particular leadframe. In order to measure the adhesion of each epoxy molding compound, five bimaterial samples of each Cu/EMC structure were used for the fracture test using the 4-ENF test. Fig. 8.21 shows the load-displacement curve of four Cu/**MC-1** samples. The advantage of the 4-ENF test is that the crack propagation is stable and the scatter of fracture results is smaller than 4PB and 3-ENF delamination test.

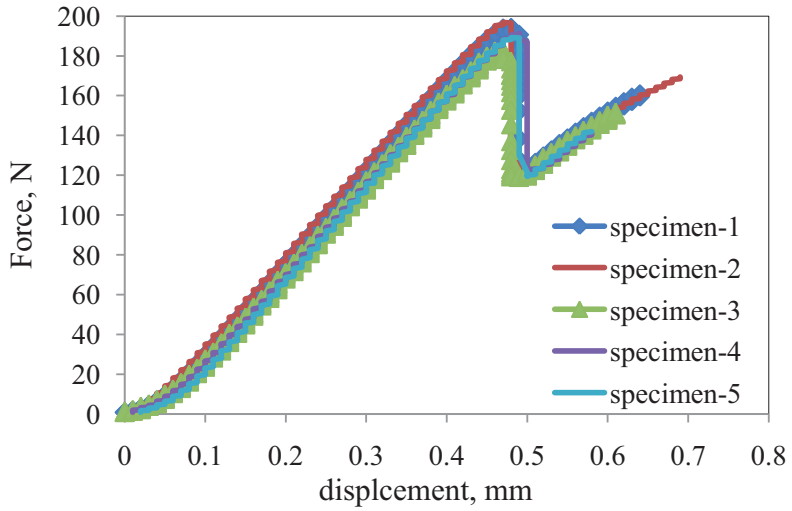

Figure 8.21 Load-displacement curves of five Cu/EMC samples (molding compound: **MC-1**) in a 4-ENF delamination test.

The peak point in the load-displacement of a 4-ENF test represents the required load for the propagation of crack across the interface. This force leads to the interface delamination and its value is demonstrated for each of samples with different EMCs in Fig. 8.22. The scatter of the maximum loads was within 10 % of the average value, which shows the good repeatability of the fracture tests. This suggests that the 4-ENF is a quite stable characterization method and can be used instead of the conventional 3-ENF testing method, if only a qualitative comparison between the EMC materials is needed. However, if the fracture results are desired to be used later for the analysis of the interface delamination in a package, where an exact value of G_c is required, 3-ENF testing method provides more reliable fracture toughness results and should be preferred as will be discussed in the next section.

Based on critical load analysis, the molding compound material that provides the highest strength against interface fracture is **MC-3** because it shows an average critical load of 230.83 N, which is slightly higher than **MC-1** (229.9 N) and considerably higher than **MC-2** (159.42 N). This interpretation is similar to adhesion analysis based on shear tests, which qualifies the EMC materials based on the fracture load in the shear test. However, the main drawback of these shear tests is that a higher fracture load does not necessarily mean that the adhesion between the EMC and leadframe is better. In the following, the intrinsic fracture toughness of these samples will be calculated and will be shown that based on these values, a successful EMC material is not the one with higher fracture load.

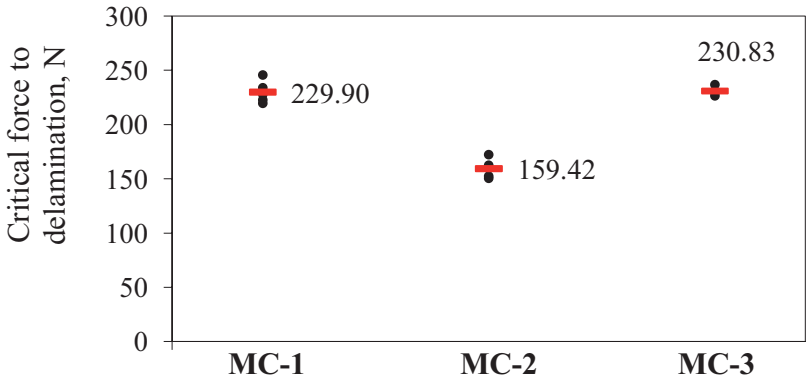

Figure 8.22 Critical loads leading to the interface delamination for three EMC materials on a copper leadframe using 4-ENF delamination test.

In order to find the fracture toughness results, the critical forces for each EMC material in Fig. 8.22 were used for three-dimensional FE analyses. The viscoelastic material characterization and cure and CTE measurements are introduced in Chapter 3. Fig. 8.23 summarizes the interfacial fracture toughness (G_c) results of the copper/EMC interface for all three types of epoxy molding compounds. The mechanical analysis of the fracture toughness shown in Fig. 8.23 means that the fracture toughness value was determined by considering only the maximum force leading to the crack propagation (*apparent* interfacial fracture toughness). The results of the mechanical analysis manifest the same trend as the critical loads in Fig. 8.22. This means that a material with a higher critical force in the fracture test, results in apparently higher fracture toughness if only the critical load is considered. However, there are two fundamental disadvantages if the cure- and thermo-mechanical stresses are not considered in the analysis of the fracture toughness results. First, as shown in Fig. 8.23 the amount of interfacial fracture toughness was underestimated when the residual stresses were not considered in the case of 4-ENF fracture tests. Second, when fracture mechanics is applied to qualify a superior molding compound among various available EMC materials, neglecting the residual stresses in the FE models, may cause a totally wrong EMC selection. As shown in Fig. 8.23 the fracture results analyzed by considering only the mechanical load suggest that **MC-1** and **MC-3** have equally a stronger adhesion (higher *apparent* interfacial fracture toughness) than **MC-2**. Considering the warpage results of Chapter 3, it is well obvious that the **MC-3** undergoes lower residual stresses at room temperature comparing to **MC-1**, meaning that the force required to bring the specimen **Cu/MC-1** to the flat condition is larger than that for the **Cu/MC-2** sample. When the total process induced (cure + thermo-mechanical) stresses were considered in the second analysis, it was revealed that the *intrinsic* interfacial fracture toughness of the material **MC-1** is much higher than the other two materials, suggesting that if adhesion is of major concern, the material **MC-1** is the successful candidate to fulfill the packaging requirements.

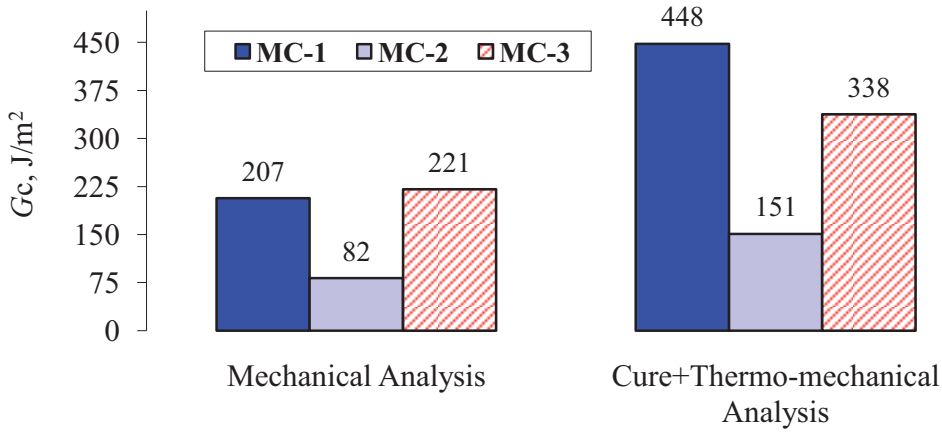

Figure 8.23 *Apparent* interfacial fracture toughness (using mechanical load only) *vs. intrinsic* interfacial fracture toughness (using cure & thermo-mechanical FEA).

The direct conclusion of this section is that if an EMC material is going to be nominated among other ones for a better adhesion performance, a fracture mechanics analysis on its own is not sufficient and the fracture results must be complemented by correct material data. The main reason is that, not all of the measured force during a fracture test leads to the crack propagation along the interface. Some portions of the measured forces act against the residual stresses arising from the manufacturing of the samples. A simple glance at the warpage results shown in Chapter 3 reveals that more energy is needed to overcome the initial positive warpage of the bi-material beam **Cu/MC-1** prior to the fracture tests, compared to the beam **Cu/MC-2**.

8.6 Effect of Mode Mixity

A crack at an interface is subjected to mixed mode conditions and propagates in mixed mode while the preferred fracture path is at the interface. Mode mixity is the relative proportion of tractions ahead of the crack tip in mode II and mode I fracture. Typically, the total fracture toughness depends on the mode mixity and it increases as the contribution of the mode II fracture increases. Fig 8.24 shows the influence of mode angle on the interfacial fracture toughness. The scatter of results together with the average value of each test is also shown. The 4PB test measures the mixed mode interfacial fracture toughness with mode I fracture dominating. However, the 3-ENF test measures the interfacial fracture toughness close to mode II fracture. The toughness values from the 4-ENF tests are not depicted in this figure. This is due to the fact that the 4-ENF does not provide the quantity of G_c correctly and results in large toughness values due to friction between substrate and adhesive.

For the calculation of mode mixity (mode angle) the method proposed by Beuth (1996) was used. A MATLAB routine was written in order to calculate the Δa-independent mode mixity from G_{Ic}, G_{IIc}, and G_{IIIc} found by using VCCT. It can be concluded that the interface strength with respect to shear loading is greater than its strength with respect to tensile loading.

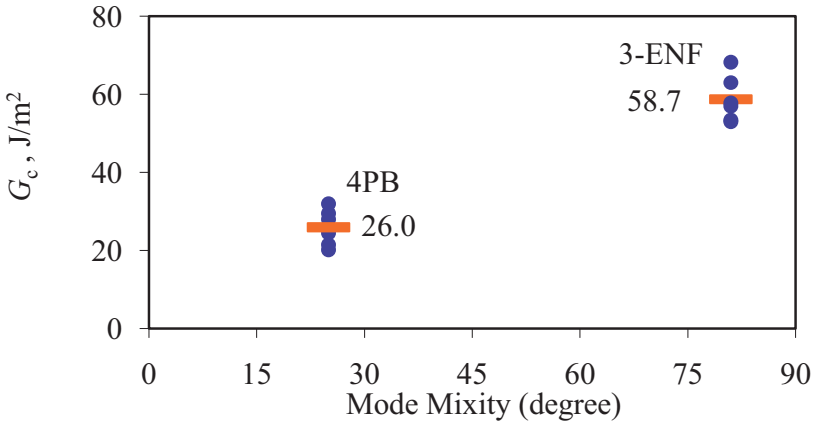

Figure 8.24 Effect of mode angle on the interfacial fracture toughness of Cu/EMC (mold compound: **MC-1**) interface.

The effect of mode mixity on the interfacial fracture toughness has been widely investigated. For instance, Liechti and Chai (1991) proposed a method to establish the range of in-plane fracture mode mixity and contact zone that can be obtained from bimaterial samples. They measured the crack opening displacement and matched the obtained values with finite element solutions to extract the mixed mode fracture parameters. They obtained interfacial fracture energy as a function of mode mixture as shown in Fig 8.25. This figure shows the interfacial fracture toughness curve obtained for an epoxy/glass interface for two different lengths scale and for two different roughness λ of the glass surface. These results and those found by Liu *et al.* (1995) are all in agreement with those found in this work and it can be generally concluded that the fracture toughness of interfaces is mode dependent, with interfaces being tougher against the mode II fracture than mode I.

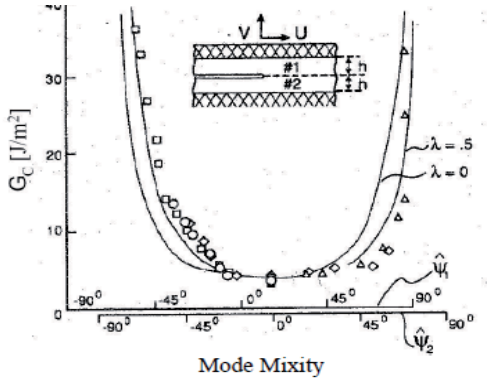

Figure 8.25 Interfacial fracture toughness as a function of mode mixity for an epoxy/glass interface (Liechti and Chai, 1991).

8.7 Discussion on Fracture Tests

As observed in Section 8.5, although both 3-ENF and 4-ENF testing methods provide toughness values of mode II, fracture tests showed that the 4-ENF results in generally a higher toughness values compared to 3-ENF. Schuecker and Davidson (2000) used VCCT to analyze the 3-ENF and 4-ENF tests, and showed that by using the typical test setup the effect of frictional force in the 4-ENF test is more significant than that in the typical 3-ENF. Davidson and Sun (2005) examined the effect of friction on 3-ENF and 4-ENF and suggested that the effects of geometric nonlinearities and friction of rollers on the SERR increase with decreasing outer span length, increasing roller diameter, and increasing friction coefficient. They used a "direct compliance calibration" technique, which allows the perceived toughness to be recreated by FE simulation. In this method, the compliance C of the pre-cracked 4-ENF test specimens is measured against the crack length a and fitted to a linear relation. The derivate of the compliance curve $m=\partial C/\partial a$ is calculated and by using the critical load P_c at onset of fracture, the G_{IIc} is calculated from $G_{IIc}^{4\text{-ENF}} = P_c^2 m/2B$, where B is the width of the test specimen. The numerical results were found to be always higher than those from other researchers and they recommended that 4-ENF tests should be conducted with stiff fixtures and a small span length. Fan and Ben (2007) studied the role of friction surfaces during the delamination in the measurement of delamination resistance of fiber-reinforced composites. Based on the results for the frictional force effect they concluded that the frictional force between the contact surfaces cannot be fully responsible for the inconsistence of the delamination resistance determined by using 3-ENF and 4-ENF tests and other factors, such as fiber-bridging, may also play a significant role in the inconsistence. Recently, Yoshihara (2008) proposed a "data reduction method" using the strain at the crack-free portion for the 4-ENF test specimen to obtain a relation between the mode II energy release rate and crack length. It was suggested that the 4-ENF test should be conducted under a large span length with reducing the frictional forces between the crack surfaces. Shindo *et al.* (2008) studied the mode II interlaminar fracture and damage behavior of fiber-reinforced polymers by beam theory and finite element solutions to generate results of G_{IIc} and found larger values of G_{IIc} from a nonlinear FE analysis when compared with a linear one and attributed it to the fact that damage causes an increase in G_{IIc}.

8.8 Conclusions

Adhesion and adhesion degradation in microelectronic devices are key reliability concerns in semiconductor industry. In a fracture mechanics approach for the analysis of the interface reliability, the strain energy release rate (SERR) is compared against the (intrinsic) fracture toughness (G_c). This approach enables us to determine as to whether the available crack would satisfy the failure criterion. In this chapter the fracture tests for determining the fracture toughness of Cu/EMC samples were introduced. For the determination of intrinsic interfacial fracture toughness, the following important points should be considered:

First, the sample manufacturing history such as cure shrinkage of polymers during fabrication, stress relaxation because of viscoelasticity, and swelling/shrinkage during moisture absorption/desorption should be considered for the estimation of intrinsic interfacial fracture toughness. Significant influence of the residual stresses on the measured energy release rate was observed, which suggests that using the analytical solutions for the calculation of energy release rate can cause errors. Compressive stresses in general impede the crack propagation while tensile stresses facilitate it. Residual stresses contribute to the stored energy in the specimen. Therefore, geometric parameters such as adhesive thickness may have direct effect on the outcome of the test, unless the residual stresses are considered in a finite element analysis.

Second, the mode angle plays a significant role in the magnitude of interfacial fracture toughness. In general, the strength of the interface increases when the contribution of mode II fractures increases.

Third, the selection of a proper fracture setup is very important. If the fracture tests are performed in order to select the most suitable EMC material in terms of adhesion, 4-ENF may be a good choice due to its simplicity. However, if the interfacial fracture toughness values are needed for the delamination prediction in an IC package, 3-ENF and 4PB tests together with FEA should be applied in order to determine the mode-dependent toughness values and use them for comparison with the SERR in the package.

Finally, for the polymer/metal interfaces, linear elastic fracture mechanics may be still acceptable if the load-displacement curve of the delamination test up to delamination is linear and if the delamination tests are conducted within time periods that are short compared to the time needed for stress relaxation of the polymer. In case of epoxy molding compounds viscoelastic material law together with LEFM for the cracks at Cu/EMC interface was found to be a correct approach.

Chapter 9 Mechanism of Adhesion Degradation of Epoxy Molding Compounds

9.1 Introduction

Electronic packages used in automotive industry are prone to harsh environmental attacks that make the qualification of these devices more challenging than those of packages used in consumer electronics. There are typically two environmental effects that influence the structural integrity of these devices. Degradation of the material characteristics during the storage at elevated temperatures and diffusion of moisture prior to surface mount technology and during the service life of these devices pose significant reliability challenges. A crucial point in long term reliability and life prediction of microelectronic assemblies is an understanding of the interfacial adhesion, failure mechanisms due to lack of adhesion, and associated debonding behavior of the interfaces within these assemblies. The delamination between the copper leadframe and the epoxy molding compound has a negative influence on the durability of these packages and is a common failure mode during their qualification process. In addition, the delamination can affect long term package reliability by yielding enhanced transport of moisture along the epoxy/copper interface through moisture wicking.

This chapter investigates various effects of temperature and moisture on the adhesion between epoxy molding compounds and copper leadframe. When talking about temperature, there are basically two types of effects that elevated temperature can cause. The first effect is similar to the temperature dependency of material parameters. For example, as elastic modulus and ultimate strains of materials change with increasing temperatures, the isotropic fracture toughness of bulk materials and interfacial fracture toughness of an interface vary with temperature. This phenomenon is called the temperature dependency of material parameters. The second effect associated with temperature is the effect of thermal aging on the material parameters. This effect is not restricted to elevated temperatures because the behavior of polymers changes with time even at low temperatures. However, at elevated temperatures, polymeric materials change their prop-

erties more rapidly. The aging of polymers is a complex process which is generally due to a continuous curing of these materials at elevated temperatures.

The main objective of this chapter is to understand the mechanism of adhesion change under moisture and thermal loading and correlate the adhesion results to the other results explained in Chapters 5 and 6 regarding the mechanism of moisture diffusion and hygroscopic swelling of epoxy molding compounds.

9.2 Theories of Adhesion

In the performance of adhesive joints, the physical and chemical properties of the adhesive are the most important factors. The mechanical behavior of the bonded structure in turn is influenced by the details of the joint design and by the way in which the applied loads are transferred from one adherend to the other. Implicit in the formation of an acceptable adhesive bond is the ability of the adhesive to wet and spread on the adherends being joined (Encyclopædia Britannica, 2009). Attainment of such interfacial molecular contact is a necessary first step in the formation of strong and stable adhesive joints. Once wetting is achieved, intrinsic adhesive forces are generated across the interface through a number of mechanisms.

The precise nature of adhesion mechanisms has been the object of physical and chemical study since at least the 1960s, with the result that a number of theories of adhesion exist. The main mechanism of adhesion is explained by the adsorption theory (Kinloch, 1979 and 1987). The adsorption theory of adhesion is the most widely applicable theory that provided sufficiently intimate molecular contact is achieved at the interface; the materials will adhere because of the interatomic and intermolecular forces which are established between the atoms and molecules in the surface of the adhesive and substrate. The most common such forces are van der Waals forces and these are referred as secondary bonds. In other words, this theory states that substances stick primarily because of intimate intermolecular contact. In adhesive joints this contact is attained by intermolecular or valence forces exerted by molecules in the surface layers of the adhesive and adherend.

In addition to adsorption, four other mechanisms of adhesion have been proposed. The first, mechanical interlocking, occurs when adhesive flows into pores in the adherend surface or around projections on the surface. The second, interdiffusion, results when liquid adhesive dissolves and diffuses into adhered materials. In the third mechanism, adsorption and surface reaction, bonding occurs when adhesive molecules adsorb onto a solid surface and chemically react with it. Because of the chemical reaction, this process differs in some degree from the simple adsorption as described above, although some researchers consider a chemical reaction to be part of a total adsorption process and not a separate adhesion mechanism. Finally, the electronic, or electrostatic, attraction theory suggests that electrostatic forces develop at an interface between materials with differing electronic band structures.

In general, more than one of these mechanisms play a role in achieving the desired level of adhesion for various types of adhesive and adhered. However, in the studies performed on Cu leadframe/EMC interfaces, most of researches believe, that the contributions of interfacial diffusion and electrostatic forces between the adhesive and substrate causing adhesion is far lower than the effects of mechanical interlocking and adsorption (Ferguson, 2006). Since the copper substrates in this study were polished to a mirror finish, the effects from mechanical interlocking of the adhesive into irregularities present on the substrate surface will be small compared to the effects from intermolecular secondary forces between the atoms and molecules in the surfaces of the adhesive and substrate. Consequently, adsorption theory will dominate the adhesive bonding at the EMC/copper interface. This theory was further developed by Ferguson (2006 and 2007) to describe the adhesion degradation of leadframe/underfill interfaces.

9.3 Test Matrix

In this work both effects of temperature namely the temperature dependence of fracture toughness and thermal aging of the interface are investigated. Moreover, various effects of moisture on the interfacial fracture toughness are discussed.

The fracture tests were divided into four categories as explained below. The aim was to investigate the effects of temperature, thermal aging, interfacial moisture diffusion, and the intrinsic effect of moisture absorption separately.

In test category 1, the fracture toughness of Cu/EMC just after their fabrication are determined at six temperatures. The test temperatures selected were room temperature (25°C), 85°C, 130°C, 175°C, 210°C, and 250°C. The first three temperature values are under the glass transition temperature (T_g) of the selected EMC (**MC-1**), while the rest lie above the T_g.

The second effect of temperature associated with thermal aging is investigated in test category 2. Two aging temperatures of 85°C (test category 2a) and 175°C (test category 2b) were selected to investigate the effect of aging in dry conditions (thermal aging) on the interfacial adhesion between Cu and EMC. These two temperatures are very often used in electronic packaging industry. The 85°C is the recommended temperature by JEDEC standard to accelerate the moisture diffusion at 85% RH. Consequently, the role of thermal aging (without the presence of moisture) should be investigated in order to isolate the effect of thermal aging as explained by Ferguson (2006). The second temperature used to investigate the effect of thermal aging was chosen to be 175°C. This is the conventional mold temperature for the fabrication of plastic IC packages. At this temperature, the residual stresses are very low (although not zero because of the effect of cure shrinkage). Consequently, at this temperature the warpage of the bimaterial beam is small and hence the stresses are insignificant. This means that if any degradation in adhesion is observed at this thermal aging condition, the degradation can be directly attributed to the effect of thermal aging only, because almost no damage is caused by very low stresses during the aging.

The effect of moisture diffusion on the adhesion between leadframe and epoxy molding compound was investigated from two aspects. One aspect is the degradation of adhesion due to diffusion of moisture along the interface path, for which a higher diffusion coefficient than for the bulk materials is normally observed. The second aspect is the diffusion through the bulk EMC and hence existence of uniform moisture content across the interface. This causes an intrinsic degradation of adhesion due to the uniform presence of water molecules at the interface.

Fig. 9.1 illustrates two types of samples used in this study. These two sample types differ in two characters, namely the thickness of EMC layer and the diffusion path of water molecules, as will be discussed later.

Test categories 3a-3e were aimed at understanding the phenomenon of interfacial diffusion. For this test purpose, several type II samples were put in a moisture chamber at 85°C/85%RH and each week 5 samples were removed from moisture chamber and the fracture test was carried out at room temperatures. This larger EMC thickness allows for the characterization of adhesion degradation due to interfacial moisture diffusion along Cu/EMC interface, because the moisture travels along the interface much faster that along the bulk EMC, as was discussed in Section 5.2.2.

Finally, the test category 4 aimed at understanding the intrinsic effect of adhesion degradation due to uniform moisture content and the possible recoverability of adhesion loss upon a subsequent baking. In contrast to test category 3 the diffusion path along the interface was blocked for the samples of test category 4 by using type I samples. In the fabrication of type I samples, the mold compound was injected in such a way that it covered the both sides of samples across the width so that the molding compound effectively was a barrier for moisture transport at interface. If any humidity aging was needed prior the fracture tests (test categories 4a, 4b, and 4c), the sample was first exposed to moist environment, after moisture preconditioning the extra mold flake on sample sides was remove by a grinding machine. This process guarantees that in test categories 4a-4c, uniform moisture content existed at the interface.

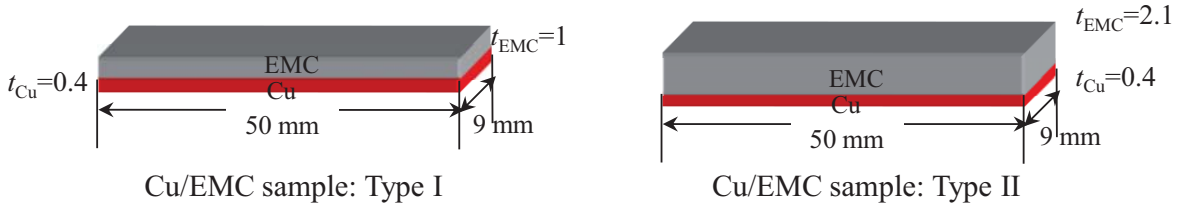

Figure 9.1 Bimaterial samples used to determine the environmental effect on the Cu/EMC adhesion.

A summary of the experimental test matrix is given in Tables 9.1-9.4. For each test category at least five samples were used for the fracture tests.

Table 9.1 shows the test matrix for the measurement of interfacial fracture toughness at various temperatures which will be discussed in Section 9.4.

Table 9.1 Tests category 1: Effect of test temperature on the interfacial fracture toughness.

Test category	Aging Environment	Test Temperature	Cu/EMC Sample type	Test objective
1	-	25°C	Type I	Control value
1a	-	85°C	Type I	Temperature effect
1b	-	130°C	Type I	Temperature effect
1c	-	175°C	Type I	Temperature effect
1d	-	210°C	Type I	Temperature effect
1e	-	250°C	Type I	Temperature effect

Table 9.2 shows the test matrix for the investigation of the effect of thermal aging in dry conditions. The results will be discussed in Section 9.5.

Table 9.2 Tests category 2: Effect of thermal aging in dry condition on the interfacial fracture toughness.

Test category	Aging Environment	Test Temperature	Cu/EMC Sample type	Test objective
2a	2 weeks in dry condition at 85°C	25°C	Type I	Thermal aging effect
2b	2 weeks in dry condition at 175°C	25°C	Type I	Thermal aging effect

In Section 9.6 the effect of moisture on the interfacial fracture toughness of Cu/EMC interface will be presented. A review of literature together with the available theories for adhesion degradation under moisture will be presented. Then the fracture results will be discussed.

In Section 9.6.1 the degradation effect of moisture diffusion through the interface will be discussed. Table 9.3 summarizes the test matrix.

Table 9.3.Tests category 3: Effect of interfacial moisture diffusion on the interfacial fracture toughness

Test category	Aging Environment	Test Temperature	Cu/EMC Sample type	Test objective
3a	-	25°C	Type II	Interfacial diffusion
3b	1 week at 85°C/85%RH	25°C	Type II	Interfacial diffusion
3c	2 weeks at 85°C/85%RH	25°C	Type II	Interfacial diffusion
3d	3 weeks at 85°C/85%RH	25°C	Type II	Interfacial diffusion
3e	4 weeks at 85°C/85%RH	25°C	Type II	Interfacial diffusion
3f	5 weeks at 85°C/85%RH	25°C	Type II	Interfacial diffusion

In Section 9.6.2 the intrinsic effect of moisture on the interfacial fracture toughness of Cu/EMC will be discussed. The purpose of this test category was to ensure a uniform moisture concentration at the interface when the fracture tests were performed. As stated in Chapter 5, there are at least two mechanisms of moisture diffusion when epoxy molding compounds are exposed to humid environment. The first mechanism was found to be mostly reversible when the samples were baked, however, the second mechanism was irreversible and upon baking the samples residual

moisture content was detected. In Section 9.6.2 the influence of first and second phase of moisture diffusion on the interfacial fracture toughness will be investigated by fracture tests of samples after both short and long sorption times followed by baking. Table 9.4 tabularizes the test category 4.

Table 9.4 Tests category 4: Study of the intrinsic degradation of fracture toughness and a possible recoverability of adhesion loss upon subsequent baking.

Test category	Aging Environment	Test Temperature	Cu/EMC Sample type	Test objective
4a	2 weeks at 85°C/85%r.h.-	25°C	Type I	Moisture diffusion effect
4b	2 weeks at 85°C/85% RH followed by baking at 125°C for 24 h	25°C	Type I	Effect of 1st phase of moisture absorption
4c	4 weeks at 85°C/85% RH followed by baking at 125°C for 24 h	25°C	Type I	Effect of 2nd phase of moisture absorption

It must be noted that due to the significant reduction in the elastic modulus of the EMC at higher temperatures, the mode mixity in the test categories 1b-1e is different from other test categories. For other tests, the mode mixity remains almost constant, because the elastic modulus of EMC is almost independent of the moisture content.

9.4 Effect of Temperatures on the Interfacial Fracture Toughness

As electronic devices are used in more and more demanding structural application at high temperatures, understanding their reliability tolerance becomes increasingly important. IC devices are usually exposed to elevated temperature in the SMT process as well as during service life and it is generally agreed that exposing surface-mount plastic parts to high-temperature reflow profiles can generate package failures if delamination is present. Consequently, there is an additional concern that unexpected failures could occur when these devices are exposed to elevated temperatures. This section investigates the behavior of interfaces when subjected to elevated temperatures. Since the pure effect of temperature is desired to be understood all the samples used in this section were tested just after their fabrications to reduce possible effects of storage.

Delamination tests were performed at six temperatures namely room temperature (25°C), 85°C, 130°C, 175°C, 210°C, and 250 °C. In order to perform each test, the sample was placed on the inner supports of a 4PB test setup, the environmental chamber was closed and the temperature inside the chamber was allowed to stabilize for 5 minutes for all the tests. At each temperature, a constant displacement rate of 10 mm/min was performed. This relatively high rate was selected because of high stress relaxation of the EMC at elevated temperatures when small rates were applied. For example at 210°C no delamination was observed by using the displacement rates of

0.1 mm/min and 1 mm/min, and the EMC layer broke before interface delamination happened. Consequently, the displacement-rate of 10 mm/min was selected for all the tests of test category 1 for the sake of consistency. During each test, load and displacements were recorded along with the temperature data.

Fig. 9.2 shows the change of interfacial fracture toughness with temperature. The scatter of the results together with the average value at each temperature is also depicted. . The results are normalized to the fracture toughness values at room temperature. It can be observed that the fracture toughness initially increases from room temperature to temperatures close to the glass transition temperature of the molding compound. Then it starts to decrease significantly.

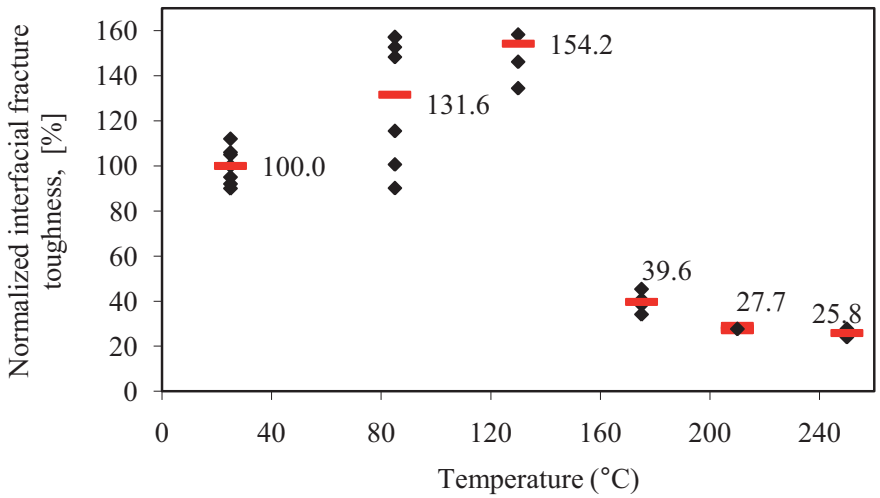

Figure 9.2 Effect of temperature on the interfacial fracture toughness of Cu/EMC interface.

It must be noted that for testing at elevated temperature and at time scales where viscoelastic deformation may cause changes in fracture toughness, the use of linear elastic fracture mechanics is believed to be valid because the load-displacement curves were all linear up to the point of delamination propagation. In this case any significant viscoelastic deformation that may be occurring in a specimen is assumed to occur on a very local scale in the crack tip region as part of crack growth process. Additionally, Guojun *et al.* (2007) and Tay *et al.* (1998) conducted ENF tests at various high temperatures and loading rates. They found that the time of maximum loads matched exactly with the time of maximum energy release rates. They concluded that the fracture toughness of the interface between the molding compound and copper increases with temperature when the viscoelastic behavior of the molding compound is taken into account.

Reeder *et al.* (2003) studied the effects of temperature and loading rate on delamination growth of composites for high speed aircraft applications at 149°C, 177°C, and 204°C. At each temperature the tests were performed with a variety of loading rates so that the delamination initiated over the range of time from 0.5 sec to 24 hrs. The fracture results showed that the delamination resistance is a complicated function of both time and temperature with the effect of temperature either increasing or decreasing the fracture toughness depending on the time scale. The results

also showed that the fracture toughness changed by as much as a factor of three as the time scale changed over the five orders of magnitude. The effect of increasing temperature caused a decrease in toughness at higher load rates but an increase in toughness at lower load rates. Park *et al.* (2007) investigated the interfacial fracture toughness between passivation layers and underfills at elevated temperatures by 4PB delamination tests. They observed that if temperature was increased, the interfacial toughness also increased up to glass transition temperature. Beyond this temperature they observed that interfacial fracture toughness decreased. Their results were in complete agreement with those of this work. They attributed their results to the thermal motion of molecules. As temperature is increased, the thermal motion of molecules is increased. Thus the adhesion strength at interface is decreased as the interaction is decreased. Therefore, the combination of decrease in Young's modulus and decrease in interfacial interaction at high temperature determines as to whether the interfacial fracture toughness increases or decreases. Loo *et al.* (2007) employed Brazil-nut specimens and determined the interfacial fracture toughness of an adhesively sandwiched joint. They observed that generally for the same loading angle, an increase in strain rate causes an increase in interfacial fracture toughness. For viscoelastic materials at low strain rates, the viscous effect was dominant. They suggested that this viscous effect results in creep during low strain rates and causes interfacial fracture toughness to decrease. On the other hand, at higher strain rates, the elastic effect is dominant. This means that the material is able to undergo more "stretching" before fracture. The interfacial fracture toughness in this case will increase.

It seems that the fracture toughness results of Fig. 9.2 can be explained by the combined effects of adhesion strength and elastic modulus of the EMC material. The effect of increasing temperature on the interfacial fracture toughness caused an increase in toughness at temperatures below the T_g, and a decrease of toughness at temperatures above it. As shown in Chapter 4, the value of elastic modulus of EMC decreases from room temperature to elevated temperatures almost an order of magnitude.

9.5 Effect of Thermal Aging on the Interfacial Fracture Toughness

Plastic encapsulated microelectronic devices exhibit evolving properties that change significantly with environmental exposures such as isothermal aging and thermal cycling. Such aging effects are accelerated at higher temperatures, which is a typical phenomenon of thermal cycle qualification tests for harsh environment electronic packaging. In order to determine as to whether a long term exposure to elevated temperatures will result in a change of the adhesion between EMC and leadframe, samples were exposed to two different temperatures for a period of 2 weeks. Two thermal aging temperatures of 85°C and 175°C (both in dry state) were selected. As described earlier, these two temperatures are especially important in electronic packaging. The aim of the storage at 85°C was to isolate the pure effect of moisture when the samples are exposed to 85°C/85%RH condition. The storage at 175°C is also important, because this is the temperature of the transfer molding process and it is normally assumed that the residual stresses at this tem-

perature are very low and, consequently, the adhesion loss at this aging temperature can be attributed to the degrading effect of long-term thermal aging without damage being influenced by stresses in the sample.

There have been several investigations on the effects of isothermal aging (with and without humidity) on the polymeric materials. These studies have primarily focused on the evolution/degradation of interfacial failure properties with duration of exposure. For example, Luo and Wong (2005) showed that there are dramatic reductions in the interfacial adhesion strength of the underfill/soldermask interface in lap shear specimens exposed to a combined humidity-temperature exposure (60°C and 95% RH for 168 hours). They observed that a change in the constitutive behavior of their lap shear specimens after thermal/humidity aging has occurred.

Chaware *et al.* (2004) showed that dry aging at 85°C for 3 weeks prior to testing had little effect on the reliability of flip chip assemblies made with several different underfills. However, combined hygro-thermal exposures at 85°C and 85% RH had a significant effect on all of the configurations examined. Both underfill fillet cracking and delamination at the underfill to the passivation interface were accelerated during thermal cycling testing that occurred after the environmental exposures. In recent work Lin *et al.* (2009) used a microscale tension testing machine to evaluate the uniaxial tensile stress-strain and creep behaviors of an underfill material at several stresses and test temperatures, after various durations of isothermal aging. The evaluated underfill illustrated softening behaviors at temperatures exceeding 100°C, although the documented T_g ranged from 130-140°C. They showed that both the effective elastic modulus (initial slope) and ultimate tensile strength (highest stress before failure) increase monotonically with the amount of isothermal aging or aging temperature, regardless of whether the aging temperature was below, at, or above the T_g of the material. In general, the changes (increases) in E and UTS (Ultimate Tensile Stress) with aging were typically in the range of 10-40% of the non-aged values. From the creep results, it was seen that at a given time, the creep strains were much lower for the aged samples relative to the non-aged samples.

Fig. 9.3 shows the effect of aging in dry environment on the interfacial fracture toughness of Cu/EMC (**MC-1**) interface. The control value (dry sample without any storage prior to fracture test) is also shown. All of the test results are again normalized to the average fracture toughness of the control value. While thermal aging in dry condition at 85°C (test category 3a) had no significant effect on the interfacial fracture toughness, aging at 175°C (test category 3b) degraded the interfacial fracture toughness significantly.

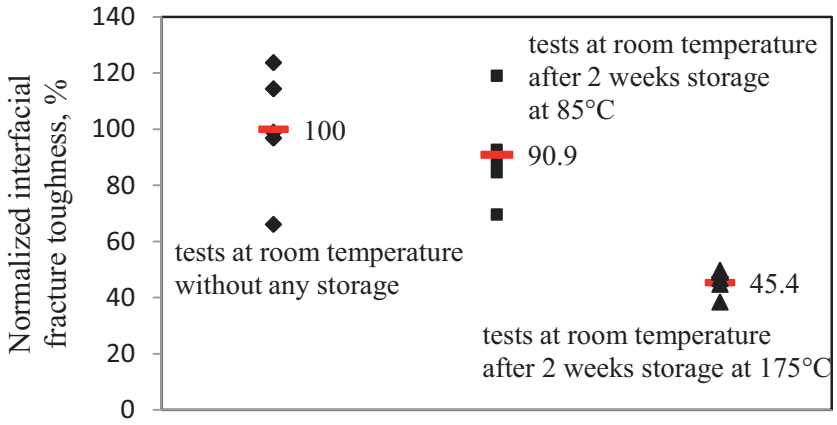

Figure 9.3 Effect of 2 weeks thermal storage at 85°C and 175°C dry conditions.

As shown in Fig. 9.3 the interfacial fracture toughness decreased to 45.4% of initial un-aged value after 2 weeks of storage at 175°C. The significant adhesion loss at this condition is most probably due to two simultaneous mechanisms:

The first one can be explained by adsorption theory, which explains the interfacial integrity by van der Waals forces. Apparently these forces get weaker when the bimaterial structures are stored at elevated temperatures due to degradation of polymers.

An equally important mechanism in the adhesion degradation of Cu/EMC interface is the degradation of leadframe surface due to its oxidization. The exact mechanism of oxide layers and their influences on the adhesion to polymers is the subject of many studies and is beyond the scope of this work. However, it was tried to understand as to whether the locus of the fracture changes when the specimens are stored. Figs. 4a-4d show the effect of both time and temperature on the oxide layer of the leadframe studied in this work. Fig. 9.4a is an SEM picture of the leadframe just before the sample fabrications. Fig 9.4b shows the increase in oxide layer during one minute storage at 175°C which is the approximate time the leadframes are heated during the transfer molding process. Fig. 9.4c shows the oxide layer after 4 hours storage at 175°C, which is comparable to the times needed for post mold cure of the plastic parts. As shown in this figure the oxide layer ranges from 10-70 nm. However, these tests were performed for bare open face leadframes that were exposed directly at elevated temperatures in conventional heat chambers. In reality the thickness of oxide layer in the bimaterial samples is lower, because the leadframes are adhered to the molding compounds and are not directly exposed to air. Finally, Fig 4.9d shows the thickness of oxide layer after 4 hours storage at 175°C followed by 5 minutes at 260°C. This is the worst case can happen in an IC package with an initial delamination at interface subjected to solder reflow process. The thickness of oxide layer was reached a value of 214 nm.

This oxide layer together with the degradation of EMC materials is most probably responsible for the remarkable degradation of interfacial fracture toughness when samples were stored 2 weeks at 175°C. Since the aging at 85°C did not significantly alter the interfacial fracture toughness, it can be concluded that storage at elevated temperatures above the T_g of EMC is one of the most de-

grading scenarios because both mechanisms of EMC degradation and Cu oxidization act simultaneously.

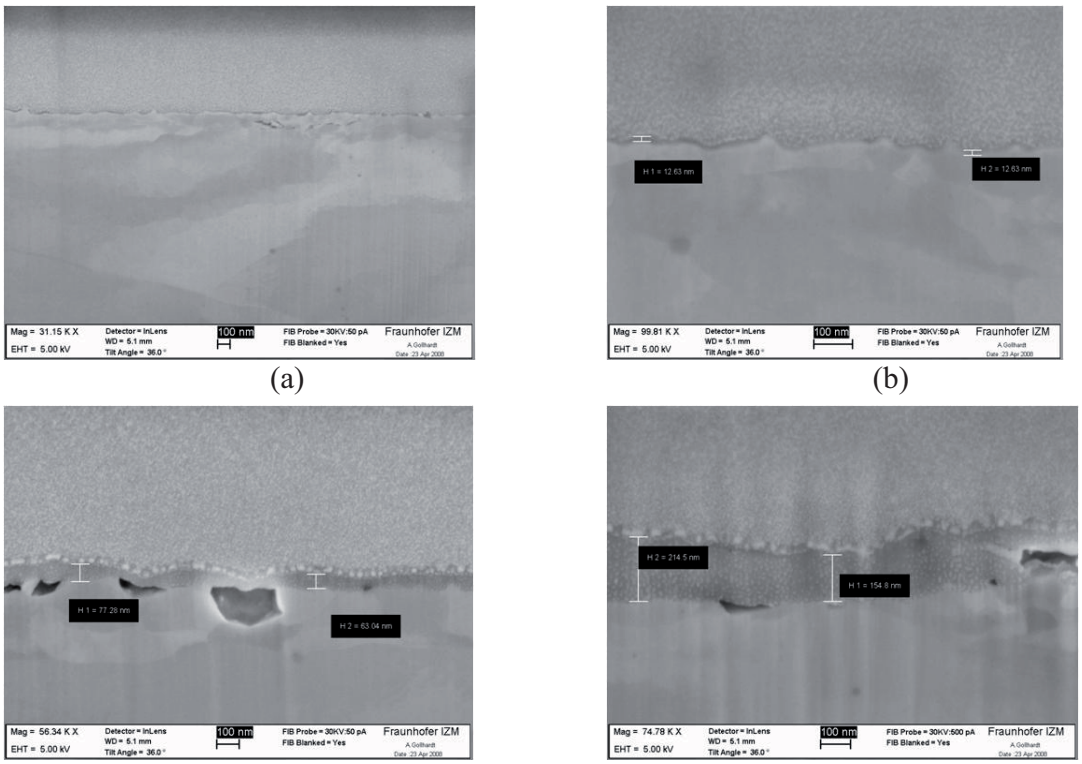

Figure 9.4 Increasing the copper oxide layer with storage: (a) without storage (b) 1 min at 175°C (c) 4 hrs at 175°C (d) 4 hrs at 175°C followed by 5 min at 260°C.

There are also some other works that study the influence of surface oxidization of Cu leadframes on their adhesion to molding compounds. Chong *et al.* (1995) studied the presence of a copper oxide layer on the leadframe of plastic IC packages. Copper oxide was found to cause delamination at the diepad/mold compound interface. They suggested that at high temperatures the failure mechanism was the presence of voids at the oxide/metal interface, which increased as the degree of oxidation was increased. Elevated temperature processes used in assembly, such as die attach curing and wire bonding, were found to be the primary causes of oxidation. However, an important observation was that the duration of post mold curing had a great impact on the interfacial integrity of the oxidized interface within an encapsulated package. Their work also describes the method of characterizing oxidation using SIMS (Secondary Ion Mass Spectroscopy) depth profiling. They suggested that at temperatures below 200°C the oxidation of leadframes was insignificant. Lahiri *et al.* (1998) also worked on the oxidization problem of copper leadframes in an effort to identify the factors which may lead to the formation of brittle and/or poorly adhering oxides. The kinetics of oxidation of leadframes in air was investigated by measuring the oxide thickness as a function of time at temperatures ranging from 200 to 300°C. The oxidation was found to occur fairly rapidly in this temperature range. The oxide had the appearance of incohe-

rent platelets and it consisted of CuO and Cu_2O. Analysis of the oxidation data indicated a logarithmic growth law in the 100–1400 nm thickness range. Recently, Abdullah *et al*. (2009) analyzed the reliability of two condition types of copper leadframe, namely, good and oxidized. The oxidized leadframe provided a poor surface to adhesive and a higher microstrain on cyclic load, resulting in a negative effect on package reliability, such as a crack phenomenon at the epoxy interface between the die and the leadframe.

Lee and Park (2002) also investigated the failure path at the interface of copper leadframe with epoxy molding compound. They forced black-oxide and/or brown-oxide layers to be formed on the surface of copper-base leadframe sheets in hot alkaline solutions, and then the oxide-coated leadframe sheets were molded with epoxy molding compound. The molded bodies were machined to form sandwiched-double-cantilever-beam specimens, and the adhesion strength between oxide-coated leadframes to EMC was measured in terms of critical energy-release rate (G_{Ic}). They observed that untreated leadframe and Cu_2O-coated leadframe showed almost no adhesion to EMC. However, once a continuous CuO layer formed on the leadframe surface (brown oxide) or on the Cu_2O layer (black oxide), G_{Ic} increased to around 80 J/m^2. After the fracture toughness tests of the brown oxide-coated leadframe/EMC interface, they carried out analyses of the fracture surface and the failure path was revealed: When the oxidation time was less than 2 min, the failure path lied over near the CuO/EMC interface and inside the EMC. However, when the oxidation time was more than 2 min, the failure path lied near the CuO/EMC interface and inside the CuO.

These studies are in agreement with the fracture results presented in this section where the interfacial fracture toughness of Cu/EMC interface upon 2 weeks of storage at 175°C was found to be significantly lower than that of un-aged samples.

9.6 Effect of Moisture on the Interfacial Fracture Toughness

Water is often regarded as the main agent in reducing the service life and reliability of adhesive joints, electronic devices and composite materials. The mechanism of adhesion loss at a critical relative humidity is the subject of much speculation (O'Brien, 2003, Fan *et al.*, 2008a,b,c and 2009, Shirangi, 2010). The dramatic reduction in adhesion strength has been attributed to both physical and chemical changes resulting from the moisture absorption in either the bulk adhesive or at the interface between the adhesive and substrate.

Moisture can influence the interfacial adhesion through three mechanisms. The first mechanism is the intrinsic aggregating effect of water molecules upon direct presence at the interfaces and degrading the interfacial adhesion by bonding to the polymer chains (Brewis, 1990). The second mechanism is that the absorbed moisture changes the mechanical properties of polymeric materials. For example Dudek *et al.* (2002) and Ferguson *et al.* (2005) reported that moisture can change the elastic modulus and shift the glass transition temperature of polymers to lower values. This mechanism leads normally to a slight difference in the mode mixity of the measured fracture

toughness of moist sample when compared to that of dry ones. The third mechanism is the swelling of polymeric materials upon exposure to moist environments and causing an additional mismatch between volumetric expansions of substrate and adhesives. This is even more pronounced if the joint between a polymer and a metal is investigated. Since the metallic substrate is impermeable to moisture only the polymeric adhesive absorbs moisture and causes a mismatch in hygroscopic strains. In order to measure the intrinsic fracture toughness of a moisture preconditioned bi-material sample, the influence of hygroscopic swelling which induces an apparent change in the measured fracture toughness should be isolated.

There are many reports in the literature regarding different mechanisms of adhesion degradations. Brewis *et al.* (1990) proposed that the weakening of molecular bonds at interface is the basic cause for adhesion loss. They suggested that bonds attributable to secondary forces at the interface are broken up by moisture, hydration of the oxide surfaces, and/or water condensation due to lowering of vapor pressure by the presence of salt impurities at the interface. In contrast to them Lefebvre *et al.* (2000) suggested that the change in the bulk properties of the epoxy adhesive is responsible for the observed onset of adhesion loss at a critical relative humidity. They reported that the solubility or mass of absorbed water, as a function of relative humidity increased abruptly at the critical relative humidity. Their study suggests that capillary condensation and the depression of glass transition are not responsible for the adhesion loss. They proposed that inter-chain hydrogen bonds are broken by absorption of water. However, using nuclear magnetic resonance, McBrierty *et al.* (1999) opposed the theory that inter-chain hydrogen bonds are broken by absorption of water. They showed in epoxies based on the Diglycidyl Ether of Bisphenol that no disruption of the hydrogen bonding network occurs at room temperature in the hydrated epoxy resin.

Ferguson (2004) suggested that there are three mechanisms that contribute to water penetration at the interface in epoxy adhesively structures. Bulk diffusion, wicking along the interface and capillary action associated with micro-cracking. The first mechanism was discussed in the Chapter 5 where it was shown that the diffusion of moisture in epoxy molding compounds does not follow the conventional Fickian diffusion theory and a dual-stage absorption curve was observed. The second mechanism for moisture transport to interface is attributed to wicking along the interface and was discussed in Section 5.2.2 as interfacial diffusion. It was found that the diffusion of moisture in a plastic package was faster than that in a bulk EMC material. This high rate of interfacial diffusion has also a significant role in the adhesion loss as will be discussed in the next section. The final mechanism for moisture transport to the interface is by capillary action associated with voids and cracks present in epoxy or epoxy composite. Lu *et al.* (1998) found that the addition of fillers to polymers resulted in faster sorption kinetics when compared to the bulk polymer alone. They concluded that water was not only absorbed by the epoxy, but also by the interfaces inside the epoxy introduced by addition of filler.

In order to understand the mechanism of adhesion degradation in Cu/EMC interfaces, the fracture tests used throughout this work are further applied similar to the methodology introduced in Chapter 8. The pure effect of moisture on the interfacial fracture toughness cannot be understood unless the effect of moisture on the bulk EMC material is well identified. In the following the

results from other chapters are shortly reviewed in order to enable a better understanding of the logical sequence of the Chapters 3-8.

In Chapters 3 and 4 the required material characterization together with experimental verifications of FE analyses were introduced. These data are used to model the stresses in the bimaterial samples. In Chapter 5, the mechanism of moisture absorption and desorption in EMC materials was discussed. In Chapter 6, the hygroscopic swelling of epoxy molding compounds was investigated. It was found that this phenomenon is responsible for a change in the warpage of bimaterial samples upon exposure to humid environments. This is especially important, because as shown for the case of cure and thermal stresses, modeling the residual stresses plays an important role in the accuracy of fracture toughness analysis. Finally, the fracture mechanics approach described in the Chapters 7 and 8 is used to determine the intrinsic interfacial fracture toughness of Cu/EMC interfaces. VCCT is used for the determination of strain energy release rate. This method was benchmarked in Chapter 7.

In the following, the mechanism of adhesion degradation due to moisture is discussed in two parts. In Section 9.6.1, the mechanism of interfacial moisture diffusion is introduced. Bimaterial samples of type II as shown in Fig. 9.1 are used to investigate the interfacial moisture diffusion. In Section 9.6.2 bimaterial samples of type I are applied in order to investigate the adhesion degradation under uniform moisture content at the interface.

9.6.1 Adhesion Degradation by Interfacial Diffusion

Table 9.3 shows the test matrix for the investigation of adhesion loss from a direct diffusing of moisture through the interface. Fracture tests performed in this section are similar to those introduced in previous sections. Five samples of Cu/EMC interface of type II were immediately tested after the fabrication in order to prevent any moisture diffusion. The average fracture toughness of these samples was used as a control value. 30 other Cu/EMC samples were placed in a humidity chamber in 85°C/85%RH condition. Each week five samples were removed from the humidity chamber, the samples were allowed to reach the room temperature, and the fracture tests were performed. It is important to note that the thickness of EMC layer in type II samples is 2.1 mm, which is relatively high. This means that moisture needs at least 8 weeks to reach the quasi-saturation state at the interface, if it only transfers from the top surface of EMC. However, the dominating diffusion path for the type II samples is the diffusion through the interface. This problem was described in Section 5.2.2 where the moisture diffusion of a plastic package was compared to that of a bulk EMC material. It was found that the diffusion through the lead/EMC interfaces was faster than through the EMC. This section describes the interfacial moisture diffusion from the adhesion point of view and supports the results of Section 5.2.2.

Fig. 9.5 shows the dominating diffusion path for the type II samples exposed to a humid environment. Although moisture also diffuses from the top surface of the EMC layer, it is not depicted in this picture. The time needed for moisture to reach the interface from the top surface of EMC was calculated by an FE analysis. It was revealed that the diffusion along the both sides of

sample is the dominating path as shown in Fig. 9.5b because of the higher diffusion rate through interface, compared to bulk EMC. However, it should be noted that there was always a gradient of moisture concentration at the crack front when these fracture tests were performed. This means that the fracture toughness results are the average of both wet and dry parts of interface delamination as shown in Fig. 9.5b.

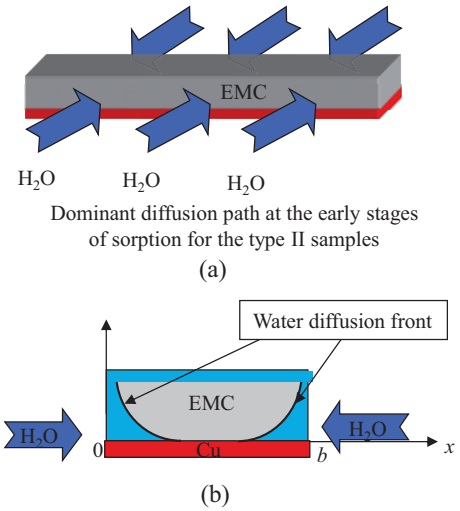

Figure 9.5 (a) Dominant diffusion path for type II samples in humid environment.
(b) Cross-section of type II sample, showing the diffusion path.

The fracture toughness values were determined from the experimental tests and a subsequent FE analysis using VCCT as described earlier. The average interfacial fracture toughness for each test category was normalized to the value of the dry samples. Fig. 9.6 shows the interfacial fracture toughness values at different aging times. As shown in Fig. 9.6, it was observed that most of the adhesion loss happened immediately within the first week of moisture sorption where the highest decrease in toughness values (from 100 to 69.2%) occurred, followed by a small decrease during the second week of sorption (from 69.2 to 65.3%). Finally, the interfacial adhesion reached almost a constant value after approximately three weeks of exposure to moisture and further exposure to moisture did not affect the toughness values significantly.

These results of rapid adhesion degradation can be attributed to the high rate of moisture diffusion along the interface between the EMC and the leadframe. Moreover, the fracture results can be justified by the sorption comparisons in Section 5.2.2 which showed a higher diffusion rates across the interfaces than the bulk EMC.

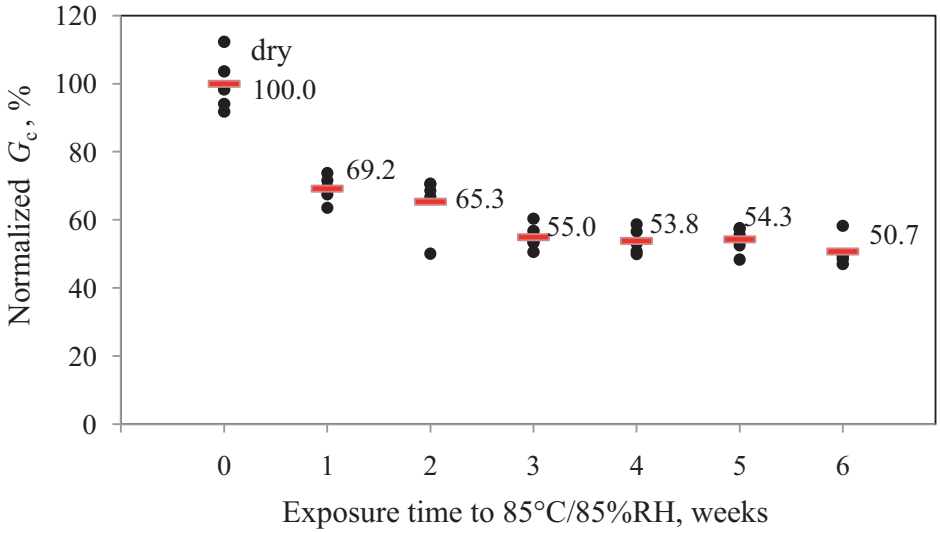

Figure 9.6 Adhesion degradation of Cu/EMC interface due to interfacial moisture diffusion

Comyn *et al.* (1994) support the theory of higher interfacial diffusion rate. They found that the rate of wicking of glass-to-lead alloy joints bonded with an epoxide adhesive could not be accounted for by the rate at which water enters the epoxide adhesive by bulk diffusion alone. They concluded that water must also enter the interface by "wicking" along debonded zones along the interface.

Davis *et al*. (2000) utilized the technique of electrochemical impedance spectroscopy and investigated epoxies bonded to aluminum with various surface preparations that resulted in either a weak or strong interface and observed that the rate of crack growth was slower for strong interfaces. However, for weak interfaces crack growth was detected almost immediately as moisture appeared at the interface and resulted in a fast rate of crack growth. Zanni *et al.* (1993) compared the calculated diffusion rates between non-bonded adhesive specimens and bonded adhesive joints. They observed that the interfacial diffusion coefficient was greater than the diffusion of bulk adhesives and hypothesized the phenomenon of "capillary diffusion," where the higher surface energy of the dry adhesive effectively pulls moisture along the interface.

These examples all suggest that the diffusion of water into the adhesive joints is not a simple process and may involve several pathways for the moisture ingress, dependent on the system chemistry and interfacial morphology. The most important result of this section is that, for bimaterial samples that are exposed to humid environments, the rate of adhesion degradation is much higher than the diffusion rate across the bulk polymer samples. In the next section the geometry of the fracture test is changed, so that no moisture molecule diffuses through the interface and enable uniform moisture content at the interface. In this way, it is possible to investigate the effect of moisture concentration level on the adhesion as well as its reversibility upon a subsequent baking.

9.6.2 Intrinsic Effect of Moisture on Interfacial Fracture Toughness

This section describes a test methodology to investigate the effect of uniform moisture content on the interfacial fracture toughness of Cu/EMC interface. The term *intrinsic* is again used in this section, because there are two primary differences between the results of this section and those shown in the previous section.

First of all, bimaterial samples of type I (Fig 9.7) are used in this investigation. In the design of the mold cavity some changes were made so that the molding compound covered both sides of the bimaterial sample acting as a barrier for interfacial diffusion. This procedure guarantees the moisture content across the width of the samples to be uniform as shown in Fig. 9.7.

Second, in the determination of interfacial fracture toughness, the complete residual stresses were considered. In Chapter 8 the effect of cure and thermal residual stresses on the apparent interfacial fracture toughness of Cu/EMC samples were investigated. It was shown that the fracture toughness results may be completely misinterpreted if these stresses are not taken into account. The situation gets more complicated if hygroscopic strains are also present, because they also change the overall warpage and stress state of the samples as shown in Chapter 6.

In order to determine the intrinsic effect of moisture on the interfacial fracture toughness, the residual stresses during the manufacturing process and moisture preconditioning of the samples were considered as follows:

First, the chemical cure shrinkage during the molding process was introduced in the FEA model as shown in Chapter 4. Then the cooling process from mold temperature (175°C) to room temperature (25°C) was taken into account. Later the hygroscopic swelling during the moisture aging was modeled from the data found in Chapter 6. Finally, the introduction of a precrack, which leads to some stress relaxations in the sample, was modeled by decoupling the selected nodes at the interface and the critical load from experimental results was applied. After a complete modeling of the sample, the critical load from fracture tests together with the crack length were applied in the stress analysis. Based on the results of the nodal forces and displacements obtained from the finite element analysis VCCT was used to estimate the interfacial fracture toughness.

Fig 9.8 shows the flowchart for determining the intrinsic interfacial fracture toughness of Cu/EMC samples upon humid aging.

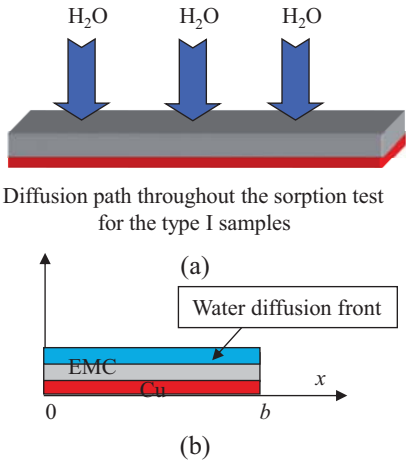

Figure 9.7 Moisture diffusion path for type I samples in humid environment. (b) Cross-section of type I sample, showing the diffusion path

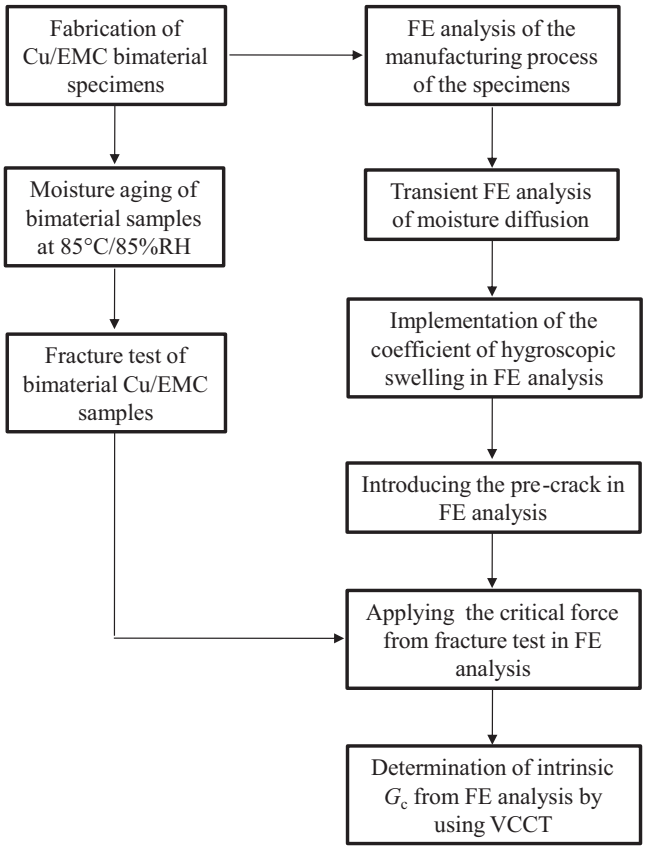

Figure 9.8 Methodology for determining the intrinsic adhesion loss of Cu/EMC interface.

Table 9.4 shows the test matrix to determine the interfacial fracture toughens of Cu/EMC interface under moisture and baking condition. It is evident that the level of moisture concentration at the interface increases with sorption time. This moisture concentration level plays an important role in the fracture results of bimaterial samples. More importantly, this concentration level de-

termines the behavior of interface after a sample is baked to remove the moisture content. Consequently, in what follows, the moisture absorption and desorption results of Chapter 5 will be used to interpret the fracture tests.

Fig. 9.9 shows the intrinsic effect of aging in humid environment on the interfacial fracture toughness of the Cu/EMC interface. All fracture tests were conducted at room temperature with a displacement-controlled rate of 0.1 mm/min using the 3-ENF fracture testing method. In addition, the effect of moisture on the elastic modulus of the EMC was investigated using three-point bending of bulk EMC bars. It was found that the combination of moisture absorption at 85%RH and thermal aging at 85°C does not affect the elastic modulus of EMC materials significantly. Hence, all fracture toughness measurements can be assumed to be at a constant mode angle. Using the diffusion coefficient from the experimental results the time to quasi-saturation of the samples was found numerically to be almost two weeks (0.21 % weight gain of the whole sample). Results show that the interfacial fracture toughness initially being 100 % in dry condition reduced to 44.8 % when the quasi-saturation level at the interface was reached as shown in the first and second column of Fig. 9.9.

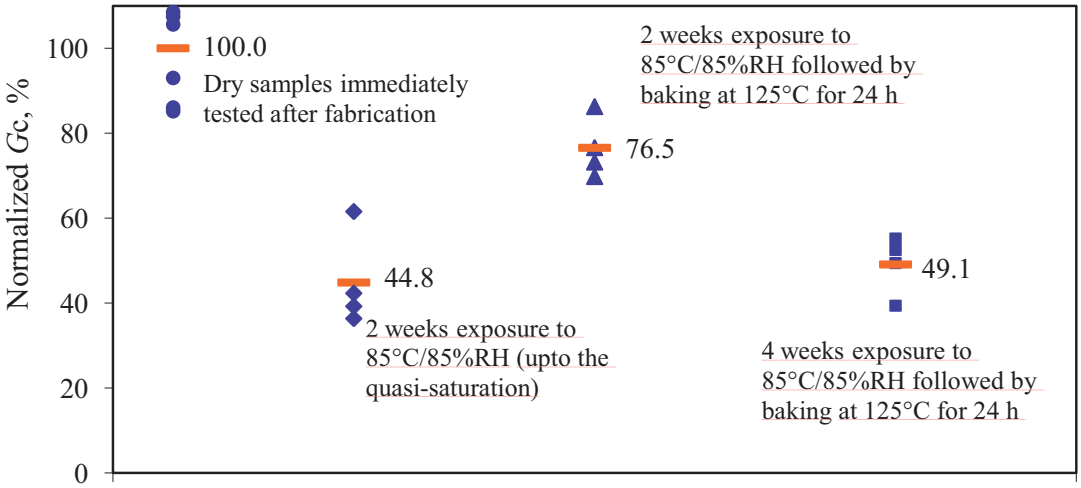

Figure 9.9 Effect of Moisture absorption, sorption time and the subsequent desorption on the adhesion of Cu/EMC interface.

In order to study the effect of an absorption/desorption cycle on adhesion, moist samples were baked for 24 h at 125°C reaching a virtually dry state. Then the fracture tests were performed on these samples at room temperature. Some of the adhesion loss due to moisture absorption up to quasi-saturation was recovered after drying (76.5 %) as shown in Fig. 9.9. This means that if the level of moisture concentration at the interface is within the quasi-saturation level (as described in Chapter 5) it is possible that some portion of the adhesion be recovered if the sample is baked properly. In other words, the adhesion loss due to an absorption / desorption process depends on the level of moisture content in the absorption process.

A longer exposure to moisture was also investigated by 4 weeks of aging in humid condition (0.25% weight gain of the sample) and subsequent baking for 24 h at 125°C. The fracture tough-

ness of these samples was measured again at room temperature. It was observed that samples which remained 4 weeks in humid conditions showed almost no recoverability upon annealing (49.1 %). In other words, if the level of moisture content at interface reaches the second phase state (as defined in Chapter 5) then baking the samples could not improve the adhesion between the Cu and EMC. This is an important result, which shows the extreme degrading effect of the second phase of moisture absorption. The moisture absorption during the first phase degrades the adhesion due to intrinsic effect of the presence of water molecules at the interface, which is partially reversible if a proper heating is performed. However, the second phase of moisture absorption seems to destroy the adhesion bonds permanently, and none of the adhesion loss may be recovered if the moisture level at the interface reaches this critical content

These results are in agreement with the results of Dodiuk *et al.* (1984) who evaluated the effect of moisture on the lap shear strength of four commercial epoxy adhesives to aluminum. They found that the exposure of moisture caused a reduction in lap shear strength; however, if the moisture concentration was below 0.3%, the strength was fully reversible after drying, indicating that adhesion loss may be recovered if the moisture content at the interface is still low. They gave no explanation for their results. However, the fracture results depicted in Fig. 9.9 together with the sorption model depicted in Fig. 5.15 can be helpful to understand the moisture-induced degrading effects. The key to conceptual understandings of adhesion loss and its recoverability or non-recoverability is the secondary phase of moisture absorption curve, which causes a permanent degradation in adhesion by destroying the secondary bonds between polymer and the substrate. Similarly, Orman and Kerr (1971) showed that although some of the strength lost in the epoxy-bonded aluminum joints studied was recovered, there was noticeable permanent damage from moisture suggesting an irreversible disruption at the interface as a result of attack by water.

There are some researchers that observed a critical moisture content for the adhesion degradation. Kinloch (1987) found that epoxy/mild-steel joints suffered no loss in adhesion from environment attack at 50%RH, even though the adhesive still absorbed water up to an equilibrium concentration. As a direct consequence of this observation, Kinloch proposed that a minimum, critical concentration of water must be a requirement for the loss of adhesion due to the presence of moisture. Ferguson and Qu (2004) used a water-proof perimeter to the bimaterial test specimens before moisture preconditioning to force 1-D moisture uptake through the top surface of the test specimen and prevent wicking along the interface. This can allow for the assumption of uniform concentration at interface by utilizing the inherent moisture absorption characteristics of the adhesive. They observed that a large portion of the loss in elastic modulus from moisture uptake was recovered upon subsequent drying. They also observed a permanent weight increase in epoxy samples after subsequent fully drying which suggests that at least part of the irreversible damage resulted from hydrolysis with a greater extent occurring at higher humidity levels. When they investigated the adhesion under moisture, they observed significant reduction in interfacial adhesion even for low concentrations and concluded that the loss in interfacial fracture toughness from moisture was not recovered upon fully drying. They explained the permanent loss in adhesion with adsorption theory as a primary bonding mechanism for the underfill/copper interface.

Contrary to these report regarding the permanent adhesion loss, there are a few evidences in the literature that reported a full recovery in adhesion upon subsequent drying. The reversibility of adhesion was reported for organosilicate glass film by Lin *et al.* (2007). Also Shaw *et al.* (1992) found that nearly all of the strength lost after immersing steel/epoxy lap shear joints in distilled water for three weeks was recovered after drying. They attributed the loss in strength after moisture preconditioning to plasticization of the epoxy adhesive, which is generally regarded as a reversible process. Similarly, Buehler and Seferis (2000) found samples soaked in water at 71°C for 1200 hours exhibited varying degrees of reversible and irreversible damage to both the flexural modulus and flexural strength upon drying at 50°C for 450 hours. However, more time was needed to fully dry the specimens in this study as well, with 3% weight concentrations of moisture still existing in the specimens at the time of testing after drying.

9.7 Conclusions

In this chapter the influence of temperature, thermal aging and moisture diffusion on the interfacial fracture toughness between a copper leadframe and an epoxy molding compound was investigated. Fracture mechanics was employed and bimaterial Cu/EMC samples were used to determine the interfacial fracture toughness. Three-dimensional finite element analysis was used to determine the interfacial fracture toughness from the experimental tests. For the determination of intrinsic fracture toughness, the process of sample fabrication was taken into account. Three sources of residual stresses were found to influence the apparent interfacial fracture toughness. First, the cure shrinkage of molding compound was implemented in the FE-analysis. Then the thermal stresses due to the mismatch between the CTE values of Cu and EMC was taken into account. For the samples under moisture, the effect of hygroscopic swelling was also considered. After modeling the residual stresses and applying the critical loads found from each fracture test, it is possible to determine the fracture toughness values using VCCT. The effects of test temperature, thermal aging and moisture diffusion were investigated in fracture tests and the results can be summarized as follows:

- First of all, the test temperature was found to affect the interfacial fracture toughness significantly. It was found that the fracture toughness values demonstrate two scenarios when the temperature rises. First, increasing the temperature from room temperature to the glass transition temperature of the molding compound resulted in an increase in the interfacial fracture toughness. However, the fracture toughness was found to demonstrate an opposite behavior at temperatures above the glass transition temperature of the EMC. These results were attributed to two major mechanisms that dominate the adhesion between polymers and metals. The decrease in elastic modulus of EMC with increasing temperature and the increase in the thermal motion of molecules are the primary reasons of adhesion change. In other words, the combination of decrease in Young's modulus and decrease in interfacial interaction at high temperatures determines if the interfacial fracture toughness increases or decreases.

- The second problem discussed in this chapter was the effect of dry aging at elevated temperatures. It was found that the storage of bimaterial samples at temperatures below the glass transition temperature of EMC did not affect the interfacial fracture toughness significantly. However, the storage at 175°C for a period of two weeks caused significant adhesion loss. There are two mechanisms responsible for this adhesion degradation. The first mechanism was attributed to the degradation of secondary bonds between molecules and atoms of adhesive (here EMC) and substrate (here copper leadframe). The second mechanism impacting the adhesion was found to be the oxidization of the surface of copper leadframe.
- Finally, the effect of moisture diffusion at 85°C/85%RH condition was investigated in details. Two types of bimaterial samples were used to investigate the effect of moisture on the adhesion between the copper leadframe and EMC layer:
  - For the samples that allowed for the diffusion of moisture along the interface, it was found that the rate of adhesion loss was much higher than the rate of moisture diffusion in the bulk EMC layer. This rapid adhesion degradation was attributed to the fact that the diffusion coefficient of moisture at the interfaces is almost an order of magnitude larger than that at a bulk material. This high diffusion rate was attributed to nano- or micro-pores and voids at the interface which facilitate the moisture transfer. Moreover, since these interfaces are under residual stresses, the stresses also contribute to the faster diffusion of moisture.
  - For the rest of samples the diffusion path from the interface was blocked and diffusion was forced to occur only from the EMC layer. Consequently, a uniform moisture concentration was available at the interface. Two levels of moisture content (quasi-saturation and second phase diffusion) that were identified during the moisture absorption of EMC materials were investigated. Both short term (2 weeks) and long term (4 weeks) sorption conditions resulted in a significant reduction in the interfacial fracture toughness. Similarly to the residual moisture content identified from desorption tests of EMC samples, adhesion recoverability tests were also carried out. For samples that were aged shortly in the humid environment, the adhesion was partially reversible by applying an appropriate heat treatment at 125°C. However, long-term aging in humid condition caused permanent adhesion loss, which was attributed to the degradation of hydrogen bonding between water molecules and polymer chains at the interface.

The important result from the moisture diffusion experiments is that the adhesion tests gave reasonable predictive values, in agreement with the observations in moisture absorption and desorption behavior. These realistic test conditions can enable a correlation to the response of microelectronic packages to humid conditions. To the author's best knowledge there is no other evidence in the literature that combines all of the responsible effects for understanding the adhesion degradation mechanism of polymer/metal interfaces. The results of this section provide invaluable information on various effects of moisture-induced adhesion loss, many of which may not direct have to do with moisture, but in reality contribute to the results of fracture tests.

Chapter 10 Applications and Case Study

10.1 Introduction

This chapter provides some examples that explain the applications of the methods developed in this work for the assessment of reliability in plastic IC packages. These examples show how the qualification of these devices can be done faster and more efficiently by selecting proper materials and by making small changes in the design of IC packages.

Early works of treating the problems associated with cracking in electronic devices were restricted to computational limitations. Most of these works treated the problem of fracture by 2D stress analysis. For instance, Kitano *et al.* (1998) studied package cracking by means of a moisture-diffusion analysis of the plastic, deformation and stress analysis of the package, and measurement of some high-temperature properties of the plastic. The validity of the analysis was confirmed by measurement of the deformation of packages heated by infrared radiation. They claimed via examples that it is possible to evaluate package cracking by the presented method quantitatively.

Le Gall *et al.* (1996) were one of the first who published results on a fracture mechanics analysis to understand cracking along the chip-fillet interface. They used linear elastic fracture mechanics and showed that the energy release rate for an underfill increased and subsequently decreased with crack length. Lau *et al.* (2000) presented a similar approach to delamination along the passivation-underfill interface. They reported that the equivalent plastic strain in the solder increased as the crack grew closer to the solder joint. Fan *et al*. (1999) investigated the underfill delamination in flip-chip modules under temperature cycling and categorized the stress intensity factor in electronic packaging into three groups: (1) angular corner of homogeneous materials, (2) angular corner of bimaterial wedge and (3) bimaterial wedge with adhesion. Saitoh *et al*. (2000) combined the elastic thermo-mechanical finite element method for nonlinear contact problems with a linear interface fracture mechanics approach. They conducted analyses to make the tendency of delamination growth clear and presented results on the effect of geometry and material parameters on the delamination between the silicon chip and encapsulant/die bonding material in a package. Wong and Cheng (2000) studied the initiation of interface delamination and the sub-

sequent delamination propagation in plastic IC packages. They used a numerical scheme, based on the assumption that interfaces are the weakest planes, where delamination is the most favorable failure mode. They used a traction-separation law that allows for the assumption of the interface being fully bonded or fully debonded. Results showed that the moisture-induced vapor pressure and interface adhesion quality were two major factors controlling popcorn failure. Under thermal loading alone without moisture, interface delamination progressed in a stable fashion; a well baked plastic IC package would therefore be resistant to popcorn failure during the solder reflow process. Under combined thermal and vapor pressure loading, delamination would propagate in a highly unstable manner. An unbaked package with low interface adhesion properties would therefore be susceptible to popcorn failure. They concluded that the relative geometries of the die, die-pad and molding compound would also influence the initiation of delamination.

Harries and Sitaraman (2001) used numerical fracture models to determine the effect of various thermo-mechanical property parameters on the growth of delamination at the encapsulant-backplate interface of a VSPA package. Results from these parametric studies showed that the energy release rate of interfacial delamination could be greatly reduced by use of an encapsulant with a lower CTE and lower modulus of elasticity. In contrast, the SERR was found to be practically insensitive to the die-attach adhesive and backplate CTEs and elastic moduli. Mercado *et al.* (2000) realized that the understanding of interface failure is critical to package reliability and performance. They developed an FE analysis methodology to validate the known solutions for mechanical loading and thermal loading for a Flip-Chip PBGA package. The simulation results indicated that packages with metal substrates had much higher chances of interface delamination than packages with FR-4 substrates.

In the next sections, some of the methods studies in this work are applied to evaluate the reliability of plastic IC packages. In Section 10.2, the moisture diffusion of a plastic IC package is discussed. Section 10.3 presents delamination risk of the same package under thermal loading. Finally, Section 10.4 shows how a fracture mechanics analysis may help us optimize the package geometry in order to minimize the delamination risks.

10.2 Evaluation of Critical Moisture Content in a TQFP Package

The moisture diffusion in a package prior to the surface mount process and during the storage is the primary reason for the initiation of interface delamination during the solder reflow process. As described in Chapter 5, the moisture diffusion curve of an EMC material consists of two regions. The primary region is the first linear part of the moisture absorption curve with an apparent saturation. The secondary region is the second liner part of the curve. For short sorption times, a Fickian diffusion model may be adequate. However, for long sorption times at high humidity levels, a more complex model proposed in Chapter 5 shall be applied. Fig. 10.1 shows the moisture content in the epoxy molding compound in a TQFP-epad package in 85°C/85%RH condition. Taking benefit from the symmetry of the package, only one-eighth of the package was

modeled. Since the leadframe and chip are impermeable to moisture, only the molding compound has been simulated.

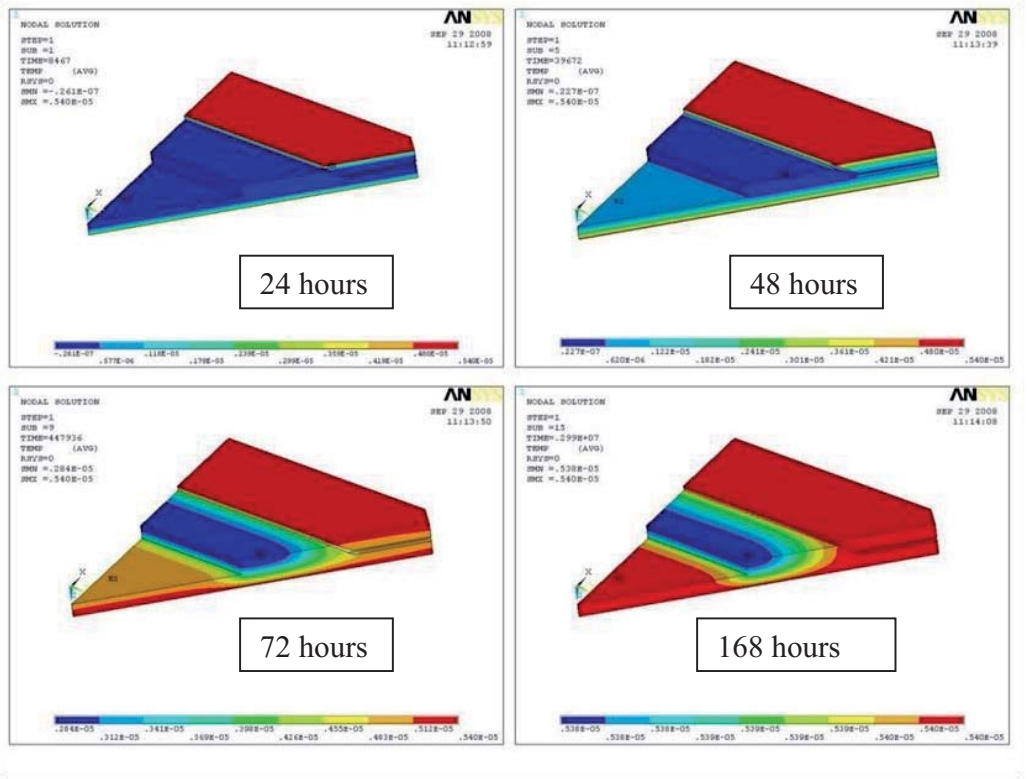

Figure 10.1 local moisture concentration in the molding compound of a TQFP-epad package in 85°C/85%RH condition.

As indicated in these plots the moisture content increases with exposure time to humid environment. The moisture concentration at the leadframe/EMC interface, one of the weakest internal joints in the package, is an important parameter for the occurrence of delamination during the solder reflow process. When the moisture sensitivity level as defined by the JEDEC standard is known, then the moisture sensitivity performance can be analyzed. This can help us reduce the number of experiments required to qualify the IC devices significantly. In some experiments it has been observed that when a critical moisture concentration at interface is reached, the interface delamination during a subsequent thermal loading is more probable.

In order to investigate the desorption model suggested in Chapter 5, the desorption process of this package was also analyzed. For the simulation with FEA, the package has been assumed to be initially saturated and the parameters listed in Table 5.3 were used. Fig. 10.2 shows the residual moisture weight of the package at the end of desorption process. This information on the local moisture concentration of plastic packages is of particular concern, because as suggested by Tay and Lin (1996) it is the local moisture concentration in the package and not the overall moisture content which induces interfacial delamination and failure. Moreover, it is usually accepted that the magnitude of vapor pressure induced at elevated temperatures is highly dependent on the local moisture concentration (Fan *et al.,* 2009).

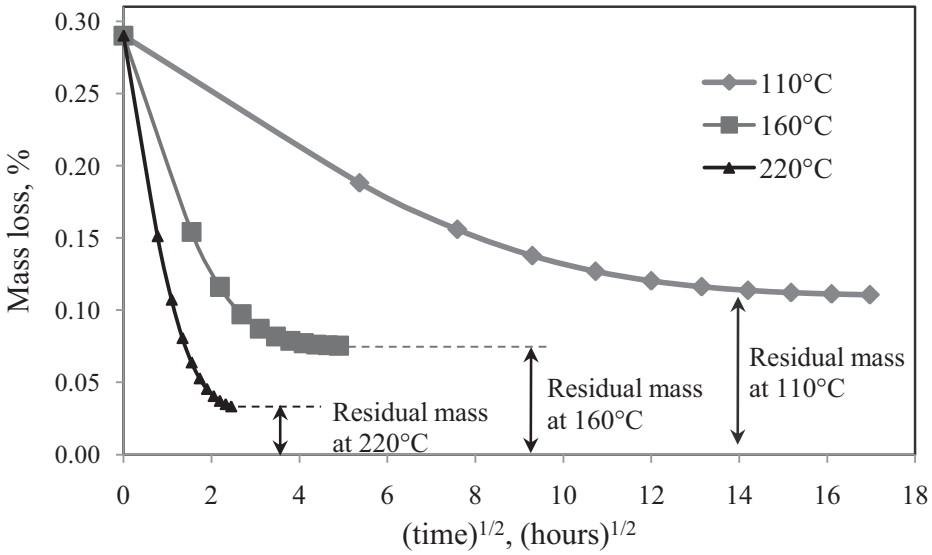

Figure 10.2 Weight loss of the TQFP-epad package with exposure to dry air using finite element analysis of the desorption model for different temperatures.

10.3 Thermo-mechanical simulation of a TQFP-epad package

This section presents some results from thermo-and hygro-mechanical FE analysis that provide valuable information about the behavior of plastic IC packages during a thermal or moisture loading. These analyses were carried out on a TQFP-epad package that uses **MC-1** epoxy molding compound described in previous chapters. This material is completely characterized for a complete thermo-hygro-mechanical FE analysis. Fig. 10.3 shows FE results of this package. Fig. 10.3a shows the state of the deformations in package during the transfer molding while the epoxy molding compound is still in fluid state. When the EMC material starts solidification during the polymerization, it shrinks and causes the first deformation of the package at molding temperature. Fig. 10.3b shows the deformed state of the package upon molding while the package is still at 175°C molding temperature. When cooling to room temperature, the mismatch between the CTE values of different package materials causes thermal strains to develop. This is the second mechanism causing deformation in the package as shown in Fig. 10.3c. A third mechanism shown in Fig. 10.3d is the moisture-induced hygroscopic swelling. Since the chip and leadframe of these packages are impermeable to moisture, the absorption of moisture by EMC materials causes a further deformation in package as shown in Fig. 10.3d.

These examples indicate that any temperature change or moisture absorption can act as a driving force for interface delamination. In the following the same package will be investigated under temperature cycle test. This example attempts to show how fracture mechanics can be used to predict interface delamination between the copper-based leadframe and epoxy molding compound. By adding a precrack to an interface in the model it is possible to find the strain energy release rate.

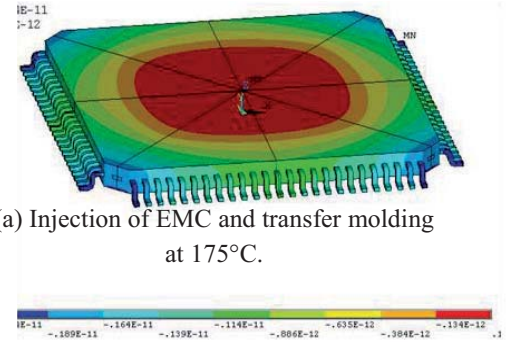

(a) Injection of EMC and transfer molding at 175°C.

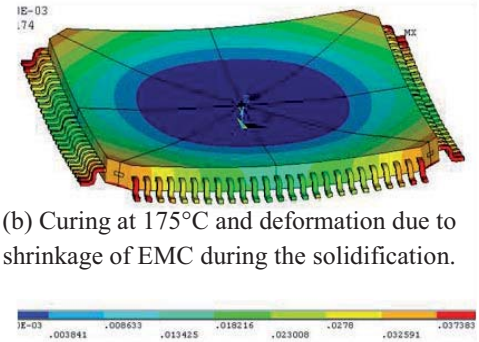

(b) Curing at 175°C and deformation due to shrinkage of EMC during the solidification.

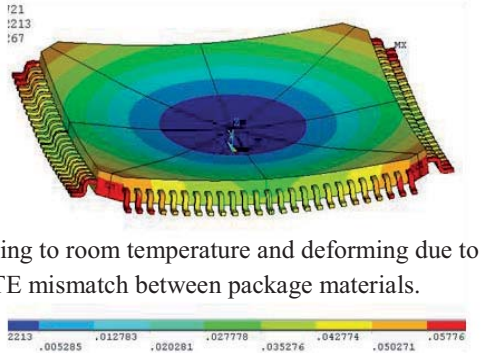

(c) Cooling to room temperature and deforming due to CTE mismatch between package materials.

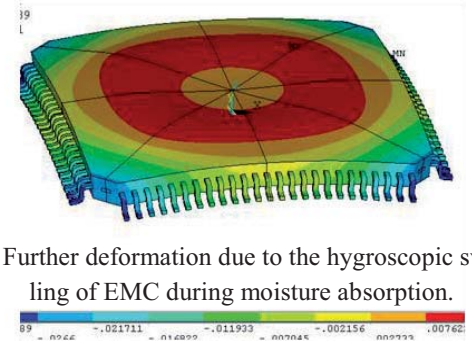

(d) Further deformation due to the hygroscopic swelling of EMC during moisture absorption.

Figure 10.3 Deformation of a TQFP-epad package after (a) mold injection (b) manufacturing (c) cooling (d) moisture preconditioning.

Once the interfacial fracture toughness is known, it is possible to predict as to whether the loading condition is able to force an existing crack to propagate. A major challenge to model cracked IC packages is the huge variation of length scales, the complexity of microstructures, and diverse materials properties. In this example, we simplified the structure and neglected the small local features of integrated circuits.

Fig. 10.4a shows an FE-simulation of this package with a very short pre-crack length at leadframe/epoxy molding compound interface. The FE model was done using a parametric script for the finite element tool ANSYS. The crack length was varied and the analysis was carried out at each step. Fig. 10.4b shows the same package while the pre-crack length was assumed to be quite larger. The nodal loads and displacements were exported for the further post-processing to determine the components of the strain energy release rate. A temperature change of 150°C to -40°C was used as the loading, which mimics the first cycle of temperature cycle test.

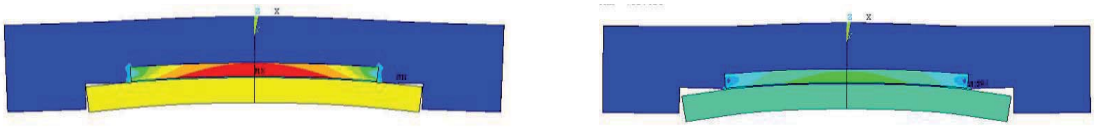

(a) (b)

Figure 10.4 FE modeling the crack at leadframe/EMC interface of a TQFP-epad package. (a) short crack, (b) large crack.

The energy release rate and the mode angle of crack at the leaframe/EMC interface based on the asymptotic linear elastic stress field are determined by VCCT. Fig 10.5 shows the strain energy release rate as a function of the crack length. From this figure it is evident that the energy release rate in this package depends on the crack length at the interface. For short crack lengths the strain energy release rate remains almost constant at moderate values. The *G* value is smaller than the interfacial fracture toughness found in Chapter 8 for the respective mode mixity. This means that an existing crack with the length below a certain length does not pose a potential risk regarding the crack propagation during a temperature cycle. This is in agreement with the experimental temperature cycles performed on these packages, where it was observed that the length of delamination after the solder reflow process determines if the crack would propagate during subsequent temperature cycles.

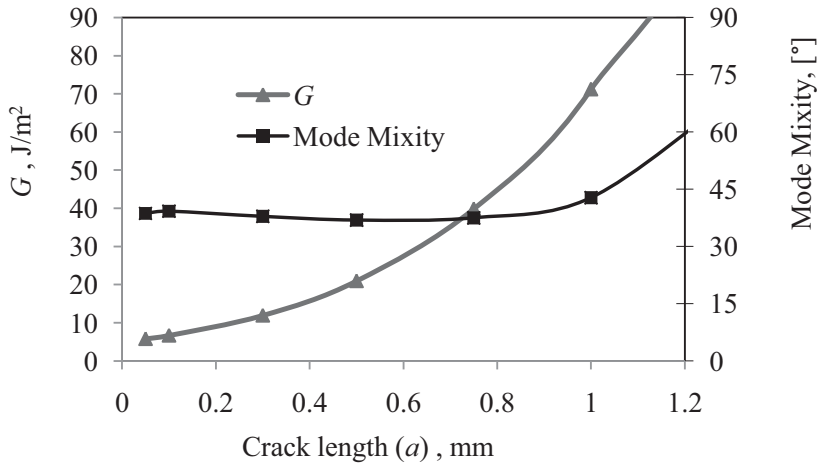

Figure 10.5 Normalized strain energy release rate and mode mixity of interfacial crack are plotted as a function of crack length.

As shown in this figure, the mode mixity at the crack tip varies between 4 degrees for very short cracks up to approximately 15 degrees for large cracks of around 1 mm length. This means that the fracture mode in this package is mainly dominated by mode I fracture. Since the interfacial fracture toughness of this interface (Cu/**MC-1**) is known through the experimental part of Chapters 8 and 9, it is possible to determine the critical pre-crack length, which leads energy release rate to exceed the interfacial fracture toughness and hence enable crack propagation. Obviously, this critical length of the pre-crack is different for packages that have experiences various humid environments. This is because of the fact that by exposure to moisture the adhesion strength of interfaces decrease as observed in Chapter 9.

It is important to note that this analysis was performed for a package at dry state. When moisture is available, the first step is to determine the state of moisture concentration similar to the example in Section 10.2. In a most simple form, by assuming one week sorption at 85°C/85%RH (Fig. 10.1d) the interfacial adhesion is almost 40% lower than that for dry package. Due to the relatively short diffusion path to interface because of thin geometry of package, the moisture concentration may most probably reach the second phase of the absorption curve as described in Chapter

5. This means that there would be no recovery in adhesion when the samples are baked prior to temperature cycle. As a result of adhesion degradation, in the case of one week prior sorption at 85°C/85%RH, the critical crack length of moisture-preconditioned package is almost 0.2 mm. This indicates that crack propagation at the interface of moisture treated samples is possible with smaller initial crack length as compared to dry samples.

10.4 Material Selection and Design Change

This section presents an example of designing more reliable packages with higher resistance against interfacial delamination and shows how the methods described in this work can help the packaging engineers develop the electronic packages more easily, letting decision making be more reliable and hence saving time and money. The package under investigation is a Hiquad (MO-188) power package with the materials and geometry shown in Fig. 10.6. Although, in this work only the interfacial fracture toughness between EMC and leadframe was determined, it is also possible to investigate other interfaces using the same method.

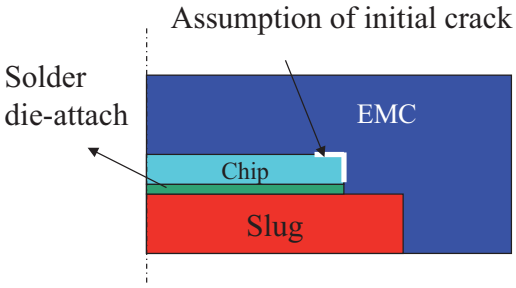

Figure 10.6 Investigation of the effect of slug thickness and EMC material on the reliability of chip/EMC interface.

In the FE modeling a viscoelastic model was assigned to the EMC material and an elasto-plastic model was used for the solder die-attach. The other materials were treated as linear elastic. From two available EMC materials and two possible slug thicknesses a combination must be selected that shows the least delamination risk at the chip/EMC interface. Three cases are investigated by using a parametric FE analysis as shown in Table 10.1. A comparison between case 1 and case 2 will reveal if by using a higher slug thickness the delamination risk will change. Moreover, by comparing case 1 with case 3 it is possible to predict which EMC material may yield the least strain energy release rate and hence the highest resistance to interface delamination.

Table 10.1 Three cases of material/geometry combinations to be investigated for a reliable interface.

	Slug thickness (mm)	EMC material used in package
Case 1	0.9	**MC-1**
Case 2	1.4	**MC-1**
Case 3	0.9	**MC-2**

By using the viscoelastic material data together with the cure shrinkage values shown in Chapter 4 warpage analyses of the three cases were carried out. In the absence of moisture the warpage of a package is mainly dominated by the cure shrinkage of the molding compound and the coefficient of thermal expansion of the package materials. As shown in Fig. 10.7, the warpage of case 3 is in all temperatures higher than that for the other two cases. This means that a combination of a thin slug together with using **MC-2** as EMC material will lead to the highest stresses in the package and, hence, increasing the delamination risk.

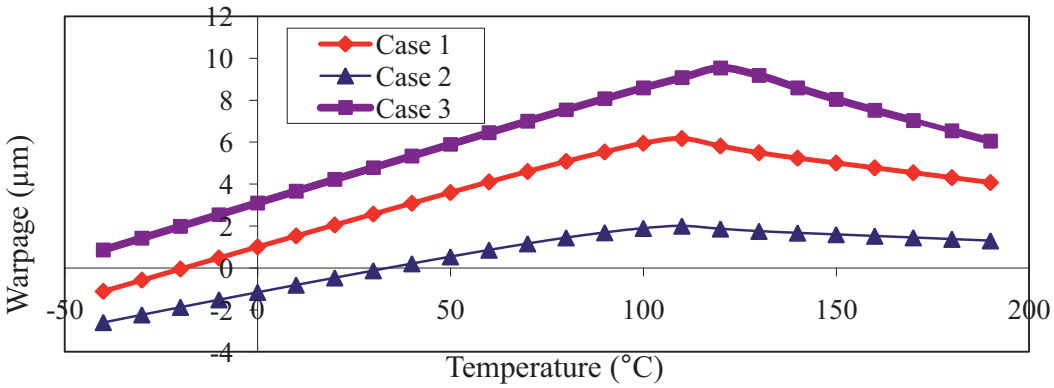

Figure 10.7 Comparison between the warpage curves of three cases.

Warpage simulation shows that case 2 leads to the lowest warpage at elevated temperatures. This means that the package at these temperatures is under lower stresses and the structural integrity can be likely preserved. Obviously, when talking about the delamination risk, fracture mechanics is a more reliable approach. However, the problem associated with this approach is that in contrast to Cu/EMC interface, a fracture toughness value for chip/EMC interfaces of these materials is not available. However, a quantitative comparison between these cases is possible by comparing the strain energy release rates. In this case it is possible to make a consistent comparison between the *G* values as shown in Fig. 10.8. In this figure the strain energy release rate at the tip of the crack is determined using the VCCT method for a temperature change of 150°C to -40°C. As evident, the case 3 yields the highest *G* value while case 2 leads to the lowest *G*. This means that by increasing the slug thickness the delamination risk can be significantly reduced, while using the **MC-1** seems to induce smaller warpage values than **MC-2**. The successful candidate for the least delamination risk is according to these analyses case 2.

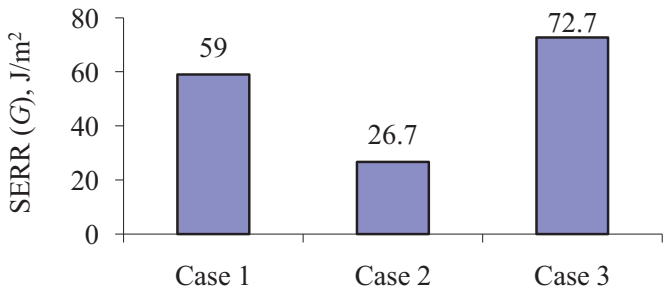

Figure 10.8 Comparison between the strain energy release values of three cases.

Chapter 11 Concluding Remarks and Outlook

11.1 Concluding Remarks

One of the main concerns in the reliability of electronic packages is their structural integrity during their fabrication, surface mounting process, and service life. A prominent example of failure in electronic assemblies is the interface delamination between dissimilar materials. This failure mode is accelerated when the polymeric materials absorb moisture from humid environments. Moisture results in degradation of material properties, induces additional deformation due to hygroscopic swelling and, more importantly, degrades the adhesion strength.

Due to the complexity of the problems a broad experimental and analytical study was performed to identify the physical mechanisms and the critical factors that influence the loss in interfacial adhesion as a result of moisture. Several micromechanical aspects of the effect of moisture on the epoxy molding compounds were taken into consideration. From a global perspective, the primary aspects considered include moisture diffusion behavior, hygroscopic swelling, and the effect of moisture on interfacial adhesion. Based on the experimental results and on corresponding numerical analysis, the following fundamental conclusions can be made:

- Moisture transport in epoxy molding compounds shows essentially a non-Fickian diffusion behavior. The moisture uptake curve consists of two parts. The first part is similar to the conventional Fickian curve with a so-called saturation. However, if the samples are exposed to humid environments for a longer period, the second part of the moisture uptake curve, which is a straight line can be observed.
- From the large number of experiments on different sample geometries and preconditioning environments it was concluded that the second linear part of the absorption curve is a nonreversible process and is responsible for a permanent increase in the weight of the plastic parts. In other words, residual moisture content upon desorption tests is the direct consequence of the second linear part of the absorption curve.

- The sorption history of the EMC samples was also investigated. It was observed that, in general, the storage of EMC materials at elevated temperatures results in the formation of new micro-pores in polymers and, consequently, an increase in the diffusivity.
- A remarkable identification from the experimental parts of this study is the difference between the diffusion of moisture through bulk EMC samples and that along the interface between two materials. Two types of experimental analyses support the hypothesis that the diffusion coefficient along the EMC/Cu interface is much larger than that in the bulk EMC sample:
  - First, gravimetric analyses showed that the moisture uptake of structures with interfaces (plastic packages and bimaterial beams) was much faster than that for bulk EMC materials.
  - Second, the adhesion degradation of bimaterial beam samples was found to be remarkably faster than the diffusion of moisture in bulk EMC materials. This suggests that water molecules diffuse much faster along the interfaces and is the reason that the bimaterial samples with unsealed interfaces showed more susceptibility to short-term exposure to moisture than those samples with protected interfacial diffusion path.

In order to use simulation tools for the reliability analysis of plastic IC packages detailed material characterization is required. Several mechanical material parameters were found experimentally. These material parameters are essential for a successful thermo-mechanical FE analysis. However, there are some characteristics that cannot be estimated directly by using the mechanical testing methods. For example, the analysis of stresses by thermo- or hygro-mechanical FE analysis requires the cure shrinkage and hygroscopic swelling coefficient of polymers. These two factors were estimated through a series of experimental-numerical studies as follows:

- The cure shrinkage of the epoxy molding compound due to the polymerization process was found to play a significant role in the overall structural behavior of plastic parts.
- Since the EMC suppliers do not usually provide information on the amount of shrinkage of the materials during the fabrication, a simple bimaterial beam was applied to find the amount of shrinkage. The warpage of the beam was measured at various temperatures, the thermal strains were modeled analytically, and the cure shrinkage was estimated.
- Once the cure and thermal strains and the material constitutive law are known, it is possible to run an FE analysis and find the stresses in the plastic parts.
- Hygroscopic swelling of polymers also contributes to the residual stresses in the multi-layered structures. Depending on the geometry, coefficient of hygroscopic swelling, and the behavior of other materials, diffusion of moisture may increase or decrease the stresses in these samples. It is essential to account for these stresses, because otherwise it may be possible that the state of stress (compressive or tensile) is predicted incorrectly. The simple bimaterial samples were used to estimate the hygroscopic swelling coefficient by warpage analysis.

Adhesion between the epoxy molding compound and the copper-based leadframe was also investigated. It was found that the determination of the intrinsic interfacial fracture toughness requires

a detailed understanding of the residual stresses. This means that the analytical solutions for the estimation of the strain energy release rate are not applicable for polymer/metal interfaces because they do not account for the residual stresses. Consequently, in order to determine the intrinsic interfacial fracture toughness of Cu/EMC samples, in this study a series of experimental-numerical analyses were performed as follows:

- First, fracture tests were performed in order to find the critical load that leads to propagation of a precrack at interface. This load was used as an input for the FE analysis of the fracture test.
- Next, the modeling of the fracture test using FE analysis was performed. Since the samples are under residual stresses, the sample fabrication and sorption history was modeled. Then the critical load and the precrack reported from the experimental investigation were modeled.
- Finally a fracture mechanics numerical method was employed and the interfacial fracture toughness was estimated.

A large number of environmental and test conditions were investigated and the effect of each individual factor was studied. The fracture tests results can be summarized in the following statements:

- The effect of test temperature on the interfacial fracture toughness is different for temperatures below and above the glass transition temperature of the EMC materials. While at low temperatures below the glass transition of EMC the interfacial fracture toughness increases with increasing the temperature, the fracture toughness decreases significantly at elevated temperatures above the T_g.
- Aging in dry conditions was also investigated. It was found that the aging at low temperature does not influence the toughness values significantly. However, aging at 175°C caused a remarkable decrease in the interfacial fracture toughness. This can be attributed to the breakage of van der Waals bonds as a consequence of high temperature storage.
- A large number of test specimens were dedicated to the investigation of the effect of moisture on the interfacial fracture toughness. It was found that the presence of water molecules at the interface of the EMC/Cu results in a dramatic loss in the adhesion. However, the storage time in humid environment has a significant effect on the recoverability of adhesion upon baking of the samples.
    - Samples that were stored in humid environment for short time showed higher fracture toughness values after baking in comparison to those samples that were aged for a longer time in humid condition.
    - The main consequence of dual-stage moisture uptake was observed in the fracture toughness results. The effect of second phase of moisture absorption was the destruction of secondary bonds and hence the permanent loss in adhesion strength.

The desorption tests of the bulk EMC samples together with the fracture tests upon baking of preconditioned samples gave a fundamental understanding of the effect of moisture on the EMC materials: The adhesion loss in epoxy molding compounds is due to the replacement of second-

ary bonds between adhesive and substrate with the hydrogen bonds between water molecules and polymer chains.

The experimental-analytical technique developed in this research could also be extended to account for delamination analysis of plastic IC packages. For example, the delamination risk of a plastic IC package under thermal cycle was investigated. It was shown that the selection of material combination can significantly result in the reduction of delamination risk. This technique could be successfully used to predict the most suitable material and geometry combinations.

11.2 Recommendations and Future Work

It is important to note that the fracture mechanics method is essentially a very time-consuming and expensive approach. It needs a large number of material characterizations, sample fabrication, precondition time and testing facilities. From the design to the fabrication of proper samples it might take several weeks time and cost a lot. However, to the author's best knowledge, the benefits of this approach are so many so that fracture mechanics is still the most promising feature in the reliability analysis of interfaces. Future work can be built from this study to expand the knowledge of moisture degradation mechanisms to yield more robust products not only in microelectronic packaging applications, but also in other areas like adhesive joints, composite, and coating materials.

Future contributions are needed to advance the understanding of the role of moisture in the reliability of polymers on the micro- and nano-scale. For example early works of molecular dynamics simulation have shown that this method is able to provide valuable information on the relation between the molecular structures of the materials with their macroscopic diffusion behavior. This method may be used for the moisture-related issues, such as interfacial fracture due to interfacial moisture diffusion.

With the increasing use of nano-particles in all aspects of material science, the development of nano-filled epoxy molding compound would be a logical extension to this work. This is obviously not an easy task, because many reliability aspects, such as adhesion, cure shrinkage, and swelling of these materials may change by introducing nano-particles.

The effect of moisture on the behavior of the Cu/EMC interfaces under fatigue loading conditions will complete the picture of delamination under different environmental conditions and may be a good topic for future researches.

Modern numerical approaches such as using cohesive zone elements and XFEM have gained more attention in recent years. Especially the latter is the subject of many current studies and may soon be used in the industrial sectors.

References

1. Abdullah S., Abdullah M.F:, Ariffin A., Jalar A. (2009), "Effect of leadframe oxidation on the reliability of a Quad Flat No-Lead package," *J. Electron. Packaging*, Vol. 131, Issue 3, pp. 31002-31009.
2. Adamson, M.J. (1980), "Thermal expansion and swelling of cured epoxy resin used in graphite/epoxy composite materials," *Journal of Material Science*, Vol. 15, pp. 1736-1745.
3. "adhesive," (2009), *Encyclopædia Britannica*. 2009. Encyclopædia Britannica Online. 15 Oct. 2009 <http://www.britannica.com/EBchecked/topic/5823/adhesive>.
4. Agraeal A., Karlsson A.M. (2006), "Obtaining mode mixity for a bimaterial interface crack using the virtual closure technique", *Int J Frac* (141), pp. 75-98.
5. Agrawal A., Karlsson A.M. (2007), "On the reference length and mode mixity for a bimaterial interface," *Transactions of the ASME*, Vol. 129, pp. 580-587.
6. Anderson T.L. (2005), "Fracture mechanics: fundamentals and applications, New York.
7. Ardebili H., Wong E.H., Pecht M. (2003), "Hygroscopic swelling and sorption characteristics of epoxy molding compounds used in electronic packaging," *IEEE Trans. Comp. Package Technology*, Vol. 26, pp. 206-214.
8. Ardebili H., Hillman C., Natishan M.A.E., McCluskey P., Pecht M.G., Peterson D. (2002), "A comparison of the theory of moisture diffusion in plastic encapsulated microelectronics with moisture sensor chip and weight-gain measurements," *IEEE Transaction on Components and Packaging Technologies*, Vol. 25, pp. 132-139.
9. Asao N., Isao H., Naotaka T. (1992), "A new method for measuring adhesion strength of IC molding compounds," *J. Elect. Packaging* (114), pp. 402-412.
10. Auersperg. J, Seiler B., Cadalen E., Dudek R., Michel B. (2005), "Fracture mechanics based crack and delamination risk evaluation and RSM/DOE concepts for advanced microelectronics applications," *Proc 6th Int. Conf. EuroSime*, pp. 197-200.
11. Bagchi A., Evans A.G., (1996), "The mechanism and physics of thin film decohesion and its measurement," *Interface Science 3*, pp. 169-193.
12. Beuth J.L. (1996), "Separation of crack extension modes in orthotropic delamination models" *Int. J. Fracture*, Vol. 77, pp. 305-321.
13. Bowden F.P., Throssell W.R. (1951), "Adsorption of water vapor on solid surfaces," *J. Nature*, Vol. 167, pp. 601-602.
14. Brewis D.M., Comyn J., Raval A.K:, Kinloch A.J. (1990), "The effect of humidity on the durability of Aluminum-Epoxide joints," *Int. J. Adhesion and Adhesive,* Vol. 10, pp. 247-253.
15. Brown W., ed., 1999, *Advanced* Electronic Packaging with Emphasis on Multichip Modules, *IEEE Press*, New York.

16. Buchwalter, L.P., (1996), "Polyimides: Fundamental aspects and applications," *Adhesion of polyimides to various substrates.* New York, Marcel Dekker, pp. 587-628.

17. Buehler F., Seferis J. (2000), "Effect of reinforcement and solvent content on moisture absorption in epoxy composite materials," *Composites: Part A: Applied Science and Manufacturing*, Vol. 31, pp. 741-748.

18. Celik E., Guven I., Madenci E. (2007), "Experimental and numerical characterization of non-Fickian moisture diffusion in electronic packages," *Proc. Electron. comp. Technology Conf. (ECTC2007)*, pp. 1069-1073.

19. Chan E., Yuen M. (2007), "Study of interfacial moisture diffusion at Cu/Epoxy interface by FTIR-MIR technique," *Proceedings of Electronic and Component and Technology Conference*, pp. 1782-1787.

20. Charalambides P.G., Lund J., Evans A.G., McMeeking R.M. (1989), "A test specimen for determining the fracture resistance of bimaterial interface*", J Appl Mech*., (111), pp. 77-82.

21. Chaware R., Vichare N., Borgesen P., Blass, D., Srihari, K. (2004), "Accelerated testing of flip chip underfills and the effect of moisture and temperature on the aging of underfills," *Proceedings of 2004 Surface Mount Technology Association International*, pp. 374-380.

22. Chen X., Zhao S. (2005), "Moisture absorption and diffusion characterization of molding compound," *J. Electronic Packaging*, Vol. 127, pp. 460-465.

23. Chew S., Tan A. (2003), "Evaluating the influence of post mold cure and additives on the viscoelastic properties of a low stress epoxy molding compound," *IEEE Tans. Electronic Packaging Manufacturing*, Vol. 26, Nr. 3, pp. 211-215.

24. Chong C.T., Leslie A., Beng L.T., Lee C. (1995), "Investigation on the effect of leadframe oxidation on package delamination," *Proc. IEEE Electronic Components and Technology Conference 1995*, pp.463-469.

25. Comyn J, Groves C., Saville R. (1994), "Durability in high humidity of glass-to-lead alloy joints bonded with an epoxide adhesive," *International Journal of Adhesion and Adhesives*, Vol. 14, pp. 15-20.

26. Databeans Research Group Report (2009), ISBN/SKU: DB4569 "Automotive semiconductors," February 2009.

27. Dauskardt R.H., Lane M., Ma Q., Krishna N. (1998), "Adhesion and debonding of multi-layer thin film structures," *Engineering Fracture Mechanics* 61, pp. 141-162.

28. Davidson B.D., Sun X. (2005), "Effects of friction, geometry, and fixture compliance on the perceived toughness from three- and four-point bend end-notched flexure tests," *Journal of reinforced plastics and composites*, (24), pp. 1611-1629.

29. Davis D., Krebs A., Drzal L.T., Rich M.J., Askeland P. (2000), "Electrochemical sensors for nondestructive evaluation of adhesive bonds," *J. Adhesion.*, 72, pp. 335-358.

30. De Morais A.B. (2004), "Analysis of mode II interlaminar fracture of multidirectional laminates," *Composites Part A* (35), pp. 51-57.

31. Dermitzaki E., Wunderle B., Bauer J., Walter H., Michel B. (2008a), "Structure property correlation of epoxy resins under the influence of moisture; and comparison of Diffusion Coefficient with MD-Simulations," *Proc. 9th Eurosime2008,* pp 204-211.

32. Dermitzaki E., Wunderle B., Bauer J., Walter H., Michel B. (2008b), "Structure Property Correlation of epoxy resins under the influence of moisture and temperature; and comparison of Diffusion coefficient with MD-simulations," *Proc. ESTC* 2008, Greenwich, UK, pp. 897-902.

33. Dodiuk H., Dori L., Miller J. (1984), "The effect of moisture in epoxy film adhesives on their performance: I. lap shear strength," *Journal of Adhesion*, Vol. 17, pp. 33-44.

34. Dreßler M., Rohde H., Liebing G., Becker K.-F., Wunderle B., Reichl H. (2006), "Influence of assembly process, material properties geometry on the reliability of flip-chip interconnections on MID for automotive applications," *Proceedings of 7th international congress of molded interconnect devices*, Fürth, Germany.

35. Dudek R., Walter H., Michel B. (2002), "Studies on moisture diffusion and popcorn cracking," *Proc. EuroSimE2002.*, pp. 225-232.
36. Dundurs J. (1967), "Effect of elastic constants on stress in composite under plane deformation," *J Compos Mater* 1(3), pp. 310–322.
37. Dundurs J. (1969), "Discussion: edge-bonded dissimilar orthogonalelastic wedges under normal and shear loading," *Trans ASME J Appl Mech*, pp. 650–652.
38. Fan C., Ben Jar P.Y., Cheng J.R. (2007), "A unified approach to quantify the role of friction in beam-type specimens for the measurement of mode II delamination resistance of fiber-reinforced polymers," *Composites Science and Technology* (67), pp. 989-995.
39. Fan X.J., Wang H.B. Lim T.B. (1999), "Investigation of the underfill delamination and cracking in flip chip modules under temperature cyclic loading," *Proceedings of the Electronic Components and Technology Conference*, pp. 994-1000.
40. Fan, X.J., Zhou, J., Zhang, G.Q. (2004), "Multi-physics modeling in virtual prototyping of electronic packages - combined thermal, thermo-mechanical and vapor pressure modeling," *Journal of Microelectronics Reliability*, Vol. 44, pp. 1967-1976.
41. Fan, X.J., Zhou, J., Zhang, G.Q., Ernst, L.J. (2005), "A micromechanics based vapor pressure model in electronic packages," *ASME Journal of Electronic Packaging,* 127 (3), 262-267.
42. Fan, X.J., (2008a), "Mechanics of moisture for polymers: fundamental concepts and model study," *Proc.9th EuroSime2008*, pp. 159-172.
43. Fan, X.J., Zhang, G.Q., van Driel, W.D., Ernst, L.J. (2008b), "Interfacial delamination mechanisms during reflow with moisture preconditioning," *IEEE Transactions on Components and Packaging Technologies*, 31(2), pp. 252-259.
44. Fan X.J., Zhou J., Chandra A. (2008c), "Package structural integrity analysis considering moisture," *Proc. electon. Comp. Technol. Conf. (ECTC)*, pp. 1054-1066.
45. Fan, X.J., Lee, S.W.R., Han, Q., (2009), "Experimental investigations and model study of moisture behaviors in polymeric materials," *Microelectronics Reliability*, Vol. 49, pp. 861–871
46. Ferguson, T. (2004), "Moisture and interfacial adhesion in microelectronic assemblies," *Dissertation for the degree of Doctor of Philosophy.* Atlanta, Georgia: Georgia Institute of Technology.
47. Ferguson T., Qu J. (2005), "Elastic modulus variation due to moisture absorption and permanent changes upon redrying in an epoxy based underfill," *IEEE Trans. Comp. Package Technologies.* Vol. 29, pp. 105-111.
48. Franks, F. (1998), "Water science reviews 3," Cambridge University press, Cambridge.
49. Galloway, J.E., Miles B.M., (1997), "Moisture absorption and desorption predictions for plastic ball grid array packages," *IEEE Transactions on Components, Packaging and Manufacturing Technology* 20(3), pp. 274-279.
50. Guojun H, Tay A, Yongwei Z., Chew S. (2007), "Experimental and numerical study of the effect of viscoelasticity on delamination in plastic IC packages," *Proc. ECTC2007*, pp.1062-1067.
51. Hae-Soo Oh (2004), "Accurate mode-separated energy release rate for delamination cracks," *Journal of computational physics*, Vol. 193, Issue 1, pp. 86-114.
52. Harries R.J. Sitaraman S.K. (2001), "Numerical modeling of interfacial delamination propagation in a novel peripheral array package," *IEEE Transactions on components and Packaging Technologies*, VOL. 24, NO. 2, pp.256-264.
53. He Y., Fan X.J. (2007), "In-situ characterization of moisture absorption and desorption in thin BT core substrate," *Proc. Electronic Copm. Tech. Conf.*, pp. 1375-1383.
54. "Hitachi Molding Compound website," (2009) *Hitachi Co.* <www.hitachi-chem.co.jp>.
55. Hofinger I., Oechsner M., Bahr H., Swain M. (1998), "Modified four-point bending specimen for determining the interface fracture energy for thin, brittle layers," *Int J Fract*, (92), pp. 213-220.
56. Hozoji H., Horie O., Ogata S., Numata S., Kinjo T. (1990), *Japanese Journal of Polymer Science and Technology*, 47, 483.

57. Huang Z., Suo Z., Xu G., He J., Prevost J.H., Sukumar N. (2005), "Initiation and arrest of interfacial crack in a four-point bend test," *Eng Frac Mech* (72), pp. 2584-2601.
58. Hutchinson J.W., Suo Z. (1992), "Mixed mode cracking in layered materials," *Adv. Appl. Mech*. 29(11), pp. 63-191.
59. Hwang S-J., Chang Y-S., "P-V-T-C equation of epoxy molding compound (2006)," *IEEE Transactions on components and packaging technologies*, Vol. 29, No. 1, pp. 112-117.
60. Irwin GR (1957), "Analysis of stresses and strains near the end of a crack traversing a plate," *J Appl Mech* (24), pp. 361–364.
61. Keller J. (2005), "Micro- and nanoscale characterization of polymeric materials by means of digital image correlation technique," *Dissertation for the degree of Doctor of Philosophy,* Cottbus, Germany: Brandenburgische Technische Universität , May 2005.
62. Kook S.-Y., Dauskardt R.H. (2002), "Moisture-assisted subcritical debonding of a polymer/metal interface," *Journal of Applied Physics*, Vol. 91, Nr. 3, pp. 1293-1303.
63. KPMG Report (2005), "Value, growth and profit in the global semiconductor industry," *A Survey of Industry Executives,* Second Quarter 2005.
64. Kinloch A. (1979), "Interfacial fracture mechanical aspects of adhesive bonded joints---A Review," *Journal of Adhesion*, Vol. 10, pp. 193-219.
65. Kinloch A. (1987) , "Adhesion and Adhesives Science and Technology", Chapman and Hall, London.
66. Kitano M., Nishimura A., Kawai S., Nishi K. (1998), "Analysis of package cracking during reflow solder process," *Proc. IEEE 26th Reliability Physics Symposium*, pp. 90-95.
67. Komori S., Sakamoto Y. (2009), "Development trend of epoxy molding compound for encapsulating semiconductor chips," In D. Lu, C.P. Wong (eds.), Materials for Advanced Packaging (pp. 339-363), Springer Science + Business Media.
68. Krueger R., Minguet O.J. (2002), "Influence of 2D finite element modeling assumptions on debonding prediction for composite skin-stiffener specimens subjected to tension and bending," NASA/CR-2002-211452.
69. Krueger R. (2002), "The virtual crack closure technique: history, approach and applications," NASA technical report for Langley Research Center.
70. Lahiri S.K., Waalib Singh N.K., Heng K.W., Ang L., Goh L.C. (1998), "Kinetics of oxidation of copper alloy leadframes," J*ournal of Microelectronics*, Vol. 29, Pages 335-341.
71. Lam W.K., Yeung T.S., Teng A., Yuen M.F. (2000), "A method for evaluating delamination between epoxy molding compounds and different plated leadframes," *IEEE International Symposium on Electronic Materials & Packaging 2000*, pp. 214-219.
72. Lau J.H., Lee R.S., Chang C. (2000), "Effects of underfill material properties on the reliability of solder bumped flip chip on board with imperfect underfill encapsulants," *IEEE Transactions on Components and Packaging Technologies*, Vol. 23, No. 2, pp. 323-333.
73. Leblanc F. (2004), "Contribution to methodology for the analysis of fracture phenomena in encapsulated components," *Dissertation for the degree of Doctor of Philosophy,* Robert Bosch GmbH, Stuttgart, and L'Universite de Valenciennes, France, December 2004.
74. Lee H.Y., Park G.S. (2002), "Failure paths at copper-base leadframe/epoxy molding compound interfaces," Journal of Materials Science, Vol. 37, pp. 4247-4257.
75. Lee K.C., Alpern P. (2007), "On the physics of failure in the case of moisture induced delamination in plastic encapsulated microelectronic devices," *IEEE 45th Annual International Reliability Physics Symposium, Phoenix, 2007*. pp. 102-106.
76. Lefebvre D.R., Elliker P.R., Takahashi K.M., Raju V.R., Kaplan M.L. (2000), "The critical humidity effect in the adhesion of epoxy to glass: role of hydrogen bonding," *J. Adhesion Science and Technology*, Vol. 14, Number 7, pp. 925-937.
77. Le Gall C.A., Qu J., McDowell D.L. (1996), "Delamination cracking in encapsulated flip chips," *Proceedings of the Electronic Components and Technology Conference*, pp. 430-434.

78. Lekatou A., Faidi S.E., Ghidaoui D., Lyon S.B., Newman R.C. (1997), "Effect of water and its activity on transport properties of glass/epoxy particulate composites," *J. Composites Part A: applied science and manufacturing*, Vol. 28, pp. 223-236.

79. Liechti K.M., Chai Y.-S. (1991), "Biaxial loading experiments for determining interfacial fracture toughness", *Transaction of the ASME*, Vol 58, 680-687.

80. Lin C., Suhling J.C., Lall P. (2009), "Isothermal aging induced evolution of the material behavior of underfill encapsulants," *Proc Elect Comp Tech Conf ECTC,* pp. 134-149.

81. Lin Y., Tsui T.Y. and Vlassak J. (2007), "Water diffusion and fracture in organosilicate glass film stacks," *Acta Materislia*, Vol. 55, pp. 2455-2464.

82. Lin, Y.C. (2006), "Investigation of the moisture-desorption characteristics of epoxy resin," *Journal of Polymer Research*, Vol. 13, pp. 369-374.

83. Loh W.K., Crocombe A.D., Abdel Wahab M.M., Aschroft I.A. (2005), "Modeling anomalous moisture uptake, swelling and thermal characteristics of a rubber toughened epoxy adhesive," *Int. J. Adhesion & Adhesives,* Vol. 25, pp. 1-12.

84. Loo S., Zhang X., Shen NG H., Yan Tee T., Mhaisalkar S.G. (2007), "Impact of thermal, moisture, and mechanical loading conditions on interfacial fracture toughness of adhesively bonded joints," *Journal of Electronic Materials*, Vol. 36, pp. 110-116.

85. Lu X., Hofstra P., Bajkar R. (1998), "Moisture absorption, dielectric relaxation, and thermal conductivity studies of polymer composites," *Journal of Polymer Science: Part B: polymer Physics*, Vol. 36, pp. 2259-2265.

86. Lu, M., Shim, M., Kim, S., (2001), "Effects of moisture on properties of epoxy molding compounds," *Journal of Applied Polymer Science*, Vol. 81, pp. 2253-2259.

87. Luo S., Wong C.P. (2005), "Influence of temperature and humidity on adhesion of underfills for flip chip packaging," *IEEE Transactions on Components and Packaging Technologies*, (28), pp. 88 – 94.

88. Malyshev BM, and Salganik RL (1965), "The strength of adhesive joints using the theory of cracks," *Int J Frac* (1), pp. 114–128.

89. McBrierty V.J., Martin S.J., Karasz F.E. (1999), "Understanding hydrated polymers: the perspective of NMR," *Journal of molecular liquids.* Vol. 80, Number 2, pp. 179-205.

90. Mercado L.L., Sarihan V., Hauck T. (2000), "An analysis of interface delamination in flip-chip packages," *Proceedings of the Electronic Components and Technology Conference*, pp.1332-1337.

91. Morgan, R., O'Neal, J., Fanter, D. (1980), "The effect of moisture on the physical and mechanical integrity of epoxies," *Journal of Materials Science*, Vol. 15, pp. 751-764.

92. Nguyen T., Byrd B., Alsheh D., McDonough W., Seiler J., "Interfacial water and adhesion loss of polymer coatings on a siliceous substrate," *Mater. Res. Soc.,* 1995, pp. 57-63.

93. O'Brien, E. P. (2003), "Durability of adhesive joints subjected to environmental stress," *Dissertation for Doctor of Philosophy,* Virginia Polytechnic Institute.

94. Orman S., Kerr C. (1971), "Aspects of Adhesion" (Ed. D.J. Alner), University of London Press, London.

95. Østergaard R.C., Sørensen B.F. (2007), "Interface crack in sandwich structures," *Int J Frac*, (143), pp. 301-316.

96. Pan J, Curry R., Hubble N., Zwemer D. (2007), "Comparing techniques for temperature-dependent warpage measurement", *Report of AkroMetrix LLC*, Atlanta, Georgia.

97. Park S., Tang Z., Chung S. (2007), "Temperature effect of interfacial toughness on underfill for ob-free flip chip packages," *Proc. IEEE Electronic Components and Technology Conference 2007*, pp. 105-109.

98. Pecht M.G., Nguyen L.T., Hakim E.B. "Plastic-Encapsulated Microelectronics," New York : Wiley, 1995.

99. Reeder J.R., Allen D.H., Bradley W.L. (2003), "Effect of elevated temperature and loading rate on delamination fracture toughness," *ICCM 14th International Conference on Composite Materials,* 14-18 Jul. 2003, USA.

100. Rice J.R., Sih G.C. (1965), "Plane problems of cracks in dissimilar media," *J. Appl. Mech*. 32, pp. 418-423.
101. Rice J.R. (1998), "Elastic fracture mechanics concept for interfacial cracks," *J Appl Mech Trans. ASME* 55(1), pp. 98-103.
102. Roham S., Hight T. (2006), "Role of residual stress on crack penetration and deflection ata bimaterial interface in a 4-point bend test," *Microelectronic Engineering* Vol. 84, pp. 72-70.
103. Rosen S., (1993), "Fundamental Principles of Polymeric Materials," John Wiley and Sons, New York.
104. Rybicki E.F., Kanninen M.F. (1977), "A finite element calculation of stress intensity factors by a modified crack closure integral," *Eng Frac Mech,* (9), pp. 931–938
105. Saether E., Ta'asan S. (2004), "A hierarchal approach to fracture mechanics," NASA Langley Research Center Hampton, Virginia Report: 23681-2199.
106. Saitoh T., Matsuyama H. Toya M., (2000), "Linear fracture mechanics analysis on growth of interfacial delamination in LSI plastic packages under temperature cyclic loading," *IEEE Transactions on Components, Packaging and Manufacturing Technology*, Vol. 21, No. 4, pp. 422-427.
107. Sandor M., Evans K. (2000) "Plastic parts delamination validation using failure analysis methods," *NASA Electronic Parts Program, technical report ID 20060040443*.
108. Schlottig G., Pape H., Wunderle B., Ernst L. (2009), "Induced delamination of silicon-molding compound interfaces," *Proc. of 10th EuroSimE*, Delft, the Netherlands, pp. 731-734.
109. Schlottig G., Xiao A., Pape H., Wunderle B., Ernst L. (2010), "Interfacial strength of silicon-to-molding compound changes with thermal residual stress," *Proc. of 11th EuroSimE*, France, 2010.
110. Schreier-Alt T., Schindler-Saefkow F., Wittler O., Kittel H. (2008), "Encapsulation of system in package- process characterization and optimization," *Proc. Electronics System Integration Technology Conference ESTC2008*, pp. 1017-1022.
111. Schuecker C., Davidson B.D. (2000), "Evaluation of the accuracy of the four-point end notched flexure test for mode II delamination toughness determination,", Composites Part A, (60), pp. 2137-2146.
112. Seraphim D., Lasky R.C., Li C. (1989), "Principles of electronic packaging," McGraw-Hill Education.
113. Shaviv R., Roham S., Woytowitz P. (2005), "Optimizing the precision of four-point bend test for the measurement of thin film adhesion," *Microelectronic Engineering* (82), pp. 99-112.
114. Shaw G., Rogers V., Payer J. (1992), "The effect of immersion on the breaking force and failure locus in an epoxy/mild steel system," *Journal of Adhesion*, Vol. 38, pp. 225-268.
115. Shen C.H., Springer G.S. (1976), "Moisture absorption and desorption of composite materials," *J. Composite Materials*, Vol. 10, pp. 2-20.
116. Shi X., Zhang Y., Zhou W., Fan X.J. (2008), "Effect of hygrothermal aging on interfacial reliability of silicon/underfill/FR-4 assembly," *IEEE Trans. Comp. Packaging Technol.*, Vol. 31, pp. 94-103.
117. Shindo Y., Sato T., Narita F., Sanada K. (2008), "Mode II interlaminar fracture and damage evaluation of GFRP woven laminates at cryogenic temperatures using the 4ENF specimen," *Journal of Composite Materials*, (42), pp. 1089-1101.
118. Shirangi M.H., Auersperg J., Koyuncu M., Walter H., Müller W.H., Michel B. (2008a), "Characterization of dual-Stage moisture diffusion, residual moisture content and hygroscopic swelling of epoxy molding compounds," *Proc. 9th EuroSime2008*, pp. 455–462.
119. Shirangi M.H., Fan X.J., Michel B. (2008b), "Mechanism of moisture diffusion, hygroscopic swelling and adhesion degradation in epoxy molding compounds," *Proc. 41st International Symposium on Microelectronics (IMAPS2008)*, pp. 1082-1089.
120. Shirangi M.H., Gollhardt A., Fischer A., Müller W.H., Michel B. (2008c), "Investigation of fracture toughness and displacement fields of copper/polymer interface using image correlation technique," *Proc. 41st International Symposium on Microelectronics (IMAPS2008)*, pp. 917-923.
121. Shirangi M.H., Wunderle B., Wittler O., Walter H., Michel B. (2009a), "Modeling cure shrinkage and viscoelasticity to enhance the numerical methods for predicting delamination in semiconductor packages," *Proc. 10th EuroSime2009.* Delft, the Netherlands.

122. Shirangi M.H., Müller W.H., Michel B. (2009b), "Effect of nonlinear hygro-thermal and residual stresses on interfacial fracture in plastic IC packages", *Proc. 59th Electronic Components and Technology Conference (ECTC)*, San Diego, USA, pp. 232-238.
123. Shirangi M.H., Müller W.H., Michel B. (2009c), "Determination of Copper/EMC interface fracture toughness during manufacturing, moisture preconditioning and solder reflow process of semiconductor packages," *Proc. int. Conf. Fracture (ICF12)*, Ottawa, Canada.
124. Shirangi M.H., Michel B. (2010), "Mechanism of moisture diffusion, hygroscopic swelling and adhesion degradation in epoxy molding compounds," X. Fan, E. Suhir (*eds.*), Moisture Sensitivity of Plastic Packages of IC Devices, *Micro- and Opto-Electronic Materials, Structures, and Systems*, DOI 10.1007/978-1-4419-5719-1_2, @ Springer Science+Business Media, LLC 2010.
125. Soles C., Yee A. (2000), "A discussion of the molecular mechanisms of moisture transport in epoxy resins," *Journal of polymer science, Part B: Polymer Physics*, Vol. 38, pp. 792-802.
126. STMicroelectronics, "Introduction to semiconductor technologz," *AN900 Applications notes*.
127. Stellrecht E., Han B., Pecht M.G. (2004), "Characterization of hygroscopic swelling of mold compounds and plastic packages," *IEEE Trans. Comp. Package Technologies*, Vol. 27, pp. 499-506.
128. Sun X., Davidson B.D., "A direct energy approach for determining energy release rates in three and four point bend end notched flexure tests," *International Journal of Fracture*, Vol. 135, 2005, pp. 51-72.
129. Sun C.T., Qian W. (1997), "The use of finite extension strain energy release rate in fracture of interfacial cracks," *Int. J. Solid Structures*, Vol. 34, No. 20, pp. 2595-2609.
130. Takahashi, M.K. (1990), "ac impedance measurements of moisture in interfaces between epoxy and oxidized silicon," *J. Appl. Phys*, Vol. 67, pp. 3419-3429.
131. Tay, A., Lin, T.Y., (1996), "Moisture diffusion and heat transfer in plastic IC package," *IEEE Transactions on components and Packaging Technologies*, Vol.27, No. 3, pp. 186–193.
132. Tay A., Lin T. (1998), "Influence of temperature, humidity and defect location on delamination in plastic IC packages," *Proc. IEEE International Conference on Electronic Packaging Technology 1998*, pp.179-184.
133. Tencer, M. (1994), "Moisture ingress into nonhermetic enclosures and packages- A quasi steady state model for diffusion and attenuation of ambient humidity variations," *Proc. electon. Comp. Technol. Conf. (ECTC)*., pp. 196-209
134. Teverovsky A. (2002), "Moisture characteristics of molding compounds in PEMs," *NASA technical report, QSS Group, Inc./Goddard Operations*.
135. Teverovsky, A. (2002a), "A rapid technique for moisture diffusion characterization of molding compounds in PEMs," *NEPP Report, GSFC*.
136. Tummala, R., ed., 2001, Fundamentals of Microsystems Packaging, *McGraw Hill*, New York.
137. Van Driel W.D., Habets P.J., van Gils M.A.J., Zhang G.Q. (2005), "Characterization of interface strength as a function of temperature and moisture condition," *Proc. 6th EPTC*, pp. 687-692.
138. Van Driel W.D. (2007), "Virtual Thermo-Mechanical Prototyping of Microelectronics Devices," *Dissertation for the degree of Doctor of Philosophy*, Delft, Technical university of Delft, The Netherlands.
139. Van Gils, M.A.J. van Driel W.D., Zhang G.Q., Bressers H.J.L., et al. (2007), "Virtual qualification of moisture induced failures of advanced packages," *Microelectronics Reliability*, Vol. 47pp. 273–279.
140. Van Roosmalen A.J.(2006), "Microelectronics technology," In Zhang G.Q., van Driel W.D., Fan X.J. (eds.), Mechanics of Microelectronics, pp. 1-34, Springer Netherlands.
141. VEDDAC/MicroDAC, Chemnitzer Werkstoffmechanik GmbH, www.cwm-chemnitz.de.
142. Vine K., Cawley P., Kinloch A.J. (2001), "The correlation of non-destructive measurements and toughness changes in adhesive joints during environmental attack," *Journal of Adhesion.*, Vol. 77, pp. 125-161.
143. Vogel D., Dudek R., Keller J., Michel B. (2003), "Combining DIC technique and finite element analysis for reliability assessment on micro and nano scale,", *Proc 5th EPTC*, pp. 450-455.

144. Vreugd J., Jansen K.M.B, Ernst L.J., Bohm C., Kessler A., Preu H. (2008), "Effects of molding compound cure on warpage of electronic package," *Proc. EPTC2008*, pp. 675-682.

145. Walter H., Dermitzaki E., Shirangi M.H., Wunderle B., Hartmann S., Michel B. (2009a), "Influence of moisture on the time and temperature dependent properties of polymer systems," *Proc. 10th EuroSime,* April 2009*,* Delft*,* The Netherlands.

146. Walter H., Shirangi M.H., Dermitzaki E., Wunderle B., Michel B. (2009b), "Study on the effect of moisture and elevated temperature on the fracture properties of viscoelastic polymers," *Proc. int. Conf. Fracture (ICF12)*, July 2009, Ottawa, Canada.

147. Wang B., Siegmund T. (2008), "A modified 4-point bend delamination test," Microelectronic Engineering 85, pp. 477-485.

148. Wang Y., Han B., Bar-Cohen A. (2008), "Simultaneous measurements of effective chemical shrinkage and modulus evolution during polymerization," *Proc. Electronic Component and Technology Conference ECTC2008*, pp. 724-728.

149. Weitsman, Y.J. (2006), "Anomalous fluid sorption in polymeric composites and its relation to fluid induces damage," *J. of Composites Part A: applied science and manufacturing,* Vol. 37, pp. 617-623.

150. Williams ML (1959), "The stress around a fault or crack in dissimilar media," *Bull Seismol Soc. Am.*, 49, pp. 199-204.

151. Wittler O. (2004), "Bruchmechanische Analyse von viskoelastischen Werkstoffen in elektronischen Bauteilen," *Dissertation for the degree of Doctor of Philosophy,* Robert Bosch GmbH, Stuttgart and Technische Universität Berlin, Berlin, Germany, February 2004.

152. Wittler O., Sprafke P., Walter H., Gollhardt A., Vogel D., Michel B. (2000), "Time and temperature dependent mechanical characterization of polymers for Microsystems application," *Proceedings: Materials Week 2000,* München, Germany, pp. 25-28,

153. Wong E.H., Teo Y.C. Lim T.B. (1998), "Moisture diffusion and vapor pressure modeling of IC packaging *Proc. electon. Comp. Technol. Conf. (ECTC)*, pp. 1372-1378.

154. Wong, E. H., Chan, K. C., Rajoo, R., Lim, T.B. (2000), "The mechanics and impact of hygroscopic swelling of polymeric packaging materials in electronic packaging," *Proc. 50th Electronic Component Technology Conf (ECTC2000*), pp. 576–580.

155. Wong W.H., Cheng L. (2000), "Initiation and propagation of interface delamination in plastic IC packages," *Proceedings of the Electronic Components and Technology Conference*, pp. 277-282.

156. Wong E.H., Rajoo R., Lim T.B. (2005), "Swelling and time-dependent subcritical debonding of underfill during temperature-humidity aging of flip chip packages," *IEEE Transactions on Components and Packaging Technologies*, Vol. 28(4), pp. 862 – 868.

157. Wu W.L., Orts W.J., Majkzak C.J. (1995), "Water absorption at a polyimide/Silicon wafer interface," *Polym. Eng. Sci.*, 12, pp. 1000-1004.

158. Wunderle B. (2003), "Thermo-mechanical reliability of flip-chip assemblies with heat-spreaders," *Dissertation for the degree of Doctor of Philosophy,* Robert Bosch GmbH, Stuttgart and Technische Universität Berlin, Berlin, Germany, June 2003.

159. Wunderle B., Nüchter W., Schubert A., Michel B., Reichl H., "Parametric FE-approach to flip-chip reliability under various loading conditions," *Journal of Microelectronics Reliability, Elsevier*, 2004, pp. 1933–1945.

160. Xie, B., Fan X.J., Shi, X.Q., Ding, H. (2009), "Direct concentration approach of moisture diffusion and whole field vapor pressure modeling for reflow process: Part I – theory and implementation," *ASME Journal of Electronic Packaging, 131(3),* pp. 031011.1-031011.6.

161. Yang D.G., Jansen K.M.B., Ernst L.J., Zhang G.Q., van Driel W.D., Bressers H.J.L., Fan X.J. (2004), "Prediction of process-induced warpage of IC packages encapsulated with thermosetting polymers," *Proc. Electronic Components and Technology Conferen*ce ECTC2004, pp. 98-105.

162. Yao Q., Qu J., "Effect of thermal residual stresses on the apparent interfacial fracture toughness of polymer/metal interface," *Proc. Electronic Conference and Technology Conference*, 1999, pp. 365-368.

163. Yoshihara H. (2008), "Theoretical analysis of 4ENF tests for mode II fracturing in wood by finite element method," *Eng Fract Mech*, (75), pp. 290-296.

164. Zanni-Defarges M.P., Shanaham M.E.R. (1993), "Evaluation of adhesive shear modulus in a torsional joint: influence of aging," *International Journal of Adhesion and Adhesives*, Vol. 13, pp. 41-45.

165. Zhang J., Lewandowski J.J. (1997), "Delamination study using four-point bending of bilayers," *Journal of Materials Science*, (32), pp. 3851-3856.

166. Zhang Z. (2007), "Thermomechanical reliability of microelectronics," *Dissertation for the degree of Doctor of Philosophy*, Cambridge, Harvard school of engineering and applied science, USA.

167. Zhou J., Lahoti S., Kallolimath K. (2005), "Investigation of non-uniform moisture distribution on determination of hygroscopic swelling coefficient and finite element modeling for a flip chip package," *Proc. 6th EuroSimE2005*, pp. 112-119.

168. Zhou, J. (2006), "Sequentially-coupled finite element transient analysis with hygroscopic swelling," *Proc. 7th EuroSimE2006*, pp. 1-6.